

---

# Human-machine-centered design and actuation of lower limb prosthetic systems

---



TECHNISCHE  
UNIVERSITÄT  
DARMSTADT

Vom Fachbereich Maschinenbau an der  
Technischen Universität Darmstadt  
zur Erlangung des akademischen Grades eines  
Doktor-Ingenieurs (Dr.-Ing.)  
genehmigte

**Dissertation**

vorgelegt von

Dipl.-Ing. Philipp Beckerle  
aus Wiesbaden

Berichterstatter: Prof. Dr.-Ing. Stephan Rinderknecht  
Mitberichterstatter: Prof. Dr. rer. nat. Oskar von Stryk

Tag der Einreichung: 06.05.2014  
Tag der mündlichen Prüfung: 08.07.2014

Darmstadt 2014  
D17

---



---

## Abstract

---

People with lower limb loss or congenital limb absence require a technical substitute that restores biomechanical function and body integrity. In the last decades, mechatronic prostheses emerged and especially actuated ones increased the biomechanical functionality of their users. Yet, various open issues regarding the energy efficiency of powered systems and the impact of user-experience of the prosthesis on technical design remain. As tackling the latter aspect urgently requires the consideration of user demands, this thesis proposes a novel human-machine-centered design (HMCD) approach for lower limb prosthetics. Further, it contributes to the design and control of elastic (prosthetic) actuation.

The HMCD approach describes a framework that equally considers technical and human factors. Therefore, seven human factors influencing lower limb prosthetic design are determined, analyzed, and modeled using human survey data: *Satisfaction, Feeling of Security, Body Schema Integration, Support, Socket, Mobility, and Outer Appearance*. Based on the application of quality function deployment (QFD), those factors can be considered as a HMCD focus in systems engineering. As an exemplary application, a powered prosthetic knee concept is elaborated with the HMCD approach. The comparison of the HMCD focus with a purely technical one, which is determined with a control group, reveals distinct differences in the weighting of requirements. Hence, the proposed method should lead to different prosthetic designs that might improve the subjective user-experience. To support this by integrating users throughout the systems engineering process, two concepts for human-in-the-loop experiments are suggested.

As an enabling technology of powered lower limb prostheses, variable (series) elastic actuation and especially such with variable torsion stiffness (VTS) is investigated. Inverse dynamics simulations with synthetic and human trajectories as well as experiments show that the consideration of the actuator inertia is crucial: Only by including it in advanced models, the whole range of natural dynamics and antiresonance can be exploited to minimize power consumption. A corresponding control strategy adapts the actuator to achieve energy efficiency over a wide range of operational states using these models.

The exemplary design of the powered prosthetic knee with respect to the HMCD prioritization of requirements confirms the fundamental suitability of VTS for integration in prosthetic components. In this, considering actuator inertia enables the determination of an optimal stiffness for serial elastic actuation of the human knee during walking that is not found in previous studies. A first simulation considering the changed dynamics of prosthetic gait indicates the potential to reveal lower design requirements. The designed knee concept combines promising biome-

---

---

chanical functionality and long operating time due to elastic actuation and energy recuperation.

Beyond lower limb prosthetics, the proposed HMCD framework can be used in other applications with distinct human-machine interrelations by adjusting the human and technical factors. Likewise, the insights into variable elastic actuation design and control can be transferred to other systems demanding energy-efficient performance of cyclic tasks.

---

## Kurzfassung

---

Menschen mit Beinamputation oder angeborener Beinverkürzung benötigen einen technischen Ersatz, der biomechanische Funktion und Körperintegrität wiederherstellt. Mit der Entwicklung mechatronischer und speziell aktuierter Prothesen wurde die biomechanische Funktionalität der Nutzer in den letzten Jahrzehnten erweitert. Dennoch verbleiben offene Fragen bezüglich der Energieeffizienz von aktuierten Prothesen und zum Einfluss des Nutzererlebens von Prothesen auf deren technische Entwicklung. Da die Bearbeitung des zweiten Aspekts die Berücksichtigung von Nutzeranforderungen dringend benötigt, schlägt diese Arbeit einen neuartigen Ansatz zur Mensch-Maschine-zentrierten Entwicklung (MMZE) in der Beinprothetik vor. Sie liefert zudem Beiträge zum Entwurf und der Regelung von elastischen (Prothesen-)antrieben.

Der Ansatz zur MMZE stellt ein Rahmenwerk zur gleichwertigen Berücksichtigung von Human Factors und technischen Aspekten dar. Dazu werden sieben Human Factors mit erhobenen Daten bestimmt, analysiert und modelliert: *Zufriedenheit, Sicherheitsempfinden, Körperschemaintegration, Unterstützung, Schaft, Mobilität und Außenwirkung*. Durch die Anwendung von Quality Function Deployment (QFD) finden diese Faktoren im Systems Engineering als MMZE-Schwerpunkt Berücksichtigung. Als Anwendungsbeispiel dient hierbei die Konzeptionierung eines aktuierten Prothesenknes mit dem MMZE-Ansatz. Der Vergleich des MMZE-Schwerpunkts mit einem rein technischen, der mit einer Kontrollgruppe erarbeitet wurde, zeigt deutliche Unterschiede in der Priorisierung von Anforderungen. Demnach sollte die vorgeschlagene Methodik zu neuartigen technischen Lösungen führen, die das subjektive Erleben von Beinprothesennutzern verbessern könnten. Um dies durch die Einbeziehung der Nutzer im gesammten Systems Engineering zu unterstützen, werden zwei Konzepte für Human-in-the-loop Experimente vorgeschlagen.

Als Grundlagentechnologie für aktuierte Beinprothesen werden variable (seriell-) elastische Aktuatoren und besonders solche mit variabler Torsionssteifigkeit (VTS) untersucht. Rückwärtsdynamik-Simulationen mit synthetischen und am Menschen gemessenen Trajektorien sowie Experimente zeigen, dass die Berücksichtigung der Aktorträgheit hierbei von entscheidender Bedeutung ist: Nur durch ihre Einbeziehung in erweiterte Modelle können Eigendynamik und Antiresonanz zur Senkung des Leistungsverbrauches ausgenutzt werden. Eine entsprechende Regelungsstrategie passt auf Basis dieser Modelle den Aktuator für einen effizienten Betrieb über einen breiten Bereich an.

Die beispielhafte Konzeptionierung der aktuierten Knieprothese anhand der MMZE-Priorisierung bestätigt die grundsätzliche Eignung von VTS zur Integra-

---

---

tion in prosthetischen Komponenten. Hierbei erlaubt die Berücksichtigung der Aktuatorträgheit im Gegensatz zu früheren Studien die Bestimmung einer optimalen Steifigkeit für die seriell-elastische Aktuierung des menschlichen Knies beim Gehen. Eine erste Gang-Simulation, die zudem die veränderte Dynamik mit der Prothese berücksichtigt, deutet auf das Potential hiermit niedrigere Anforderungen für den Entwurf zu ermitteln hin. Das konzeptionierte Prothesenknie kombiniert durch die elastischen Aktuierung und Energierückgewinnung vielversprechende biomechanische Funktionalitäten und eine lange Betriebszeit.

Neben der Beinprosthetik kann das vorgeschlagene MMZE-Rahmenwerk in anderen Anwendungen mit starken Mensch-Maschine-Wechselwirkungen durch die Anpassung der Human Factors und der technischen Aspekte verwendet werden. Ebenso können die Erkenntnisse zum Entwurf und der Regelung von elastischer Aktuierung auf andere Systemen übertragen werden, die eine energieeffiziente Durchführung von zyklischen Aufgaben verlangen.

---

---

## Contents

---

Symbols . . . . .	viii
Abbreviations . . . . .	x
List of figures . . . . .	xv
List of tables . . . . .	xvi
<b>1 Introduction</b>	<b>1</b>
1.1 Motivation . . . . .	1
1.2 Aim and structure . . . . .	3
1.3 Contributions . . . . .	6
<b>2 Biomechanics and state-of-the-art</b>	<b>9</b>
2.1 Biomechanics of human gait . . . . .	9
2.2 Variable stiffness actuation . . . . .	12
2.2.1 Actuator designs . . . . .	13
2.2.2 Motion control . . . . .	16
2.2.3 Stiffness control . . . . .	18
2.3 Powered lower limb prosthetics . . . . .	20
2.3.1 Psychological evaluation . . . . .	23
2.3.2 Design approaches . . . . .	24
<b>3 Human-machine-centered design approach</b>	<b>27</b>
3.1 Methods . . . . .	27
3.1.1 Technical factors . . . . .	29
3.1.2 Human factors . . . . .	31
3.1.3 Transfer methodology . . . . .	36
3.1.4 Systems engineering . . . . .	39
3.2 Results . . . . .	41
3.2.1 Technical factors . . . . .	41
3.2.2 Human factors . . . . .	45
3.2.3 Transfer methodology . . . . .	54
3.2.4 Systems engineering . . . . .	57
3.2.5 Human-machine-centered design framework . . . . .	62
3.3 Conclusion . . . . .	64

---

---

---

<b>4</b>	<b>Actuator design considering natural dynamics</b>	<b>67</b>
4.1	Methods . . . . .	67
4.1.1	Actuator configurations . . . . .	68
4.1.2	Advanced modeling . . . . .	69
4.1.3	Natural dynamics analysis . . . . .	72
4.1.4	Power consumption analysis . . . . .	75
4.1.5	Experimental evaluation . . . . .	78
4.2	Results . . . . .	85
4.2.1	Natural dynamics analysis . . . . .	85
4.2.2	Power consumption analysis . . . . .	88
4.2.3	Experimental evaluation . . . . .	93
4.3	Conclusion . . . . .	101
<b>5</b>	<b>Variable stiffness control exploiting natural dynamics</b>	<b>105</b>
5.1	Methods . . . . .	105
5.1.1	Modeling of stiffness adjustment mechanism . . . . .	106
5.1.2	Stiffness control strategy . . . . .	108
5.1.3	Forward dynamics simulation . . . . .	110
5.1.4	Experimental evaluation . . . . .	112
5.2	Results . . . . .	113
5.2.1	Forward dynamics simulation . . . . .	113
5.2.2	Experimental evaluation . . . . .	119
5.3	Conclusion . . . . .	124
<b>6</b>	<b>Exemplary design of a powered prosthetic knee</b>	<b>127</b>
6.1	Methods . . . . .	127
6.1.1	Human-machine-centered requirement analysis . . . . .	128
6.1.2	Concept of the actuation system . . . . .	128
6.1.3	Optimization with respect to human data . . . . .	128
6.1.4	Actuation integration and implementation . . . . .	130
6.1.5	System integration issues . . . . .	131
6.2	Results . . . . .	133
6.2.1	Human-machine-centered requirement analysis . . . . .	134
6.2.2	Concept of the actuation system . . . . .	136
6.2.3	Optimization with respect to human data . . . . .	138
6.2.4	Actuation integration and implementation . . . . .	144
6.2.5	System integration issues . . . . .	148
6.3	Conclusion . . . . .	151

---

---

7	Overall discussion and conclusion	155
7.1	Overall discussion . . . . .	155
7.1.1	Human-machine-centered design . . . . .	155
7.1.2	Variable stiffness actuation . . . . .	157
7.2	Overall conclusion . . . . .	161
A	Appendix	165
A.1	Human and technical factors . . . . .	165
A.2	Model parameters of the proposed prosthetic concept . . . . .	173
A.3	Component list of the variable torsion stiffness prototype . . . . .	173
	Acknowledgements	175
	Bibliography	177

---

## Symbols

---

$a(x)$	Part of the input transformation in feedback linearization
$b_\xi$	Numerator coefficient $\xi$ of a transfer function
$c_\xi$	Denominator coefficient $\xi$ of a transfer function
$C(\dot{q}_l, q_l)$	Matrix of coriolis and centrifugal effects (general)
$d$	(Walking) distance
$D_p$	Matrix of parallel damping
$D_s$	Matrix of serial damping
$E$	Energy
$f$	Frequency
$f(x)$	Vector function of nonlinear state space representation
$F$	Force
$g$	Gravitational acceleration
$g(x)$	Vector function of nonlinear state space representation
$G(q_l)$	Matrix of gravitational effects (general)
$i_\xi$	Gear ratio of transmission $\xi$ )
$I_\xi$	Inertia of segment(s) $\xi$
$I_t$	Torsional moment of inertia
$k_\xi$	Vector of state feedback control gains for coordinate $\xi$
$k_{\xi,a}$	Acceleration gain for coordinate $\xi$
$k_{\xi,i}$	Integral control gain for coordinate $\xi$
$k_{\xi,j}$	Jerk gain for coordinate $\xi$
$k_{\xi,p}$	Position gain / proportional control gain for coordinate $\xi$
$k_{\xi,v}$	Velocity gain / differential control gain for coordinate $\xi$
$K_p$	Matrix of parallel stiffness
$K_s$	Matrix of serial stiffness
$K_{s,\xi}$	(Serial) stiffness of component(s) $\xi$
$K_{s,a}$	(Serial) stiffness for adjustment to antiresonance
$K_{s,n2}$	(Serial) stiffness for adjustment to the second natural mode
$\bar{K}_{s,ec}(q_s)$	Analytical solution of torsional stiffness characteristics
$l_\xi$	Length of segment(s) $\xi$
$l_{str}$	Stride length
$m, m_\xi$	Mass (of segment / component $\xi$ )
$M(q_l)$	Matrix of inertial effects (general)
$M_p(q_l)$	Matrix of inertial effects (DA/PEA)
$N_\xi$	Number of participants of study $\xi$
$p_\xi$	Position of the center of gravity of segment $\xi$ regarding its axis of rotation

$P$	Power
$P_k$	Knee power
$P_{m,\xi}$	Mechanical power of actuator $\xi$
$\bar{P}_{m,\xi}$	Mechanical power of actuator $\xi$ (calculated as in [98])
$P_{m,\xi,a}$	Average mechanical power consumption of actuator $\xi$ without energy recuperation
$P_{m,\xi,r}$	Average mechanical power consumption of actuator $\xi$ with energy recuperation
$q$	Vector of joint variables / coordinates
$q_\xi$	Variable / coordinate of joint $\xi$
$s$	Laplace variable
$S(q_l)$	Matrix of inertial couplings
$S_{\xi\xi}(\omega)$	Power spectral density of signal $\xi$
$r$	(Inner) radius
$R$	Outer radius
$t$	Time
$t_m$	Duration of measurement/evaluation
$u$	Eigenvector
$U$	Unity matrix
$v$	Control input of feedback-linearized state space system
$v_a$	Angular velocity of a actuator-transmission unit ( $= \dot{q}_a$ )
$x$	State vector
$z$	Transformed state vector
$\gamma$	Linearized gravitational torque of a pendulum
$\Gamma$	Material-specific modulus of elasticity in shear
$\eta_a$	Efficiency of an actuator-transmission unit
$\lambda$	Ratio factor of inner radius and outer radius in a cylinder
$\mu$	Friction coefficient
$\pi$	Ratio of a circle's circumference to its diameter
$\varrho$	Product-moment correlation coefficient (Pearson)
$\tau$	Torque vector
$\tau_\xi$	Torque at degree of freedom $\xi$
$\omega_\xi$	(Natural) angular frequency
$\square_d$	Desired value of a variable
$\square_{eq}$	A variable in equilibrium state
$\Delta\square$	Relative error
$\frac{d\square}{dq}$	Derivative of a variable with respect to the vector of joint variables

---

$\dot{\square}$ , $\frac{d\square}{dt}$	Derivative of a variable with respect to time
$\ddot{\square}$	Second derivative of a variable with respect to time
$\dddot{\square}$	Third derivative of a variable with respect to time
$\square^{(n)}$	nth derivative of a variable with respect to time
$\hat{\square}$	Peak value of a variable / signal
$\tilde{\square}$	Control error of a variable ( $= \square_d - \square$ )

---

## Abbreviations

---

ABIS	Amputee body image scale [28]
ACT	Actuation / drive train (technical factor)
AC1	Agreement Coefficient 1 [85]
AMASC	Actuator with mechanically adjustable series compliance [105]
ANELS	Auator with non-linear elastic system [120]
AMP-Foot 2.0	Ankle Mimicking Prosthetic Foot 2.0 [33]
AMP	Amputee mobility predictor [66]
AwAS	Actuator with adjustable stiffness [111, 110]
BAVS	Bidirectional antagonistic variable stiffness [65]
BSI	Body schema integration (human factor)
cap.	Capacity
CCEA	Continuous-state coupled elastic actuation [101]
comp.	Component
CON	Controls (technical factor)
DA	Direct actuation
DC motor	Direct current motor
DLR	Deutsches Zentrum für Luft- und Raumfahrt e. V. (German Aerospace Center)
FOS	Feeling of security (human factor)
FSJ	Floating spring joint [249]
FUN	Functionality (technical factor)
GATECH-SEA	Serial elastic actuator of Georgia Institute of Technology [150]
GER	Germany
GPR	Gait planning / state recognition (technical factor)
HDAU	Hybrid dual actuator unit [118, 203]
HF	Human factor
HM	Human-machine
HMCD	Human-machine-centered design

---

---



---

MACCEPA	Mechanically adjustable compliance and controllable equilibrium position actuator [229]
MARIONET	Moment arm adjustment for remote induction of net effective torque [214]
MEC	Mechanics / kinematics (technical factor)
MESTRAN	Mechanism for varying stiffness via changing transmission angle [173]
MIA	Mechanical impedance adjuster [153]
MMZE	Mensch-Maschine-zentrierte Entwicklung
MOB	Mobility (human factor)
OPT	Operating time (technical factor)
OUT	Outer appearance (human factor)
PDAU	Parallel dual actuation unit [203]
PEA	Parallel elastic actuation
PEQ	Prosthesis evaluation questionnaire [133, 132]
P/I/D	Proportional (P), integral (I) and derivative (D) feedback / control
PPAM	Pleated pneumatic artificial muscle [232]
PWM	Pulse width modulation
QA-Joint	Quasi-antagonistic joint [56]
QFD	Quality function deployment
ran.	Rank
recup.	Recuperation
REJ	Reject
rel.	Relative
req.	Required
rHEA	Rotational hydro-elastic actuator [212]
SAT	Satisfaction (human factor)
SEA	Series elastic actuation / actuator [172]
SEMG	Surface electromyography
SEN	Sensors (technical factor)
SIZ	Size / volume (technical factor)
SOC	Socket (human factor)
SUP	Support (human factor)
sys.	System
TAPES	Trinity amputation and prosthesis experience scales [67]
TF	Technical factor
US(A)	United States (of America)
val.	Value

---

VNSA	Variable negative stiffness actuation [251]
VSJ	Variable stiffness joint [34]
VS-Joint	Variable stiffness joint [250]
VSA	Variable stiffness actuator [222, 187]
vsaUT	Variable stiffness actuator (of University of Twente) [175, 81]
VSA-HD	Variable stiffness actuator based on harmonic drives [31]
(V)-SLIP	Variable spring-loaded inverted pendulum [30]
VSSEA	Variable stiffness series elastic actuator [221]
VTS	Variable torsion stiffness [195]
V2E2	Very versatile energy efficient (actuator) [213]
w/	With
WEI	Weight (technical factor)
w/o	Without

---

---

## List of figures

---

1.1	Basic aims and approach. . . . .	4
1.2	Thesis structure. . . . .	5
2.1	Human gait cycle and phases. . . . .	9
2.2	Model and coordinate definitions from [137]. . . . .	11
2.3	Averaged human gait data for walking and running. . . . .	11
2.4	Principle of series elastic actuation. . . . .	12
2.5	Variable stiffness: Basic categories and examples. . . . .	13
2.6	Examples of powered prostheses. . . . .	22
3.1	Fundamental concept of the human-machine-centered design framework. . . . .	28
3.2	Human survey data. . . . .	29
3.3	Pair-wise comparison of technical factors based on [63]. . . . .	30
3.4	Human factor model according to [10, 246] inspired by [70]. . . . .	32
3.5	Principle template of quality function deployment based on [109]. . . . .	37
3.6	V model as a macro cycle according to [231]. . . . .	40
3.7	Structured list of technical solutions, criteria and further information. . . . .	42
3.8	Exemplary V model application. System: Powered prosthetic knee. Component example: Series elastic actuation. . . . .	58
3.9	Functional concept and units of Prosthesis-User-in-the-Loop based on [12]. . . . .	60
3.10	Functional concept and interfaces of the Int <sup>2</sup> Bot based on [14]. . . . .	61
3.11	Complete framework of the human-machine-centered design approach. . . . .	62
4.1	Mechanical models of the investigated mechanical actuator-elasticity configurations. . . . .	69
4.2	Sketch of the investigated pendulum and actuator-elasticity configurations. . . . .	71
4.3	Concept of variable torsion stiffness and elasticity implementation. . . . .	78
4.4	Prototype of a variable torsion stiffness actuator with series elasticity and stiffness adjustment mechanism. . . . .	79
4.5	Schematic lateral section of the variable torsion stiffness prototype. . . . .	80
4.6	Transfer functions from $\tau_a$ to $q_l$ of SEA and PEA. . . . .	85
4.7	Transfer functions in serial elastic actuation ( $\tau_a$ to $q_a$ and $q_a$ to $q_l$ ). . . . .	87

4.8	Average power consumption $P_{m,a,a}$ for sinusoidal trajectories without recuperation. . . . .	88
4.9	Average power consumption $P_{m,a,r}$ for sinusoidal trajectories with recuperation. . . . .	89
4.10	Natural frequencies in comparison with power contour plots for sinusoidal trajectories. . . . .	90
4.11	Average power consumption $P_{m,a,r}$ for dual-sine trajectories with recuperation. . . . .	91
4.12	Natural frequencies in comparison with power contour plots for dual-sine trajectories. . . . .	92
4.13	Maximum actuator torque $\tau_a$ of SEA (left) and PEA (right) for dual sine case. . . . .	93
4.14	Experimental evaluation of the elastic element. . . . .	94
4.15	Contour plots of elastic torque $\tau_e$ compared with natural frequencies. . . . .	95
4.16	Positions, torques and powers during chirp experiments at different stiffness values. . . . .	96
4.17	Positions, torques and powers during sinus experiments at lower stiffness values and different frequencies (1). . . . .	97
4.18	Positions, torques and powers during sinus experiments at lower stiffness values and different frequencies (2). . . . .	98
4.19	Positions, torques and powers during sinus experiments at higher stiffness values and different frequencies. . . . .	99
5.1	Mechanical model of the investigated pendulum incorporating rotational serial elastic actuation and stiffness adjustment. . . . .	106
5.2	Sections of the variable torsion stiffness prototype. . . . .	107
5.3	Block diagram of stiffness control strategy based on [13]. . . . .	108
5.4	Sinusoidal trajectory matched with antiresonance or second natural frequency. . . . .	113
5.5	Chirp trajectory matched with antiresonance or second natural frequency. . . . .	115
5.6	Spectrograms and stiffness trajectories $K_s$ for chirp trajectory. . . . .	116
5.7	Dual-sine trajectory matched with antiresonance or second natural frequency. . . . .	117
5.8	Spectrograms and stiffness trajectories $K_s$ for dual-sine trajectory. . . . .	118
5.9	Dual-sine trajectory matching frequencies deviating from antiresonance. . . . .	118
5.10	Positions, torques and powers during dual-sine experiments at lower stiffness values and different frequencies. . . . .	119

---

5.11	Positions, torques and powers during dual-sine experiments at higher stiffness values and different frequencies. . . . .	120
5.12	Variable stiffness control for sinusoidal and dual-sine trajectories. . .	121
5.13	Variable stiffness control for a chirp trajectory. . . . .	123
6.1	Peak powers related to subject weight versus stiffness and powers required during a gait cycle for peak power optimization. . . . .	139
6.2	Angular velocity $\nu_a$ versus torque $\tau_a$ at the transmission output for peak power optimization. . . . .	140
6.3	Optimized energy consumptions related to subject weight and stride length versus stiffness and powers required during a gait cycle without recuperation. . . . .	141
6.4	Angular velocity $\nu_a$ versus torque $\tau_a$ at the transmission output for energy consumption optimization. . . . .	142
6.5	Optimized energy consumptions related to subject weight and stride length versus stiffness and powers required during a gait cycle with recuperation. . . . .	143
6.6	CAD models of the proposed prosthetic knee in combination with an active foot. . . . .	147
6.7	Spectrograms of shank motion trajectories and comparison of natural limb dynamics with power consumption contour. . . . .	149
6.8	Inverse dynamics simulation of human gait with and without prosthesis. . . . .	151
A.1	Complete list of technical solutions, criteria and further information.	172

---

## List of Tables

---

2.1	Categorized overview on actuation concepts with variable elasticity based on [16]. . . . .	15
3.1	Items of the English questionnaire investigated in [38]. . . . .	34
3.2	Additional items regarding body schema integration. . . . .	35
3.3	Description of technical factors. . . . .	43
3.4	Data from pair-wise comparison by $N_P = 6$ experts: Individual sums of higher importance rating of specific factors. . . . .	44
3.5	Correlation matrix of the items from [38]. . . . .	46
3.6	Satisfaction correlations of data from [36]. . . . .	48
3.7	Human factor set and factor descriptions. . . . .	50

3.8	Frequency distribution for category assignments from [191]. . . . .	52
3.9	Results of quality function deployment with 0/1/3/9 rating scale. . . . .	54
3.10	Results of quality function deployment with 0/1/2/3 rating scale. . . . .	55
3.11	Comparison of technical factor rankings obtained with the purely technical and the human-machine-centered approach based on QFD with 0/1/3/9 scaling. . . . .	56
4.1	Inertial and gravitational parameters of the pendulum based on the VTS test rig [17, 59]. . . . .	71
4.2	Numerator coefficients of transfer functions. . . . .	73
4.3	Denominator coefficients of transfer functions. . . . .	73
5.1	Inertial and friction parameters (param.) of the stiffness adjustment mechanism. . . . .	107
6.1	Dynamics properties of the right leg in the human model from [248].	132
6.2	First version of the (human-machine-centered) list of requirements considering actuation of a powered prosthetic knee. . . . .	135
6.3	Stiffness, peak power and related energy consumption values for optimization of peak power and energy consumption. . . . .	142
6.4	Updated (human-machine-centered) list of requirements considering actuation of a powered prosthetic knee. . . . .	145
6.5	Characteristic frequencies of natural dynamics in the prosthetic system.	149
A.1	German items of the custom-built questionnaire. . . . .	165
A.2	English items of the custom-built questionnaire. . . . .	168
A.3	German items on body schema integration. . . . .	170
A.4	English items on body schema integration. . . . .	171
A.5	Dynamics properties of the proposed prosthetic concept. . . . .	173
A.6	Component list of variable torsion stiffness prototype. . . . .	174

---

## 1 Introduction

---

People with lower limb loss or congenital limb absence have the need for a technical substitute of the missing part of their body. Freely translating the definition from [121], prostheses can be described as “artificial substitutes for parts of the human body made from non-body material”. Specifically, the recreation of biomechanical function as well as appearance of the lost limb by prosthetic components reflect basic design requirements: In case of the lower limb, this comprises the replacement of the (partially) missing leg and the function of the musculoskeletal system in combination with the recovery of an intact appearance. Thus, from a mechatronic perspective, prostheses should replace leg mechanics, actuation, sensing, and control in postural and movement tasks. Among those tasks, the realization of stance and swing phase of different types of gaits is a crucial one, as it has a direct impact on mobility and security of users [19]. Beyond this, various non-technical challenges occur, as prosthetic devices are also required to create an intact outer appearance of their users and give them the feeling of body integrity [243].

In the last three decades, mechatronic approaches led to a significant progress in lower limb prosthetic technology especially regarding biomechanical function and comfort regain. As shown in [19, 252], development started from micro-processor controlled knees adjusting the dynamic characteristics of the system in swing phase and evolved those to vary dynamic parameters in stance phase and provide additional functionalities, e. g., different types of gait or specific modes for activities like cycling. Recently, first commercial knee and ankle devices integrate active components like electrical motors to further provide power to the human-machine system comprising user and prosthesis during locomotion [19, 233], while academic research starts focusing on multi-joint prosthetic systems often aiming at optimizing power consumption as in [71].

---

### 1.1 Motivation

---

A motivation of this work and prosthetic research in general is the high and increasing number of people with amputation shown in various studies: In [92], 55,000 lower limb amputations are counted in Germany in 2003. Another German study estimates 40,000 to 50,000 amputations per year [77]. Major reasons of amputations are diabetes mellitus and arterial diseases [92, 171] or country-specific causes like veterans suffering from limb loss in the United States of America (US) [171].

---

The development of the number of people with amputation in the US is estimated in [253]. According to this study, 1.6 million persons with lower limb amputations were living there in 2005 and an increase to 3.6 millions is projected for 2050.

As losing a limb has an enormous psychological impact [157], people with lower limb amputation are confronted with several challenges in multiple domains including physical as well as psychological factors: As stated in [183], their disability is not only a result of the obvious physical impairment but also caused by social and personal issues. The study further reports a relation of those psychological variables to prosthetic use and thus recommends to consider them in prescription. In [8], it is pronounced from a medical and orthopedic point of view that the patient should always be the focus of treatment as well as rehabilitation and not the medical intervention method or prosthetic technology. The positive impact of modern approaches, such as micro-processor controlled or even powered lower limb prosthetic devices, on the biomechanical disability has been shown for knee [19] and ankle parts [233]. However, various open questions result in psychological issues concerning the users as well as technical potentials compared to the versatile and efficient biological counterpart.

Technical potentials concern functional aspects like gait flexibility or energy consumption of user or prosthesis: Although current prostheses allow for selecting walking speed in a specific range, only few like those in [95, 18] enable the user to run for instance. Regarding energy consumption, powered prostheses are able to improve walking economy of the user [6], while actuation concepts incorporating elasticity can additionally reduce power required from the prosthesis [98]. Therefore, stiffness has to be designed “to work at resonance in rhythmic tasks like walking“ [62], which can be adapted to “different activities or walking speeds and for rejecting unexpected disturbances“ [242]. Yet, the usage of such elastic actuation at varying gait velocities demands additional power to adjust the variable elastic actuator [229, 13] that might (but not necessarily will) affect the benefit of the concept. Potentials regarding human factors are indicated by ingruent questionnaire feedback in [38], where users reported satisfaction with their prosthesis although regularly experiencing pain, for instance.

In contrast to the advice from [8], prosthetics research is scientifically not only motivated by user demands, but also by the multi-disciplinary challenge connecting a variety of aspects like:

- Mechatronic design, actuation, and integration.
- Robot kinematics, dynamics, and control.
- Biomechanical understanding, simulation, and inspiration.

- 
- Psychological background, impact, and intervention.
  - Medical care, treatment, and assistance.

Anyhow, the translation of findings in these fields into practical benefits for the users of prostheses should finally be possible and thus be in compliance with the requirements of [8] again. Yet, a completely human-centered design might overvalue human factors [94] and thus affect the technical solution in a way that the final result is not optimal for the user. Hence, a human-machine-centered approach in analogy to the general idea from [94] is expected to be more appropriate to cover the (partially implicit) user demands in prosthetics. Beyond this, insights from investigations of the fields mentioned above might be useful in other applications concerning human-mechatronic systems with distinct human-machine interaction.

---

## 1.2 Aim and structure

---

The fundamental approach of this thesis is based on the assumption that prosthetic technology can be improved in a novel human-machine-centered way by equally considering human and technical factors. This finally aims at the design of prostheses that integrate with the human as a synergetic human-mechatronic system. To satisfy the multi-disciplinary nature of this task, psychological issues have to be considered as well as biomechanical requirements and technical possibilities. In consequence, issues from different disciplines have to be solved. Regarding human factors in lower limb prosthetics, crucial open questions are:

- Which human factors are relevant and what is their impact on design?
- How can human factors be considered in technical design to meet user requirements?
- What goals can only be achieved by considering human factors in technical design?

As powered lower limb prostheses show the capability of decreasing energy required from the user and elastic actuation can increase energy efficiency, those technical approaches are expedient to overcome biomechanical deficits accompanying limb loss or congenital limb absence. Thus, engineering issues include mechatronic hardware and control software design resulting in the following fundamental questions:

- How can variable elastic actuation support system energy efficiency and the user?

- What technical requirements emerge when considering human factors in design?
- Can the interactions of human user and technical system be considered in design?

Figure 1.1 presents the basic aims and approach of this thesis. With the initial situation of limb loss or absence shown in the middle, the subject suffers from biomechanical deficits and experiences a psychological impact. Contemporary technical solutions focusing on technical and biomechanical requirements in design lead to an artificial replacement of the lost limb (left in Figure 1.1). Such replacements are assumed to deliver a functional regain without completely restoring biomechanical capabilities and to leave open relevant psychological issues. It is further hypothesized that the final goal of a fully integrated replacement can only be achieved by human-machine-centered design and considering the changed dynamics of the prosthesis instead of those of the biological leg (right in Figure 1.1). The consideration of human factors and changed dynamics is assumed to enable the design of prostheses that lead to completely restored biomechanical functionality and the feeling of body integrity. Therefore, a set of human factors is determined, assessed and modeled based on survey data from users and experts to enrich common product design schemes regarding user issues and requirements leading to a human-machine-centered design approach. To foster this, human-in-the-loop experiments allowing for the integration of users during all phases of technical design or the investigation of specific human factors are proposed. As variable stiffness actuation is a promise-

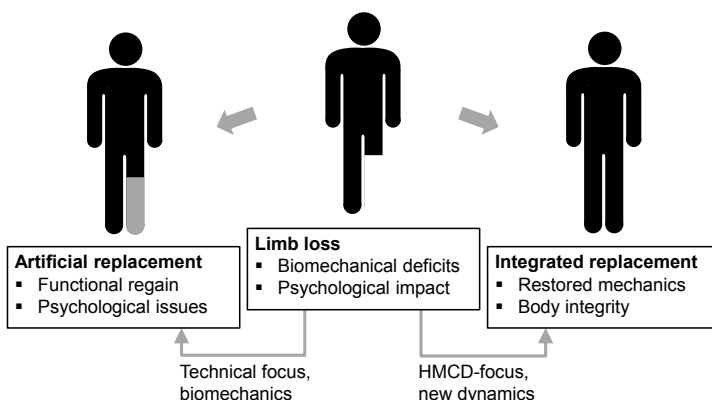


Figure 1.1: Basic aims and approach.

ing enabling technology for powered prostheses, such designs and their control are examined in detail. To illustrate the approach, methods, and results of this thesis, the development of a powered prosthetic knee joint is selected as an application example.

The structure of this thesis is based on this concept and shown in Figure 1.2. A comprehensive and research-oriented state-of-the-art of variable stiffness actuation and powered lower limb prostheses is given in Chapter 2 along with biomechanical fundamentals of human gait. In this, variable stiffness actuation designs as well as corresponding stiffness and motion control algorithms are reviewed. The prosthetic part covers technical solutions, psychological issues, and design approaches regarding (powered) lower limb prosthetics.

Subsequently, Chapter 3 presents the novel human-machine-centered design approach. After a description of the determination, assessment, and modeling of the technical and human factors, a transfer methodology is utilized to bridge the gap between the user and engineering domain. Applying it, a design focus considering human and technical factors equally is determined and compared to a purely technical approach. In systems engineering, the design methodology considers this focus by a prioritization of technical design aspects. Further, it aims at geometric and functional system integration and involving users throughout the whole design process utilizing survey data and human-in-the-loop experiments. For that purpose, the *Prosthesis-User-in-the-Loop* simulator concept [12], which is meant to allow for

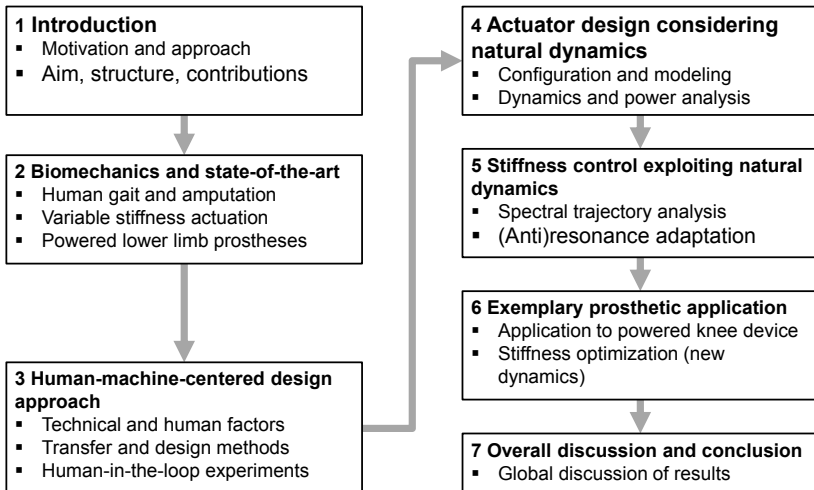


Figure 1.2: Thesis structure.

---

simulating mechanical interactions between user and prosthesis in a virtual environment for pre-prototype testing, is suggested. Additionally, the *Int<sup>2</sup>Bot* [11] is presented as a specific human-in-the-loop approach regarding the feeling of body integrity with the prosthesis.

As an aspect of enabling technologies, Chapter 4 deals with the consideration of natural dynamics in the technical actuator design process. Using advanced models, possible actuator-elasticity configurations are analyzed regarding their natural dynamics and mechanical power requirements to clarify impacts of natural behavior on energy efficiency. The findings are validated with the prototypical test rig of *Variable Torsion Stiffness (VTS)* [195, 17]. To exploit the optimized dynamics of the mechatronic actuation system with respect to energy efficiency, Chapter 5 deals with a control strategy for adjusting stiffness in variable stiffness actuation. It utilizes spectral analysis of the desired trajectory and adapts stiffness based on the advanced models. Those investigations are performed by simulative analyses and experiments with the prototype.

In Chapter 6, an exemplary prosthetic device to substitute the biological knee joint is designed with focus on actuation based on measured human data from [137]. By considering the determined human-machine-centered design focus, the potential of the design framework is evaluated. Further, the example is used to examine possibility to integrate variable torsion stiffness in a prosthesis. Therefore, the elastic drive train is optimized by design simulations and the potential of considering the changed dynamics of the human-mechatronic system is discussed based on first simulations using the model from [248].

To provide a clear separation, Chapters 3 – 6 are each subdivided into sections describing the utilized methods, presenting the results, and concluding those. Based on these chapter-specific conclusions, Chapter 7 gives a global discussion of the overall results of this thesis, along with concluding remarks and an outlook to future works.

---

### 1.3 Contributions

---

In prosthetic design, this thesis contributes a novel human-machine-centered approach and proposes a corresponding set of human factors. This set is modeled based on statistical evaluations of user and expert studies with a custom-built questionnaire (see A.1) that is specifically designed for this purpose. Yet, it is not statistically validated to this point and thus remains subject to future research. Anyhow, the new insights on human factors enable to determine insights on user requirements. The application of a transfer methodology reveals the impact of the modeled human factors on lower limb prosthetic design for the example of a powered

knee device. Further, a common method from systems engineering is extended to suit user requirements based on the results from the transfer step and integrating human-in-the-loop experiments. With Prosthesis-User-in-the-Loop and Int<sup>2</sup>Bot, experimental setups for involving users in the design process and investigating the experience of body integrity are presented. Indications regarding the influence of human and technical factors in prosthetic systems engineering are given along with an outlook suggesting a user-stereotype-specific adaptation.

Regarding variable stiffness actuation, possible actuator-elasticity configurations are assessed considering their natural dynamics and the interrelation of those to energy efficiency. In contrast to other studies, the impact of drive inertia is considered by advanced modeling and discussed intensively with respect to power consumption. Comparing natural dynamics with stiffness values yielding minimum power consumption, the interrelations of those are clarified and can be considered in design and control. As an experimental example, the very first implementation of variable torsion stiffness is presented and experimental results on its mechanical power requirements are shown.

This thesis further contributes to the field of variable stiffness control. Based on the advanced models and spectral trajectory analysis, stiffness is adapted to match the natural dynamics of the system to the trajectory frequency. By this, energy efficiency and functional versatility of the actuation system can be improved. As the adjustment of stiffness itself requires additional energy, modeling is extended to cover and analyze this aspect. Aiming at prosthetic application, such investigations could be used to assess which frequency of adjustment is beneficial: Varying stiffness during the gait cycle, once every cycle or once during several cycles.

A concept for the implementation of variable torsion stiffness in a powered knee prosthesis is proposed using design simulations with human data. By this, the potential of energy recuperation in mechatronic prosthetic knees is examined. The application of advanced modeling in optimization simulations shows essential aspects of natural dynamics to be considered in design. In the simulations, a step towards considering the change of dynamics through the prosthesis is done by introducing the inertial parameters of the prosthetic leg for a first approximation.



---

## 2 Biomechanics and state-of-the-art

---

Based on biomechanical fundamentals, this chapter reviews state-of-the-art powered prosthetics and variable stiffness actuation as a key technology for such systems. Regarding human biomechanics, a brief introduction to human gait is given based on [244] and gait data from [137]. Further, different types of amputation are explained. As many prosthetic concepts from research rely on actuation with (variable) elasticity, this basic technology from robotics is described by a comprehensive review of actuator designs and corresponding approaches to motion and stiffness control are explained. Subsequently, technical solutions of powered lower limb prostheses are presented and analyzed regarding their hardware and software components based on the systematic review from [247]. A focus is set on powered knee devices, as such a system is used as an application example in the remainder of this thesis. Beyond this, tools for evaluating psychological issues in general prosthetics and approaches to technical design are briefly described. A review and an analysis of the human factors themselves is presented as a main aspect of Chapter 3.

---

### 2.1 Biomechanics of human gait

---

Human gait and its cyclic nature can be described by a sequence of events and phases that are depicted in Figure 2.1. In [244], one gait cycle is defined as the

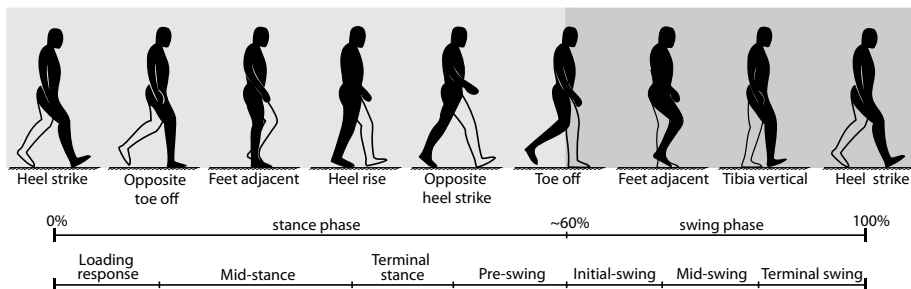


Figure 2.1: Human gait cycle and phases (Copyright: Jochen Schuy and Sabine Backhaus, Institute for Mechatronic Systems in Mechanical Engineering, Technische Universität Darmstadt, modified with permission and based on [244]).

duration between two successive occurrences of the repetitive events of the gait cycle. A common way to interpret the gait cycle is starting with heel strike of the leg in consideration (black in Figure 2.1). The observed sequence of events and phases is divided into a stance and a swing phase depending on the ground contact of the considered foot [244]: Starting with heel strike, the stance phase comprises loading response, opposite toe off, mid-stance, heel rise, terminal stance, opposite heel strike and pre-swing. The transfer from stance to swing takes place with toe off of the considered leg. Swing phase is described by initial swing, feet adjacent, mid-swing, tibia vertical, terminal swing and ends with heel strike of the considered foot marking the beginning of the next cycle. Stance phase lasts about 60%, while swing phase is about 40% of the gait cycle [244]. Between heel strike of one leg and toe off of the other, a phase of double support, where both feet are on the ground, is observed in walking [244]. With increasing gait speed, the duration of swing phase increases and double support duration decreases until it finally disappears and a flight phase occurs marking the transition from walking to running [244]. The spatial distance covered by two heel strikes represents the stride length [244]. Gait speed is often reflected as a distance per time in  $\text{m s}^{-1}$  or as a cadence in  $\text{steps min}^{-1}$  according to [244].

An important aspect of gait for users of lower limb prostheses is their energetic effort. It is often assessed via the metabolic cost, which can be determined by measuring the oxygen consumption of the human [239]. In [239], which is frequently cited, the effects of different levels of amputation on the efforts of users, their walking speeds and stride lengths are compared to those of unharmed humans: Considering the results obtained for subjects with amputation above knee level (transfemoral) and below knee level (transtibial) shows that reduced cadence and stride length is observed in both. Additionally, metabolic efforts are found to increase by 42% and 63% for subjects with transtibial and transfemoral amputation, respectively. Anyhow, subjects experienced lower energetic cost when using a prosthesis instead of crutches. Since the study presented in [239] was performed in 1976, it can be assumed that mechanical prostheses without any actuation have been considered, as those did not emerge even in academic research before the 1980s [252]. Later works report that subjects using any kind of mechatronic prostheses show decreased metabolic efforts (e. g., [19, 6]), although the situation of an unharmed human is so far not restored.

For prosthetic design, analyzing the requirements during gait from human data is crucial. Therefore, gait analysis as performed in [137] can provide insights in desired joint motion ranges and velocities as well as in torque and power requirements. The corresponding model of the lower limbs is reduced to sagittal plane, which divides the body into left and right portions [244]. It is given in Figure 2.2 in

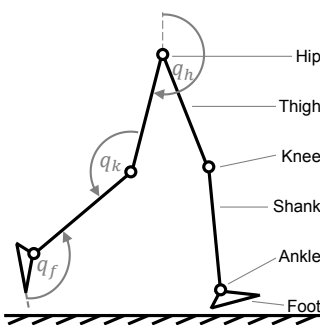


Figure 2.2: Model and coordinate definitions from [137].

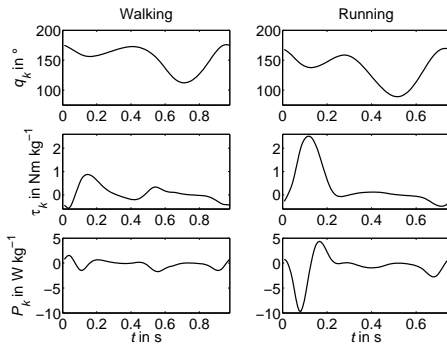


Figure 2.3: Averaged human gait data for walking at  $1.6 \text{ m s}^{-1}$  (left column) and running at  $2.6 \text{ m s}^{-1}$  (right column) from [137]: Knee angle  $q_k$ , knee torque  $\tau_k$  and knee power  $P_k$  related to body weight.

compliance with the one used for gait analysis in [137]. In this, the joints and segments of both human legs are depicted as circles and lines, respectively. Further, coordinates describing hip  $q_h$ , knee  $q_k$ , and foot motion  $q_f$  of the considered leg are defined. Based on these coordinates, Figure 2.3 gives knee joint motions  $q_k$ , torques  $\tau_k$  and power  $P_k$  of one gait cycle with respect to time  $t$ . Those are averaged from measurements with 21 subjects without amputation (average height 1.73 m, average weight 70.9 kg). In the left column plots of Figure 2.3, results for walking at  $1.6 \text{ m s}^{-1}$  are shown, while such for running at  $2.6 \text{ m s}^{-1}$  are given on the right. It becomes clear that a wider range of joint motion is covered during running and higher joint velocities occur due to this. Further, the knee torque  $\tau_k$  increases by about a factor of 2 regarding its peak value. It is depicted related to body weight for comparability between subjects. Hence, required joint power of the knee  $P_k$  is distinctly increased in running, as it depends on motion and torque. Anyhow, from an engineering point of view, the alternating nature of power in both gait types appears promising with respect to reusing energy due to the repetition of the gait cycle. According to [244] positive powers have to be generated by the muscles, while negative powers have to be absorbed by those in humans.

---

## 2.2 Variable stiffness actuation

---

Generally, robot mechanisms are built as serial, parallel or hybrid structures of links that are connected by joints and driven by actuators [134]. Conventional approaches require precise, fast, repetitive positioning and thus benefit from high mechanical stiffness in motion control with strategies as given in [116, 201]. Hence, conventional robots are designed based on rigid links and joints using actuators with high output power. Therefore, such robots usually work in restricted areas avoiding interaction with humans and preventing those from being harmed. In the last two decades, design and control paradigms changed in the field of robotics due to an increasing demand for closer human-robot interaction [86, 166, 135]. Resulting from this, series elastic joint actuation concepts coupling actuator and joint by an elastic element are increasingly applied, and various concepts to vary its stiffness depending on the actual operating conditions were introduced [227, 135]. The principle of series elastic actuation (SEA) is shown in Figure 2.4, where the link (dotted) is moved around a rotational joint by a motor M1 via a linear elasticity. As the introduced elastic elements are passive mechanical structures, this kind of actuation is commonly referred to as passive compliant or elastic actuation (e. g., [227]). Based on the SEA approach, variable stiffness (series elastic) actuation concepts provide high stiffness to enable enhanced precision, repeatability, and speed, while they can change to low stiffness, if safety is required in human-robot interaction. Further, such actuators allow for increasing energy efficiency in performing cyclic motions by matching the natural behavior of the system to the frequency of the desired trajectory [172, 229]. Beyond this, elastic joints and actuators can protect the mechanical part of the robot by decreasing loads from impacts like ground contact and allow for better force control [172]. In powered lower limb prosthetics, series elastic actuation is often implemented for energetic reasons [6, 62] and the variation of stiffness is utilized to optimize efficiency depending on body mass [96] or gait velocity [80, 79]. Further, it can be used to adapt to different activities and to reject unexpected disturbances [242].

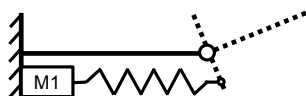


Figure 2.4: Principle of series elastic actuation.

## 2.2.1 Actuator designs

Passive elastic actuation in robotics emerged in the middle of the 1990s with the presentation of the series elastic actuator [172] and the mechanical impedance adjuster (MIA) [153], which are both capable to change joint stiffness. The series elastic actuator uses a fixed-stiffness spring in series with a stiff actuator and force-controlled stiffness variation [172], while the mechanical impedance adjuster is based on a leaf spring and stiffness can be varied by changing the active length of this spring [153]. After the introduction of those actuators, a variety of variable elastic actuators with different principles of stiffness adjustment has been presented. Those can be categorized into four groups considering their fundamental principles [227]: Equilibrium-controlled, structure-controlled, mechanically controlled, and antagonistic-controlled stiffness. In a more recent review [228], the latter three are categorized as actuators with adaptable compliance properties in contrast to such with fixed compliance like the equilibrium-controlled ones. Those latter ones change the equilibrium position of a fixed-stiffness spring to generate a desired force or stiffness by means of control [96].

An overview of the three classes that are part of both categorizations (but not completely coherent) is given in Figure 2.5. In this, categories according to [227] are given in bold face, the depicted example is explained in brackets and the corresponding category from [228] is printed bold and italic. All examples show a link element (dotted) that is attached to a rotational joint, while two motors M1 and M2 are used to move it and/or adjust joint stiffness. The antagonistic-controlled

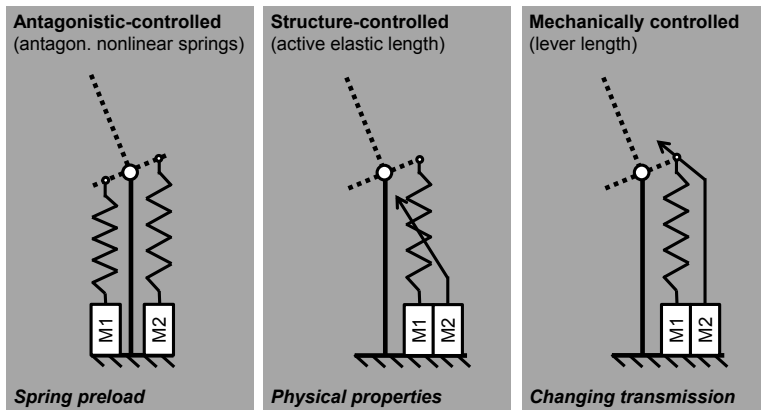


Figure 2.5: Variable stiffness: Basic categories and examples.

principle depicted on the left is using two or more actuators, coupled antagonistically via fixed stiffness elastic elements and working against each other similar to human muscles [227]. Joint stiffness becomes variable, if nonlinear springs are chosen [227]. In structure-controlled elastic actuators, as shown in the middle of Figure 2.5, the variation of stiffness is achieved by modifying the physical structure of the elastic element, e. g. changing its moment of inertia or the effective elastic length [227]. In contrast to this, the characteristics of the elastic elements in mechanically controlled elastic actuators are constant and stiffness is adjusted by modifying the attachment of the elasticity to the structure, which corresponds to a change of pretension or preload [227], as presented on the right of Figure 2.5.

Most actuator concepts can be sorted into the four categories of [227]: Beyond the original series elastic actuator [172], the SEA from the iCub robot [223] and the CompAct [124] belong to the group of equilibrium-controlled stiffness. Among structure-controlled approaches, JackSpring [96], VSJ [34], and VTS [195] are found besides the mechanical impedance adjuster [153]. The class of mechanically controlled concepts comprises MARIONET [214], Tunable Spring [225], V2E2 [213], rHEA [212], VS-Joint [250], MACCEPA [229], HDAU [118, 203], vsaUT [175, 81], AwAS [111, 110], MESTRAN [173], FSJ [249], and VNSA [251]. Concepts based on pneumatic muscles like PPAM are usually implemented in antagonistic setups [232] and are thus interpreted to belong to the antagonistic-controlled group. Other antagonistic-controlled stiffness concepts are AMASC [105], ANELS [120], GATECH-SEA [150], VSA [222, 187], VSSEA [221], PDAU [203], Edinburgh-SEA [152], CCEA [101], VSA-HD [31], and BAVS [65]. A related concept is found in the quasi-antagonistic approach QA-Joint [56] that combines a main, serial elastic actuator with stiffness variation through an additional antagonistic actuator. An overview over the mentioned variable elastic actuator examples sorted by category is given in Table 2.1.

In addition to the type of stiffness variation, the configuration of elastic elements has a significant influence on the dynamic and energetic properties of an elastic actuator concept. Most contemporary concepts with variable stiffness utilize an elastic element in series with the actuator, as this allows increasing energy efficiency and safety in human-robot interaction. Yet, parallel elastic elements or combinations of serial and parallel elastic elements can also be used to reduce energy and peak power requirements as proposed in [149, 78]. Investigations using an underactuated planar two-link pendulum showed that the total energy consumption can significantly be reduced by applying a tuned parallel spring mechanism to the actuated joint [149]. In [78], peak power and total energy requirements of serial elastic, parallel elastic, and combined serial and parallel elastic actuators are compared using simulations of a powered ankle-foot prosthesis. With appropriate parameters, all

configurations are able to decrease peak power and energy in comparison to direct actuation of the joint (without incorporating elasticity). It is shown that serial elastic configuration reduces total energy consumption best, while a pretensioned parallel elastic configuration is superior in decreasing peak power requirements and combinations resulted in a trade-off of these results. In [61] and [60], these investigations are extended regarding unidirectional springs and damping showing that unidirectional parallel elasticity can further decrease energy requirements, while damping can be beneficial in descending stairs. Anyhow, safe human-robot interaction benefits distinctly from a series elasticity due to resolving the rigid coupling of actuator and link.

In the design of elastic actuators with variable stiffness, dynamic system properties like inertial or gravitational effects have a high significance due to their distinct influence on the natural dynamics [15, 16]. Yet, design is mostly focused on drive properties in early publications like [172], although models for simulation include the properties of actuator and link as in [154]. Up to now, the dynamic interaction between actuator and link is not sufficiently considered for dimensioning in many cases, as current research focuses on energy efficiency by storing energy [227] and thereby often neglects the smaller inertia of the actuators through interpreting them

Equilibrium-controlled	Structure-controlled	Mechanically controlled	Antagonistic-controlled
SEA [172]	MIA [153]	MARIONET [214]	PPAM [232]
iCub SEA [223]	JackSpring [96]	MACCEPA [229]	AMASC [105]
CompAct [124]	VSJ [34]	Tunable spring [225]	ANELS [120]
	VTS [195]	V2E2 [213]	GATECH-SEA [150]
		rHEA [212]	VSA [222, 187]
		HDAU [118, 203]	VSSEA [221]
		VS-Joint [250]	PDAU [203]
		AwAS [111, 110]	QA-Joint [56]
		MESTRAN [173]	Edinburgh-SEA [152]
		FSJ [249]	CCEA [101]
		vsaUT [175, 81]	VSA-HD [31]
		VnSA [251]	BAVS [65]

Table 2.1: Categorized overview on actuation concepts with variable elasticity based on [16]. Abbreviations explained in list of abbreviations of this thesis.

---

as ideal torque or position generators. Thus, only link dynamics are considered and the impact of actuator properties is hence not investigated, e. g., in [110, 214, 250]. Such assumptions are also used in [229, 195] for the analysis of power consumption in various variable stiffness actuation concepts, which hence does not show the complete characteristics of those systems. This is also the case in several publications aiming at prosthetic design like [98, 96, 97, 80, 79, 78, 195, 61, 60] due to the calculation of power for stiffness optimization or power analysis, which is explained in detail in Sections 4.1.4 and 4.2.2. So far, the properties of both components are especially considered in complex antagonistic-controlled concepts like AMASC [105] and VSA [222]. In AMASC, the influence of the interaction between the inertias does not show significant impact [105], while it is not examined in the case of VSA [222]. Among structure-controlled solutions, inertial properties of actuator and link are considered in the complex VLJ [34], but comparably low as in AMASC.

Based on linearized models of a prototypic implementation of the VTS concept from [195], the impact of inertial parameters and gravitation on the natural dynamics of the elastic actuation system are investigated by the author of this thesis in [15, 17, 16]. Due to the relatively high value of actuator inertia, its impact on the natural frequencies is rather distinct and can be investigated well. Based on insights from these works, more versatile possibilities in selecting stiffness by exploiting natural frequencies and an antiresonance mode of the system are derived [17]. Hence, a wider range of operation can be covered. The effect of various actuator-elasticity configurations on these possibilities is examined in [16] and in Chapter 4.

---

## 2.2.2 Motion control

---

A main challenge in motion control of variable stiffness actuated systems is nonlinearity, as many of those have robotic structure with segmented link chains under the influence of gravity [3]. Thus, motion control techniques developed to cope with unintended elasticities in robotic joints since the 1980s can be applied as well as such designed for variable stiffness actuation. Beyond common criteria to assess control quality like stability and accuracy, control systems for (variable) elastic joint robots are often required to work without additional sensors compared to rigid systems [3, 162] and to be robust against unknown changing loads as it is also demanded in rigid ones [210, 211]. To reach these various goals, model-based strategies incorporating system knowledge are often used. Considering the review in [162], non-model-based methods like proportional (P), integral (I), and derivative

---

(D) feedback are mostly used in combination with model-based approaches rather than on their own.

Important contributions on the model-based control of robots with flexible joints were made in the second half of the 1980s: In [205], a widely adopted model for robots with elastic joints and motion control based on feedback linearization is proposed. When model and real system match perfectly, the input and state transformations of feedback linearization lead to a globally decoupled linear system that can be controlled by linear techniques [50, 208]. Yet, feedback linearization techniques are stated to generally require accurate nonlinear modeling and to be computationally expensive [143]. Tracking performance improves with increasing joint stiffness according to [200]. To ensure the robustness of such controllers against model deviations, they can be extended by sliding mode control [205, 200]. A different class of strategies is based on singular perturbation theory that can be combined with integral manifolds [209, 208]. Those strategies are separated in a fast inner and a slower outer control loop. The inner control loop is used to dampen joint oscillations and enable the application of rigid robot control laws for the outer motion control loop in case of high joint stiffness [208]. Utilized methods from rigid robotics are computed torque control or adaptive algorithms [208, 206]. A comprehensive review on major developments based on these initial works considering adaptive algorithms, robust stability and implementation issues is given in [162] for instance. Indications regarding the choice of an appropriate control algorithm are given in [208]: Feedback linearization is stated to yield good results in low stiffness scenarios as the modeled elasticity is integrated into control design, although accuracy increases with stiffness as found in [200]. In case of higher joint stiffness, good performance in combination with simple implementation can be reached using singular perturbation approaches. Both, feedback linearization as well as singular perturbation based approaches can further be used as a basis for force or impedance control instead of motion control, as shown in [207].

An extended version of the elastic joint robot model from [205] considering inertial coupling between subsequent joints is used in [51, 47]. Based on this, general feedback linearization [51] as well as feed-forward and PD-type feedback control are investigated [47, 3]. Further, extensions for the control of robots with visco-elastic joints by feedback linearization approaches are given in [48]. Passivity based controllers represent a third common class of model-based nonlinear controllers and a promising approach to combine good tracking performance and robustness [29, 3, 161]. According to [161], where passivity based impedance control is described, this approach virtually decreases the apparent motor inertia and thus improves the dynamic behavior of the controlled robot.

---

In contrast to the observations from early flexible joint control reviewed previously, non-model-based PD- and PID-based approaches are applied in variable stiffness actuator control. In [222], a PD-controller is used for control of the VSA. The HDAU [118] and the HSVA [119] are both controlled by PID-controllers, while in the DLR hand-arm system PD-control is applied in combination with a model-based compensation of gravity and coriolis effects [125]. Despite the nonlinear dynamics, linear state feedback controllers are proposed to control variable stiffness actuators in several publications: Gain-scheduled state feedback for active vibration damping in the VS-Joint and QA-Joint of a variable compliance arm [4], gain-scheduled state feedback for the linearized DLR hand-arm system that is decoupled by eigenmode analysis after torque feedback aiming at robustness and damping [169], general linear quadratic regulation in MACCEPA and the Edinburgh SEA [100] or gain-scheduled linear quadratic regulation with feed-forward components in AwAS [181, 182]. Among those, the ones based on gain-scheduling use the variation of feedback gains to cope with nonlinearities.

Those effects are directly considered by the application of feedback linearization techniques like the combined approach to control motion and stiffness in VSA-II [49] or the control of VTS [17]. Further, a similar technique extended by a smooth sliding mode to improve robustness is shown in [164], while a combination of a sliding mode with gain adaptation by a neural network is used in VSA [104, 103]. Singular perturbation based approaches are proposed for application with VSJ [34] as well as in [165].

Beyond feedback techniques, feed-forward methods are applied in several variable stiffness actuators. In vsaUT-II, limit cycles are used to create motions [30]. Further approaches use optimal control methods to maximize link velocity in SEA and VSA [69] or the DLR hand-arm system [87]. In [88] optimal control is suggested to maximize potential energy in elastic joints. A method to optimize torque and stiffness control for throwing tasks with the DLR hand-arm system are given in [26, 27].

As an alternative to motion control, impedance and force control, which can be based on feedback linearization and singular perturbation techniques [207], can be applied especially to ensure safety in human-robot interaction. Since active impedance and force control are closely correlated with the stiffness control in variable stiffness mechanisms, such solutions are reviewed in the following.

---

### 2.2.3 Stiffness control

---

For the variable stiffness actuation concepts described previously, various methods for controlling stiffness adjustment have been proposed. Common criteria that are

---

considered in stiffness control design are the reduction of power consumption [230, 17], the adjustment of global stiffness in workspace coordinates [165], keeping injury measures below certain constraints for user-safety [222] as well as stability [104, 103], damping and robustness [4, 169].

Simple stiffness controllers are using PD- or PID-type feedback. Considering VS- and QA-Joint, PD-controllers are used [4]. In [181, 182], stiffness of AwAS is derived analytically and adjusted by a PID-controller regarding the perceived stiffness on the link side. PID-controllers are also used in HSVA [119] and for damping control in CompAct [122, 123]. Further, a PD-approach is proposed to vary stiffness of VTS in a way to exploit natural frequencies and an antiresonance mode of the system aiming at reduced power consumption by the author of this thesis [17]. Another class of approaches to stiffness control relies on nonlinear feedback methods like sliding mode control and feedback linearization. The control of the VSA combines sliding mode control with a neural network for adaptation aiming at increased robustness [104, 103]. Feedback linearization is used for decoupled stiffness and motion control in the VSA-II [49] and combined with a smoothed sliding mode for robustness in the control design presented in [164].

Beyond feedback approaches, there are feed-forward stiffness control techniques and methods for stiffness distribution regarding the kinematics of the system. The aim of [230] is the reduction of energy consumption by adapting stiffness to the trajectory and exploiting natural dynamics of a PPAM driven bipedal robot. Therefore, stiffness is chosen as the analytical derivative of required torque with respect to the desired trajectory. A feed-forward method based on the specific characteristics of HDAU is proposed in [118]. In [100], required stiffness is calculated derivating the required joint torque with respect to the position in MACCEPA and the Edinburgh-SEA. For the distribution of joint stiffness to match desired values in workspace coordinates, inverse kinematics are considered in [165]. In [30], an approach to generate stiffness commands from limit cycles is presented for vsaUT-II. Further, the calculation of stiffness from a V-SLIP model that models gait as a variable spring loaded inverted pendulum is set by a P-controller for the knee torque in [117] considering a bipedal robot actuated by vsaUT-II. In the DLR hand-arm system, quasi static variation of stiffness is assumed using motion trajectories generated from limit cycles [125]. A subgroup of feed-forward techniques applied in stiffness control are such using optimal design. Investigating SEA and VSA, an optimal control scheme to maximize link velocity is suggested in [69]. In addition to maximizing link velocity [87], the potential energy in the DLR hand-arm system is maximized using methods of optimal control in [88].

The group of impedance and force control based methods can substitute motion control methods. Anyhow, it is directly connected to stiffness control, as effective

---

joint stiffness can be influenced passively by a variable stiffness mechanism or actively by means of impedance and force control. Considering pneumatic actuation, sliding mode control and linear optimization are used with additional PD-type loops for independent stiffness and force control in [199]. In [245], the effective stiffness of a cable/tendon mechanism of a finger in the DLR hand-arm system is controlled by combining inverse calculations of required tendon positions with impedance and force control. Further, the combination of passive joint stiffness and active impedance control is used to adjust Cartesian stiffness of the DLR hand-arm system in [168]. Considering a bipedal walking robot based on vsaUT-II, a controller switching between stiffness control in stance and motion control in swing phase is proposed in [117].

---

### 2.3 Powered lower limb prosthetics

---

Historically, lower limb prostheses developed from completely passive mechanisms to micro-processor controlled knees. The first realizations of the latter class were able to adjust the dynamic characteristics of the artificial limb in swing. Such concepts that provide this adaptation during swing and stance phase have been investigated in academic research since the middle of the 1980s before commercial products were introduced in the early 1990s [252]. Contemporary, manifold academic research on powered lower limb prosthetics is performed (e.g., in [6, 71]) and first products like the PowerKnee from Össur, Reykjavík, Iceland or the BiOM AnkleSystem from Personal Bionics, Bedford, MA, USA are commercialized. Although the benefits of such mechatronic prostheses regarding biomechanical function have been shown for knee [19] and ankle parts [233], the versatility and efficiency of the biological counterpart is not yet met: As mentioned above, open issues concern walking economy of the users [6], power required from the prosthesis [98] and enabling activities like running, which is only possible with few systems [95, 18, 102].

Regarding their kinematic setup, the majority of knee devices reviewed in [247] combine a rotational single-axis joint or a multi-bar linkage with an electromechanic actuator via a ball-screw or belt transmission [114, 22, 64, 224, 99, 170]. Further, the knee part of the integrated powered ankle-knee prosthesis from [217, 218, 128] is implemented using a ball-screw and a slider-crank mechanism, while a combination of a four-bar linkage with a linear actuator is found in [72, 73]. Contrary designs are found in the agonist-antagonist knee from [146, 145, 144] that uses two series elastic actuators attached to the same joint and working against each other as well as the antagonistic setup with pneumatic actuation proposed in [240]. Two novel concepts aim at increased energy efficiency: In the first, a clutch added in parallel with the motor of a serial elastic actuator allows to disengage the motor

and make the system completely passive in certain situations [179]. In the second, a passive knee is coupled with an active ankle to exchange energy and thus decrease ankle requirements [71]. This is possible due to the dissipative nature of the knee during level walking described in [145]. Yet, this kinematic approach might not be beneficial in other gaits, as power has to be provided in the knee in stair climbing or running for example [176, 79]. Most actuators applied in powered knee prosthetic are electromechanic ones like brushed direct current (DC) motors [64, 22, 204, 146, 145, 217, 144, 224, 128, 99], brushless DC motors [218, 170] or linear stepper motors [72, 73]. Pneumatic actuation by means of double-acting cylinders [215, 216] or artificial muscles [240] as well as hydraulic actuation [52] both appear in significantly fewer concepts. While those concepts actuated by fluids use inherent elastic characteristics [215, 216, 240], others incorporate such to store and release energy during gait as the antagonistic setup from [146, 145, 144] or the clutched series elastic actuator in [179]. Yet, elasticity is used often in the ankle but not in the knee of systems like in [217, 218, 128]. Another solution uses a complex elastic mechanism in the knee but only actuates the ankle [71]. For power supply, all autonomous systems rely on (Lithium Polymer) batteries as energy source [146, 144, 218, 72, 128, 73, 99], while other prototypes use external power supplies [215, 64, 216, 217, 52].

Nearly all concepts comprise some kind of joint motion sensor like encoders or potentiometers, as such are often used for state recognition and control purposes [114, 215, 64, 216, 217, 22, 146, 145, 144, 218, 224, 240]. In some systems, mechanical loads of joints or actuators [64, 224, 99] are acquired, while the systems from [216, 217, 218] use an additional load cell under the socket to assess loads at the interface to the user. Two very common types of sensing are the acquisition of limb motions by accelerometers or inertial sensors [215, 204, 22, 146, 145, 218, 130, 128] and assessing ground contact using force resistors, Hall effect sensors or pneumatic bladders [64, 217, 146, 145, 144, 240, 99]. Based on such information, state recognition and controller selection are performed as in [218]. Another aspect of state recognition is the detection of user intentions. For this purpose, the sockets of two systems are equipped with surface electromyographic (SEMG) sensors that measure muscle activity to estimate human intent [204, 99]. In [99], this is applied to realize volitional control by the user, while it is used to extend *Echo Control* approaches in [204].

Echo control generates motions based on measuring motion of the intact leg and imitating it shifted by a half gait cycle on the prosthesis [22, 204] and is thus limited to walking even numbers of steps and to people with unilateral amputation. The extension with SEMG sensing in [204] solves the first of those issues. However, the most prevalent methods to recognize the state of

the prosthesis, user intention and environmental conditions use finite-state machines, which are also interpreted as high-level controllers, as they adapt the system to certain states by switching lower-level motion or force/torque controllers [114, 64, 215, 146, 216, 217, 218, 144, 130, 240, 128]. Techniques of artificial intelligence like adaptive fuzzy algorithms [22] or recurrent neural networks [52] as well as motion generation by bio-inspired central pattern generators that represent nonlinear oscillators [73] are only used in individual solutions.

To finally perform motion tasks, feedback control approaches regarding position [22], actuator currents [52] or force [99] are applied. Yet, one of the most important types of such lower-level controllers is impedance control, which is used to adjust the mechanical characteristics of the limb, while providing power to it at the same time [64, 215, 216, 217, 218, 128]. Through the specific implementations, torques are generated according to those of a passive spring and damper system instead of controlling positions. With such algorithms, the prosthesis shows more predictable behavior and thus allows for better interaction with the user [216]. A comparable approach is used in [240], where a robust sliding-mode torque control is commanded by an impedance-based torque generator. Two other techniques aim at optimizing energy efficiency: In [146, 145, 144], a *quasi-passive equilibrium point control* is regulating the engagement of the springs in the antagonistic setup and thus the transformation of potential into kinetic energy, while the approach from [224] switches between a mode that imposes joint power and another that dissipates it by using the motor as a generator.

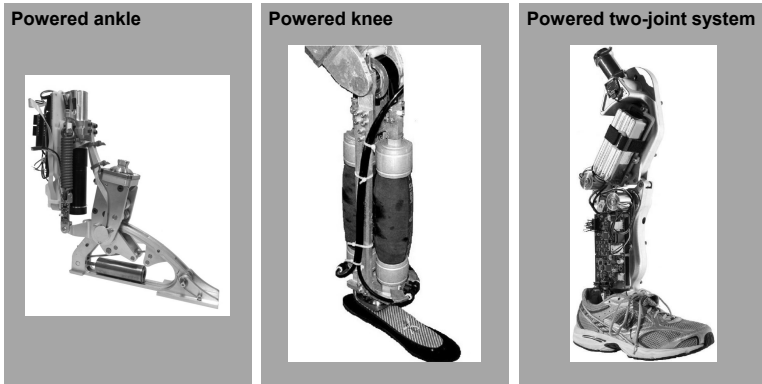


Figure 2.6: Examples of powered prostheses (all with permission): AMP-Foot 2.0 (left, [33]), knee powered by pneumatic artificial muscles (middle, [240]) and powered two-joint system (right, [129]).

Considering these aspects regarding ankle, knee and two-joint lower limb prosthetic systems (refer to Figure 2.6 for examples), comparable components and specific characteristics are found: Many ankle prostheses like the ones from [95, 18, 6, 33] use series elastic actuation with electromechanic motors to cope with the high power requirements at the joint. In contrast to the ankle, certain knees do not use series elastic actuation [217, 218, 224] or no actuation at all [71], since power can even be regenerated during level walking as shown in [224]. Yet, the activities of daily life comprise other types of gait [252] with higher power requirements and less potential of regeneration [176]. Prosthetic systems combining powered ankle and knee joints are not available as commercial products and are rather rare in research: A pneumatically actuated approach shown in [215, 216], one system with hydraulic actuation [52], an electromechanically actuated one including elasticity in the ankle drive train [217, 218], a second generation of the former one utilized and described in [102, 127, 129] and the cyberlegs- $\alpha$  prototype combining a passive knee and an ankle with series elastic actuation to exchange energy [71]. An approach similar to the cyberlegs- $\alpha$  prototype is successfully applied for the design of the completely passive WalkMECH prosthesis that transfers knee power to the ankle, which is not actuated [226]. In addition to avoiding conversion losses, such mechanical transfers allow for reducing required actuator power in contrast to electrical regeneration and transfer of energy between joints, as the mechanical requirements at the specific joint are reduced. Anyhow, purely mechanical solutions are not adaptable to different gait types or velocities.

---

### 2.3.1 Psychological evaluation

---

As motivated in Chapter 1, amputation has a dramatic psychological impact on the life of the concerned persons. Currently, there are two major tools assessing psychological issues in lower limb prosthetics: The Prosthesis Evaluation Questionnaire (PEQ) [133, 132] and the Trinity Amputation and Prosthesis Experience Scales (TAPES) [67]. In the PEQ, prosthetic function, mobility and psychosocial aspects are evaluated by different scales [133, 132]. The functional ones concern usefulness, residual limb health, appearance and sounds, while mobility is treated individually and differentiated in ambulation and transfers. The psychosocial scales are perceived responses, frustration and social burden. Further, the issue of well-being is treated as a scale itself. The subscales of the three sections of TAPES are determined and validated by a factor analysis in [67]. Like the PEQ, TAPES contains psychosocial subscales that are general adjustment, social adjustment and adjustment to limitation. Functional restriction, social restriction and athletic activity restriction are clustered as subscales of activity restriction in contrast to the func-

---

tional scales of PEQ. Further, TAPES comprises functional satisfaction, aesthetic satisfaction and weight satisfaction as satisfaction subscales.

Beyond these general tools, questionnaires or measures for specific psychological issues exist. The Amputee Body Image Scale (ABIS) examines correlations between the body image of people with amputation and their self-esteem, anxiety and depression [28]. In [147], tools not specifically designed for people with amputation are used to investigate their body awareness and schema. The body schema is an important aspect and describes the representation of the characteristics of the own body in a subconscious, neurophysiological and multisensory way [147, 68].

Research described in [186, 184] aims at exploring the values and preferences of prosthetic users towards their devices and their perception of alternative prosthetic options. Based on combined user and practitioner knowledge, a list of the essential elements for prosthetic prescription to improve outcomes is developed to finally improve fitting rates and user satisfaction. A subsequent Delphi study [185] concludes that psychosocial factors related to service provision and prosthetic use are not widely recognized or incorporated into clinical practice and demands the creation of standardized measures incorporating psychosocial factors for optimal prosthetic prescription. In [70], the factors influencing prosthetic design are categorized as enabling, predisposing and reinforcing factors. As only enabling ones can be influenced by technical development, the author of this thesis proposed to investigate the impact of human factors, the connections between enabling and predisposing factors and to use the obtained insight to consider such factors in technical design [9, 10]. According to this approach, several studies aiming at modeling human factors with focus on their integration to prosthetic design have been performed [57, 91, 36, 38, 246, 191, 192]. The survey data and results of those studies represent the human data basis of this thesis and are used to tackle the impact of human factors and their impact on the design in Chapter 3 and Chapter 6.

---

### 2.3.2 Design approaches

---

Analyzing the design and criteria of the powered prosthetic knee concepts described above, gives an overview over the main issues considered and the resulting approaches. In most designs, important criteria are joint or actuator velocities [114, 22, 216, 146, 170, 71, 179] and joint or actuator forces / torques [114, 215, 216, 217, 218, 146, 144, 72, 224, 240, 99, 170, 71, 179]. Further, common aims are to decrease power required from the actuator [216, 217, 218, 146, 99, 71, 179] and reducing the energetic effort [216, 146, 224, 179, 71] to find a technical solution coping with the demanding biomechanical requirements. Considering those, mimicking stiffness [64, 146, 216, 217, 71] and damping [64] characteristics as well

---

---

as the kinematic functionality [146, 216, 217, 144, 218, 240, 99, 71] of the biological limb are design objectives. The consideration of size or weight of the prosthetic component [146, 144, 240] is often connected with compliance to the anthropometric dimensions by adaptation to the size range of the user population [215, 216, 217, 218, 224, 240, 99] and sufficient structural strength to sustain the required range of user weights [215, 216, 217, 218, 240].

Although requirements like suiting anthropometric dimensions concern the user, they are rather technology-oriented than human- or human-machine-centered just like the resulting design processes. Furthermore, questionnaires like the PEQ are mainly used to evaluate existing designs as in [90, 115] but do not specifically aim at integrating human factors during design or at identifying related technological potentials. Other psychological evaluations presented in Section 2.3.1, focus more on the assessment of the psychological state of the person than on technical potentials. First steps towards considering psychological aspects in a human-centered way during technical design are described in [9, 10] by the author of this thesis and are treated in Chapter 3.

In [94], the term human-machine-centered is used regarding ergonomic issues of machines in general. Although this concept has similar overall objectives as the approach proposed in this thesis, it rather considers aspects of classical ergonomics (e. g., [54]) than such distinct human-machine interrelations and interaction as those that occur in prosthetics. Due to these differences, the term human factor comprises more than the user-friendly design of the system or environment in this case and is subject to psychology as can be seen from [133, 132, 67].

Beyond the lack of considering human factors in prosthetic design, biomechanical requirements are usually determined based on gait analysis and simulation of unharmed subjects like in [98, 96, 97, 5, 234, 95, 80, 79, 78, 61, 60] and thus do not consider the changed dynamics of the prosthetic system. Those changes mostly find first consideration in experiments with prototypes as in [6, 218, 144] and can hence not influence design earlier than at prototype level. Specific simulation models enabling to consider the properties of the prosthesis during its design are available [1, 248]. Further, such allowing for the simulation of pathological gait [53] or the investigation of muscle-reflex control for application in prosthetics [74] exist. Yet, they seem not to be used as tools for prosthetic design up to now.



---

### 3 Human-machine-centered design approach

---

According to [63], it is important for the success of products that those meet customer requirements, which results in an increasing consideration of such requirements during the engineering design processes. This is a complex task in general, as only parts of the demands are expressed explicitly by the customer, while the other ones are implicit requirements that can negatively affect product acceptance if they are not covered [63]. In prosthetic design, the patient should always be the focus of treatment and rehabilitation as described above [8]. Anyhow, psychological factors in general and psychosocial ones in particular recently seem not to be incorporated into clinical practice, while standardized measures for that purpose are missing according to [185].

The human-machine-centered design approach presented in the following specifically aims at coping with that and considers the open questions stated in Chapter 1. This comprises the investigation of which human factors are relevant and what is their impact on technical design. Beyond this, it is unclear how human factors can be considered in technical design and what can be reached by this. As a possible solution, a design framework aiming at a balanced consideration of human and technical factors is proposed. This strives for the long-term objective of designing prostheses that integrate with their users as synergetic human-mechatronic systems. The approach is specifically applied to lower limb prosthetics here, but can be used to design other human-mechatronic systems with distinct body-proximity and human-machine interrelations as well. Therefore, technical and human factors can be adapted, since the framework relies on general approaches from product development. In the deduction of the framework, human factors and their impacts are emphasized, since the user perspective is less investigated and technical aspects are discussed extensively in the literature (compare review in Chapter 2).

---

#### 3.1 Methods

---

This section describes the methods used in the elaboration of the human-machine-centered design framework. Those comprise literature analysis, user and expert studies to assess user issues as well as product development and systems engineering techniques.

The fundamental concept of the proposed human-machine-centered design framework is presented in Figure 3.1. The steps left open in this envelope are

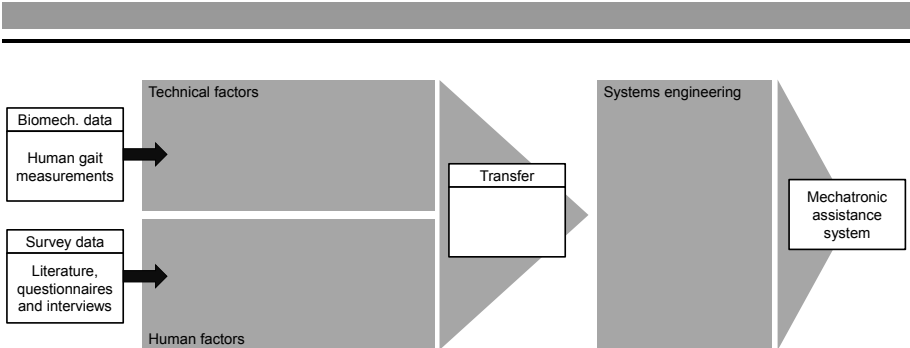


Figure 3.1: Fundamental concept of the human-machine-centered design framework.

elaborated and completed in the following. In contrast to the methodology described in [10, 246], this concept is intended to integrate technical and human factors within a human-machine-centered design approach leading to a closed development process instead of extending technical design regarding human factors. Therefore, two parallel analysis tracks for the consideration of technical and human factors are fed with different types of user data. While biomechanical data for technical requirement analysis is acquired by human gait and motion measurements, survey data is obtained from literature as well as questionnaires and interviews with users and experts for human factor examination. In a transfer step, a methodology from product development is utilized to bring the results from the two parallel paths to a joint domain and make them usable for technical design. Therefore, a design focus that gives a human-machine-centered prioritization of design requirements is elaborated. This design focus is used in a systems engineering step for the final development of the mechatronic assistance system.

While all methods regarding human factors are applied to (powered) lower limb prostheses in general, technical factors, transfer methodology and systems engineering steps are performed for the application example of a powered prosthetic knee with focus on its actuation. Yet, the approach could be applied to other prosthetic or orthotic systems as well as wearable robotics in general.

In this thesis, biomechanical data from gait analyses reported in [137] is utilized. Literature from the systematic review in [247] is analyzed to extract the main technical factors and assess their impact based on contemporary powered prosthetic research. To cope with user requirements, a set of relevant human factors is proposed based on literature and questionnaire data as well as examined in an expert study. With the statistical analysis of the latter study from [191, 192], human factor set is analyzed, first indications regarding the impact of the factors are given

User data		Expert data	
Questionnaire evaluation $N_1 = 29$	Interview study $N_3 = 11$	Pair-wise comparison $N_P = 6$	<i>Technical factor ranking, tech. development focus</i>
<i>Human factor modeling, technical potential</i>	<i>Body integrity, proprioception</i>	<i>QFD discussion <math>N_Q = 5</math></i>	<i>Relations of human/tech. factors, HM-centered focus</i>
Questionnaire evaluation $N_{2a} = 29, N_{2b} = 21$	Expert study $N_E = 22$	<i>Questionnaire optimization, human factor validation</i>	
<i>Human factor modeling and correlations, tech. potential</i>			

Figure 3.2: Human survey data utilized for: Ranking of technical factors, human factor identification, assessment and modeling as well as determining the human-machine-centered design focus.

and relations between them are described. To consider human and technical factors in design, the *quality function deployment* (QFD) method to be conducted with an expert team is proposed and performed. Inspired by [109, 246, 63], interrelations between technical and human factors are assessed to determine a human-machine-centered focus for technical development and component-specific consideration of user requirements. For mechatronic systems engineering, V model development methodology as given in [231] is presented as a common example. Beyond taking into account the development focus determined by QFD in the V model, indications for mapping human factors impact to it are given and the influences of technical factors are discussed. For better understanding, Figure 3.2 gives an overview on user and expert data acquired for the deduction of this approach. It presents the different studies and the corresponding numbers of participants ( $N$ ). The objectives of the particular studies are printed italic. User data from the custom-built questionnaire given in Appendix A.1 and interviews as well as expert data are used in human factors investigation. Additional expert data is used for pair-wise comparison of technical factors as well as an expert discussion within the QFD-method used in the transfer step.

### 3.1.1 Technical factors

During early development of a technical product, the definition of a list of requirements that can be obtained from persons, products or documents is a crucial step [63]. The requirements on this list include interests of the customer and are thus not purely technical. To separate technical and human factors for an individ-

ual analysis of both, technical ones are understood as components or properties of the technical systems in this thesis.

As powered prosthetics design recently is more a field of research than of industrial product development, the corresponding technical factors are determined based on scientific publications. To create a structured list of such factors for the example of a powered prosthetic knee design, the systems resulting from the systematic literature review on powered lower limb prostheses from [247] and described in Section 2.3 are considered. In this review, 22 papers containing information on the design of powered prosthetic knees are found: [22, 52, 64, 71, 72, 73, 99, 114, 130, 128, 146, 145, 144, 170, 179, 204, 215, 216, 217, 218, 224, 240]. These papers are analyzed regarding the mechanical design, actuation, controls and sensors of the described prostheses. Further, algorithms for recognition of gait, user intent and environment as well as information on energy source and system weight are collected and the design criteria applied in the particular papers and comments on other criteria describing practical issues of such systems are gathered. Those aspects are chosen based on the engineering knowledge of the author.

The resulting collection of technical solutions, criteria and further information is generalized by simplifying it, analyzing interrelations and clustering it into groups and subgroups. This leads to a structured list of items that represent the variety of design solutions or issues influencing those according to the investigated literature. From this list, the main technical factors, which are assumed to be represented by the top-level groups, are determined and descriptions defining them are elaborated based on the lower-level items of the list. As a benchmark for the human-machine-centered approach proposed in this thesis, a technically motivated ranking of those factors is determined by a pair-wise comparison based on [63]. For that purpose, an international group of engineering experts from prosthetics research ( $N_P = 6$ ) was asked to compare the determined technical factors among each other using the scheme shown in Figure 3.3. The participants were employees of university groups or other research institutes and have a mean age of 29.17 years ranging from 24 to 33 years. All are male and not familiar with the specific human-machine-centered approach of this thesis. In the example given in Figure 3.3, three factors A, B and C are compared. The more important one of two factors is written into the

	A	B	C	0		Val.	Ran.	
A		B	C	0		A	0	3
B			C	0		B	1	2
C						C	2	1
						1	2	

Figure 3.3: Pair-wise comparison of technical factors based on [63].

corresponding field of the left table. If B is more important than A for example, B is put in the first row of the second column. For evaluation, the frequency of the preference of the individual factors is counted considering in the rows and columns corresponding to these factors. The number of their preference is counted in the rightmost and bottom rows. These are summed and the resulting values (val.) are written into the middle column of the right table. Depending on these values, the technical ranking (ran.) is determined by increasing factor importance with an increased resulting value. In the example, C would be ranked highest, as it received higher importance than both other factors. As six individual ratings are obtained from the participants in this case, an overall rank is determined based on the averages of the individual ratings. As the method is appropriate for use in engineering teams, it might also be used to determine factor rankings in an expert group discussion alternatively.

---

### 3.1.2 Human factors

---

The International Ergonomics Association defines human factors by: “Ergonomics (or human factors) is the scientific discipline concerned with the understanding of interactions among humans and other elements of a system, and the profession that applies theory, principles, data and methods to design in order to optimize human well-being and overall system performance“ [106]. According to [180], “the focus of human factors is on the application of knowledge about human capabilities, limitations, and other characteristics to the design of human-machine systems“, where a human-machine system is further defined as a system in which interaction occurs between people and other (technical) components. Yet, a human factor in (lower limb) prosthetics comprises more than issues of user-friendly design, e. g., coping with losing a part of the own body and integrating a technical replacement, and should thus be subject to psychological research as in [133, 132, 67].

The determination of human factors and their impact is performed using different methods and data presented in Figure 3.2 in this thesis: First, researched literature is used to determine a fundamental orientation, a basic human factor model and indications for relevant human factors. Second, an analysis of user requirements is performed using the results of a custom-built questionnaire co-developed by the author of this thesis [57] to support the determination of relevant human factors. Third, results of an interview study reported in [91] are used as a source of detailed and user-specific information. Fourth, an expert study co-developed by the author of this thesis and conducted with experts from technical and medical professions as well as user groups. The aim of this study is to optimize the custom-built questionnaire and validate the set of human factors proposed based on the results

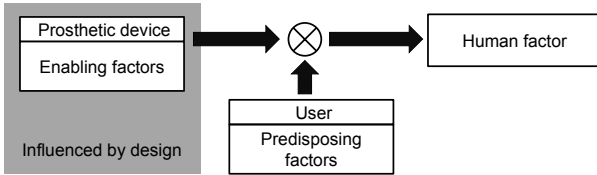


Figure 3.4: Human factor model according to [10, 246] inspired by [70].

from the previous steps. By analyzing the expert ratings, the proposed set of human factors is statistically substantiated [191, 192] and prepared to be validated in with a subsequent and optimized questionnaire.

In order to determine and assess the relevant human factors in prosthetic design, a model of those has to be specified. As described in [70], the factors influencing experience of a prosthetic device can be categorized as enabling factors, predisposing factors and reinforcing factors. Enabling factors cover the functions and characteristics of the prosthetic device, while predisposing ones include the attitude and experience of users. In contrast to enabling factors, predisposing ones can only be influenced indirectly by technical development, while reinforcing factors such as family support cannot be tackled by technology at all. The corresponding basic human factor model applied in this thesis is shown in Figure 3.4. It considers that the user as well as the prosthetic device influence human factors by enabling and predisposing factors, although only the prosthesis itself can be altered by design. The human factor model is used to determine how the subjective assessment of predisposing factors can be influenced by means of technology (enabling factors) and furthermore to analyze the impact of those on design.

Since enabling factors contribute on psychological outcome and can be approached by technical design, those are facilitated in development considering their interrelation with predisposing factors and their impact on human factors. This particular focus on identifying influences on technical development differentiates the proposed human factor model from the approaches based on PEQ [132] and TAPES [67], which focus on psychological, activity and health aspects. Emphasizing the investigation of human factors impact on technical design, specific human survey data is acquired in several studies comprising questionnaire, interview and expert data as shown in Figure 3.2.

The custom-built questionnaire from [57] consists of 85 items. The non-demographic and non-freetext items among those are listed in Appendix A.1. Those collect user data on satisfaction, usability, appearance, pain and handling of the prosthesis in different motor situations. In contrast to other prosthetic questionnaires like PEQ [132] and TAPES [67], the major subject of the questionnaire is to

identify potentials for technical development in powered lower limb prostheses. The questionnaire was announced by several internet platforms, user groups and magazines connected to prosthetics. Data is collected online and offline by a German version and an English one that was reviewed by a native speaker before data acquisition. The items include statements like “Are you satisfied/restricted...”, “How satisfied/restricted...”, “Do you feel/have...” and can be answered using a numeric rating scale. Numeric values are described verbally like 1 = “very satisfied”, 2 = “somewhat satisfied”, 3 = “dissatisfied”, and 4 = “very dissatisfied”. No statement was coded with the value 5 = “missing value”. The first evaluation considers data from  $N_1 = 29$  experienced prosthesis users with lower limb amputation collected from 80 items of the German version [36]. In this evaluation, the values 1 and 2 are interpreted to code satisfaction with the related issue, while the values 3 to 4 are interpreted as being not satisfied. The satisfaction correlations evaluated from this data are not completely given in [36] but are used to support human factor determination in this thesis. In [38], only a subset of user data from the German and the English version is evaluated. Therefore, two groups of experienced participants with transfemoral amputation ( $N_{2a} = 29$ ) or lower levels of amputation ( $N_{2b} = 21$ ) are selected from a total of 65 participants (15 female, 50 male). Subjects range from 15 to above 71 years of age and from 0 to 63 years in the duration of using prosthetic devices. Among all participants, 30 used microprocessor-controlled prostheses, 26 mechanical ones, 2 active devices and 7 other ones. To emphasize results, the threshold of satisfaction is set to answers coded between 1 and 2 instead of interpreting 3 and above as dissatisfied. Further, a correlation matrix of the items shown in Table 3.1 is presented but not interpreted completely in [38]. By interpreting all correlations, a detailed investigation of specific human factors is performed in this thesis. All correlations are evaluated and assessed using the (Pearson) product-moment correlation coefficient  $\rho$  [23].

The study from [91] is based on semi-structured interviews with 13 participants of which 5 are female and 8 are male. User-specific data collection aims at the identification of psychological issues and the analysis of technical development potential. Regarding psychological issues, focus is set on body integrity, proprioception, phantom sensations, coping with the amputation and the impact of gender. The interview population consists of 11 subjects with amputation above knee level and 2 individuals with amputation below the knee. In the evaluation, only transcribed interviews with members of the first group are considered ( $N_3 = 11$ ). The average age is 51 years ranging between 41 and 74 years, while the average period of time since the amputation is 17 years and ranges from 3 months to 70 years. All participants used microprocessor-controlled prostheses and reasons of the amputations are stated as follows: 6 caused by tumor, 3 by trauma and 1 by an infectious disease.

One participant did not make a statement. In this thesis, ratings and statements of individual subjects or subgroups from this study are investigated to substantiate the examination of human factors with focus on body integrity and proprioception.

Using the results from literature and the previously described studies, a set of relevant human factors is derived in this thesis. A study with a group of  $N_E = 22$  experts from technical and medical professions as well as user groups is designed and conducted as described in [192] to examine this set. In contrast to other expert studies aiming at prosthetic prescription [185] or user expectations [184], the objectives of this one are optimizing the custom-built questionnaire to reveal technical optimization potential and structured investigation of human factors according to the major orientation of this thesis. The expert group has a mean age of 39.9 years (standard deviation 11.4 years) ranging from 25 to 65 years and the following frequencies of expertise: 59.1% from technical or engineering professions, 13.6% user group members and 27.3% experts with medical or psychological background. The mean professional experiences was 11 years for technical/engineering experts, 17.3 years for user group members and 16.8 years for experts from medicine and psychology. The gender distribution is 82% male and 18% female. In the study, the

Table 3.1: Items of the English questionnaire investigated in [38].

Acronym	Item
A	Are you satisfied with your prosthesis in everyday life?
B	Are you restricted in everyday life by the size of your prosthesis?
C	Do you feel socially restricted?
D	How many times a day do you have problems because of a swollen stump?
E	Are you satisfied with your appearance in public?
F	Do you think you have a natural gait pattern?
G	Would you prefer more mechanical/electronic aid during the extension of the prosthesis?
H	Do you feel comfortable when you cannot change your gait speed?
I	Do you have problems with your prosthesis while changing your gait speed?
J	Are you satisfied with the transition from standing to walking?
K	Do you feel uncertain with your prosthesis as a mechanical aid?
L	Do you feel certain and stable when you have to compensate the loss of balance (e. g., to stabilize the body in the event of imbalance during a lunge/sidestep)?
M	Would you prefer a foot prosthesis which adjusts to different heel levels?

participants were asked to assign 85 items into categories representing the categories proposed in the human factor set or to reject them aiming at two goals: On the one hand, the categorization by experts is used to evaluate the proposed set of human factors. On the other hand, the questionnaire can be shortened based on the feedback if the experts agree on the rejection or completely disagree on the categorization. For the conduction, experts could choose between an online sorting-game and an offline print version with the same instructions but different layout. In the statistical evaluation of expert data according to [191], the AC1 value (Agreement Coefficient 1) is used to assess inter-rater agreement [85]. Further, the distribution frequencies of the items to the factors are considered to examine the human factor set. The 85 items investigated here comprise the 74 non-demographic and non-freetext items of the German questionnaire developed in [57] extended by 13 new items. Those new items were designed to specifically aim at issues of body schema integration in the lower limb jointly by the author of this thesis and Dr. Oliver Christ (Institute Humans in Complex Systems, University of Applied Sciences and

Table 3.2: Additional items regarding body schema integration.

Class	Item
Ownership	Does your prosthesis seem to be a part of your body when you look at it in daily life? Did your perception of the prosthesis approach the one of the according real part of the body? Do you have the feeling that the prosthesis belongs to you? Do you have the feeling that the prosthesis is your new real leg? Do you have the feeling that the prosthesis is part of your body?
Location	Do you perceive the prosthesis in the location where you would localize the corresponding part of the body? Is the prosthesis in the location where your former real extremity was located? Do you feel the spatial position of your prosthesis without looking at it? Do you feel the structure of the ground surface through your prosthesis? Do you perceive contacts with the prosthesis as contacts with the corresponding part of the body?
Agency	Does it seem to you like you can control the prosthesis at any time? Do you have the feeling to be able to control the movements of your prosthesis? Can you relieve itching at the corresponding part of the body by scratching the prosthesis?

Arts Northwestern Switzerland). The items are inspired by the ones applied for investigation of the rubber hand illusion in [140, 139] the discussion of rubber hand illusion questionnaires in [39]. Those are adapted to lower limb prosthetics and are categorized in the three subcomponents *ownership*, *agency* and *location* as proposed in [140]. Table 3.2, shows an English version of the additionally developed items regarding body schema integration. In the expert study the German versions given in Appendix A.1 were used.

---

### 3.1.3 Transfer methodology

---

As a product development method, quality function deployment (QFD) has the goal to identify and explore the relations of customer-based product requirements and engineering-based design parameters [189, 109]. A multifunctional team assesses the importance of the engineering characteristics of the product leading to a prioritization [25]. This makes it a promising tool for human-machine-centered design in prosthetics as a multidisciplinary issue. QFD is further described as a method of quality engineering, since customer demands are rated to be the primary objective of quality engineering and hence development [138, 25, 63]. Additionally, it can help to methodically complete product requirements [63] and translate customer demands, which are partially available in a vague description only, into describable, quantifiable and thus realizable requirements [63] or product characteristics [63]. Therefore, QFD interprets customer demands as the guiding principle of product innovation and planning [63]. By running through a sequence of four QFD-processes, planning of the overall product, its parts or development, processing and operation can be investigated sequentially [189, 25, 163]. Yet, it shows weaknesses in the planning of highly innovative products, as unknown customer demands might not be identified and the early fixation of product characteristics limits novel concepts [196, 63].

Anyhow, QFD is used in various industries [189, 32], is established in the German-speaking countries [63], has been applied successfully in the development of products, services as well as software [189] and can be used for rehabilitation engineering issues [109, 138]. In [109], seven steps of QFD are applied for the example of a myoelectric prosthetic hand. The approach proposed in this thesis is inspired by this work but differs in specific steps and does not make use of all of them. A major difference is that the user of the lower limb prosthesis is considered as the customer instead of service technicians and therapists. By this, QFD is used as a method for the consideration of human factors in human-machine-centered design and to examine interrelations of user requirements and engineering design parameters. Based on this, a weighted development focus for technical design with

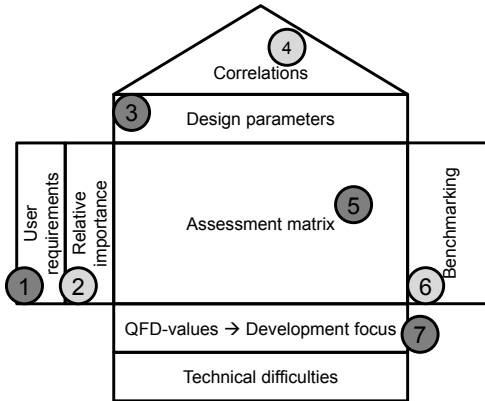


Figure 3.5: Principle template of quality function deployment based on [109].

regard to enabling and predisposing factors is deduced. This focus is considered as a prioritization of technical aspects in systems engineering.

The process of QFD is represented by the template or *house of quality* given in Figure 3.5. In the first step, the functional requirements [109] or customer demands [63] to be compared to the design parameters are listed. The relative importance of the customer requirements or demands is rated in the second step. Third, the engineering perspective is integrated to the template in terms of the design parameters. The roof of the house of quality can be used to identify interrelations of the design parameters in the fourth step. Fifth, the interrelations of user requirements and design parameters are assessed in the assessment matrix. This represents the main component of QFD and is generated by consensus of the design team using a specific scaling to assess interrelations. The sixth step can be used for benchmarking purposes by comparison to competing products on the market or previous versions of the existing one. In the final seventh step, the QFD-matrix is evaluated according to [109, 63] giving the following insights:

- The column totals (referred to as QFD-values) show the importance of the design parameters considering the user perspective. They further indicate the difficulty of improving those.
- The interrelations in the assessment matrix can be used to explore the conjunctions of specific pairs of functional requirements and design parameters.

Based on this assessment of engineering parameters and effort, the human-machine-centered development focus for the subsequent (system) design process

is defined. To consider the user perspective, the proposed approach considers the human factors as customer demands, while the design parameters are represented by the technical factors. The analysis of their interrelations in QFD is considered by prioritizing the corresponding technical requirements in systems engineering. According to [63], using QFD leads to:

- An improved determination of a list of requirements considering customer demands.
- The identification of crucial product/system functions regarding the user.
- The definition of critical technical requirements and identification of critical components.

In this thesis, QFD is applied to the example of product planning for a powered prosthetic knee. Thus, only one QFD-process is passed and later phases of the product life cycle are not considered in the example, although they can be met by the method. The colors of the steps in Figure 3.5 indicate, which steps are conducted (dark grey) and which are not covered (light grey). For the preparation of the QFD, indications for the user requirements are extracted from survey data and human factor identification as mentioned above in the first step of QFD. To model and cluster those, the determined set of human factors is used. An appropriate assessment of their relative importance in the second step is subject to future works in this respect, since the evaluation of more user data from an optimized questionnaire is required to confirm and rate the factors identified in the first step by a factorial analysis. Thus, equal relative importance is assumed here. Engineering input marking the third step is realized by interpreting the technical factors determined in the technical analysis path of the overall framework as design parameters. Steps four and six are not considered, since interrelations between the design parameters are only assessed descriptively in step four and market benchmarking is not relevant due to the research characteristics of this thesis.

The engineering team that elaborated the assessment matrix in the fifth step consists of three research associates of the faculties of mechanical engineering, computer science and sports science of *Technische Universität Darmstadt*, Germany as well as two orthopedic technicians from *Sanitätshaus Klein*, Dieburg, Germany. The mean age of those experts ( $N_Q = 5$ ) is 31 years and their professional experience averages 7.2 years. Before the discussion of the assessment matrix, the QFD-process as well as the human and technical factors were explained in an introduction of 0.5 hours. The main discussion took 4.5 hours distributed over two meetings. In contrast to [109], where a linear scale rating interrelation as *moderately negative / none / weak / strong* encoded as  $-1/0/1/2$  is used, the experts were asked to use a

---

0/1/3/9 scale encoding *none / weak / medium / strong* here. Such scales are used in early works on QFD from Japan like [2] and are referred to as logarithmic ones in [7]. They further have been adopted in most subsequent studies according to [7] and can thus be found in [7, 219, 138, 198, 25]. To assess the impact of such different scales, the results for a linear 0/1/2/3 scale are simulated by transcoding and compared to the real results. As the experts were asked to use the 0/1/3/9 scale, results from this calculation are not valid for design applications but can indicate the impact of different scales and thus the sensitivity of the method. For both QFD-matrices, QFD-values and a corresponding ranking of the design parameters are calculated and interpreted. Beyond this, the row sums of the QFD-matrix are evaluated as well to investigate the overall impact of specific human factors. This is not common in product development but is used to support the exploration of human factors in this thesis.

In human-machine-centered design, the technical factor ranking obtained from the QFD-method replaces a purely technically motivated assessment. As the ranking that results from pair-wise comparison of the technical factors represents such kind of an assessment, it is used for comparison to reveal differences between a purely technical focus and human-machine-centered design. Therefore, the differences of both rankings are calculated and it is assumed that a difference with an absolute value of 3 or more indicates a change regarding the rank of the specific technical factor. This approach represents a descriptive one that explores potentials for an alteration of engineering decision by the human-machine-centered design approach, since no inference statistic evaluation is performed. As the comparison is performed based on the rankings encoded by numbers, they do not depend on the method and can be compared. Yet, the determination of the ranking differs in both methods and thus the result might be influenced (or confounded) by the methods. Anyhow, they should be suitable for a first examination, since they are widely adopted in engineering design.

---

### 3.1.4 Systems engineering

---

To achieve system integration in terms of functional and geometric integration in mechatronic design, V model design methodology is offering a generic, widely adopted and frequently applied procedure of systems engineering. According to [189], keys to successful systems engineering are:

- Comprehensive definition of requirements at all levels.
- Not to attempt higher levels of integration until development is complete at lower levels.

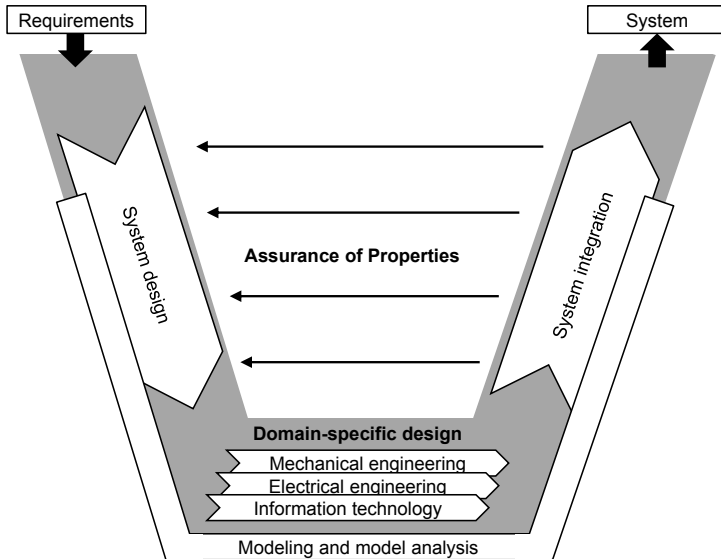


Figure 3.6: V model as a macro cycle according to [231].

Those are met by V model design, as requirements and a basic concept are elaborated on system level before components are designed and finally integrated to the global system. Further, design results are corrected iteratively during development based on short feedback loops [163].

Figure 3.6 shows the V model as a macro cycle according to [231]. Starting point of development is the definition of system level requirements that are used as quality criteria for system assessment during and after design. From those requirements, a basic system concept describing the fundamental functionality of the system is defined. For detailed design, the system is divided into subfunctions and appropriate solutions for those are determined by cross-domain design on a global system level. Based on this, a domain-specific design on component level is performed by experts in a more detailed way to ensure the performance of the function itself. The subfunctions are joined in system integration: Distributed components such as actors or sensors are connected via signal and energy flows. Further, the defined modules are coupled via unified interfaces and components are spatially integrated to form complex functional units.

By continually investigating the components as well as the overall system regarding functionality and performance, the required properties defined in system design are assured. If crucial requirements are not fulfilled, the process feeds back

---

---

to system design, for a redefinition of system or component requirements. Throughout the development procedure from system design to system integration, modeling and model analysis, e. g., by simulation, is used to examine and assess component and system functionality.

According to [231], the final system or product is usually not the result of one macro cycle, but of running through several of those in an interlaced way. The system to be designed reaches different degrees of maturity between laboratory specimen and final product during this. For an effective design, process modules for recurrent working steps can be defined [231]. Beyond computer-aided simulation, the verification and validation of realized individual components can be performed using hardware-in-the-loop setups. In those, the real environment of the specific subsystem is simulated to test it before the overall system is finalized.

---

## 3.2 Results

---

This section describes the results regarding the human-machine-centered design approach. The technical factors determined by clustering design criteria from literature and generalizing those are presented. With this, the technically motivated ranking of these factors is determined based on pair-wise comparison. Subsequently, the determination and modeling of human factors from literature, user data and expert knowledge as well as their analysis are described. The factors resulting from both paths are implemented in the QFD-matrix and the interrelations of technical factors and human factors are assessed by an expert team. This leads to a human-machine-centered design focus that prioritizes technical requirements, which is compared to the technically motivated ranking. Finally, the application of V model design methodology for human-machine-centered prosthetic design with regard to system integration is explained. In this, concepts for the integration of simulation and hardware-in-the-loop tests are described and extended by human-in-the-loop approaches. Further, indications for the mapping of human factors to the V model and the influences of technical factors are discussed.

---

### 3.2.1 Technical factors

---

The results of the collection of technical solutions, criteria and further information are presented as a structured list in Appendix A.1. A condensed version of this list that only shows the first two levels of list items is presented in Figure 3.7. The top-level categories of the hierarchy are based on the most frequent aspects in the papers and have been balanced by means of rearrangement.

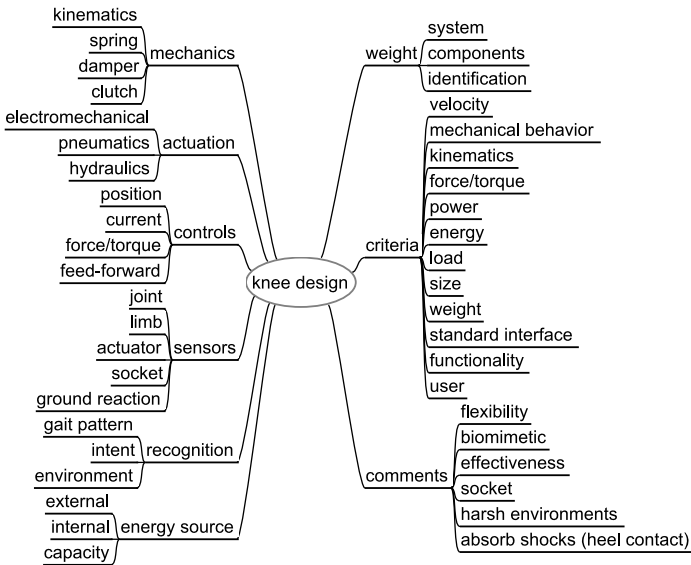


Figure 3.7: Structured list of technical solutions, criteria and further information.

The top-level categories in this scheme are: Mechanics, actuation, controls, sensors, aspects of recognition, energy source and weight as well as a variety of criteria and additional comments. These categories mainly describe hardware components, software components, and system properties, which are reviewed in Section 2.3. Definitions of the corresponding technical factors specified using the structured list are presented in Table 3.3 and explained in the following. The technical factors are defined out of the determined top-level categories and their lower level components. Factors representing hardware components comprise *Mechanics / kinematics* (MEC), *Actuation / drive train* (ACT) and *Sensors* (SEN). In this, kinematics are interpreted as a subgroup of *Mechanics / kinematics*, while gears are seen as a part of the drive train and thus as a subgroup of *Actuation / drive train*. The software components are gathered in two groups labeled *Gait planning / state recognition* (GPR) and *Controls* (CON). The differentiation between them is based on the fact that algorithms recognizing gait, user-intent or environmental conditions are mostly used for higher-level and strategic aspects of control like switching trajectories or lower level controllers like in [130, 128]. The lower level controllers that directly command the drives are represented by *Controls*.

Table 3.3: Description of technical factors.

Factor	Description
Mechanics / kinematics	This factor comprises the mechanical components of the prosthesis. Beyond structural, supporting parts as tubes or adaptors, this mainly includes kinematics like cranks or polycentric linkages and the resulting motion possibilities. Further mechanical aspects are the adjustment to the size of specific users and mechanical elements like couplings, springs or dampers.
Actuation / drive train	This category covers all actuation components that contribute to the support of the user. This includes all types of electromechanical, pneumatic or hydraulic drives. Further, gears like ball-screws or belt drives as well as elastic energy storages are part of it.
Sensors	Sensors are all measuring elements that serve the observation of the prosthesis, its environment and the user. This comprises devices for measuring positions, velocities, accelerations and forces/torques of the joints and/or links as well as such at the socket or for detecting ground contact.
Gait planning / state recognition	This means algorithms that detect the current state of gait, user intention or environmental situation and are using this information to plan gait strategically. Thus, these algorithms represent a higher planning level of software and the user-interface for controlling the prosthesis simultaneously.
Controls	Controls describe the software component that controls the actuators based on measured data and gait planning/state recognition. Therefore, commands to achieve specific objective criteria (motion, force trajectory, etc.) are calculated, sent to the drives and, if necessary, data measured by the sensors is compared with those objective criteria to adjust the commands in the case of deviations.
Weight	Weight describes the mass of the prosthetic component (i. e., the knee in this case) in kilograms for example, which should be inspired by the human leg.
Size / volume	Size / volume is the volume taken up by the prosthetic component (i. e., the knee in this case) in cubic meters for example, which should be inspired by the human leg.
Operating time	Operating time of the prosthesis describes the possible useful life without recharging the energy source. It is hence influenced by the activity of the user, the efficiency of actuation and the capacity of the energy source. It can be specified as a time of operation or a walking distance in steps, for example.
Functionality	(Biomechanical) functionality of a prosthesis includes the types of motion like walking (e. g., on even ground, inclines or stairs), running, standing, jumping or transitional movements (e. g., standing up from sitting) that are possible with the system. Additionally, it includes the adaption of the prosthesis to varying situations such as changing gait velocity or ground surface.

System properties are selected as the third category, since many items of the structured list in Figure 3.7 correspond or can be traced to such. *Weight* (WEI) and *Size / volume* (SIZ) are among those and not directly considered in the hardware components, although they are important to the users. Those require decreased metabolic energy, which can be achieved better by a lightweight prosthesis, and want the prosthesis to suit a human-like envelope for example. Additionally, *Operating time* (OPT) is chosen as a technical factor among system properties, since several components impact on it and it is connected to criteria assessing energy issues like efficiency. The energy source itself is considered to be a relevant hardware component that is not treated separately but integrated in this factor. Another group including various aspects is *Functionality* (FUN). It is hence chosen as a technical factor and comprises possible motions and the adaptation of motions or to the environment. There also occurs a large group of user-related requirements, e. g., restoring motion capabilities or decreasing asymmetric kinematics. In contrast to the human factors investigated in the following, those are not considering psychological issues. They mainly represent issues of biomechanical functionality, which are considered as aspects of the other technical factors in this thesis.

The results obtained from  $N_P = 6$  engineering experts in pair-wise comparison of the technical factors are given in Table 3.4. In the upper part, it shows the individual ratings evaluated from the comparison matrices of the individual experts. Those matrices implemented a pair-wise comparison of the nine technical factors according to the example in Figure 3.3. Based on the averages of the individual ratings, an overall ranking is determined in descending order starting from the highest overall rating. In this, *Weight* is distinctly assessed to be the most important factor. *Functionality*, *Controls*, *Gait planning / state recognition*, *Sensors* and *Size / volume* follow with decreasing rating. The lowest ranks are achieved

Table 3.4: Data from pair-wise comparison by  $N_P = 6$  experts: Individual sums of higher importance rating of specific factors.

	Expert	MEC	ACT	SEN	GPR	CON	WEI	SIZ	OPT	FUN
Individual sums	1	3	1	3	0	4	8	7	4	6
	2	3	2	6	3	7	4	2	0	8
	3	6	5	1	4	3	8	7	2	0
	4	4	5	7	7	6	2	0	2	3
	5	5	3	0	4	2	4	5	5	8
	6	0	5	8	7	5	5	2	1	3
Sum average		3.50	3.50	4.17	4.17	4.50	5,17	3.83	2.33	4.67
Overall rank		7	7	4	4	3	1	6	9	2

by *Mechanics / kinematics*, *Actuation / drive train* and *Operating time*, which is distinctly rated lowest by the experts despite they were asked to consider a powered knee device. Although those results are not statistically validated and thus might differ considering other experts, they are utilized for a first, explorative comparison with the results of the human-machine-centered approach aiming at discovering its potentials.

---

### 3.2.2 Human factors

---

Subsequently, the results of human factor determination, analysis, and modeling are presented. Therefore, the factors are explained and integrated in a set of human factors to be used in the QFD-process.

**Satisfaction (SAT)** is a major issue of prosthetic acceptance and can be interpreted as kind of an overall assessment of the prosthesis by the user. Influences on this factor are found in the characteristics, functionality, and appearance as well as the usability features of the prosthetic device based on the evaluation of the custom-built questionnaire in [38]. A factorial analysis of the TAPES questionnaire revealed three satisfaction subscales that are functional satisfaction, aesthetic satisfaction and weight satisfaction [67]. Hence, results from both studies show the global characteristics of *Satisfaction*. In [38], it is further found that subjects with different types of amputation showed no significant differences in terms of *Satisfaction*. The results given in the correlation matrix from [38] are shown in Table 3.5. Those reveal inconsistent results regarding *Satisfaction*: Satisfaction with the prosthesis showed a significantly positive relationship to the experiences of problems due to a swollen stump ( $\rho = 0.39, N_{2a}$ ) and satisfaction with the transition from standing to walking was positively associated with swollen stumps ( $\rho = 0.56, N_{2a}$ ). These positive correlations are concluded to be incongruent and may be interpreted as acceptance of dissatisfaction [38]. The findings on incongruent *Satisfaction* assessment receive certain support by literature, as perceived benefits obtained by using a micro-processor controlled knee did not encourage the participants of [220] to increase their everyday activity level in the short term. Beyond this, the correlation matrix in Table 3.5 shows consistent negative correlation regarding the relation of *Satisfaction* with the transition from standing and walking to feeling uncertain with the prosthesis ( $\rho = -0.43, N_{2a}$ ). Further, *Satisfaction* with appearance is in negative and thus consistent relation with being restricted with the prosthesis in everyday life ( $\rho = -0.41, N_{2a}$ ) and feeling socially restricted ( $\rho = -0.41, N_{2a}$ ).

**Feeling of Security (FOS)** describes the security perceived by the prosthetic user and hence does not exactly match with objective security. In the PEQ, patients rated balance to be highly important to prosthetic use [132]. Many people with

amputation show a reduction in balance and an impairment of their physical capabilities [93]. This increased risks of stumbling and falling as well as the resulting fear of falling have considerable influence on the *Feeling of Security* [151]. Among 228 transtibial and 168 with transfemoral amputation, 50% of the participants had fallen in the month before the survey evaluated in [70]. Considering the correlation matrix from [38] in Table 3.5 for the analysis of the results from the custom-built questionnaire [57], several issues concerning *Feeling of Security* can be found: Problems with the prosthesis when changing speed are negatively correlated with satisfaction regarding the transition from standing to walking ( $\rho = -0.52$ ,  $N_{2a}$ ) as well as feeling certain and stable when compensating a loss of balance ( $\rho = -0.42$ ,  $N_{2a}$ ). Additionally, uncertainty with the prosthesis as a mechanical aid is negatively correlated to satisfaction with the transition from standing to walking ( $\rho = -0.43$ ,  $N_{2a}$ ). Those correlations represent consistent results and show a distinct connection between predisposing factors and enabling ones, since providing the ability to change gait speed should be a part of prosthetic functionality.

**Body Schema Integration (BSI)** is based on the psychological concept of the body schema, which describes the representation of the characteristics of the own body in a subconscious, neurophysiological and multisensory way [68, 147]. The main changing processes after the amputation are changes in the body image as well as the body schema of the person with amputation according to [197]. Studies report about subjects perceiving a prosthesis as a part of their own body [155], as a functional extension of their body [42] or that they experience it in a proprioceptive way [156]. An obvious manifestation of *Body Schema Integration* is observed in [75], where users could relieve itching of their phantom limb by scratching the

Table 3.5: Correlation matrix of the items from [38] that are given in Table 3.1.

A	B	C	D	E	F	G	H	I	J	K	L	M
A			0.39									-0.39
B				-0.41								
C				-0.41								
D	0.39							0.56				
E		-0.41	-0.41									
F									-0.42	0.44		
G							-0.37					
H						-0.37						
I					-0.42			-0.52				-0.42
J					0.44			-0.52			-0.43	
K									-0.43			
L									-0.42			
M	-0.39											

prosthesis. Recently, such effects receive increasing attention in upper [178] and lower limb prosthetics [36]. Regarding the lower limbs, appearance is understood as a descriptor for subjective *Body Schema Integration* and hence as an important factor associated with perception and motions [36]. As prosthetic devices should replace the perception of missing body parts besides its functionality [35, 36, 38], users should perceive their bodies as being intact including them. Thus, a successful integration of the prosthesis into the body schema requires the feeling of control and sensory perception and understanding it as an integral part of the own body instead of viewing it as a foreign artifact [35]. Interpreting appearance as a descriptor for *Body Schema Integration* and taking into account the significant correlation of it with voluntary movements ( $\varrho = 0.63$ ,  $N_1$ ), the consideration as a human factor is expected to be very useful to optimize biomechanical functionality. More specific information can be drawn from the interview study presented in [91], where body integrity and proprioception in persons with amputation are part of the study focus. There, 7 of 11 subjects experienced the prosthesis like a part of their body, while 1 experienced it as an accepted external part like a shoe and 3 saw it as a foreign artifact. Regarding proprioception, the study reports that 8 subjects perceived ground surface through the prosthesis during walking, while only 2 perceived their leg or foot positions during sitting. Yet, there are negative effects connected to *Body Schema Integration*, as the user might feel other-directed by the prosthesis: In [243], highly active prosthetic users report such feelings during using a micro-processor controlled knee. One of the participants in the interview study [91] confirms this effect by assessing the same knee as “inhibiting“ (German: “hemmend“).

Due to the missing **Support (SUP)** through the muscles lost by amputation, the metabolic effort of walking increases with height of amputation [239]. Hence, people with transfemoral amputation are assessed to be less efficient ambulators than such without [93]. The literature survey in [93] shows that statistically significant increases as well as not significant increases of energy efficiency are reported for the C-Leg from Otto Bock, Duderstadt, Germany. Anyhow, it is concluded that there is sufficient evidence to suggest increased efficacy of the C-Leg in energy efficiency compared with other prosthetic knees for transfemoral amputees. In [167], 3 different prosthetic knee devices are tested with only 1 subject: The subject is observed to walk the farthest and fastest, with an overall lower rate of oxygen consumption and oxygen cost in comparison to the other knee devices when wearing the C-Leg. Hence, the study as well concludes that walking with the C-Leg is the most efficient method of ambulation for the investigated subject. Newer studies with advanced prosthetic devices from academic research also investigate energetic cost: Examinations in [45] indicate that reduced ankle push-off contributes to an increased

metabolic energy expenditure accompanying ankle impairments. Compared to an ankle joint designed to store and shift energy during the gait cycle, this is used to demonstrate that energy recycling can be used to reduce such cost [45]. Investigating a powered ankle-foot prosthesis, an average decrease by 14% compared to the conventional passive-elastic prostheses is found in the metabolic cost of transport of the subject by evaluating oxygen consumption [6]. The item “Prosthesis does not require a lot of energy for use” in the utility category of the PEQ aims at the required energy expenditure to ambulate [132]. It shows the connection of reduced energy expenditure and facilitation motor functionality. This is substantiated by gait analysis results with elderly participants on inclines in [235]. Those show that subjects with amputation have reduced speed, knee and hip range of motion and hip torques along with increased muscle activity compared to healthy people.

The **Socket (SOC)** is one of the major technical [252], medical [8] and psychological [132] issues in lower limb prosthetics. It thus is appropriately considered as “Theme One: The Fit of the Socket with the Residual Limb” in a study using the PEQ [132], as the topic most often mentioned by the subjects was the fit of their residual limb with the socket independently of them being complimentary or critical. It is further found there that the fit of the prosthesis is highly important to most participants, as those rated the fit of the prosthesis being the most important issue (with a mean score of 98.1). The avoidance of blisters or sores on the residual limb is rated third (mean score 96.7) and avoidance of rashes on the residual limb fourth (mean score 95.2). These results are extended by the custom-built questionnaire evaluation in [36] indicating a lack of satisfaction with the prosthesis shaft irrespective of the prosthesis technology. The satisfaction correlations given in Table 3.6 are based on unpublished data from [36]. There, satisfaction with the socket shows significant correlations to walking ( $\rho = 0.82, N_1$ ) and standing ( $\rho = 0.70, N_1$ ) and thus reflects the connection to prosthetic functionality. This is substantiated by a positive correlation between problems due to a swollen stump and the satisfaction with gait transitions ( $\rho = 0.56, N_{2a}$ ) as shown in Table 3.5. Although improved biomechanical understanding advanced the science of socket fitting, most insights in experienced residual limb stresses have not led to enough

Table 3.6: Satisfaction correlations of data from [36].

	Socket	Appearance	Walking	Standing
Socket	1	0.61	0.82	0.70
Appearance	0.61	1	0.63	0.59
Walking	0.82	0.63	1	0.64
Standing	0.70	0.59	0.64	1

---

clinical consensus to fundamentally alter clinical practice according to [142]. Statements in the interview study [91] emphasize the efforts made by the users to get a good socket: 6 participants stated to travel several hundreds of kilometers to have their socket being produced by a particular orthopedic technician, while one participant was even producing his own sockets for about 10 years.

Two scales of **Mobility (MOB)** are considered in the PEQ [132]: Ambulation and transfers. Their evaluation in [132] shows that patients rated the ability to walk with the prosthesis being the second most important of the investigated issues in prosthetic use. Other items rated at high importance included the ability to walk on sidewalks and the ability to walk up and down stairs. Among the subscales of TAPES identified by factor analysis in [67], the activity restriction subscales functional restriction and athletic activity restriction as well as the satisfaction subscale functional satisfaction deal with the *Mobility* of the subject. With the Amputee Mobility Predictor (AMP) investigated in [66], a validated clinical tool specifically designed to assess ambulation and functional potential of subjects with lower limb amputations exists. The evaluated criteria consider transfers, sitting and standing balance as well as various gait skills. Anyhow, various other methods for measuring mobility with different scales and questionnaires are available [177]. According to [89], the physical change due to amputation of the lower limb is often associated with functional limitations like impaired ability to transfer or ambulate. Additionally, results of [36] indicate a lack of satisfaction in voluntary ( $\rho = 0.82, N_1$ ) and postural ( $\rho = 0.70, N_1$ ) motor functioning independent of the used prosthetic devices (compare correlations in Table 3.6). Particular interview participants of [91] stated that a natural gait pattern and the adaptation of the prosthesis to different gait speeds is important. Similar effects can be observed in Table 3.5: Feeling uncomfortable, when changing gait speed is not possible, is negatively correlated to the question if more technical aid would be helpful ( $\rho = -0.37, N_{2a}$ ). Further, satisfaction with transition from standing to walking is correlated to the sense of having a natural gait pattern ( $\rho = 0.44, N_{2a}$ ), while problems in changing speed are negatively correlated to this sense ( $\rho = -0.42, N_{2a}$ ).

**Outer Appearance (APP)** is represented by two of the four function scales determined with the PEQ in [132], which are appearance and sounds. Thus, the study considers it in “Theme Three: Other Qualities of the Prosthesis”. The importance of *Outer Appearance* is confirmed in [67], as the factor analysis of the TAPES questionnaire reveals three satisfaction subscales including aesthetic satisfaction. Correlations can further be observed between appearance and functionality during voluntary ( $\rho = 0.63, N_1$ ) and postural movements ( $\rho = 0.59, N_1$ ). The correlation matrix in Table 3.5 shows that the ratings of satisfaction with appearance in public are significantly negative correlated with feelings of social restriction ( $\rho = -0.41$ ,

$N_{2a}$ ) and restriction in everyday life ( $\rho = -0.41$ ,  $N_{2a}$ ). In the interview study [91] the majority of female subjects (4 of 5) attached importance to cosmetic covers imitating leg appearance, while most male participants (4 of 6) rated this to be not important. Among the male ones, 3 subjects stated that they use a cosmetic cover but require it to not limit functionality.

Table 3.7: Human factor set and factor descriptions.

Factor	Description
Satisfaction	Satisfaction with the prostheses is a central factor for the use of it. It can be interpreted as some kind of overall assessment by the user of the prosthesis and is influenced by: Features, functionality, appearance and usability characteristics of the prosthesis.
Feeling of Security	In contrast to objective security, feeling of security describes the experience of security by the user of the prosthesis. Besides reduced balance, many of those also show limited physical functionality themselves. The increased frequency of stumbling and falling and the resulting fear of falling have significant influence on the subjective experience of security.
Body Schema Integration	Prostheses are meant to substitute the functionality of the lost part of the body as well as having the users experience it as a part of their own bodies. Users should feel like “complete humans” and experience the prosthesis not as a body foreign object, but rather as a part of their bodies. A successful integration to the body schema implies that the user develops a feeling for the control and the sensory perception of the prosthesis.
Support	Support of the user could induce a reduction of his energy expenditure or facilitate certain motor situations.
Socket	The socket is the interface between user and prosthesis. A major share of everyday problems and limitation of people using prostheses can be traced to a socket that is fitted inappropriately. It thus has strong impact on the acceptance und hence on the use and function of the prosthesis.
Mobility	A central objective of prosthetic development is the extension of the mobility of the user. This comprises the possible types and situations of movement like locomotion, stance or situations of transition (e. g., standing up) intended by the user.
Outer Appearance	Outer appearance as a technical aspect of the prosthesis includes aspects like appearance and acoustics. Those characteristics of the prostheses have influence on the personal and social acceptance by the prosthetic user and his environment.

Based on the presented aspects, a set of seven human factors is proposed for the consideration in human-machine-centered design and presented in Table 3.7. It comprises *Satisfaction*, *Feeling of Security*, *Body Schema Integration*, *Support*, *Socket*, *Mobility* and *Outer Appearance*. Those all include psychological issues like the assessment and experience of the prosthesis in terms of predisposing factors. Yet, they further aim at the exploration of technical development potentials in powered lower limb prosthetics. *Satisfaction* might be used for an overall assessment of technical solutions, while *Feeling of Security* gives detailed information on aspects concerning perceived security. *Body Schema Integration* considers the key aspect of aiming at a fully integrated replacement, since it might reveal potentials for new interfaces and control approaches. *Support* and *Mobility* are assumed to provide essential information on the benefits expected from powered lower limb prostheses, while the *Socket* as the mechanical interface between human and prosthesis represents a major and general issue. *Outer Appearance* is an important factor to the user population and appearance seems to be a descriptor for subjective body schema integration according to [36].

The statistical analysis of the expert study examines the assignments of the items from the custom-built questionnaire to the categories representing the human factors through the participants [191]. By evaluating this, it is investigated whether those confirm the determined human factors by assigning the items to the corresponding category. Based on the resulting inter-rater agreement, the statistical validation of the human factor set can be discussed. The AC1 assessing the rating agreement in the expert study is calculated in [191] according to [85]. It has a value of 0.39 and thus shows fair agreement of the experts on the benchmark scale from [126], where moderate agreement would start from a value of 0.41. Discussions in [191] state that this comparably low result seems to be due to the exploratory state of questionnaire development and should not have been caused by an inappropriate choice or professional experience of the participating experts.

Table 3.8 shows the results of the expert study. The number of items (#) assigned to the particular categories shows how the seven human factors are covered by the questionnaire items and extension regarding body schema issues. More than 10 items are assigned to all factors except *Support* with 9 and *Outer Appearance* with 4 items. Further, the frequency distribution gives information about the diversity of the factors and how often those are rejected (REJ, mostright column). Taking into account the fair expert agreement by considering distributions over 15% as threshold for a interrelation of factors, only *Body Schema Integration* with a maximum frequency of 10.14% does not show issues regarding interference with other factors. From the 13 new items presented in Table 3.2, 10 were assigned to *Body Schema Integration*. The ones on feeling ground structure and controlling

the prosthesis were categorized to belong to *Feeling of Security*. *Feeling of Security* further shows slight relations to *Body Schema Integration* with 15.60% as well as *Support* with 16.06% and *Mobility* with 16.42%. *Socket* and *Outer Appearance* share ratings with *Satisfaction* in 18.43% and 16.09% respectively. Items assigned to *Satisfaction* itself show high frequencies in other categories peaking at 30.01% regarding *Mobility*. As *Satisfaction* is understood as some kind of overall assessment of the prosthesis, these results are in line with the concept of the human factor set. In the case of *Mobility*, the category frequencies are higher: 20.82% are observed regarding *Feeling of Security*, 19.03% considering *Support* and 16.09% to *Satisfaction*. *Support* is the most critical factor, as it shows the highest rejection ratio of 29.59% and distinct interrelations to *Satisfaction* (22.55%), *Feeling of Security* (22.22%) and *Mobility* on the one hand. On the other hand, the interrelation to *Mobility* shows the peak category frequency of 48.83% indicating uncertainties in the separation of those two factors by the experts. Besides lowest rejection rates, also the least diverse ratings are found in *Outer Appearance*, *Socket* and *Body Schema Integration*. Regarding *Outer Appearance*, the very distinct results might be due to the lower number of items assigned to this category. Hints towards the further development of the questionnaire can be drawn from the specific AC1 scores of the items and their frequency distribution as given in [191] considering only 20 subjects.

Reviewing the factor distribution in the expert study, interrelations described in the literature and observed in the other studies, allows for comparing and assessing the connections of the modeled human factors: The interdependence of *Support*, *Socket*, *Mobility* and *Outer Appearance* with *Satisfaction* observed in the results of the expert study coincides with its interpretation as an overall assessment of the prosthesis comprising functional as well as aesthetic aspects. *Feeling of Security*

Table 3.8: Frequency distribution for category assignments from [191].

Assigned categ.	#	Category frequency							
		SAT	FOS	BSI	SUP	SOC	MOB	APP	REJ
SAT	14	-	9.60%	10.50%	13.78%	5.71%	30.01%	13.39%	14.91%
FOS	14	9.51%	-	15.60%	16.06%	4.90%	16.42%	1.91%	14.82%
BSI	11	10.14%	6.03%	-	0.00%	2.30%	1.28%	5.74%	9.33%
SUP	9	22.55%	22.22%	8.65%	-	4.29%	48.83%	2.98%	29.59%
SOC	15	18.43%	3.48%	2.01%	9.64%	-	5.21%	1.28%	7.81%
MOB	15	16.09%	20.82%	2.27%	19.03%	0.95%	-	2.79%	14.07%
APP	4	16.58%	6.05%	1.39%	0.00%	1.39%	0.00%	-	1.67%

shows slight relations to *Mobility*, *Support* and *Body Schema Integration* in the expert study. The highest score is observed regarding *Mobility*, which is confirmed by the correlation between *Feeling of Security* and the satisfaction with biomechanical functionality representing *Mobility* as shown in Table 3.5. The factor *Body Schema Integration* does not show distinct interdependencies in the expert study as well. Anyhow, it seems to be linked to biomechanical functionality and thus *Mobility* as well as *Outer Appearance* according to the literature: In [38], it is stated that it is important to prevent the consolidation of residual limb pain in the residual limb due to repetitive noxious stimulation that may cause swelling, as it may interfere with the integration of the prosthesis in the body schema [147]. The interviews in [91] show that participants further connected perception of body integrity to good motion feedback (55%) and recovering *Mobility* (2 of 11). *Support* shows interrelation with *Satisfaction*, *Feeling of Security* and *Mobility* in the expert study. Among those, the relation to *Mobility* shows the highest distribution frequency. In the derivation and description of the human factor set, such relationships are not considered, as *Support* is mainly motivated as a human factor based on literature on the energy expenditure. Yet, the observed results seem to reflect the users situation, since higher *Mobility* and thus also increased *Satisfaction* and a stronger *Feeling of Security* can be caused by lower energetic effort through *Support*. The fact that the *Socket* only interferes with *Satisfaction* in the expert study might be due to the influence of its manifold issues on overall prosthetic assessment that documented in the literature. Beyond the results reported so far, it is shown in [36] that satisfaction with the prosthesis *Socket* is significantly correlated with the satisfaction in voluntary ( $\varrho = 0.82$ ) and postural ( $\varrho = 0.70$ ) movements. In [91], the participants connected the perception of *Body Schema Integration* with the fitting of the *Socket*. *Mobility* shows relationships to *Satisfaction*, *Feeling of Security* and *Support* in the expert study. The correlation with *Satisfaction* is confirmed in the factor analysis of TAPES in [67] and the investigations in [38]. Regarding items assigned to *Outer Appearance* the lowest frequencies in other categories are observed in the expert study. Anyhow, the results of [36] show significant correlation to satisfaction with the *Socket* ( $\varrho = 0.61$ ) as well as voluntary ( $\varrho = 0.63$ ) and postural ( $\varrho = 0.59$ ) movements. The latter ones describe biomechanical functionality and thus represent a subset of *Mobility*. This connection can also be observed in the correlation matrix in Table 3.5 based on the results from [38]. In the expert study *Outer Appearance* only shows relevant relationship to *Satisfaction*, which complies with the aspect of aesthetic satisfaction considered in TAPES [67].

### 3.2.3 Transfer methodology

The results of the exemplary application of quality function deployment (QFD) for the design of a powered prosthetic knee show interrelations of user requirements and design parameters leading to a human-machine-centered development focus. By using this focus instead of the results of pair-wise comparison of the technical factors for further development, the technical requirements are filtered considering user issues and a human-machine-centered design is achieved. As the expert study indicates the basic applicability of the human factor set, it is used to represent the user requirements. Due to the exploratory state of the questionnaire and the consequent studies and evaluations, the human factors are rated at equal relative importance of  $1/7 \approx 0.143$  assuming an uninformative prior distribution. A sophisticated assessment of the relative importance together with an improved human factor set, could later be derived based on extensive user data from the optimized version of the custom-built questionnaire. The design parameters are represented by the technical factors resulting from literature analysis in Section 3.2.1.

The outcome of the expert discussion and consensus using the 0/1/3/9 scale are shown in Table 3.9. During the discussion, the experts agreed to assess the interrelations based on state-of-the-art technology, which was defined by them to be the PowerKnee from Össur, Reykjavík, Iceland. Further, they considered other commercial prostheses like the C-Leg and Genium from Otto Bock, Duderstadt, Germany and the RheoKnee from Össur, Reykjavík, Iceland for comparison and agreed to interpret the interrelations as a basis for future design solutions. Considering the column sums in Table 3.9, it becomes distinct that *Gait planning /*

Table 3.9: Results of quality function deployment with 0/1/3/9 rating scale.

	User requirements	Design parameters									
		MEC	ACT	SEN	GPR	CON	WEI	SIZ	OPT	FUN	
SAT	0.143	1	3	1	9	1	3	1	3	9	3.44
FOS	0.143	9	3	1	9	3	1	0	3	3	3.56
BSI	0.143	3	9	1	9	9	3	3	1	3	4.56
SUP	0.143	9	9	3	9	3	3	1	3	9	5.44
SOC	0.143	1	3	1	1	1	3	1	0	3	1.56
MOB	0.143	3	9	3	9	1	3	1	9	9	5.22
OUT	0.143	3	9	0	1	0	0	3	3	3	2.44
<b>QFD-value</b>		4.14	6.43	1.43	6.71	2.57	2.29	1.43	3.14	5.57	
<b>Rank</b>		4	2	8	1	6	7	8	5	3	

*state recognition*, *Actuation / drive train* and *Functionality* are the most crucial design parameters according to the experts and should thus be in the design focus. *Mechanics / kinematics* and *Operating time* receive relatively high ratings followed by *Controls* and *Weight*, while the lowest results are obtained for *Sensors* and *Size / volume*.

Although the row sums of the QFD-matrix shown in the rightmost column of Table 3.9 are commonly not evaluated, three interesting aspects concerning the human factors can be observed when looking at those. The human factors *Support* and *Mobility* receive the highest row sums, although they are not separated well in the expert study for questionnaire optimization and factor modeling. Hence, those seem to be important and hard to distinguish at the same time. *Body schema integration*, which shows to be a clear concept in the expert study, is ranked third in row sums of the QFD-matrix emphasizing its importance in human-machine-centered design. The lowest row sum is achieved by the *Socket*, which might be caused by the task to consider a prosthetic knee but could also be due to the increased importance of other components in a powered mechatronic system.

The background of those results is not given in the QFD-matrix but can be drawn from protocols of the expert discussion. According to the experts, *Gait planning / state recognition* is an important software component, as the reactions of a prosthetic system in certain situations are determined by it. Conspicuously, it receives high ratings in the human factors *Satisfaction*, *Feeling of Security* and *Body schema integration* because those are related to the human-machine interface that is (partially) represented by it. *Actuation / drive train* receives a high QFD-value, since the experts interpreted it as the part of the system that basically enables

Table 3.10: Results of quality function deployment with 0/1/2/3 rating scale.

User requirements	Design parameters										
	MEC	ACT	SEN	GPR	CON	WEI	SIZ	OPT	FUN		
	SAT	0.143	1	2	1	3	1	2	1	2	3
FOS	0.143	3	2	1	3	2	1	0	2	2	1.78
BSI	0.143	2	3	1	3	3	2	2	1	2	2.11
SUP	0.143	3	3	2	3	2	2	1	2	3	2.33
SOC	0.143	1	2	1	1	1	2	1	0	2	1.22
MOB	0.143	2	3	2	3	1	2	1	3	3	2.22
OUT	0.143	2	3	0	1	0	0	2	2	2	1.33
<b>QFD-value</b>	2.00	2.57	1.14	2.43	1.43	1.57	1.14	1.71	2.43		
<b>Rank</b>	4	1	8	2	7	6	8	5	2		

locomotion *Support* and thus increases *Mobility*, which were seen as the major aim of powered prosthetics. Similar reasons caused the high rating of *Functionality*. The distinctly low ratings of *Sensors* and *Controls* were due to the assumption that those are not perceived by the user directly and are thus just required to work properly. Regarding *Weight* and *Size/ volume*, the experts assumed that those or tradeoffs affecting them are accepted if the parameters remain at an appropriate level as in state-of-the-art systems.

The house of quality calculated by transforming the 0/1/3/9 scaling to a 0/1/2/3 scaling is presented in Table 3.10. In this, it is assumed that experts would rate identically although using a different scale. As mentioned above, the results are thus not valid for design but for analyzing scale impact and method sensitivity. Comparing the results to the ones in Table 3.9 shows that the basic ranking structure would remain. Yet, the order of top- and low-ranked parameters could change. Among the three top-rated ones, *Actuation/ drive train* would be rated first instead of *Gait planning/ state recognition*, which would be ranked equal with *Functionality*. While the parameters rated medium and very low would not change ranks, *Weight* would have a higher rating than *Controls* in this case. Due to these results, the effects of QFD-scaling should be investigated by comparing results with different scales acquired with separate expert groups instead of recalculating such. Discussions with researchers from psychology support this outcome, since experts might have different rating behavior using different scales. Hence, Table 3.10 is not used for design reasons but only for this comparison.

To discover potential impacts of the human-machine-centered design focus on engineering decisions, the results of QFD are compared to those of pair-wise comparison of the technical factors that is given in Table 3.4. The results of this comparison are presented in Table 3.11 and show distinct differences between the human-machine-centered and the technical ranking. The most obvious deviations in ranking are observed for *Actuation/ drive train* and *Weight*: *Actuation/ drive train* shows a low rating in the technically motivated ranking, while it receives the second highest assessment in the human-machine-centered one. In contrast to

Table 3.11: Comparison of technical factor rankings obtained with the purely technical and the human-machine-centered approach based on QFD with 0/1/3/9 scaling.

Approach	MEC	ACT	SEN	GPR	CON	WEI	SIZ	OPT	FUN
Purely technical	7	7	4	4	3	1	6	9	2
QFD 0/1/3/9	4	2	8	1	6	7	8	5	3
Difference	3	5	-4	3	-3	-6	-2	4	-1

---

this, *Weight* distinctly loses importance in the human-machine-centered ranking. Less distinct but relevant differences are seen in *Sensors, Mechanics/ kinematics, Gait planning/ recognition, Control* and *Operating time*. *Functionality* and *Size/ volume* appear to be insensitive to the ranking approach. From an engineering perspective, it is remarkable that *Gait planning/ state recognition* and *Actuation/ kinematics*, which are the two factors rated to be most important in QFD using the 0/1/3/9 scaling, receive medium or even low ranking when assessed technically. Conversely, *Weight* and *Controls* are rated to be most important in the technical evaluation, while they are judged to be of medium to low impact in the human-machine-centered focus. Due to the distinct differences, engineering decisions might thus be made differently based on the two methods. The results indicate that especially *Gait planning/ state recognition, Actuation/ drive train* and *Operating time* receive increased weight, when considering human factors.

Anyhow, a statistical evaluation of these results based on more user and expert data is required to finally confirm these findings. Further, the impact of the methods used to determine the rankings as well as the selection of experts should be investigated. Pair-wise comparison and QFD determine rankings from human data in different ways (individual survey and expert discussion), which might have an impact on the resulting ranking. As such comparisons of methods and the incorporation of statistical evaluations are not considered for methods like pair-wise comparison as well as the QFD-method in engineering design literature like [63], both should be subject to future research.

---

### 3.2.4 Systems engineering

---

Systems engineering of powered lower limb prosthesis using V model methodology can be performed in analogy to the process described in [231], as design and integration steps are general processes and can be applied to all mechatronic systems. Yet, requirements from technical and human factors as well as the transfer step should be used as inputs of the V model to suit user requirements as proposed in the human-machine-centered design approach depicted in Figure 3.1. These comprise technical functionalities, weighted user requirements and the development focus determined with the QFD-method condensed in a human-machine-centered list of requirements. Figure 3.8 shows an exemplary implementation of the V model for a powered prosthetic knee system. Based on the results obtained using the QFD-method, *Gait planning / state recognition, Actuation / drive train* and *Functionality* are the most important components and properties and thus are to be focused on in global system and domain-specific component design.

To determine appropriate technical and user requirements, the selected technical factors and criteria, the identified human factors as well as the results of the QFD-method should be taken into account. Especially, the consideration of the derived development focus by prioritizing components and properties with high impact on human factors as *Gait planning / state recognition*, *Actuation / drive train* and *Functionality* helps to suit user requirements. Further, the impact of certain human factors on specific components or properties that are identified in the QFD-matrix are to be considered in domain-specific design. To support this, predisposing factors influenced by the enabling factors of the specific component might be investigated in specialized surveys. An important example therefore is the strong interrelation between *Gait planning/ state recognition* and the human factors *Satisfaction*, *Feeling of Security* and *Body Schema Integration*.

Additionally, results from additional tests with users can be combined with survey data from questionnaires and interviews to cope with correlations between the human factors themselves. In the case of *Support* and *Mobility*, the application of practical, biomechanical tests assessing those factors could help to separate the factors for example. This assessment can be realized using biomechanical criteria such as in the *10 Meter Walk Test* or the *Four Step Square Test* or by surveying them in specific questionnaires like the AMP [66].

The design of series elastic *Actuation / drive train* of a prosthetic knee is selected to represent component development, as such actuators promise good energy efficiency [98] along with user safety [227, 135]. Thus, they are widely adopted in lower limb prosthetics research as in [6, 71] for instance. Variable stiffness implementation

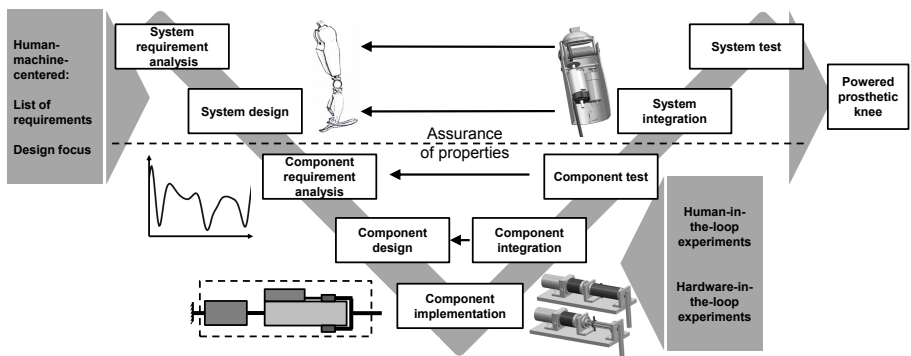


Figure 3.8: Exemplary V model application. System: Powered prosthetic knee. Component example: Series elastic actuation.

---

can further support *Functionality* in terms of adaptation to gait velocity [80, 79] or user weight [96]. Hence, this example, which is a main subject in the remainder of this thesis comprises hardware design of *Actuation / kinematics* and software design of the corresponding stiffness control aiming at improving the system property *Functionality*. Therefore, appropriate methods for design, modeling and analysis have to be selected.

Possible steps regarding variable stiffness actuation of a prosthetic knee are outlined in Figure 3.8. A more detailed description regarding a specific solution is examined and developed in Chapter 6. As shown in Figure 3.8, a basic concept of actuation is prepared as a topological model after system design. This is based on biomechanical data like required joint torques that are used to define performance requirements. Design simulations using a dynamics model of the concept are applied to determine the basic design of hardware and software, e. g., actuators and control algorithms, respectively. In this, model-based approaches support the design of hardware and software in order to exploit the natural dynamics of the actuation system and thus to decrease energetic efforts [17, 16]. A prototypical implementation of the actuation system is developed by iterations of this process and realized in the component implementation step. With this, an evaluation and optimization of the actuation system becomes possible by means of hardware-in-the-loop simulations. For continuous consideration of human factors in design, an extension by human-in-the-loop experiments is a promising approach for the evaluation of component or system concepts with users. As such experiments enable the reproduction of test scenarios and the modification of parameters, they seem to be a key technology to define specific technical requirements based on user experience. The integration of all components in system design leads to the final prosthetic system and the fulfillment of requirements and thus system functionality is continuously monitored for property assurance.

Although human factors are considered as requirements in V model development, the available user data only facilitates indications on mapping the factors to the specific steps of the V model, which might be important for their particular implementation. *Satisfaction* and *Body Schema Integration* seem to have impact on component and system design, as they are related to characteristics like weight, acoustics or size of the prosthesis, which finally depend on the single components. In contrast to this, *Feeling of Security* as the “experience of security by the user“ seems to be a more global issue, since it is directly associated with effects like the fear of falling [93] and balance confidence [151]. Such issues cannot be tackled by a single component, as they are influenced by the functionality of the whole prosthesis and thus by the interaction of all components. Anyhow, the technical factors *Mechanics / kinematics* and *Gait planning / state recognition* receive high QFD-ratings with

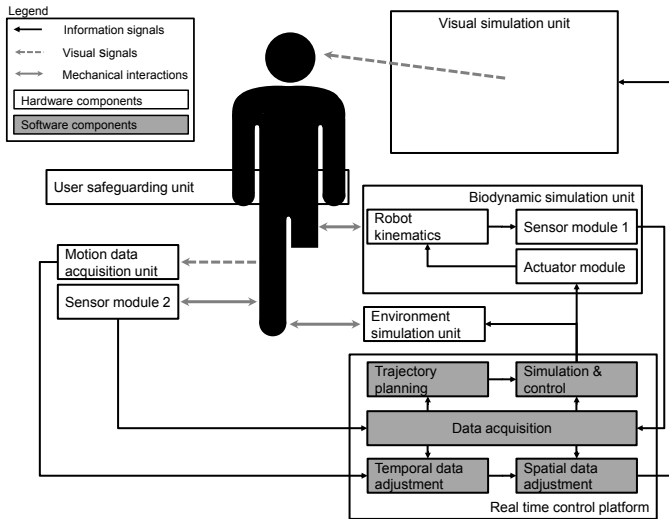


Figure 3.9: Functional concept and units of Prosthesis-User-in-the-Loop based on [12].

respect to *Feeling of Security* and are thus more relevant than other ones in the system. Further, *Outer Appearance* seems to be important in system and component design, as every single component can contribute to the acoustical and optical characteristics of the whole system. The *Socket* represents the mechanical and control interface in the human-mechatronic system and thus seems to be influenced on system level, as the global behavior of the prosthesis induces the mechanical load situation there. Since the *Socket* transfers power and information flows, it might be developed using an appropriate functional structure according to [163]. Although *Support* and *Mobility* mainly depend on the biomechanical performance of the prosthetic system, those factors can strongly be influenced by single components like motors or gears. Thus, these factors seem to be relevant on both levels.

As human-in-the-loop simulations can leverage human factor investigation and support human-machine-centered design, the Prosthesis-User-in-the-Loop simulator concept [236, 237, 41, 12], which is co-developed by the author of this thesis, is suggested to be used with the proposed framework. The main objective of this simulator is to simulate different prosthetic concepts in several gait scenarios for the user to enable comparisons of technical solutions without building those. Therefore, mechanical interactions as well as visual and auditory perception have to be included. The functional units given in Figure 3.9 simulate gait and interactions with the specific investigated prosthesis as well as a virtual environment. Envi-

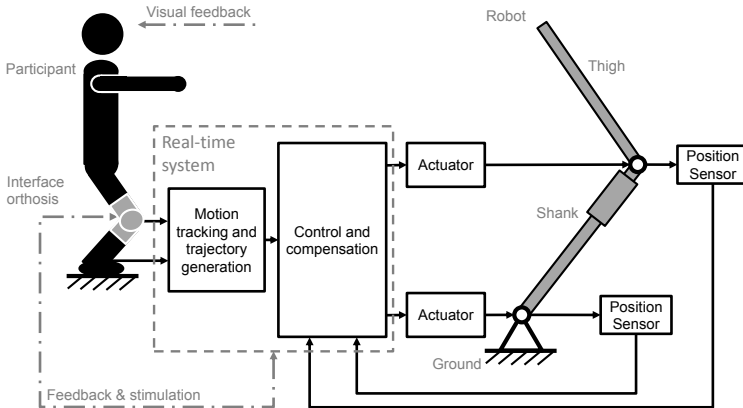


Figure 3.10: Functional concept and interfaces of the Int<sup>2</sup>Bot based on [14].

ronment is simulated to the intact leg of the subject while the residual stump is attached to an actuated and instrumented biodynamic simulation unit. This simulates the biodynamical interactions between the human subject and the investigated prosthetic concepts. Controls can be based on simulations of prosthetic gait using dynamics models of human [248] and prosthesis. A holistic illusion of walking with the simulated prosthesis is established by complementing the biomechanical simulation with a visual one [41]. Such an illusion could eventually be realized utilizing virtual or augmented reality technologies. According to [44], such setups might further support rehabilitation but also claims the need for proper validation of the results. With this specific human-in-the-loop experiment, various possibilities specify detailed technical requirements based on user experience for systems engineering emerge. Therefore, the simulator supports the isolation and individual manipulation of human and technical factors for an assessment by users [41]. For example, experiments with this simulator might help to understand why prostheses that are lighter than the real leg are perceived to be heavy as described in [44] and consider such insights in design.

A specific human-in-the-loop setup to investigate the factor *Body schema integration* and possible user-interfaces for controlling the prosthesis is the Int<sup>2</sup>Bot [11, 14] that is also co-developed by the author of this thesis. In analogy to the rubber hand illusion [39], it aims at examining the rubber leg illusion and its maintaining factors during movement using the robotic setup from [11, 14] that is shown in Figure 3.10. Such illusions describe manipulations of the body schema that induce the feeling of the ownership of an artificial limb and a measurable proprioceptive

re-calibration [24]. First experiments on transferring the rubber hand illusion to the lower limbs in terms of a rubber foot illusion during static situations show significant changes in survey data while results differ regarding the proprioceptive drift [112, 37]. To extend such investigations to postural motions, the robotic leg of the Int<sup>2</sup>Bot imitates postural motions of the subject, as postural motor functioning is correlated with appearance as an indicator of subjective body schema integration [36] ( $\rho = 0.59, N_1$ ). Therefore, movements of the participant standing close to the robot are tracked contactlessly and used for trajectory generation [40, 190]. Influences to be investigated are synchronous and asynchronous robot motion or the impact of distance between participant and robot motivated by [136] or [139], respectively. Further, an instrumented and actuated orthosis attached to the human subject extends tactile and kinesthetic feedback to examine the impacts of interfaces on multisensory integration of artificial limbs. If such feedback and interfaces can manipulate the body schema, those could be translated in engineering design requirements. Thus, the Int<sup>2</sup>Bot might support issues corresponding to the important technical factor *Gait planning / state recognition*, as this comprises the human-machine interface of the prosthesis.

### 3.2.5 Human-machine-centered design framework

Based on the obtained results, the proposed human-machine-centered design framework is completed as shown in Figure 3.11. The integration of a human-machine-centered technical design is achieved by two balanced paths that are fed by user

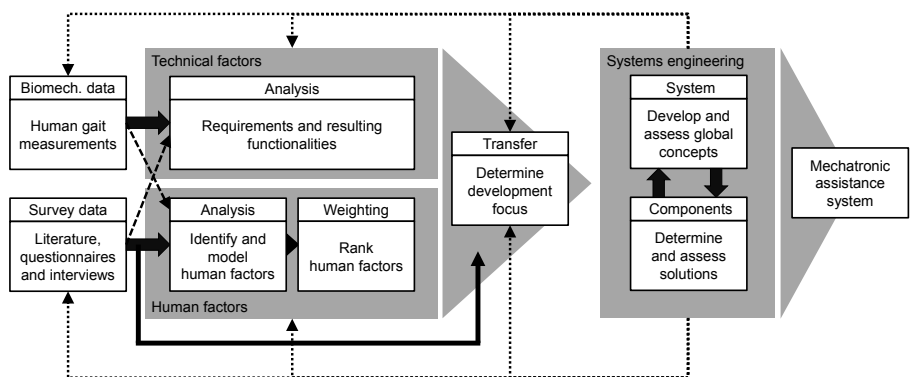


Figure 3.11: Complete framework of the human-machine-centered design approach.

---

---

data to analyze and weight technical and human factors. In the technical track, requirements and functionalities resulting from those are analyzed, while human factors are determined, modeled, and ranked in the parallel one. The dashed arrows on the left side indicate the consideration of additional data from the other domain: Utilizing measures based on biomechanical data might help to sharpen human factor modeling and assessment, while survey data can be directly used in technical design regarding aspects like outer appearance.

The transfer step joining the domains replaces purely technical assessment of the technical factors by determining a development focus using the QFD-methodology that considers the interrelation between technical factors and human factors. As these interrelations are determined within an expert discussion, additional survey data is introduced to the development process here. Based on the identified focus, the mechatronic assistance system is finally developed by systems engineering and integration of components. Those are prioritized by the design focus and tested to meet the required functionalities. Therefore, technical and user requirements are condensed to a human-machine-centered requirement list based on the results from the two analysis paths and the QFD-method.

To achieve geometrical as well as functional integration, V model design represents an approved method and is thus suggested for systems engineering. Although the concepts of systems engineering and quality function deployment are related to each other, systems engineering methods focus on the engineering point of view rather than the one of the customer [189]. Yet, by bringing V model design together with the QFD-method, a methodology combining user perspective and system integration should be reached. Therefore, results from human factor assessment and biomechanical investigations can be considered as human-machine-centered requirements in the V model by ranking the technical factors according to the results of quality function deployment. To assure the properties demanded from the system, requirements from both tracks and results from the transfer step are included as a human-machine-centered list of requirements and assessment measures within the V cycle.

During component design and integration as well as system integration the fulfillment of these requirements is checked continuously supported by hardware- and human-in-the-loop techniques like Prosthesis-User-in-the-Loop and Int<sup>2</sup>Bot. Those can also contribute to the definition of specific technical requirements in a human-oriented way, e. g., to determine weight limitations that are accepted by the user. Such issues might further be investigated based on user surveys by analyzing the correlation particular enabling and predisposing factors. If a component solution does not meet its requirements, two feedback paths allow for overcoming this. Internal feedback of the V model leads to an adaptation or redesign of the planned

---

system or components if the corresponding criteria are not met. Beyond that, the dotted arrows in Figure 3.11 indicate that it might be necessary and is possible to correct, adjust or extend the requirements and their weighting during earlier steps. Those include data acquisition, factor analysis and weighting as well as the transfer step. By feeding back to the analysis paths before transfer, the method might thereby overcome the limitation of quality function deployment in the planning of highly innovative designs.

---

### 3.3 Conclusion

---

To understand relevant human factors in powered lower limb prosthetics and assess their impact on design, seven human factors are determined and modeled. The structure of this factor set aims at revealing connections between predisposing and enabling factors and determining a human-machine-centered technical development potentials in contrast to other studies. Additionally, this research orientation is emphasized by the custom-built questionnaire as well as interview and expert studies that are designed to specifically explore such issues. The resulting human factor set comprises *Satisfaction* as an overall assessment. *Feeling of Security* represents perceived security and distinctly connects predisposing and enabling factors, while *Body Schema Integration* includes experience, control and sensory perception of the prosthesis. *Support* describes a crucial but not completely discovered aspect of powered prostheses that is related to *Mobility*, which comprises ambulation and transfer abilities. The *Socket* represents a major and manifold issue of lower limb prosthetics in general and *Outer Appearance* is correlated to functional aspects of motion and to (social) restriction. The model is basically confirmed by an expert study showing that *Body Schema Integration*, *Socket* and *Outer Appearance* are approved. Anyhow, overlapping of specific factors can be observed, e. g., regarding *Support* and *Mobility* that both concern major potentials of powered prostheses.

As a basis for considering those human factors in design, technical factors are collected, clustered and investigated regarding interrelations for the example of a powered prosthetic knee. Those factors comprise the hardware components *Mechanics / kinematics*, *Actuation / drive train* and *Sensors*. Further, the software components *Gait planning / state recognition* and *Controls* and the system properties *Weight*, *Size / volume*, *Operating time* and *Functionality* are included. Expert consensus from a quality function deployment (QFD) discussion is utilized to assess interrelations between human and technical factors. This shows that *Gait planning / state recognition*, *Actuation / drive train* and *Functionality* are the most crucial design parameters of the knee example independent of the rating scale. In QFD, *Support* and *Mobility* receive the highest weights among human factors, although

---

being not separated well in the expert study, and *Body schema integration* is ranked third emphasizing its importance in human-machine-centered design. Remarkably low ratings of the *Socket* might be due to focusing on the example of a prosthetic knee but could also be due to increased importance of other components in powered prostheses. A brief investigation of QFD-sensitivity shows that different scales do not seem to change the basic rating structure. Yet, the determined design focus might be influenced and thus different scales should be examined in future comparative studies. The potential impact of a human-machine-centered design focus is shown based on a comparison with a purely technically motivated ranking from pair-wise comparison of the technical factors. The results indicate distinct influence, as factors like *Actuation/ drive train* receive significantly increased weight in human-machine-centered ranking, while others like *Weight* are ranked lower.

Aiming at human-machine-centered prosthetic systems engineering, V model development methodology is extended to consider human factors. This is achieved by a human-machine-centered list of requirements and a corresponding design focus determined by QFD, which additionally provides factor-specific information. During the design process, human-in-the-loop experiments are integrated to consider user-experience and further investigate specific human factors. Together with an analysis of enabling and predisposing factors of specific issues, such experiments should support the definition of technical requirements. To remove the necessity of developing prototypes before integrating human subjects to the development process in terms of experiments, human-in-the-loop experiments are proposed to be included in the V cycle within the proposed framework. As possible simulators for that purpose, Prosthesis-user-in-the-loop and the Int<sup>2</sup>Bot are suggested.

The combination of the human factor set, QFD as a transfer methodology, and systems engineering by V model design is embedded in a human-machine-centered design framework. Bringing together QFD and V model allows for considering the user perspective and leads to integrated system design at the same time. Feedback paths in the framework provide an assurance of properties and the possibility to correct, adjust or extend requirements. In this framework, user requirements can be understood as quality engineering aspects considered by QFD [63]. Finally, the impact and suitability of the proposed human-machine-centered design framework can only be validated by evaluating designs developed using it with human subjects. Anyhow, the deviations between the QFD-results and the technically motivated ranking show a strong influence of the consideration of human factors on the design focus. A recent example from commercial prosthetics substantiates the demand of improved *Gait planning / state recognition* by the users, as it is also found in the high human-machine-centered rating: The improvement of software algorithms detecting and enabling additional gait and motion types in the Genium

---

knee compared to the C-Leg (both from Otto Bock, Duderstadt, Germany) results in the experience of increased safety and less difficulty of Genium users [20, 113].

The improvement and validation of the human factors based on a factor analysis of data from an optimized questionnaire are part of future works. In addition, the application of structural equation models would allow for a quantitative assessment of the relative human factor importances and interrelations [241]. Such analyses can further support assessing connections between human and technical factors in QFD as well as mapping human factors to V model levels or steps. To separate overlapping human factors, certain additional (biomechanical) tests could be adapted and integrated to the human-machine-centered design framework. To support the determination of specific design parameters, interrelations of corresponding enabling and predisposing factors should be explored, e. g., how novel technologies are experienced by users. Further, both proposed human-in-the-loop experiments are subject to future works in engineering and psychology. Since the fundamental human-machine-centered design approach is general, the framework should be extended to other lower limb prosthetic components besides knee devices or even other types of prostheses. In the first case, technical factors need to be adjusted, while in the second an identification of corresponding human factors is required.

According to [186], individual requirements of particular prosthetic users are found in perception and attitude of subjects resulting in variability of psychological outcomes. To generalize demands of different users and thus reduce effort to determine those, clustering the user population into stereotypes with compatible requirements for human-machine-centered design seems to be appropriate. Such stereotypes could be subgroups with similarities in attributes like age, gender or activity that influence their specific needs. In [133], subgroups regarding gender, age, comorbidities, amputation level and years since amputation are examined and show distinct differences. Among those, gender shows very distinct influences: Aesthetic aspects are more important to female users [157, 132], while male users focus on functionality according to [157] for instance. The interview study in [91] approves this difference regarding gender: Most women used cosmetic covers and related it to social acceptance, while many men did not use such covers for functional reasons. Looking at results from [133, 157, 91], a classification regarding gender and activity (in correlation to age) is proposed in [246]. To consider such user-stereotypes in technical design of prostheses, a validated model based on a cluster analysis and structural equation models of user data should be determined. The differences between those groups can be mapped to the relative importance of human factors in the QFD-process using the requirement classification of Kano according to [63].

---

## 4 Actuator design considering natural dynamics

---

Variable elastic actuation represents an enabling technology of powered lower limb prostheses, while open questions that are presented in Chapter 1 remain. As described in Chapter 2, a major issue is how to support system energy efficiency by variable elastic actuation design. Below, aspects of energy efficiency are discussed considering a pendulum example. The dynamics of the mechanical system are described by advanced models that enable the investigation of their natural dynamics and power consumption. Based on the results from [16], possible actuator-elasticity configurations are presented and analyzed in this section. After discarding unpromising configurations, the remaining drive train concepts are represented by advanced models including the mechanical dynamics of actuator and driven link.

The influences of the configurations and varying stiffness is analyzed in two ways: First, the frequency responses are investigated to reveal the impacts of inertial and gravitational effects on natural dynamics. Second, power consumption during cyclic motion tasks is analyzed based on the mechanical power required from the actuator. From the comparison of this with the insights on natural dynamics, the correlations between power consumption and stiffness design and variation are determined. Based on this, an appropriate configuration can be selected and required stiffness ranges can be specified. Additionally, power recuperation by the drive is considered as it might provide better energy efficiency and can further be a functionally integrated implementation of damping, which can be beneficial according to the gait situation [60]. A transfer of the obtained results to a prosthetic application is given within the remainder of this thesis. For experimental evaluation, a prototype of the series elastic variable torsion stiffness (VTS) concept [195, 17] is described and investigated.

---

### 4.1 Methods

---

As a basis for the description of the methods utilized for the analysis of natural dynamics and power consumption, promising actuator-elasticity configurations are preselected based on [16]. For modeling and analysis, the selected configurations are represented by the corresponding nonlinear equations of motion in general and for the example of moving a single degree of freedom pendulum as in the VTS prototype from [17]. Those equations are linearized and transformed to the frequency domain for the basic investigation of the impacts of actuator-elasticity configuration on the natural dynamics. Further, inverse dynamics simulations of the nonlinear

equations of motion are utilized to examine the mechanical power consumption of the systems. In this, the effects of energy recuperation as well as actuator and transmission efficiencies are considered. Energy recuperation is promising with respect to lower limb prosthetics, as “legged locomotion entails a number of functions that require net dissipation of mechanical power and “an actively powered artificial limb has the potential to leverage energy storage mechanisms for improved overall performance“ in contrast to “the human musculoskeletal system which requires net metabolic energy consumption during contraction“ [224]. The power consumptions resulting from inverse dynamics simulations are compared to the natural dynamics of the systems considering stiffness variation to identify stiffness values for power-optimized operation. For a comparison to basic modeling approaches that are often used in research, power analysis is performed for those as well. For experimental evaluation, the series elastically actuated VTS prototype and the experiments for the practical analysis of power consumption are presented. With this, equations for the dimensioning of the elasticity and the control algorithm implemented in the prototype are described.

---

#### 4.1.1 Actuator configurations

---

A fundamental decision in elastic drive train design is the selection of an appropriate mechanical actuator-elasticity configuration. The configurations investigated in this thesis are presented in Figure 4.1. Elasticities represent rotational spring elements rotating around their center axis, while  $\tau_a$  describes the torque applied by an actuator-transmission-unit. The upper left sketch shows *direct actuation* (DA), where the link is rigidly connected to the actuator and no elasticity is present in the drive train. This configuration does not belong to the class of elastic actuators but is considered for comparison, since it represents the most common method of actuation in robotic systems (compare [116, 201]). The *parallel elastic actuation* (PEA) case is given in the upper right. Here, link and actuator are rigidly connected and an elasticity fixed to the environment and working in parallel with the drive is introduced. The bottom sketch represents the *serial elastic actuation* (SEA) case. In contrast to the other configuration, drive and link are not rigidly coupled, as the elasticity is implemented between them. Beyond those basic configurations, there are combinations of the two latter ones: Serial elastic actuation can be extended by parallel elasticities on the link side, the drive side or on both. All configurations are shown and investigated in [16].

The results and conclusions from [16] show that exclusive serial and parallel elasticity can reduce power consumption if stiffness of the elastic element is adjusted to match a characteristic frequency of the actuation system to the frequency of the

trajectory. It is further found that the combinations of serial elasticity with link sided parallel elastic elements are not suitable due to increased power consumption. Only the combination of serial with drive side parallel elements might be beneficial, as those introduce additional degrees of freedom for stiffness selection. Yet, mechanical and control efforts are increased in these configurations. Thus, serial and parallel elastic actuation are preselected and compared to each other as well as direct actuation.

#### 4.1.2 Advanced modeling

Mechanical models of the investigated mechanical actuator-elasticity configurations considering single joints are given in Figure 4.1. In this,  $q_l$  represents the position of the link and  $q_a$  corresponds to the actuator position. The input torque  $\tau_a$  is generated by the actuator and transformed by the transmission of the actuator-transmission unit. The stiffness value of the elasticities is given by  $K_s$  or  $K_p$  and the combined mass and inertia of drive and link in DA and PEA is given by  $m$  and  $I$ , respectively. Regarding the SEA, the rotational inertia of the actuator-transmission unit is represented by  $I_a$ , while  $m_l$  and  $I_l$  correspond to the mass and the inertia of the link. The consideration of those in modeling can have a significant impact on design due to [16]. Although comprehensive models are available [154, 47, 3] and early publications as [172] focused on the actuator dynamics, many studies from recent research consider link dynamics only, e. g., [110, 96, 214, 250, 229, 195]. Hence, models including the dynamics of link and actuator are referred to as advanced models, while such neglecting the actuator are referred to as basic models. A general description of

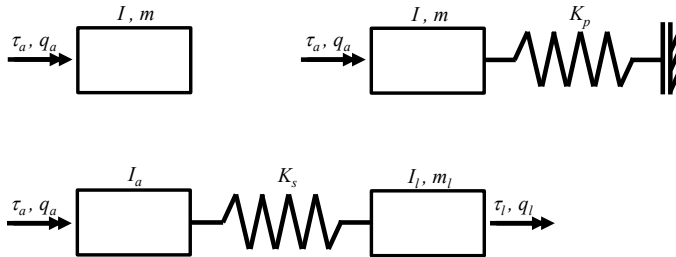


Figure 4.1: Mechanical models of the investigated mechanical actuator-elasticity configurations: Direct (top left), parallel elastic (top right), and series elastic actuation (bottom).

elastic joint dynamics considering multi-joint robotic systems is derived using the Lagrange formalism in [3]. The dynamics equations neglecting damping and friction are written as

$$M(q_l) \ddot{q} + C(\dot{q}_l, q_l) \dot{q} + G(q_l) + K q = \tau. \quad (4.1)$$

In (4.1),  $q = [q_l^T \quad q_a^T]^T$  is a vector containing the position vectors of the links and the actuators. The vector  $\tau = [0 \quad \tau_a^T]^T$ , contains the torque vector  $\tau_a$  that is introduced by the actuator-transmission units. Hence, no actuation is performed on the links directly and  $\tau_a$  acts remotely on the links via the elasticity. The matrices  $M(q_l)$ ,  $C(\dot{q}_l, q_l)$  and  $G(q_l)$  describe inertial, coriolis and centrifugal as well as gravitational effects depending on the link velocities  $\dot{q}_l$  and positions  $q_l$ . In general, the inertia matrix of a general multi-joint system is given by

$$M(q_l) = \begin{bmatrix} I_l(q_l) & S(q_l) \\ S(q_l)^T & I_a \end{bmatrix}. \quad (4.2)$$

According to [3],  $I_l(q_l)$ ,  $S(q_l)$  and  $I_a$  are square matrices with as many rows and columns as the number of joints:  $I_l(q_l)$  contains the inertias of the links,  $I_a$  is a diagonal matrix containing the constant rotational inertias of actuator-transmission units [3] and  $S(q_l)$  denotes inertial coupling effects between the rotors and link segments [47]. As coriolis, centrifugal and gravitational effects are caused by joint motion, the elements in the lower halves of  $C(\dot{q}_l, q_l)$  and  $G(q_l)$  that correspond to the actuator side degrees of freedom equal 0. The upper half elements correspond to the behavior of the links and can be derived for the specific mechanism using Lagrange equations as in rigid robotics according to [201, 116]. The structures of the matrices are hence

$$C(\dot{q}_l, q_l) = \begin{bmatrix} C_{ll}(\dot{q}_l, q_l) & C_{la}(\dot{q}_l, q_l) \\ 0 & 0 \end{bmatrix}, \quad G(q_l) = \begin{bmatrix} G_l(q_l) \\ 0 \end{bmatrix}. \quad (4.3)$$

The stiffness matrix can be derived based on the potential energies of the elasticities [3] and is given by

$$K = \begin{bmatrix} K_s + K_p & -K_s \\ -K_s & K_s \end{bmatrix}, \quad (4.4)$$

where the dimension of the square submatrix  $K_s$  containing the serial stiffness parameters on its diagonal corresponds to the number of joints. The parallel stiffness values are the diagonal elements of  $K_p$ . For the investigation of variable stiffness impact on the natural dynamics and power consumption, the stiffness values in  $K_s$

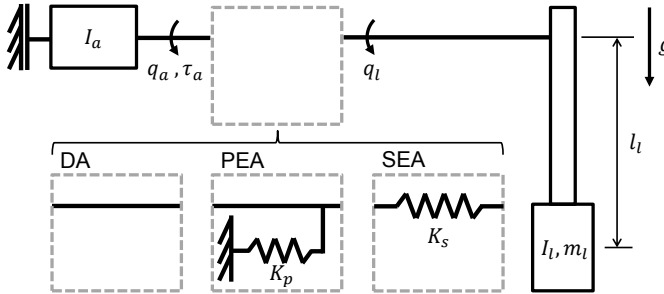


Figure 4.2: Sketch of the investigated pendulum: Dashed, grey box in the drive train is substituted with one of the actuation cases DA, PEA or SEA in the examinations. All elasticities represent rotational ones aligned with the drive train axis (parallel elasticity shown not aligned for layout reasons).

and  $K_p$  are varied in the subsequent analyses. Further, the dynamics model in (4.1) and the corresponding matrices are adapted to the investigated actuator-elasticity configurations: In direct and serial elastic configuration, the matrix  $K_p$  is zero. According to the rigid coupling of link and actuator, the degrees of freedom are reduced in direct or parallel elastic actuation. As  $K_s \rightarrow \infty$  and  $q_l - q_a \rightarrow 0$  in these cases, the degrees of freedom correspond to the number of joints, which is half of those occurring in (4.1). Hence, the dynamics equations are modified to

$$(I_l(q_l) + I_a) \ddot{q}_l + C_{ll}(\dot{q}_l, q_l) \dot{q}_l + G_l(q_l) + K_p q_l = \tau_a . \quad (4.5)$$

The corresponding inertia matrix is given by  $M_p(q_l) = I_l(q_l) + I_a$ , while it is  $M_p(q_l) = I_l(q_l)$  in basic model that neglect the actuator inertia. In the case of direct actuation  $K_p = 0$ .

To investigate the actuation concepts themselves independently from the particular application, a single joint with one degree of freedom assuming a pendulum load as shown in Figure 4.2 is examined. In this case, the position vectors  $q_l$  and  $q_a$  as well as the torque vector  $\tau_a$  reduce to scalars. Due to this, all matrices

Table 4.1: Inertial and gravitational parameters of the pendulum based on the VTS test rig [17, 59].

Parameter	$I_{a,r}$	$I_{a,g}$	$I_{a,c}$	$i_{a,g}$	$I_l$	$m_l$	$l_l$	$g$
Value	$1.80 \cdot 10^{-4}$	$0.95 \cdot 10^{-4}$	$2.47 \cdot 10^{-3}$	80	$9.41 \cdot 10^{-1}$	6.81	0.3558	9.81
Unit	$\text{kg m}^2$	$\text{kg m}^2$	$\text{kg m}^2$	-	$\text{kg m}^2$	kg	m	$\text{m s}^{-2}$

in (4.1) reduce to a dimension of 2, while those in (4.5) become scalars. Figure 4.2 shows the investigated actuator-elasticity configurations: The dashed grey box in the drive train is substituted with one of the actuation cases DA, PEA or SEA, where all depicted elasticities represent rotational ones. Although parallel elasticity is not shown aligned with the rotational axis of the drive train in Figure 4.2 for layout reasons, it should be understood as it would be and is considered in the equations accordingly. While the scalar version of (4.5) is applied for DA or PEA, the dynamics equations of a SEA driving a one-link robot are given by

$$\begin{bmatrix} I_l & 0 \\ 0 & I_a \end{bmatrix} \ddot{q} + \begin{bmatrix} G_l(q_l) \\ 0 \end{bmatrix} + \begin{bmatrix} K_s & -K_s \\ -K_s & K_s \end{bmatrix} q = \begin{bmatrix} 0 \\ \tau_a \end{bmatrix}, \quad (4.6)$$

where  $S(q_l) = 0$  according to [47],  $C(\dot{q}_l, q_l) = 0$  due to the single joint setup and  $I_l$  is a constant parameter instead of a function of  $q_l$ . Irrespective of the actuator-elasticity configuration,  $C_{ll}(q_l, \dot{q}_l) = 0$  and  $G_l(q_l) = m_l g l_l \sin(q_l)$  in the pendulum example. The corresponding basic model is obtained by choosing  $I_a = 0$ . Through this, the lower part of (4.6) reduces to  $K_s(q_a - q_l) = \tau_a$ . The parameters of the inertial and gravitational matrices given in Table 4.1 are based on the variable torsion stiffness test rig presented in [17] and updated according to [59]. Link inertia  $I_l$  is determined from the CAD-model and includes the term  $m_l l_l^2$  according to the parallel axis theorem [82] as well as those of the components connected rigidly to the pendulum. The inertia  $I_a = i_{a,g}^2 I_{a,r} + I_{a,g} + I_{a,c}$  of the actuator-transmission unit comprises reflected rotor inertia  $i_{a,g}^2 I_{a,r}$  as well as those of gear box  $I_{a,g}$  and coupling  $I_{a,c}$ . In this,  $i_{a,g}$  describes the gear ratio of the transmission that transforms the motor torque  $\tau_{a,m}$  to the actuator torque  $\tau_a = i_{a,g} \tau_{a,m}$ .

#### 4.1.3 Natural dynamics analysis

For the investigation of natural dynamics, the dynamics equations for moving the single degree pendulum are linearized regarding the equilibrium position  $q_{l,eq} = 0^\circ$  of the pendulum. The parameters of the pendulum are inspired by the VTS test rig [17, 59] that is designed in reference to the lower limbs of the biped robot named Lucy [230] for comparability to [229, 195, 17, 16, 59]. As in [16], all stiffness parameters are set to  $50 \text{ Nm rad}^{-1}$  to investigate the global characteristics of the transfer behavior of the actuator-elasticity configurations. Due to numerical reasons, negligible damping of  $D = 10^{-12} \text{ Nm s rad}^{-1}$  is introduced to the models in parallel with the investigated elasticities, which is in compliance with the Kelvin-Voigt viscoelastic damping model [107]. Hence, parallel damping  $D_p$  and serial damping  $D_s$  are scalars in the investigated single degree of freedom case. The linear equations

are transformed to frequency domain to obtain the transfer functions of the specific configuration. In DA and PEA, only one transfer function is found. This is

$$\frac{q_l(s)}{\tau_a(s)} = \frac{1}{c_2 s^2 + c_1 s + c_0} = \frac{1}{(I_l + I_a) s^2 + D_p s + K_p + m_l g l_l}, \quad (4.7)$$

for parallel elastic actuation according to (4.5), while for the DA case  $K_p = 0$  and  $D_p = 0$ . In this,  $s$  is the Laplace variable and  $\tau_a$  and  $q_l$  denote the actuator torque as input and link position as output, respectively. The corresponding numerator and denominators coefficients of these and the subsequent transfer functions are given in Table 4.2 and 4.3, respectively. In those, the factor  $m_l g l_l$  of the linearized gravitational torque is denoted as  $\gamma$ . According to [141], the natural frequency of the PEA without damping is determined from (4.7) to be

$$\omega_{p,n1} = \sqrt{\frac{K_p + m_l g l_l}{I_l + I_a}}, \quad (4.8)$$

In case of DA,  $K_p = 0$  in (4.8) and is thus dominated by the behavior of the pendulum [148]. Contrary to the majority of models like the ones from [229] or [195], two transfer functions are found in the serial elastic case with the advanced models, since rotor inertia of the actuator is not neglected here. The transfer function from the input  $\tau_a$  to the link position  $q_l$  is given by

$$\frac{q_l(s)}{\tau_a(s)} = \frac{b_{l1} s + b_{l0}}{c_4 s^4 + c_3 s^3 + c_2 s^2 + c_1 s + c_0}. \quad (4.9)$$

Table 4.2: Numerator coefficients of transfer functions.

Configuration	$b_{l0}$	$b_{l1}$	$b_{a0}$	$b_{a1}$	$b_{a2}$	$b_{q0}$	$b_{q1}$
SEA	$K_s$	$D_s$	$K_s + \gamma$	$D_s$	$I_l$	$K_s$	$D_s$
PEA	1	0	0	0	0	0	0
DA	1	0	0	0	0	0	0

Table 4.3: Denominator coefficients of transfer functions.

Configuration	$c_0$	$c_1$	$c_2$	$c_3$	$c_4$	$c_{q0}$	$c_{q1}$	$c_{q2}$
SEA	$K_s \gamma$	$D_s \gamma$	$(I_l + I_a) K_s + I_a \gamma$	$(I_l + I_a) D_s$	$I_l I_a$	$K_s + \gamma$	$D_s$	$I_l$
PEA	$K_p + \gamma$	$D_p$	$I_l + I_a$	0	0	0	0	0
DA	$\gamma$	0	$I_l + I_a$	0	0	0	0	0

The second transfer function describing the behavior between  $\tau_a$  and the actuator position  $q_a$  is

$$\frac{q_a(s)}{\tau_a(s)} = \frac{b_{a2} s^2 + b_{a1} s + b_{a0}}{c_4 s^4 + c_3 s^3 + c_2 s^2 + c_1 s + c_0}. \quad (4.10)$$

The natural characteristics of the undamped system are described by the poles of transfer functions. Those coincide with the roots of the equal denominators of (4.9) and (4.10) and yield

$$\omega_{s,n1} = \sqrt{\frac{-c_2 - \sqrt{c_2^2 - 4 c_0 c_4}}{2 c_4}}, \quad (4.11)$$

$$\omega_{s,n2} = \sqrt{\frac{-c_2 + \sqrt{c_2^2 - 4 c_0 c_4}}{2 c_4}}. \quad (4.12)$$

When the actuation system is operated at those frequencies, a very low torque  $\tau_a$  is required [141]. Beyond the natural modes, a zero representing an antiresonance mode is found in (4.10). Not considering damping, it is calculated by the roots of the numerator to be

$$\omega_{s,a} = \sqrt{\frac{K_s + m_l g l_l}{I_l}}. \quad (4.13)$$

Operation with this frequency leads to very low motions  $q_a$  of the inertia  $I_a$ , as the numerator of (4.10) becomes zero in this case [188]. The dynamic interaction between the positions of link  $q_l$  and actuator  $q_a$  that is given by

$$\frac{q_l(s)}{q_a(s)} = \frac{b_{q1} s + b_{q0}}{c_{q2} s^2 + c_{q1} s + c_{q0}} = \frac{D_s s + K_s}{I_l s^2 + D_s s + m_l g l_l + K_s}, \quad (4.14)$$

can be analyzed regarding control issues caused by missing sensor and actuator collocation [158].

Beyond the characteristic frequencies of the configurations, the relative motion of the inertias during operation with a specific natural frequency can be figured out by analyzing the corresponding eigenvectors  $u$ . No relative motion is possible for DA and PEA, as they only have a single degree of freedom. In serial elastic actuation, the eigenvectors  $u$  are calculated by solving the eigenvalue problem

$$\left( \frac{dM}{dq} \Big|_{q_{l,eq}}^{-1} \left( K + \frac{dG}{dq_l} \Big|_{q_{l,eq}} \right) - U \omega^2 \right) u = 0, \quad (4.15)$$

where  $\omega$  represents the corresponding natural frequencies [46],  $U$  denotes a unity matrix with the dimension of  $M$ . The linearizations of the inertial and gravitational effects are given by  $\frac{dM}{dq} \Big|_{q_{eq}}$  and  $\frac{dG}{dq_l} \Big|_{q_{eq}}$ , respectively.

---

#### 4.1.4 Power consumption analysis

---

Aiming at energy-efficient operation of powered prosthetic devices or robots in general, it is important to understand the power consumption of the actuated system during operation in different states. Considering human lower limb motions, periodic behavior is observed in the angular position trajectories that are cyclically repeated [244] (periodicity of knee motion can be seen in Figure 2.3). In the pendulum example analyzed here, power consumption is mainly influenced by the oscillation frequency  $f_d$  and the selected stiffness  $K_s$  or  $K_p$  in the elastically actuated cases. The investigations of the elastic actuator configurations are based on inverse dynamics calculations of the motions of the single degree of freedom pendulum. Sinusoidal link position trajectories are utilized as reference  $q_{l,d}(t)$  as in [229]. Those and their derivations  $\dot{q}_{l,d}(t)$ ,  $\ddot{q}_{l,d}(t)$  and  $q_{l,d}^{(3)}(t)$  describing the corresponding velocities, accelerations and jerks as well as  $q_{l,d}^{(4)}(t)$  are

$$\begin{aligned} q_{l,d}(t) &= 2\pi \hat{q}_l \frac{1}{360^\circ} \sin(2\pi f_d t), \\ \dot{q}_{l,d}(t) &= 4\pi^2 f_d \hat{q}_l \frac{1}{360^\circ} \cos(2\pi f_d t), \\ \ddot{q}_{l,d}(t) &= -8\pi^3 f_d^2 \hat{q}_l \frac{1}{360^\circ} \sin(2\pi f_d t), \\ q_{l,d}^{(3)}(t) &= -16\pi^4 f_d^3 \hat{q}_l \frac{1}{360^\circ} \cos(2\pi f_d t), \\ q_{l,d}^{(4)}(t) &= 32\pi^5 f_d^4 \hat{q}_l \frac{1}{360^\circ} \sin(2\pi f_d t), \end{aligned} \quad (4.16)$$

with an amplitude of  $\hat{q}_l = 10^\circ$ , a frequency  $f_d$  ranging from 0.1 Hz to 3.5 Hz and  $t$  denoting time. Further, the superposition of two sinusoidal functions, which are closer to biological motion, is investigated [230] and referred to as dual-sine. It is given by

$$q_{l,d}(t) = 2\pi \frac{1}{360^\circ} \left( \hat{q}_l \sin(2\pi f_d t) + \frac{\hat{q}_l}{2} \sin(\pi f_d t) \right), \quad (4.17)$$

and the corresponding derivations with respect to time  $t$ . While the sinusoidal trajectory can be perfectly matched by natural dynamics, the dual-sine trajectory allows for examining trajectories with multiple frequency components. The required torques to track those trajectories can be calculated solving inverse dynamics problem [47, 201]: Therefore, the reference trajectory and its derivations are inserted into the dynamics equations (4.5) or (4.6) considering the investigated

actuation type. For DA and PEA, this directly yields the torques  $\tau_{a,d}$  required from the actuator. Regarding SEA, the required torque  $\tau_{e,d} = K_s (q_{a,d} - q_{l,d})$  in the elastic element that equals the link sided load torque is calculated from the upper part of (4.1) and reorganized yielding the required positions, velocities and accelerations of the actuator. In case of the general multi-link case those are

$$\begin{aligned} q_{a,d} &= q_{l,d} + K_s^{-1} \tau_{e,d} \\ &= q_{l,d} + K_s^{-1} (I_l(q_{l,d}) \ddot{q}_{l,d} + C(q_{l,d}, \dot{q}_{l,d}) + G(q_{l,d})) , \\ \dot{q}_{a,d} &= \dot{q}_{l,d} + K_s^{-1} \dot{\tau}_{e,d} \\ &= \dot{q}_{l,d} + K_s^{-1} \left( I_l(q_{l,d}) q_l^{(3)} + \dot{I}_l(q_{l,d}) \ddot{q}_{l,d} + \dot{C}(q_{l,d}, \dot{q}_{l,d}) + \dot{G}(q_{l,d}) \right) , \\ \ddot{q}_{a,d} &= \ddot{q}_{l,d} + K_s^{-1} \ddot{\tau}_{e,d} \\ &= \ddot{q}_{l,d} + K_s^{-1} \left( I_l(q_l) q_l^{(4)} + 2 \dot{I}_l(q_l) q_l^{(3)} + \ddot{I}_l(q_l) \ddot{q}_l + \ddot{C}(q_l, \dot{q}_l) + \ddot{G}(q_l) \right) , \end{aligned} \quad (4.18)$$

according to [47]. In this, the torque  $\tau_{e,d}$  is differentiated twice with respect to time corresponding to the fourth order dynamics of the system. Considering the constant link inertia  $I_l$  and that  $C(q_{l,d}, \dot{q}_{l,d}) = 0$  for the pendulum setup, the equations simplify to

$$\begin{aligned} q_{a,d} &= q_{l,d} + K_s^{-1} (I_l \ddot{q}_{l,d} + G(q_{l,d})) , \\ \dot{q}_{a,d} &= \dot{q}_{l,d} + K_s^{-1} \left( I_l q_{l,d}^{(3)} + \dot{G}(q_{l,d}) \right) , \\ \ddot{q}_{a,d} &= \ddot{q}_{l,d} + K_s^{-1} \left( I_l q_{l,d}^{(4)} + \ddot{G}(q_{l,d}) \right) . \end{aligned} \quad (4.19)$$

Inserting those in the upper part of (4.1) or (4.6) gives the required actuators torques  $\tau_{a,d}$  in case of SEA. With the trajectories, their derivations and the calculated torques, energy required for the motion of the link via the actuator is determined by integrating the corresponding mechanical power, which is generally given by

$$P_{m,a} = \tau_a \dot{q}_a . \quad (4.20)$$

In contrast to this, several works that are specifically aiming at prosthetics like [98, 96, 97, 80, 79, 78, 195, 61, 60] calculate mechanical power in SEA by

$$\bar{P}_{m,a} = \tau_e \dot{q}_e + K_s^{-1} \tau_e \dot{\tau}_e . \quad (4.21)$$

In this alternative way to calculate power indicated by the bar in  $\bar{P}_{m,a}$ , the link sided load torque  $I_l \ddot{q}_l + G_l(q_l)$  that equals the elastic torque  $\tau_e$  is utilized. Neglecting actuator inertia  $I_a$  in the lower part of (4.6), shows that the elastic torque  $\tau_e$

and the actuator torque  $\tau_a$  are equal in this case. Considering this in the calculation of mechanical power required from the actuator according to (4.20) yields

$$\bar{P}_{m,a} = \tau_e \dot{q}_a . \quad (4.22)$$

Substituting  $\dot{q}_a = \dot{q}_l + K_s^{-1} \dot{\tau}_e$  into (4.22) shows that calculating power with (4.21) corresponds to the neglection of the inertia  $I_a$  of the actuator-transmission unit, which is also stated in [98]. Hence, powers calculated with (4.21) represent the behavior of basic models, which are shown throughout the power analysis for comparison.

In power consumption analysis, steady-state motion of the system is assumed to focus on the consumption during oscillation without transient effects. Therefore, energy contents due to the initial positions and velocities of the different systems are considered in the calculations as the initial values of integration, which is compatible with the assumptions in [229, 195]. As a measure of average required mechanical actuator power  $P_{m,a,a}$  in compliance with former studies as [98, 229, 79, 195], the energy consumption during five periods is calculated and related to the temporal duration  $t_m$  by

$$P_{m,a,a} = \frac{1}{t_m} \int_{t_m} |P_{m,a}(t)| dt . \quad (4.23)$$

This corresponds to assuming that power has to be provided to “resist and propel human motion” as in [98] and thus power is consumed for decelerating. Evaluating this measure for frequencies  $f_d$  ranging from 0.1 Hz to 3.5 Hz in steps of 0.1 Hz and investigating a stiffness interval from  $10 \text{ N m rad}^{-1}$  to  $750 \text{ N m rad}^{-1}$  in steps of  $10 \text{ N m rad}^{-1}$  leads to characteristic maps of power consumption for analysis. For the example of the dual-sine trajectory, further the corresponding characteristic map of the actuator torques  $\tau_a$  is given.

Aiming at efficient actuation, energy recuperation by using the actuator as a generator can be a promising solution to extend the time of operation. Further, this kind of regenerative braking can be used to introduce damping required during specific gait situations [60] without consuming but even regaining energy in opposition to the assumptions in [98]. Hence, average mechanical actuator power consumption  $P_{m,a,r}$  considering recuperation as in [159] is utilized as a second measure of the energy efficiency of the actuation system. It is calculated by

$$P_{m,a,r} = \begin{cases} \frac{1}{t_m} \int_{t_m} \eta_a^{-1} P_{m,a}(t) dt , & P_{m,a}(t) \geq 0 \\ \frac{1}{t_m} \int_{t_m} \eta_a P_{m,a}(t) dt , & P_{m,a}(t) < 0 \end{cases} \quad (4.24)$$

where  $\eta_a$  represents the maximum value of the combined efficiencies of actuator and transmission. Although real efficiencies vary with torque and angular velocity, this enables a fundamental investigation if efficiency consideration alters the results of power analysis. Due to its value below one, efficiency  $\eta_a$  has negative effect on power consumption during both providing and recuperating power. The measure  $P_{m,a,r}$  is evaluated considering frequencies  $f_d$  ranging from 0.1 Hz to 3.5 Hz in steps of 0.1 Hz and investigating a stiffness interval from  $10 \text{ N m rad}^{-1}$  to  $750 \text{ N m rad}^{-1}$  in steps of  $10 \text{ N m rad}^{-1}$ . Additionally, it is examined using the dual-sine trajectory from (4.17). To fundamentally clarify the relationship between natural dynamics and power consumption, the natural frequencies of the configurations calculated from the linearized transfer functions are plotted over stiffness in comparison with a contour plot of the power consumption determined from nonlinear inverse dynamics simulation. Based on this, stiffness values leading to low power operation can be mapped to frequencies and associated with natural dynamics.

Both measures  $P_{m,a,a}$  and  $P_{m,a,r}$  are based on integrating power resulting in an energy that is related to the oscillation period. Hence, they are suitable to identify power-optimized stiffness values but not for dimensioning and selection of drives and transmissions. Therefore, the peak values of required actuator velocities  $\hat{v}_{a,d}$  ( $v_{a,d} = \dot{q}_{a,d}$ ), torques  $\hat{\tau}_{a,d}$  and powers  $\hat{P}_{m,a,d}$  including resisting and propelling ones as stated by [98] are to be compared to the properties of potential components.

#### 4.1.5 Experimental evaluation

The experimental evaluation focuses on a prototype with series elastic actuation realizing the variable torsion stiffness concept that is shown left in Figure 4.3 and aims at two objectives: First, the implementation of the required stiffness characteristics of the elastic element is validated. Second, power consumption of the test rig

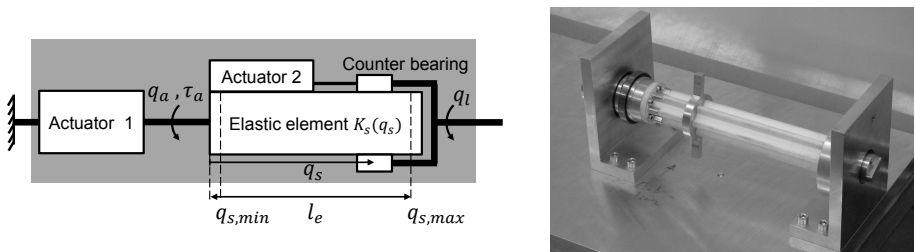


Figure 4.3: Concept of variable torsion stiffness (left, [195]) and elasticity implementation in the prototype (right).

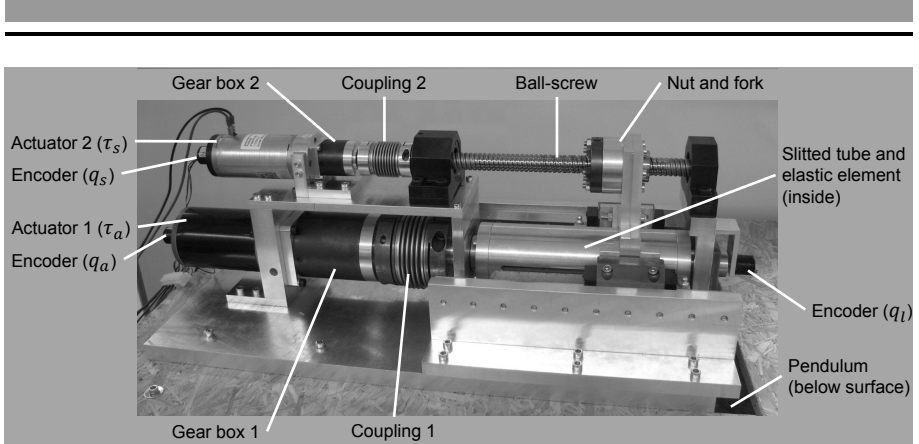


Figure 4.4: Prototype of a variable torsion stiffness actuator with series elasticity and stiffness adjustment mechanism.

is investigated for different trajectories to provide an experimental examination of the findings from the natural dynamics and power analysis. In the variable torsion stiffness concept, a series elastic configuration is chosen due to its wide adoption in prosthetics and robotics and the results of [195].

As shown left in Figure 4.3, actuator 1 applies the torque  $\tau_a$  to a torsional elastic element in serial configuration to change link position  $q_l$ . The torsional stiffness  $K_s(q_s)$  of the drive train is varied by changing the effective length  $q_s$  of the elastic element via the location of a counter bearing using actuator 2. As the actuators moving the link and varying stiffness are separated, motion and stiffness adjustment are conducted independently. According to [83], the torsional stiffness characteristics are given by

$$K_s = \frac{\Gamma I_t}{q_s}, \quad (4.25)$$

where  $\Gamma$  is the material-specific modulus of elasticity in shear and  $I_t$  denotes the torsional moment of inertia of the elastic element.

The variable torsion stiffness prototype used in the experimental evaluations is depicted in Figure 4.4. Actuator 1, which is moving the link, is realized by a 200 W direct current (DC) motor depicted left. A planetary gear box with a transmission ratio of  $i_{a,g} = 80$  transforms the torque  $\tau_{a,m}$  of the motor resulting in  $\tau_a = i_{a,g} \tau_{a,m}$ . A bellows coupling connects the gear box to the elastic element, which is realized by a torsional rod manufactured from polyamide and housed in a slotted aluminium tube. The counter bearing for stiffness adjustment is realized

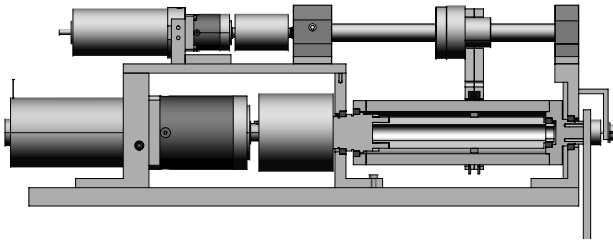


Figure 4.5: Schematic lateral section of the variable torsion stiffness prototype.

by a relocatable aluminium slider guided by the slotted tube. In the right part of Figure 4.3 the implementation of the elastic element and the relocatable slider without the surrounding components is shown. The pendulum on the right side of the prototype in Figure 4.4 is rigidly connected to the tube and corresponds to the one examined in the simulations above. To provide an appropriate transfer of the torque via the relocatable slider, six guiding rails fitting the slider geometry are placed on the tube-shape of the elastic element as depicted right in Figure 4.3. Considering the lateral section that is given in Figure 4.5, the elastic element is housed inside the horizontally aligned slotted tube and torque is transferred by the vertical relocatable slider that can be moved by means of the upper drive train.

The drive train for stiffness adjustment is placed above the one moving the pendulum. A 56 W DC motor is connected to a planetary gear box with a transmission ratio  $i_{s,g}$  implementing actuator 2. The transformed torque is transferred to a ball-screw with a lead of 0.01 m per revolution via a bellows coupling. The nut of the ball-screw is connected to a fork that surrounds and moves the relocatable slider and is supported by linear bearings. To minimize friction between the relocatable slider and the slotted tube, two ring-shaped sleeve bearing elements made of *iglidur Z* from igus GmbH, Cologne, Germany are inserted between those.

Both actuators are driven by motor drivers, which are torque-controlled based on current measurement and commanded by corresponding higher-level control algorithms. Those calculate the required torques and are implemented on a rapid prototyping control-platform. The position  $q_l$  of the pendulum is measured by an incremental encoder with 1024 counts per revolution that leads to a resolution of  $87.89 \cdot 10^{-3}^\circ$ . An incremental encoder with 360 counts per revolution or a resolution of  $3.125 \cdot 10^{-3}^\circ$  acquires the position  $q_a = i_{a,g}^{-1} q_{g,m}$  corresponding to the motion of the gear box output. A third incremental encoder with 256 counts per revolution yielding a resolution of  $0.14 \cdot 10^{-4} \text{ m}$  measures the position  $q_s$  of the stiffness adjustment drive train. All encoders are operated in quadrature mode and

positions are evaluated by encoder pulse counting, while velocities are determined with a pulse-timing method as explained in [131]. A list of the components of the prototype and information on those is given in Appendix A.3.

Geometric dimensioning of the elastic element is deduced based on the equations introduced in [195, 194]. For comparison with results from [229, 195], a stiffness range from  $50 \text{ Nm rad}^{-1}$  to  $350 \text{ Nm rad}^{-1}$  is required according to [195]. A thick-walled hollow cylinder with a ratio factor  $\lambda = r/R$  between the inner radius  $r$  and outer radius  $R$ , which are both constant with respect to the effective length  $q_s$ , is assumed. The torsional moment of inertia  $I_t = \frac{\pi}{2} (R^4 - r^4) = \frac{\pi}{2} (1 - \lambda^4) R^4$  given in [83] is substituted to (4.25) yielding

$$K_s(q_s) = \frac{\pi \Gamma (1 - \lambda^4) R^4}{2 q_s}. \quad (4.26)$$

Rearranging this, a geometry providing the maximum required stiffness  $K_{s,max}$  at the minimum active length  $q_{s,min}$  can be dimensioned by

$$R = \sqrt[4]{\frac{2 K_{s,max} q_{s,min}}{\pi \Gamma (1 - \lambda^4)}}. \quad (4.27)$$

Alternatively, dimensioning regarding a specific length can be performed by replacing maximum stiffness  $K_{s,max}$  and minimum active length  $q_{s,min}$  by minimum stiffness  $K_{s,min}$  and maximum length  $q_{s,max}$ . In order to realize the required stiffness range, an outer radius  $R = 11 \text{ mm}$  is determined in [238] and assuming that the elastic element is manufactured from polyamide ( $\Gamma = 6.3 \cdot 10^8 \text{ N m}^{-2}$ ), a minimum elastic length of  $q_{s,min} = 25.2 \cdot 10^{-3} \text{ m}$  and  $\lambda = 0.791$ . With this, the minimum stiffness of  $50 \text{ Nm rad}^{-1}$  should be achieved for  $q_{s,max} = 176.4 \cdot 10^{-3} \text{ m}$ .

To validate the accuracy of stiffness design, the approaches and experimental results from [15, 58] are considered. In [58], the static torque due to gravitation  $G_l(q_l)$  and the position difference  $q_a - q_l$  between actuator and link are measured for varying link and counter bearing positions. In this experiment, the encoder measuring  $q_l$  is replaced by an analogue rotary potentiometer to avoid limitations due to sensor resolution. Link positions range from  $-24^\circ$  to  $24^\circ$  in steps of  $2^\circ$  and counter bearing positions cover  $0.011 \text{ m}$  to  $0.151 \text{ m}$  in steps of  $0.02 \text{ m}$  as well as a final one at  $0.166 \text{ m}$ . The combined inherent stiffness of coupling  $K_{s,c} = 95,100 \text{ Nm rad}^{-1}$  and gear box  $K_{s,g} = 21,658 \text{ Nm rad}^{-1}$  is considered as

$$K_{s,cg} = \frac{K_{s,c} K_{s,g}}{K_{s,c} + K_{s,g}}, \quad (4.28)$$

according to [188, 58]. With this, the stiffness of the elastic element  $K_{s,e}$  is isolated from the measured drive train stiffness by

$$K_{s,e} = \frac{G_l(q_l)}{q_a - q_l - \frac{G_l(q_l)}{K_{s,cg}}}. \quad (4.29)$$

Assuming a linear relationship regarding position, the stiffness coefficients  $K_{s,ec}(q_s)$  are determined with a least squares regression as described in [108] for each investigated counter bearing position  $q_s$  according to [15, 58]. In these, a linear term, which is interpreted to correspond to the stiffness coefficients  $K_{s,ec}(q_s)$ , and a constant term are approximated. As determined empirically in [58], only link positions  $q_l$  with absolute values of more than  $12^\circ$  are considered in the regression to avoid affection due to sensor noise. The single stiffness coefficients are examined by plotting measured static torques  $G_l(q_l)$  versus measured deflections  $q_a - q_l$  and comparing them to the models from regression. Additionally, the stiffness characteristics of the elastic element and the suitability of design using (4.27) are investigated. Therefore, the stiffness  $K_{s,ec}(q_s)$  is plotted versus the counter bearing position  $q_s$  and compared to the analytical solution  $\bar{K}_{s,ec}(q_s)$  according to (4.25) as well as investigating the relative error

$$\Delta K_s(q_s) = \frac{K_{s,ec}(q_s) - \bar{K}_{s,ec}(q_s)}{\bar{K}_{s,ec}(q_s)}. \quad (4.30)$$

between those [174].

The experimental analysis of mechanical power consumption considers two kinds of pendulum motion trajectories  $q_{l,d}(t)$ . A cosine with linearly increasing frequency, which is referred to as chirp and given by

$$q_{l,d}(t) = 2\pi \hat{q}_l \frac{1}{360^\circ} \cos(2\pi(h_1 t + h_2 t^2)), \quad (4.31)$$

is used to determine an overview on the system dynamics that might deviate between model and prototype due to model deviations. In (4.31), the constants  $h_1 = f_0$  and  $h_2 = \frac{f_1-f_0}{2t_1}$  specify the initial frequency  $f_0$  and the final frequency  $f_1$  that is desired, when time reaches  $t_1$ . Based on this overview, sinusoidal trajectories as specified in (4.16) are examined for various frequencies to obtain detailed results covering the range of natural dynamics.

For the definition of the experiments, the structural strength of the elastic element is considered to avoid harming it during the examinations. Therefore, contour plots of the elastic torque  $\tau_e$  are investigated and a threshold frequency until which

the elastic torque  $\tau_e$  is below the maximal one of  $\tau_{e,max} = 45.1 \text{ Nm}$  [58] is determined. The contour plots are further compared to the natural frequencies, as operation is bounded by stability limitations of the controller, which are assumed to be slightly higher than the second natural frequency [58]. To ensure that all kinds of trajectories are covered, those plots are investigated considering sinusoidal trajectories according to (4.16) as well as such of dual-sine type according to (4.17), which will be subject to all experiments in the remainder of the thesis. The amplitudes of sinusoidal and chirp-type trajectories, are set considering the limitations determined for the sine case, as both trajectories include only one frequency component.

Two stiffness values of approximately  $75 \text{ Nm rad}^{-1}$  and  $150 \text{ Nm rad}^{-1}$  corresponding to counter bearing positions  $q_s$  of about  $0.12 \text{ m}$  and  $0.04 \text{ m}$  are selected for the experiments. Based on the results regarding the chirp trajectories, the frequency ranges to be investigated regarding sinusoidal ones are chosen to cover the area containing the antiresonance as well as the second natural frequency. According to (4.13), antiresonances are expected to be  $1.63 \text{ Hz}$  for  $75 \text{ Nm rad}^{-1}$  and  $2.16 \text{ Hz}$  for  $150 \text{ Nm rad}^{-1}$ . The second natural frequencies are predicted to be found at  $2.01 \text{ Hz}$  for  $75 \text{ Nm rad}^{-1}$  and  $2.80 \text{ Hz}$  for  $150 \text{ Nm rad}^{-1}$  with (4.12). To assess the power consumption, mechanical power is calculated as  $P_{m,a} = \tau_a \dot{q}_a$  according to (4.20) considering both inertias of the system. Beyond power, control issues as well as reasons and impacts of parameter uncertainties are discussed based on the results.

For motion control of the prototype, feedback linearization according to [205, 202] is selected due to its suitability for the control of low stiffness joints [208]. Further, it can be used as a basis for later implementations of impedance control [207]. For the design of feedback linearization control, the extended model of the SEA (4.6) is rewritten in nonlinear state-space representation with the state vector

$$x = \begin{bmatrix} x_1 & x_2 & x_3 & x_4 \end{bmatrix}^T = \begin{bmatrix} q_l & \dot{q}_l & q_a & \dot{q}_a \end{bmatrix}^T. \quad (4.32)$$

Hence, the system is represented by a nonlinear input affine form

$$\dot{x} = f(x) + g(x) \tau_a, \quad (4.33)$$

$$\dot{x} = \begin{bmatrix} x_2 \\ -\frac{m_l g l_l}{I_l} \sin(x_1) - \frac{K_s}{I_l} (x_1 - x_3) \\ x_4 \\ \frac{K_s}{I_a} (x_1 - x_3) \end{bmatrix} + \begin{bmatrix} 0 \\ 0 \\ 0 \\ \frac{1}{I_a} \end{bmatrix} \tau_a,$$

where the scalar system input is the actuator torque  $\tau_a$  [202]. This torque is computed using the nonlinear state feedback

$$\tau_a = \frac{I_l I_a}{K_s} (\nu - a(x)), \quad (4.34)$$

with

$$a(x) = \frac{m_l g l_l}{I_l} \sin(x_1) \left( x_2^2 + \frac{m_l g l_l}{I_l} \cos(x_1) + \frac{K_s}{I_l} \right) \\ + \frac{K_s}{I_l} (x_1 - x_3) \left( \frac{K_s}{I_l} + \frac{K_s}{I_a} + \frac{m_l g l_l}{I_l} \cos(x_1) \right), \quad (4.35)$$

and the new input  $\nu$  due to design in [205, 202]. With the coordinate transformation

$$z = \begin{bmatrix} x_1 \\ x_2 \\ -\frac{m_l g l_l}{I_l} \sin(x_1) - \frac{K_s}{I_l} (x_1 - x_3) \\ -\frac{m_l g l_l}{I_l} x_2 \cos(x_1) - \frac{K_s}{I_l} (x_2 - x_4) \end{bmatrix}, \quad (4.36)$$

the components of the new state  $z$  correspond to the link position  $q_l$ , velocity  $\dot{q}_l$ , acceleration  $\ddot{q}_l$  and jerk  $\dddot{q}_l$  and the transformed system behaves like a chain of four integrators. For this system, a linear tracking control law

$$\nu = z_d^{(4)} + k_a \tilde{z}, \quad (4.37)$$

is designed for asymptotic stabilization. In this,  $z_d^{(4)}$  corresponds to the desired value of the fourth derivation of the transformed state  $z_1$ , while  $\tilde{z} = z_d - z$  is the state control error and  $k_a = [k_{a,p} \ k_{a,v} \ k_{a,a} \ k_{a,j}]$  are the control gains. Those are determined by placing all poles to  $-12$ , which showed to be an appropriate tradeoff of tracking accuracy and control effort in the prototype. For the adaptation of the controller to stiffness variations during operation, the stiffness parameter  $K_s$  in (4.34), (4.35), and (4.36) is adapted to the current stiffness value of the drive train. Hence, feedback linearization and the suitability of the linear control design should be given for the whole stiffness range. Additionally, friction is compensated by a specific control action as described in [59], since feedback linearization is just suitable to linearize smooth nonlinearities [202]. Both, sensor data acquisition and the control loops are operating at a frequency of 1,000 Hz, while measured data is stored into the flash storage of the real-time control platform with 100 Hz.

## 4.2 Results

This section presents the results of the investigation of actuator-elasticity configurations. Insights on those obtained by analyzing their natural dynamics and their impact on power consumption are assessed with the methods presented before. As energy efficiency is a main design objective in powered prosthetics, focus is set on how power consumption can be reduced by varying elasticity. The fundamental findings on the connection of power consumption and stiffness variation are experimentally evaluated with a variable torsion stiffness prototype. Beyond this, the practical implementation of the elastic element is experimentally validated in comparison with the design requirements.

### 4.2.1 Natural dynamics analysis

The natural dynamics of the considered topologies and models are investigated based on the linearized transfer functions presented in Section 4.1.3. In this, the effects caused by actuator inertia and gravity are examined by comparing models that either neglect or include these influences. Stiffness parameters are fixed to  $K_s = 50 \text{ N m rad}^{-1}$  and  $K_p = 50 \text{ N m rad}^{-1}$ , as the impact of stiffness variation is subject to the following power analysis.

Figure 4.6 depicts the transfer functions from the actuator torque  $\tau_a$  to the link position  $q_l$  considering serial and parallel elastic actuation, respectively. For direct actuation, no plot of the frequency response is given, as it basically shows the same

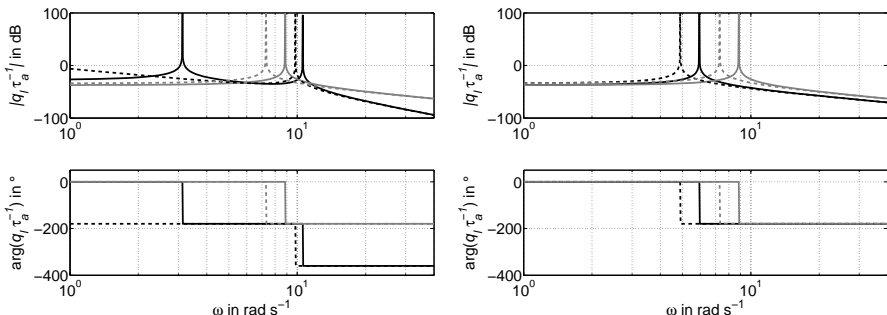


Figure 4.6: Transfer functions from  $\tau_a$  to  $q_l$  of SEA (left) and PEA (right): Neglecting (dashed) and considering (solid) gravity is indicated by line style. Neglecting (grey) and considering (black) actuator inertia is indicated by line color.

transfer behavior as the one of PEA but with  $K_p = 0$ . In Figure 4.6, dashed lines indicate that gravitational effects due to link motion are not considered, while those are included in results presented by solid lines. The line color indicates the inclusion of inertias: Results presented by grey lines are obtained neglecting actuator inertia, while it is considered in results shown in black. Regarding serial elastic configuration, results given left in Figure 4.6 show that gravity and input inertia increase the natural frequency, as the resonance peak observed in the dashed grey line has the lowest frequency of about  $7 \text{ rad s}^{-1}$ . The case of considering gravity while neglecting actuator inertia is depicted by the solid grey line. Here, the increase of the natural frequency is caused by the restoring torque induced to the pendulum by gravity, as it acts equivalent to a nonlinear spring and thus increases global system stiffness  $K_s + \gamma$ . If actuator inertia is considered and gravity is neglected, an additional rigid body mode occurs in the transfer behavior as shown by black dashed line. It is characterized by global integral behavior with a magnitude decrease of  $-40 \text{ dB}$  per decade and a phase drop of  $180^\circ$  at  $0 \text{ Hz}$  and represents the rigid body motion of the two inertias at low frequencies. If actuator inertia and gravitational effects are considered as given by the solid black line, the rigid body mode occurring with the introduction of actuator inertia is transformed to an elastic one. This is caused due to gravity that acts like a virtual fixation of the link inertia. Through this, the system has two elastic natural frequencies and rigid body motion does not occur. In contrast to the models used in previous studies like [229, 195], this advanced model allows for investigating the impacts of mechanical effects. Further, it enables the clarification of the natural characteristics observed for different configurations. The results for parallel elastic configuration depicted right in Figure 4.6, show that gravity has the same influence as in the serial elastic one. The additional virtual stiffness introduced by the gravitational torque leads to an increase of the natural frequency. A difference can be observed, if introducing actuator inertia, as this generates neither rigid body nor elastic modes. This is due to the fact that actuator and link inertia are rigidly coupled and are hence observed as a single inertia with a higher value in this case. Thus, only one elastic natural frequency with a smaller value is appearing.

The transfer function of the serial elastic configuration from  $\tau_a$  to  $q_a$  is shown left in 4.7. As this is only possible if actuator and link inertia are considered, only the influence of gravity is examined and indicated by line style. Besides the previously described natural frequencies, this transfer path shows an additional antiresonance characterized by a magnitude minimum and phase increase of  $90^\circ$ . It is observed below the elastic natural frequency for the neglection of gravity, while it occurs between the elastic modes if gravity is considered. This effect is due to the zero in the corresponding transfer function (4.10). Neglecting gravity, global integral

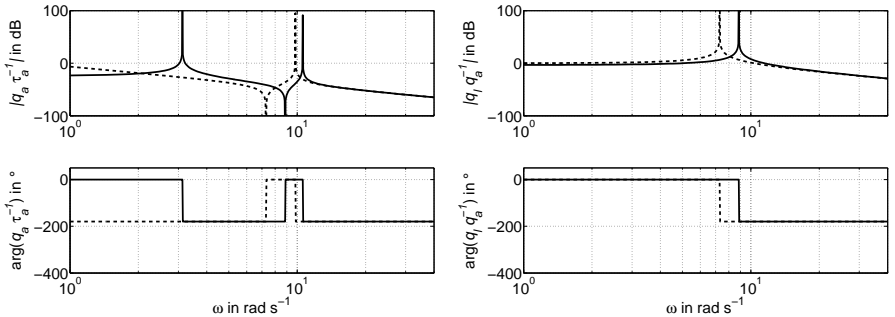


Figure 4.7: Transfer functions in serial elastic actuation: From  $\tau_a$  to  $q_a$  (left) and from  $q_a$  to  $q_l$  (right). Neglecting (dashed) and considering (solid) gravity is indicated by line style.

behavior is observed due to the rigid body mode as in the other transfer paths, while considering gravity is reflected as a virtual fixation again. In DA and PEA, this transfer function does not appear, since both have only one degree of freedom.

As shown in [58, 59], the investigation of the transfer path from  $q_a$  to  $q_l$  depicted right in Figure 4.7 is mainly important for design of motion control, as it allows for determining the frequency limit according to missing sensor and actuator collocation. Since beyond this frequency the feedback from the sensor and required action at the actuator are out of phase [158], common PID-type controllers are not able to stabilize the serial elastic mechanism there in contrast to model-based ones [58]. The right part of Figure 4.7 reflects the second order transfer behavior of this path in analogy with (4.14). At its natural frequency that coincides with the antiresonance of the transfer function from  $\tau_a$  to  $q_a$ , a resonance peak and a phase drop of  $180^\circ$  causing the disappearance of collocation can be observed. The first eigenvector of the SEA case is  $u_1 = [0.77 \quad 1]^T$  and shows that both inertias move in phase, as both vector elements have the same sign. The motions of  $q_l$  are amplified by the factor 0.77 compared to those of  $q_a$ . The second eigenvector is  $[-1.58 \quad 1]^T$ , which shows that the inertias are moving in antiphase, as the factor  $-1.58$  that amplifies link motion is negative. Results regarding both modes comply with those given in [55].

## 4.2.2 Power consumption analysis

The average power consumptions of the investigated actuator-elasticity configurations calculated from inverse dynamics simulation are presented subsequently. In the depicted plots, the power required for direct actuation is always given by a dashed black border for comparison. Both power consumption measures introduced in Section 4.1.4 are evaluated for the basic and advanced models. Powers calculated using the basic models are shown in grey, while those based on the advanced models are given in black. Further, the relations between power consumption and natural dynamics are analyzed based on the comparison of natural frequencies as functions of stiffness values to the contour plots of power consumptions.

In Figure 4.8, the average power consumptions of the serial and parallel elastic actuation considering that energy is not recuperated are plotted against the investigated frequencies and varying stiffness. For series elastic actuation, just one area of minimal power consumption can be observed investigating the basic model shown by the grey surface. Compared to the consumption of direct actuation, power consumption is distinctly decreased in this area and for combinations of higher stiffness and lower frequency that occur right of it. When considering advanced modeling, this area can be observed again. Yet, two additional areas of minimal power consumption appear: One at below 1.0 Hz that is nearly independent to stiffness variation and one left to the original one, which is very sensitive to stiffness variation. Further, the power-optimized range of operation is not located below

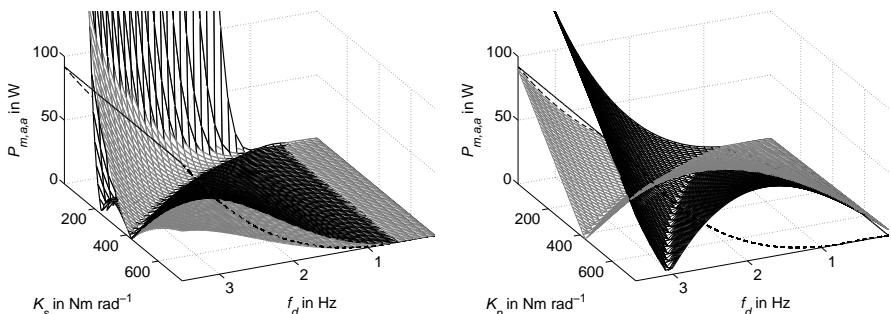


Figure 4.8: Average power consumption  $P_{m,a,a}$  for sinusoidal trajectory and considering no recuperation: SEA (left), PEA (right) and DA (dash-dotted border, both). Results shown in grey are calculated from basic models and such in black from advanced models.

the original minimum but around it at higher frequencies. Since power consumption is generally low at operational frequencies below 1.0 Hz, utilizing the power minimum located there is not suitable for optimizing power consumption by means of stiffness variation. In contrast to this, selecting stiffness to match the middle and left area will distinctly decrease power consumption. Further, those two areas cover widely across the operating range when stiffness is varied without exploiting the investigated stiffness interval. Both, the decrease of required power and the stiffness sensitivity suggests the utilization of those two areas for power-optimized operation. The results for parallel elastic actuation without energy recuperation are depicted right in Figure 4.8. Irrespective of considering actuator inertia in the models, only one power minimum is observed. Using the advanced model, this area is found at lower frequencies and higher stiffness values, respectively. In that case, the operational frequency range is not covered completely, as no power minima are found above approximately 3 Hz, and thus the interval of stiffness variation would have to be increased to suit the required range.

Figure 4.9 shows power consumption plots in analogy to the previous ones but includes energy recuperation as well as actuator and transmission efficiencies. In both, serial and parallel elastic actuation, no fundamental changes are observed, as the global characteristics and the particular areas of low power consumption remain. Hence, recuperation and efficiencies do not need to be considered for determining power-optimized combinations of operational frequency and stiffness. Due to recuperation, average power consumption lies at a generally lower level. A

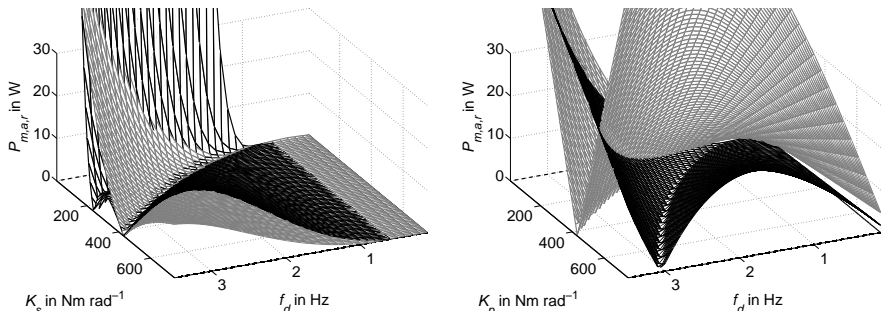


Figure 4.9: Average power consumption  $P_{m,a,r}$  for sinusoidal trajectory and considering recuperation and efficiencies: SEA (left), PEA (right) and DA (dash-dotted border, both). Results shown in grey are calculated from basic models and such in black from advanced models.

remarkable distinction compared to the previously given results can be seen for direct actuation, which hardly consumes any power. This is due to the sinusoidal reference trajectory that allows for nearly perfect energy recuperation, as energy is only lost due to actuator and transmission efficiencies. Although this seems to be promising, the higher required drive peak power does not change and hence a heavier actuator resulting in additionally increasing requirements would have to be selected. Further, non-sinusoidal trajectories will not show such beneficial results. Due to this and further unmodeled losses, peak power and energy consumption would be affected in practical implementations and thus the suitability for the application in prosthetics.

Investigating the influence of stiffness variation on natural dynamics and comparing it with power consumption is crucial for power-optimized actuator design and deducting corresponding stiffness selection strategies as shown in [17, 16]. Therefore, natural and antiresonance modes are determined by calculating the poles and zeros of the linearized transfer functions given in Section 4.1.3 for varying stiffness. Figure 4.10 compares the natural modes of the advanced models of serial and parallel elastic actuation with the corresponding average consumed mechanical powers  $P_{m,a,a}$  excluding recuperation and efficiencies. Regarding serial elastic actuation, the first elastic natural frequency plotted as a solid black line describes the power minimal area that is located rightmost in Figure 4.8 and Figure 4.9. In contrast to this, the second elastic mode given by the dashed black line is causing the leftmost power minimal area in Figure 4.8 and Figure 4.9. While the first natu-

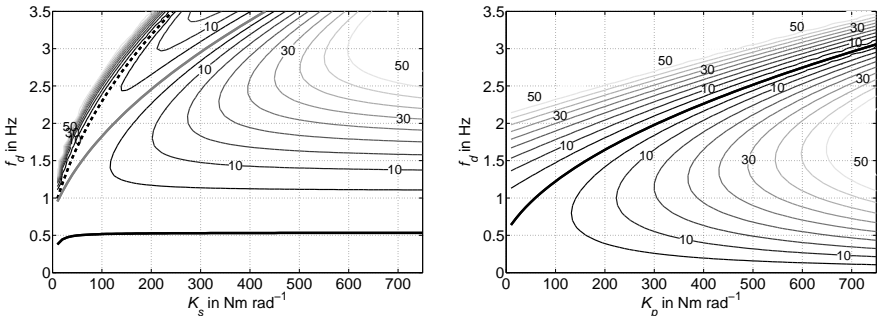


Figure 4.10: First (black, solid), second (black, dashed) natural and antiresonance (grey) frequencies in comparison with power contour plots for sinusoidal trajectory considering advanced models (isolines in W, no recuperation): SEA (left) and PEA (right).

ral frequency is influenced weakly by stiffness variation, the second one is distinctly sensitive to stiffness adjustment. In both cases, power consumption is getting minimal due to the very low torque requirements. Further, the antiresonance that is due to the zero in (4.10) is depicted by the solid grey line. It corresponds to the middle power minimal area that is caused by the small motions  $q_a$  and thus velocities  $\dot{q}_a$  of  $I_a$ . It can be manipulated well by stiffness adjustment and does only depend on the link properties. The corresponding power minimum hence ideally agrees with the one of the basic model observable in Figures 4.8 and 4.9, as this neglects actuator dynamics and thus only considers link dynamics in analogy. This accordance further explains why power-optimized stiffness values are found with both model types. Anyhow, considering the advanced model leads to more versatile possibilities to adapt stiffness according to natural frequencies and antiresonances. Considering parallel elastic actuation presented in the right part of Figure 4.10, only one natural frequency is occurring that explains the power minimal area with a lower value due to the higher inertia. Despite the trajectories exceed the range of the small-angle approximation distinctly, the modes from the linear transfer functions show good concordance with the power minima from nonlinear inverse dynamics simulation in all plots. Hence, the approximation of the nonlinear dynamics by the natural behavior of the linearized models is assessed to be appropriate.

The power consumptions during performing the dual-sine trajectory considering recuperations and efficiencies are given in Figure 4.11. For SEA, which is given on the left, the global behavior is close to that obtained with the sinusoidal trajectory

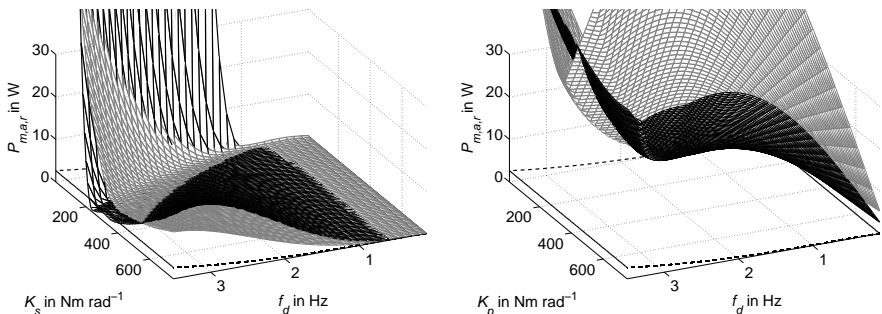


Figure 4.11: Average power consumption  $P_{m,a,r}$  for dual-sine trajectory and considering recuperation and efficiencies: SEA (left), PEA (right) and DA (dash-dotted border). Results shown in grey are calculated from basic models and such in black from advanced models.

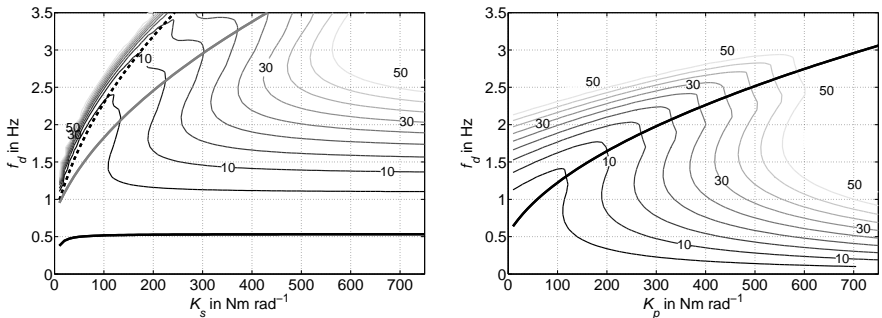


Figure 4.12: Natural frequencies in comparison with power contour plots for dual-sine trajectory considering advanced models (isolines in W, no recuperation): SEA (left) and PEA (right).

given left in Figure 4.9. Yet, the power minimal areas are less pronounced and the advanced model shows significantly reduced power consumption in the antiresonance case compared to the basic model. Further, the power required for direct actuation is higher than the one calculated for the advanced SEA model. This substantiates the possibilities to decrease power consumption with SEA and its potential in prosthetic application. The results obtained with PEA models are shown right in Figure 4.11. Although the global characteristics remain as in SEA, the level of power consumption is distinctly increased in comparison to the sinusoidal trajectory. In this case, the parallel elasticity works against link motions with a frequency that it is not adjusted to and thus increases required power. A comparison of the power contour plots obtained investigating the dual-sine trajectory without recuperation to the natural frequencies of the advanced models is given in Figure 4.12. The results for both, SEA and PEA, show that power minima and natural frequencies are fundamentally matching. Yet, a slight shift to higher frequencies can be seen regarding antiresonance, while the power minimal area connected to the second natural frequency is observed at slightly lower frequencies.

The required peak actuator torques  $\tau_a$  of SEA and PEA for dual-sine trajectories are given in the characteristic map in Figure 4.13. From the left plot, it becomes obvious that torque requirements are minimal for the first and second natural frequency in SEA. In antiresonance mode power is low due to the minimal motion of the drive. Considering the torque requirements in the PEA shown right in Figure 4.13, one can see that those are minimal at the natural frequency of the system. Yet, power requirements in this area are distinctly higher than in the minimum of

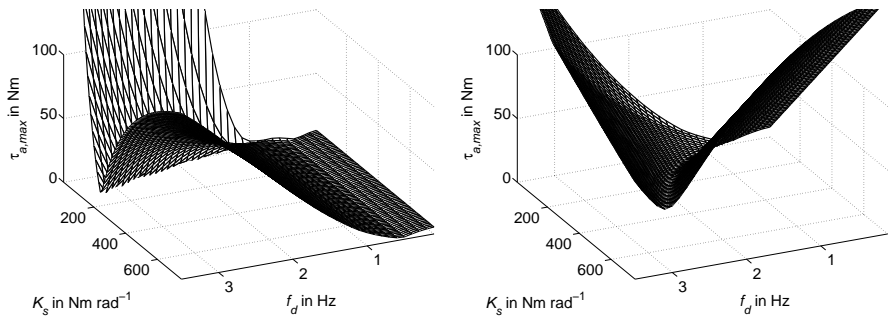


Figure 4.13: Maximum actuator torque  $\tau_a$  of SEA (left) and PEA (right) for dual sine case.

the SEA. This is due to the negative impact of the parallel elasticity, if trajectory comprises frequencies that the system is not optimized for.

#### 4.2.3 Experimental evaluation

The results of the experimental evaluation of stiffness properties are presented in Figure 4.14. On the left, the regression of torque-deflection-characteristics for different active lengths  $q_s$  is shown. In this, measured data is indicated by grey plus signs, circles, stars and squares in repetition. Those indicate the different active lengths according to the counter bearing positions  $q_s$  increasing clockwise. The black lines show the results of linear regressions of the data points for different active lengths  $q_s$ . The slopes of the linear regressions represent the current stiffness  $K_{s,e}$  and decrease with increasing active lengths  $q_s$ . This basically complies to the analytical behavior in (4.25). Further, the assumption that stiffness  $K_{s,e}$  is linear with respect to the position difference  $q_a - q_l$  is confirmed due to the good accordance of measured data and regression results. In the right part of Figure 4.14, a spline extrapolation of the stiffness characteristics  $K_{s,e}(q_s)$  is plotted versus the counter bearing position  $q_s$  in comparison with the analytical solution according to (4.25). The experimentally determined characteristics given by the black line show the same global behavior as the analytical one depicted in grey. A bar plot below the characteristics shows the relative error (rel. error) between experimentally and analytically determined stiffness values. For stiffness values below  $200 \text{ Nm rad}^{-1}$ , this relative error is below 10 % as indicated by the grey line. Above  $200 \text{ Nm rad}^{-1}$ , the relative error increases, since the stiffness determined experimentally is distinctly lower than the analytic prediction. This might

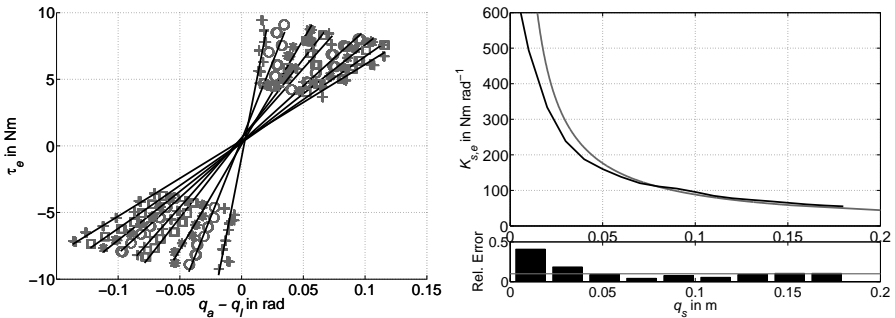


Figure 4.14: Experimental evaluation of the elastic element: Regression of torque-deflection characteristics for different active lengths  $q_s$  (left). Comparison of analytically calculated stiffness  $K_{s,e}(q_s)$  (grey) and experimentally determined stiffness  $K_{s,e}(q_s)$  (black, Spline extrapolation) characteristics with relative error over active length  $q_s$  (right).

be due to not ideally rigid components of the drive train that were not modeled in terms of stiffness in contrast to coupling and gear box. Despite these deviations, the maximum required stiffness  $350 \text{ Nm rad}^{-1}$  is covered by the elastic element, while the lowest possible value is extrapolated to be  $55.02 \text{ Nm rad}^{-1}$  at  $0.18 \text{ m}$  and hence slightly above the required value  $50 \text{ Nm rad}^{-1}$  at  $0.176 \text{ m}$ . This limitation remains, when considering the stiffness  $K_{s,cg}$ , as the lowest possible value of the global stiffness  $K_s$  reduces to  $54.84 \text{ Nm rad}^{-1}$ . Due to the results, (4.27) shows to be suitable for the design of elastic elements in VTS. To match the requirements more accurate, unmodeled elasticities in the drive train should be explored. Further, the geometry of the elastic element can be simplified based on the adapted design equations presented in [194].

The limitations of the operating range in the experiments according to the criteria stated before are depicted in Figure 4.15. To avoid structural damage of the elastic element during dynamical operation, power analysis experiments are performed with a reduced amplitude of  $\hat{q}_l = 5^\circ$  to ensure that the critical elastic torque  $\tau_{e,max}$  is not exceeded (compare torque-isolines in Figure 4.15). Beyond this, the second natural frequency (dashed black line) should not be surpassed distinctly to keep within the stability region of control. Corresponding results for dual-sine trajectories, which are subject to the remainder of this thesis, are given right in Figure 4.15. These comply with those of the sine case, while the torque levels are increased due to the superposition of two frequency components with amplitudes of  $\hat{q}_l = 5^\circ$  and  $\frac{1}{2}\hat{q}_l$ .

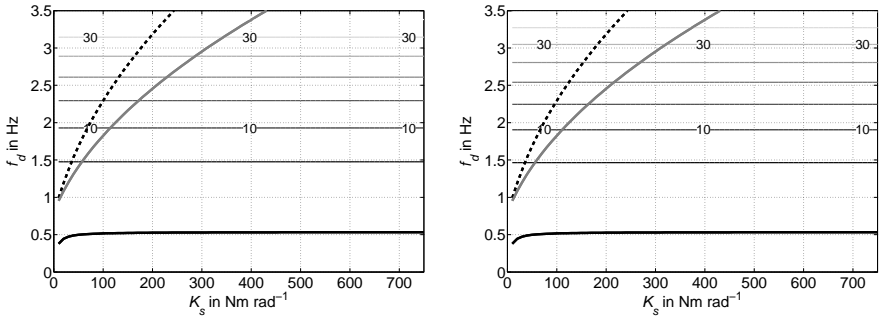


Figure 4.15: Contour plots of elastic torque  $\tau_e$  (isolines in Nm) for amplitudes of  $\dot{q}_l = 5^\circ$  compared with natural frequencies: SEA with sine trajectory (left) and dual-sine (right).

The results for tracking chirp trajectories to determine the frequency ranges to be investigated in power analysis are given in Figure 4.16. Those obtained for a stiffness of  $75 \text{ Nm rad}^{-1}$  are shown left, while the results for  $150 \text{ Nm rad}^{-1}$  are depicted right. The particular plots show positions, torques and powers during the chirp trajectories, which are ranging  $0.2 - 2.8 \text{ Hz}$  and  $0.2 - 3.1 \text{ Hz}$  in  $120 \text{ s}$ . In those, focus is set to the envelopes of the signals, as those describe global behavior.

Comparing the positions of link (black) and actuator (grey) in the left part of Figure 4.16, one can see that minimum actuator motion is required around  $1.85 \text{ Hz}$ . This corresponds to the behavior predicted for operation with the antiresonance frequency in Section 4.2.1. Hence, it is concluded that antiresonance shows to be shifted compared to the value of  $1.63 \text{ Hz}$  obtained from the model. Due to this, power consumption is also minimal at this frequency but at  $1.85 \text{ Hz}$ . Considering the measured torques, a steady increase followed by a local minimum at about  $2.10 \text{ Hz}$  can be seen. Thus, the second natural frequency seems to be shifted from  $2.01 \text{ Hz}$  to  $2.10 \text{ Hz}$ . In contrast to the simulation results, no distinct minimum is observed in power consumption, since unmodeled friction keeps the torque at a certain level even for operation in the natural modes. Further, the proximity to antiresonance might weaken the visibility in the experimental results. Reconsidering the measured torques, one can see that the torque limit is reached at about  $2.30 \text{ Hz}$ . Hence, motion tracking accuracy decreases and power consumption is reduced.

In the results for the chirp trajectory and a stiffness of  $150 \text{ Nm rad}^{-1}$  given right in Figure 4.16 a similar behavior is observed at different frequencies due to the modified stiffness. Antiresonance is found at about  $2.37 \text{ Hz}$  instead of  $2.16 \text{ Hz}$ .

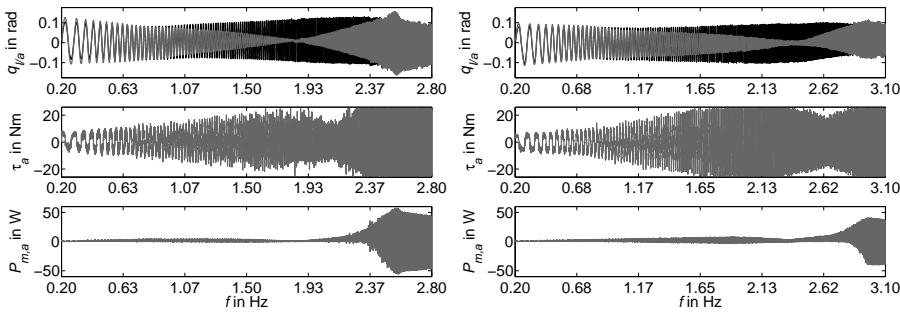


Figure 4.16: Positions, torques and powers during chirp trajectories (link - black, actuator - grey): Left, stiffness is  $75 \text{ Nm rad}^{-1}$  and frequencies range from  $0.2 - 2.8 \text{ Hz}$  in  $120 \text{ s}$ . Right, stiffness is  $150 \text{ Nm rad}^{-1}$  and frequencies are ranging  $0.2 - 3.1 \text{ Hz}$  in  $120 \text{ s}$ .

which is predicted by the model. The torque minimum due to the second natural frequency indicates that the latter one is reduced to  $2.64 \text{ Hz}$  from  $2.77 \text{ Hz}$ . Further, the torque threshold is reached for a certain time before surpassing antiresonance. Torque finally stays at its limitation for frequencies above  $2.83 \text{ Hz}$  leading to reduced tracking accuracy.

Due to the results obtained considering the chirp trajectories, the frequencies of the sinusoidal trajectories are specified to enable a more detailed investigation of the natural dynamics. Experiments for a stiffness of  $75 \text{ Nm rad}^{-1}$  are performed for frequencies ranging  $1.5 - 2.2 \text{ Hz}$  and those for a stiffness of  $150 \text{ Nm rad}^{-1}$  at  $2.0 - 2.7 \text{ Hz}$  in steps of  $0.1 \text{ Hz}$ . Figure 4.17 and Figure 4.18 present the positions, torques and powers obtained during  $3.0 \text{ s}$  of the experiments regarding sinusoidal trajectories and a stiffness of  $75 \text{ Nm rad}^{-1}$ . In both, frequency increases line-by-line from the upper left to the lower right plot. Black lines depict link data, while actuator measurements are shown in grey. In the position plots, desired trajectories of link and actuator are given as dashed lines with the corresponding colors. Those of the actuator are calculated by solving the inverse dynamics problem. When focusing on the global development of the resulting powers, it is observed that power consumption varies significantly with frequency: Peak powers required to track the periodic trajectory decreases from values of about  $4 \text{ W}$  at  $1.5 \text{ Hz}$  to such slightly above  $1 \text{ W}$  at  $1.8 \text{ Hz}$  and about  $0.8 \text{ W}$  at  $1.9 \text{ Hz}$ . This complies with the observation that antiresonance occurs at  $1.85 \text{ Hz}$  due to model uncertainties from the chirp experiment. Comparing actuator positions  $q_a$  and link positions  $q_l$ , one can see that

those change to antiphase relative motion between 1.7 Hz and 2.0 Hz. Despite the shifted frequency, this complies with the transfer behavior between those positions that is shown in Section 4.2.1. In Figure 4.7, an immediate phase drop of 180° occurring with antiresonance is seen and thus a delay of a half period between the position signals is expected for frequencies beyond it. Yet, the phase drop is distributed across a range of 1.7 – 2.0 Hz in the experimental results due to the influence of friction and damping [141]. Beyond antiresonance, power requirements are increasing steadily and reach a level of around 5 W at 2.2 Hz in the lower right plot of Figure 4.18. Comparing these results to the mechanical power requirements of direct actuation determined by inverse dynamics simulation shows the potential of the series elastic drive train. In direct actuation, peak powers of 1.37 W, 3.19 W and 5.23 W are required for operation at 1.5 Hz, 1.9 Hz and 2.2 Hz. Hence, the

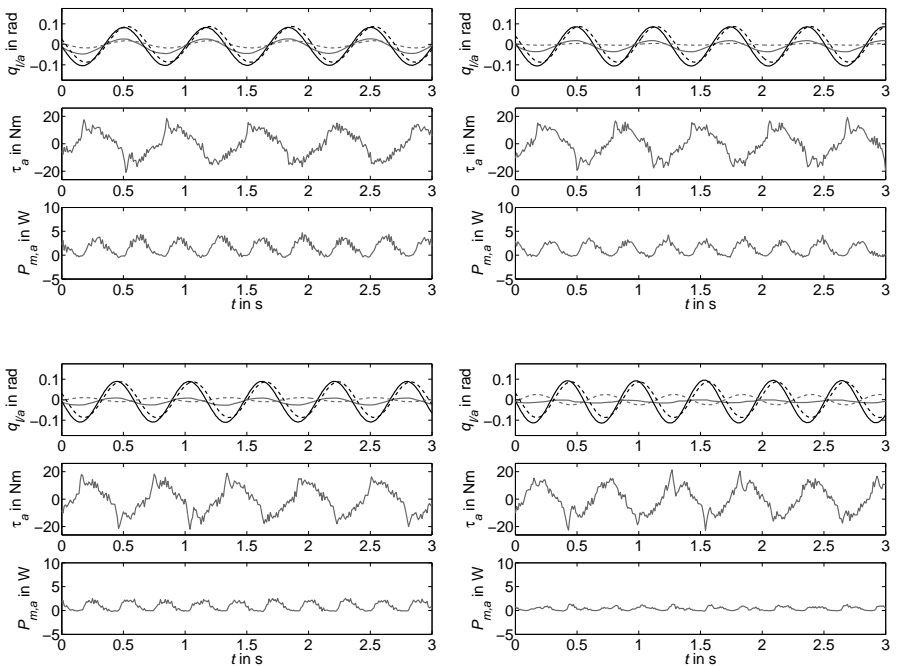


Figure 4.17: Sinus positions, torques and powers (link - black, actuator - grey, desired - dashed). Stiffness is  $75 \text{ Nm rad}^{-1}$  and frequency is 1.5 – 1.8 Hz (upper left to lower right).

actuator shows distinctly lower power consumption during experimental operation in the antiresonance than the theoretical value from inverse dynamics simulation of direct actuation. This further applies for stiffness values deviating slightly from the optimal one, since power requirements are low in a certain range around antiresonance as shown left in Figure 4.9 for instance. The second natural frequency predicted to be 2.01 Hz, is not observed distinctly in Figure 4.17 and Figure 4.18 as in the chirp experiment.

Experimental results considering a drive train stiffness of  $150 \text{ Nm rad}^{-1}$  are shown in Figure 4.19. According to (4.13) and (4.12), antiresonance and second natural frequency are expected to be at 2.16 Hz and 2.77 Hz, respectively. Yet, they are found at about 2.37 Hz and 2.64 Hz in the experiments with the chirp trajectory. This is confirmed by the results, as minimum motion and peak power of

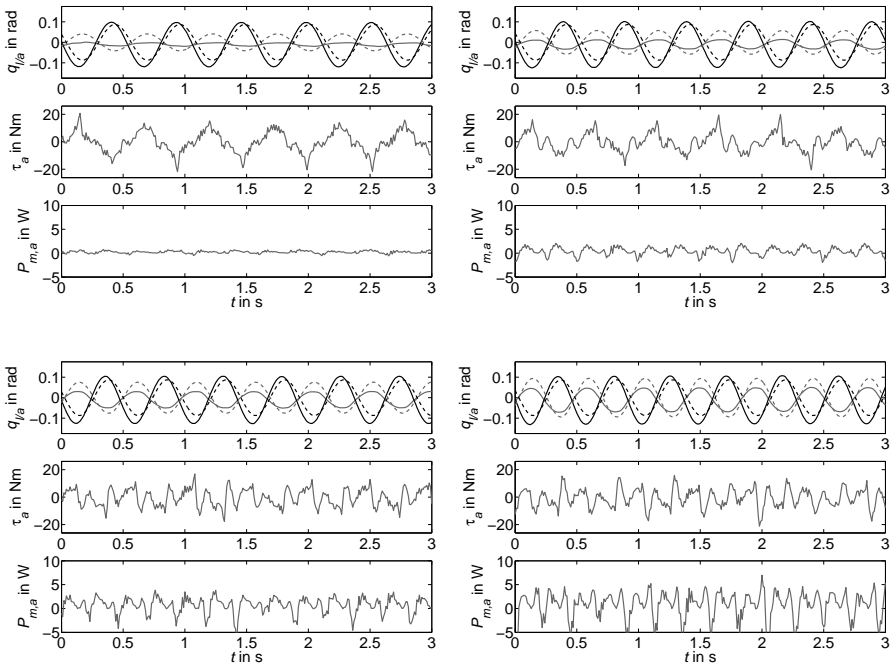


Figure 4.18: Sinus positions, torques and powers (link - black, actuator - grey, desired - dashed). Stiffness is  $75 \text{ Nm rad}^{-1}$  and frequency is  $1.9 - 2.2 \text{ Hz}$  (upper left to lower right).

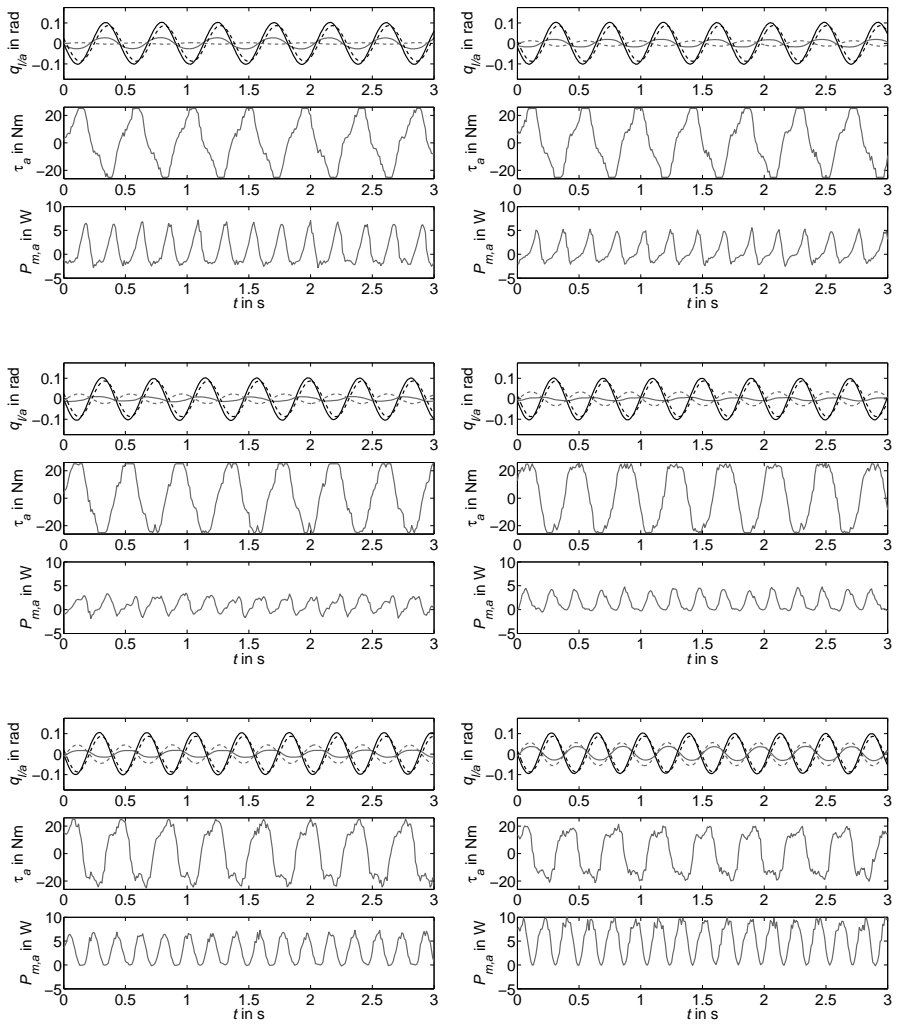


Figure 4.19: Sinus positions, torques and powers (link - black, actuator - grey, desired - dashed). Stiffness is  $150 \text{ Nm rad}^{-1}$  and frequency is  $2.2 - 2.7 \text{ Hz}$  (upper left to lower right).

---

below 3.5 W is seen for 2.4 Hz, while torques are minimal at about 2.7 Hz. Mechanical peak powers for operation at 2.2 Hz and 2.7 Hz, are found to be higher than 7 W and 10 W, respectively. Thus, the suitability of the SEA setup to reduce power consumption can be seen here as well, since peak powers of 5.23 W, 6.96 W and 10.16 W are predicted for direct actuation at 2.2 Hz, 2.4 Hz and 2.7 Hz. Considering the results presented in Figure 4.19, it becomes distinct that tracking performance is comparable to the results obtained for setting stiffness to  $75 \text{ Nm rad}^{-1}$ . Yet, as for the chirp trajectory, the torque limit is reached at 2.1 – 2.5 Hz. The phase shift of antiresonance is observed between 2.2 Hz and 2.6 Hz and the corresponding power minimum is found at 2.4 Hz in analogy to the chirp examinations.

In addition to deviations of the natural and antiresonance modes, the effect of model uncertainties can be observed in the control performance as well. The upper plots in Figure 4.16 show that link side position amplitudes are not kept ideally constant as required by the trajectory. As shown in Figure 4.17, Figure 4.18, and Figure 4.19, tracking is rather accurate with respect to phase. This is concluded to be due to deviations between the model used for feedback linearization control and the prototype plant, as the uncertain model parameters influence the global gain of the controller. Anyhow, control performance is assessed to be appropriate considering the high requirements of operating the system in or close to its natural frequencies and antiresonances. Despite the thorough determination of inertial, mass and stiffness parameters in [58], remaining uncertainties seem to cause these deviations. A major issue is found in the counter bearing position that determines stiffness, since it is manually set considering a scale that was defined before the stiffness adjustment mechanism was installed. Thus, uncertainties like stiffness offsets that would influence the natural behavior are probable. Further, effective stiffness varies throughout a trajectory period, as the nonlinear impact of gravitation depends on the pendulum position. Other effects leading to a deviating behavior of the prototype are damping and friction that shows similar influence as damping. Both are not considered in the models based on (4.6) and friction cannot be assumed to be compensated ideally by the algorithm discussed in [58, 59].

Beyond this, the link velocity signals obtained by an incremental encoder affect control performance due to its limited resolution. The effect of the resulting discontinuities in the velocity signals is observed in the motor torques that are calculated by the controller based on the positions and velocities. Instead of smooth torques generating the sinusoidal motions under ideal circumstances assumed in analytical calculation, those are superimposed with periodic and discontinuous parts. This is also due to the compensation torque added to remove friction effects by feed-forward compensation, which itself again relies on the velocity signals. Another deviation from the ideal periodic sinus is seen in the power consumption plots in

---

Figure 4.17 and 4.18. The powers are mostly positive, while positive and negative powers should have equal shares in an ideal sinus. This is caused by the compensation of Coulomb friction, which adds a constant torque with the sign of the direction of motion to the control torque. The power resulting from this part of the torque is thus always positive and causes the offset of the torque signal, as the torque level does not change significantly at 2.1 Hz.

---

### 4.3 Conclusion

---

The detailed theoretical investigation of the natural dynamics of different actuator-elasticity configurations shows the potential of exploiting natural dynamics of the drive train and its load. Therefore, the consideration of the transfer paths of serial and parallel actuation by means of linearized models gives insights in the impact of particular mechanical effects like inertias and gravitation. Gravity has the effect of a virtual fixation, as it introduces a nonlinear restoring torque to the system. Due to this and the two inertias of actuator and link, two natural frequencies and an antiresonance mode occur. In basic models that neglect actuator inertia, only one natural frequency equaling the antiresonance mode of the advanced model is found, as the latter mode only depends on the link dynamics. The antiresonance is further of importance for control design, since it determines the collocation limit that marks the transition between inphase and antiphase motion of the inertias and thus the stability limit of non-model-based controllers. Hence, considering both inertias of the system is beneficial for a detailed assessment of mechanical power reduction and from a control perspective.

Deeper insight to the power consumption of the actuator-elasticity configurations is acquired by inverse dynamics simulations using nonlinear models. A comparison of the results of those to the natural dynamics calculated from linearized models shows good accordance of both despite the linearization. As an energy measure, average mechanical power consumption is determined in several manifestations. On the one hand, the effects of efficiencies and energy recuperation are examined. On the other hand, the impact of considering and neglection of the actuator inertia is investigated. Regarding the actuator-elasticity configurations, series elastic actuation shows significantly lower power consumption than direct actuation over a wide frequency-stiffness range irrespective of the considered model. Investigating the advanced model, two power minima are found in addition to the one observed with the basic model. The resulting three minima are due to the first and second natural frequency as well as the antiresonance. The antiresonance frequency of the advanced model equals the single natural frequency of the basic one, as it only depends on the link dynamics. In terms of stiffness variation, antiresonance and the

---

second natural frequency show to be sensitive and thus promising for an adaptation of natural dynamics. As serial elastic actuation, parallel elastic one is also able to decrease power consumption distinctly. Yet, only one natural frequency occurs, since both inertias are coupled rigidly if actuator inertia is considered. Further, power consumption is not as low as for SEA, if the task contains frequencies that do not correspond to the natural behavior of the drive train.

Taking into account the influence of actuator-transmission efficiencies and energy recuperation, the global characteristics of average power consumption remain. Thus, it is not necessary to consider those when designing or controlling the stiffness of an actuation system with respect to exploitation of natural dynamics causing the power minima. Yet, energy recuperation reduces the level of power consumption significantly and thus shows high potential for increasing energy efficiency in prosthetic applications. Considering recuperation, average power consumptions close to zero are obtained for direct actuation in sinusoidal motion. Anyhow, those will not occur in practical application due to conversion losses and unmodeled effects like damping and friction. Further, purely sinusoidal motions will not occur in prosthetic application. Hence, the average power consumptions determined for dual-sine trajectories are considered as an example that is closer to application [230]. The results show the same global characteristics and especially minima due to natural and antiresonance frequencies as for sinusoidal trajectories. Yet, it can be seen that serial elastic actuation is beneficial compared to direct actuation when considering efficiencies and recuperation in this case, while parallel elastic actuation is not.

Based on these results, series elastic actuation is assessed to be the more promising technology for prosthetic applications. It shows superior reduction of power consumption in non-sinusoidal tasks and an increased versatility due to the higher number of modes available for stiffness adjustment. Further, it is advantageous with respect to security and human-robot interaction as described in Chapter 2. The reasons of the power minima that are found for SEA can be understood by considering natural dynamics analysis: Minimal actuator motion appears in antiresonance, while minimal actuator torque is required in both natural frequencies. As the product of those determines the mechanical power consumption of the actuator, it shows locally minimal values in both cases as well. Due to setting the focus on reducing mechanical power, electrical losses in the actuation system are not considered and might change the results. Such depend on the electrical actuator current  $i_a$  and thus its mechanical torque  $\tau_a$  [159]. For operation in antiresonance the torque  $\tau_a$  is only slightly higher than the one of direct actuation, while it is significantly lower in the natural frequencies. Hence, the fundamental results obtained here should be robust against considering or neglecting electrical losses.

An experimental evaluation is performed to investigate the effects observed regarding power consumption and natural dynamics in a real application. Therefore, a prototypic implementation of variable torsion stiffness according to [17] is utilized. The serial elastic drive train is controlled by feedback linearization in combination with a friction compensator. Serial stiffness can be varied by changing the active length of the torsional elastic element incorporated in the drive train. The implementation of the elastic element is examined in a static experiment, while dynamic operation is considered to analyze power consumption. In both a pendulum load corresponding to the one considered in the previous simulations is driven by the VTS drive train. The determined stiffness characteristics estimated by least squares regression based on results from static measurements show good accordance with hyperbolic characteristics that are predicted analytically. Further, if a specific stiffness is set, the elastic element act like a linear, torsional spring. Experimental examinations of power consumption with the prototype indicate a shift of natural and antiresonance frequencies compared to the model. Those are concluded to be due to model uncertainties and non-ideal friction compensation and are observed in both considered types of trajectories. Anyhow, the functional aspects of the elastic drive train can be investigated due to the sufficient accuracy and high performance of the model-based controller. The experiments with sinusoidal trajectories substantiate the feasibility of setting stiffness to the antiresonance frequency for power optimization in the prototype. Along with this, the transition from inphase to antiphase relative motion between actuator and link inertia can be observed as predicted by the advanced model. Yet, the manifestation of the two natural frequencies themselves as well as their impact on power consumption are not as distinct as expected. Hence, they are less feasible for stiffness selection in this specific practical application.



---

## 5 Variable stiffness control exploiting natural dynamics

---

As described in Chapter 2 and Chapter 4, variable stiffness actuation can be beneficial from the perspective of the user and in terms of energy efficiency. Regarding energy issues in prosthetics, the variation of stiffness can be utilized to optimize efficiency depending on body mass [96] or gait velocity [80, 79]. Beyond tuning the drive train to a power-optimized operation point minimizing actuator requirements, it can increase the acceptance by the user, e. g., by improving *Functionality*. Referring to [242], controlling stiffness helps for adaptation to “different activities or walking speeds and for rejecting unexpected disturbances“, which is beneficial in terms of functionality. Hence, finding appropriate strategies to control variable stiffness in a way to utilize the natural dynamics of elastic actuation best is an important issue in general and for the application in prosthetics.

The variable stiffness control strategy proposed by the author of this thesis suits variable stiffness actuators in general but is specifically applied for the example of variable torsion stiffness [13]. By identifying the frequency component with major power consumption from the trajectory, stiffness can be adjusted to match a natural mode or antiresonance to the specific task. Therefore, stiffness adjustment laws to exploit resonance and antiresonance effects are derived based on the linearized models from Chapter 4. Forward dynamics simulations using coupled models of the pendulum and the stiffness adjustment mechanism are used to investigate overall power consumption. Aiming at lower limb prosthetic applications, those simulations provide indications on the power share of the two actuators driving the pendulum and varying stiffness. These first results on power required for adjustment allow for an assessment of how frequent stiffness should be adapted. Experimental evaluations using the VTS prototype in analogy with the simulations are presented to validate those results. The feasibility of the overall strategy and its single components in lower limb prosthetics is addressed here but finally considered in the remainder of this thesis.

---

### 5.1 Methods

---

The methods utilized for the proposed variable stiffness control method are given subsequently. In this, the dynamics of the adjustment mechanism of VTS and its coupling with the pendulum are modeled by its equations of motion. Further methods comprise spectral analysis, the model-based stiffness adjustment laws, and feedback control of the adjustment mechanism. Finally, the forward dynamics

simulation and the experimental evaluation performed using the VTS prototype are explained.

### 5.1.1 Modeling of stiffness adjustment mechanism

According to the prototype shown in Figure 4.4, a mechanical model of the pendulum driven by the variable torsion stiffness actuator and incorporating the stiffness adjustment mechanism is given in Figure 5.1. It comprises the model of the elastic drive train with  $I_l$ ,  $m_l$  and  $I_a$  describing the inertial properties of the pendulum and actuator 1. Additionally, the reduced mass

$$m_s = i_{s,t}^2 I_{s,r} + i_{s,b}^2 I_{s,g} + i_{s,b}^2 I_{s,b} + m_{s,n}, \quad (5.1)$$

of the stiffness adjustment mechanism with respect to the counter bearing position  $q_s$  is modeled to consider its dynamical properties. It comprises the reflected rotor inertia  $i_{s,t}^2 I_{s,r}$  of actuator 2 as well as the mass of the nut  $m_{s,n}$  and the inertias of gear box  $i_{s,b}^2 I_{s,g}$  and ball-screw  $i_{s,b}^2 I_{s,b}$ . In those components, the combined transmission ratio of gear box and ball-screw is given by  $i_{s,t} = i_{s,g} i_{s,b}$ , while  $i_{s,b}$  denotes the transmission ratio of the ball-screw. These inertial parameters are given in Table 5.1. The adjustment mechanism is moved via the torque  $\tau_{s,m}$  of actuator 2 that is transformed into the force  $F_s = i_{s,t} \tau_{s,m}$  by gear box and ball-screw. Besides inertial effects, the main loads to be overcome by the drive to move the counter bearing are due to friction and subsumed by the force  $F_{s,f}$ . The corresponding Coulomb friction model according to [201] is given by

$$F_{s,f} = (\frac{\mu_{s,1}}{r_1} + \frac{\mu_{s,2}}{r_2}) |\tau_e| \text{sign}(\dot{q}_s). \quad (5.2)$$

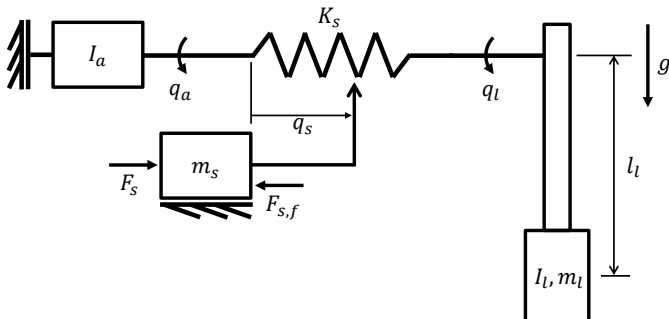


Figure 5.1: Mechanical model of the investigated pendulum incorporating rotational serial elastic actuation and stiffness adjustment.

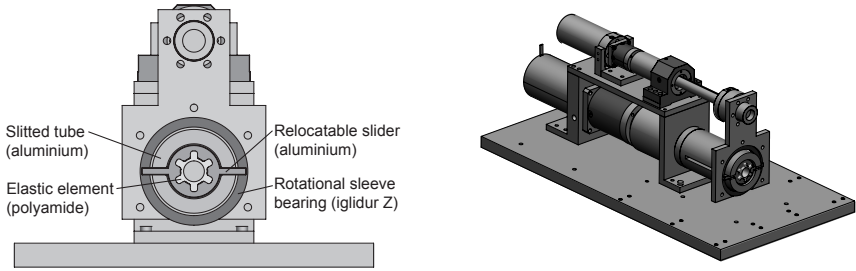


Figure 5.2: Sections of the variable torsion stiffness prototype: Elastic element in the middle. Surrounded by relocatable slider, aluminium tube and rotational sleeve bearing.

In this, friction effects at two contact surfaces shown in the section views given in Figure 5.2 are considered. The geometry of the contact between elastic element and the relocatable slider is characterized by the mean radius  $r_1$  of the surface with respect to the axis of rotation and a normal force of  $\frac{\tau_e}{r_1}$ . The mean radius  $r_2$  and normal force  $\frac{\tau_e}{r_2}$  describe the contact geometry of the relocatable slider and the slotted aluminium tube. Further, the friction coefficients are determined to be  $\mu_{s,1}$  and  $\mu_{s,2}$  based on (comparable) material combinations from [84]. The inner contact is a aluminium-polyamide combination and its friction coefficient is approximated by the value of a lubricated steel-polyamide combination. The value for the outer aluminium-aluminium contact is approximated as the mean of the range given for this material combination in [84]. The resulting friction parameters are given in Table 5.1 and represent a first approximation that might deviate distinctly from the real system. Anyhow, it should allow for a first assessment of the power requirements due to stiffness variation.

Based on this, the dynamics of stiffness adjustment are modeled by

$$m_s \ddot{q}_s = F_s - F_{s,f}. \quad (5.3)$$

As the friction force  $F_{s,f}$  depends on the torque  $\tau_e$  and thus the current drive train stiffness  $K_s$ , which is furthermore altered by the adjustment mechanism, the

Table 5.1: Inertial and friction parameters (param.) of the stiffness adjustment mechanism.

Param.	$I_{s,r}$	$I_{s,g}$	$I_{s,b}$	$m_{s,n}$	$i_{s,t}$	$i_{s,b}$	$\mu_{s,1}$	$\mu_{s,2}$	$r_1$	$r_2$
Value	$2.5 \cdot 10^{-5}$	$2.2 \cdot 10^{-6}$	$2.09 \cdot 10^{-5}$	2.23	4	628	0.1	0.375	0.014	0.029
Unit	$\text{kg m}^2$	$\text{kg m}^2$	$\text{kg m}^2$	kg	-	m	-	-	m	m

dynamics of both systems are coupled. Hence, motion control of the pendulum has to cope with the stiffness variation, while the stiffness controller has to overcome friction varying with stiffness and load.

### 5.1.2 Stiffness control strategy

The stiffness control strategy aims at exploiting natural dynamics based on adjustment of the drive train stiffness to the desired task and is proposed by the author of this thesis in [13]. A block diagram of the stiffness selection process is shown in Figure 5.3. By means of spectral analysis of the link trajectory  $q_{l,d}$ , which reflects the desired task to be fulfilled on the link side, a time-dependent approximation of the frequency component  $\omega_d$  which shows the maximum amplitude is determined. This component is assumed to have major impact on the power requirements in the considered time frame. Using  $\omega_d$ , stiffness is selected by adjustment laws initially introduced in [17] and described subsequently. With those, a stiffness  $K_{s,d}$  desired for heuristic power-optimization by matching natural dynamics and trajectory according to [172, 229] is calculated. This stiffness  $K_{s,d}$  is transformed to a desired active length or counter bearing position  $q_{s,d}$  considering the characteristics of the elastic element given in (4.25). The output of the algorithm represents a trajectory of the desired active length  $q_{s,d}$  with respect to time  $t$ . Yet, the calculated stiffness  $K_{s,d}$  corresponds to a constant stiffness of the trajectory throughout the considered time frame. Since the method is based on an analysis of the link trajectory  $q_{l,d}$  and does not require further information from the motion controller, it can be applied with several control methods. Beyond motion control techniques, this also comprises impedance control approaches that rely on desired motion trajectories [207, 201]. This is important for utilizing the method in a lower limb prosthesis, as impedance control is broadly used in this field [64, 215, 216, 217, 218, 128].

To approximate the frequency component  $\omega_d$  of the trajectory that is assumed to cause the major part of power consumption, a spectrogram of the desired link motion  $q_{l,d}$  is computed by short time Fourier transformation or a bank of Goertzel

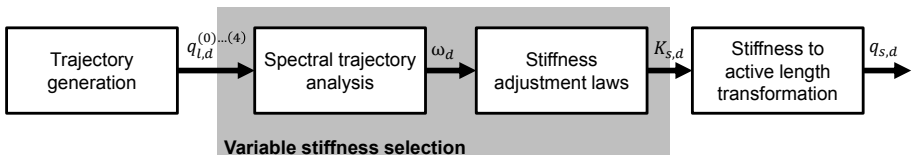


Figure 5.3: Block diagram of stiffness control strategy based on [13].

filters [160]. As those are available as ready-to-use tools in contemporary software packages, rather their use than their algorithmic implementation is presented in this thesis (considering [160] is recommended for more detailed information). The spectrogram gives the power spectral density  $S_{qq}(\omega)$  of the position trajectory  $q_l$ , which represents the power distribution of frequency components in the signal with respect to time [108]. From this, the frequency  $\omega_d$  showing the highest power share in the signal is determined. To achieve sufficient accuracy, leakage errors have to be minimized by applying an appropriate window function [160]. Further, a suitable number of samples investigated as a time segment as well as the examined frequency interval and discretization have to be selected for the spectrogram [160].

With the insights from power analysis given in Section 4.2.2 and the equations from Section 4.1.3, stiffness values optimizing power consumption of the variable torsion stiffness prototype can be derived analytically from the linearized transfer functions of SEA. Considering the advanced model, one approach to minimize power consumption is matching the antiresonance  $\omega_{s,a}$ . Thus, stiffness adjustment can be performed by

$$K_{s,a}(\omega_d) = I_l \omega_d^2 - m_l g l_l , \quad (5.4)$$

that is obtained by reformulating (4.13). Beyond this, the advanced model further facilitates selecting stiffness according to the second natural frequency  $\omega_{n2,a}$  described by (4.12) resulting in the adjustment law

$$K_{s,n2}(\omega) = -\frac{I_a I_l \omega_d^4 - I_a m_l g l_l \omega_d^2}{-(I_l + I_a) \omega_d^2 + m_l g l_l} . \quad (5.5)$$

Additionally, it becomes possible to tune the drive train considering both, the second natural or the antiresonance frequency, depending on the requirements of the current task. Anyhow, switching frequently between the two areas should be avoided, as non-power-optimal areas have to be passed and thus power consumption might stay equal or even be increased. To set the resulting desired stiffness  $K_{s,d}$  to equal either  $K_{s,a}$  or  $K_{s,n2}$  with actuator 2, those values are transformed into an active length  $q_{s,d}$  by means of the characteristics of the elastic element using (4.25). Rearranging the dependency of drive train stiffness and active length yields the transformation of stiffness values  $K_{s,d}$  to active lengths

$$q_{s,d}(K_{s,d}) = \frac{\Gamma I_t}{K_{s,d}} , \quad (5.6)$$

where  $I_t = 6.3 \cdot 10^8 \text{ N m}^{-2}$ . The trajectory of the desired active length  $q_{s,d}$  is forwarded to a feedback-controller commanding actuator 2 to track it by setting the corresponding counter bearing position.

---

### 5.1.3 Forward dynamics simulation

---

To investigate the dynamical effects of the proposed stiffness control strategy considering the pendulum setup, forward dynamics simulations are performed. In those, the model of the series elastic drive train (4.6) and the stiffness adjustment mechanism (5.3) are combined according to Figure 5.1. For the control of pendulum and adjustment mechanism, stiffness-adapted feedback linearization as presented in Section 4.1.5 and the stiffness control strategy described previously are utilized.

The spectrogram of the trajectory is calculated with a bank of Goertzel filters for a frequency range of  $0.0 - 5.0$  Hz with a frequency difference of 0.1 Hz between the filters. The time segment length of the Goertzel filters is set to 16,384 samples corresponding to 1.64 s and windowed with a 16,384-point Kaiser window with a sidelobe attenuation of 0.5. To set the desired stiffness values calculated with (5.4) or (5.5), those are transformed using (5.6). As this simulation is performed to analyze the basic effects of the variable control strategy and the link position trajectories  $q_l$  are defined previously, the whole calculation of the desired stiffness values  $K_{s,d}$  is performed before the simulation. To cope with missing values of the desired frequency  $\omega_d$  before the spectral analysis of the first time segment is finished, the stiffness values  $K_{s,d}$  resulting from the first segment is extrapolated constantly to  $t = 0$  s. Missing values during the last time segment, which are due to the usage of the Goertzel algorithm that updates every 1.64 s, are extrapolated linearly from the previous trend. To further provide a stiffness value  $K_{s,d}$  during every time step and to smoothen the trajectory, the extrapolated vector is mapped to the time vector using cubic interpolation. For tracking those trajectories by the adjustment mechanism, a computed-torque-type controller [116] is combined with a friction compensation term. The control law calculating the force  $F_s$  ensuring appropriate stiffness adjustment in the real system is given by

$$F_s = m_s \left( \ddot{q}_{s,d} + k_{s,p} \tilde{q}_s + k_{s,v} \dot{\tilde{q}}_s \right) + F_{s,f}, \quad (5.7)$$

where  $\tilde{q}_s = q_{s,d} - q_s$  and  $\dot{\tilde{q}}_s = \dot{q}_{s,d} - \dot{q}_s$  represent the position and velocity error and  $\ddot{q}_{s,d}$  is the desired acceleration that is assumed to be zero due to the slow motions of the adjustment mechanism. The control parameters  $k_{s,p}$  and  $k_{s,v}$  are weighting position and velocity feedback and are part of the first term that compensates the inertial load. The compensation of coriolis effects and gravitation as in [116] is not implemented, as such loads do not occur in the system as can be seen in (5.3). Yet, friction that represents an additional load besides inertia is ideally compensated by  $F_{s,f}$  using the friction model (5.2). Considering that the inertial

load and friction are modeled and thus compensated ideally, the resulting linearized closed-loop behavior is

$$\ddot{\tilde{q}}_s + k_{s,v} \dot{\tilde{q}}_s + k_{s,p} \tilde{q}_s = 0. \quad (5.8)$$

These closed-loop dynamics are adjusted to yield critical damping by choosing the control parameters to be  $k_{s,p} = \omega_c^2$  and  $k_{s,v} = 2\omega_c$ , where  $\omega_c$  determines the exponential decay rate of  $\tilde{q}_s$  and  $\dot{\tilde{q}}_s$  [116]. To achieve appropriate motion tracking,  $\omega_c$  is empirically set to  $50 \text{ rad s}^{-1}$ .

To investigate the mechanical power consumption including the stiffness adjustment mechanism, the power  $P_{m,a} = \tau_a \dot{q}_a$  consumed due to link motion and the power  $P_{m,s} = \tau_s \dot{q}_s$  required to set stiffness are examined without considering recuperation. As pendulum motion tasks, three types of desired trajectories  $q_{l,d}(t)$  are used: A sinusoidal one with 2.0 Hz according to (4.16), a dual-sine with 2.0/1.0 Hz as given in (4.17) and a chirp according to (4.31). The chirp is specified to have an initial frequency  $f_0 = 1.0 \text{ Hz}$  and a final frequency  $f_1 = 3.0 \text{ Hz}$  at  $t_1 = 8.0 \text{ s}$ , which marks the end of simulation. Irrespective of the investigated trajectory, the adjustment mechanisms initial position  $q_s(0)$  is set to match the initial value of the trajectory. As in Chapter 4, the sinusoidal trajectory is used to investigate matching natural dynamics ideally. The chirp trajectory allows for examining the adjustment of stiffness to a changing trajectory and the impact of the frequency of adjustment. Hence, the spectrograms resulting from spectral analysis and the corresponding stiffness trajectories are discussed.

The dual-sine trajectory shows if stiffness is tuned to the frequency with the highest impact on power consumption. In [230], an average stiffness during a trajectory cycle is found to be the power-optimal stiffness for non-sinusoidal trajectories although varying stiffness would result from mathematically optimizing it with respect to the trajectory. The approach used in this thesis complies with the concept regarding the usage of a constant stiffness over a cycle. Anyhow, power-optimal stiffness might not be found by adjusting the system to match the major frequency component of the dual-sine trajectory. To investigate if selecting frequencies between those of the two superimposed sinusoidal trajectories achieves lower power consumptions than tuning to the major one, dual-sine simulations are further performed with modified stiffness values.

As an outlook on possible implementations in lower limb prosthetics, the strategy is further applied to the link torque trajectory that corresponds to the elastic torque  $\tau_e = K_s (q_a - q_l)$  in (4.6). If the strategy shows suitable results in this case, a combination with force/torque control methods based on force/torque trajectories should be feasible. Supporting such methods, the elastic element and the two encoders measuring link and actuator positions  $q_l$  and  $q_a$  can be used to implement

---

the sensory function of a torque sensor [212]. Beyond this, it would be possible to use it with specific (impedance) control methods applied in powered lower limb prosthetics like the approach from [216, 217, 218, 128], where torques are generated based on a passive spring and damper system instead of positions.

---

#### 5.1.4 Experimental evaluation

---

For the experiments, the motion control algorithm explained in Chapter 4 is used regarding pendulum motion. Pole placement for the tracking controller and friction compensation are not changed. In addition to the investigation of sinusoidal tasks in Chapter 4, the interplay of natural dynamics and multi-frequency trajectories is examined based on dual-sines according to (4.17). Considering two stiffness values of  $75 \text{ Nm rad}^{-1}$  and  $150 \text{ Nm rad}^{-1}$ , the investigated frequency range is selected to cover the corresponding antiresonance based on the results from Chapter 4. The amplitudes of the trajectories are set to  $5^\circ$ , to ensure that the load of the elastic element stays below the critical value  $\tau_{e,max}$  as explained in Section 4.1.5. According to (4.17), the higher frequencies of the dual-sine are set to the full amplitude, while the lower ones are set to half of this value. The power consumption is assessed based on mechanical power  $P_{m,a} = \tau_a \dot{q}_a$  according to (4.20), which implies considering the influences of both inertias. Further, interrelations of power consumption and natural dynamics are investigated considering positions, torques, and powers.

Further, experiments including the automatic variation of stiffness with a first implementation of the proposed variable stiffness control strategy are performed. The effect of antiresonance adjustment on power consumption as well as the dynamics of stiffness control are examined considering sine, dual-sine and chirp trajectories. The experimental results are represented by position trajectories of  $q_l$ ,  $q_a$  and  $q_s$  as well as the mechanical powers  $P_{m,a}$  and  $P_{m,s}$  of the two actuators. For spectral analysis, a moving short time Fourier transform with point by point operation is used and windowed with a 4,096-point Hann window. The window is selected to be shorter than in the simulations, to increase the updating rate of online processing on the prototype. The stiffness value determined by antiresonance adjustment is transformed into a counterbearing position  $q_s$ . Therefore, the value is approximated by a spline interpolation of the measured stiffness characteristics. Instead of the PD-type controller and friction compensation applied in the simulations, a PI-controller with anti-windup is implemented. The parameters are set to  $k_{s,p} = 50$  and  $k_{s,i} = 6000 \text{ s}^{-1}$  heuristically, since those led to good tracking results in first experiments. The D-component is not implemented, as sufficient damping is found in the mechanism due to friction, while the I-component is introduced to eliminate steady-state control errors.

## 5.2 Results

The results of forward dynamics simulation and experimental evaluation of variable stiffness control are presented below. In this, focus is set on power consumption and how it is reduced by the proposed variable stiffness control strategy. Further, the power share of the two actuators is examined as well as detailed issues of the control strategy like dynamics and updating rate.

### 5.2.1 Forward dynamics simulation

Following, the forward dynamics simulation results of variable stiffness control regarding the sinusoidal, dual-sine and chirp trajectories are shown. The corresponding plots compare the cases of matching the natural frequency of the system to either the antiresonance (left) or the second natural mode (right). For each case, the position trajectories of actuator  $q_a$  and link  $q_l$ , desired and real stiffness as well as power consumption  $P_{m,a}$  and  $P_{m,s}$  of both actuators are presented.

Figure 5.4 gives the results for the sinusoidal trajectory. In the left part, the antiresonance of the system is matched with the trajectory frequency. In compliance with the results from Section 4.2.2, very low actuator motion  $q_a$  is observed according to the grey line in the upper plot, while link motion  $q_l$  depicted black corresponds to the desired task. A phase delay of  $180^\circ$  occurs between both motions

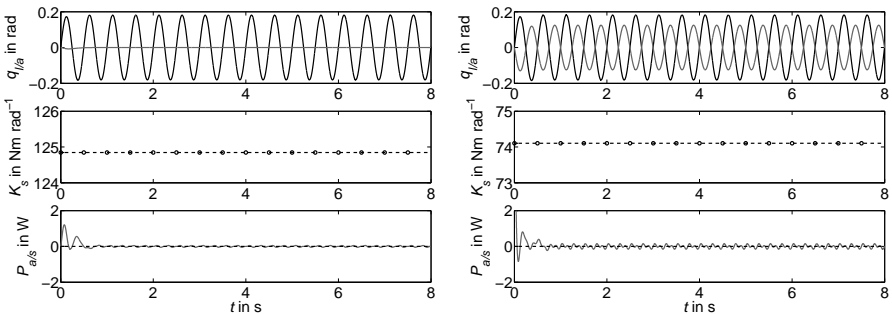


Figure 5.4: Sinusoidal trajectory matched with antiresonance (left) or second natural frequency (right): Top - Position trajectories of actuator  $q_a$  (grey, solid) and link  $q_l$  (black, solid). Middle - Desired stiffness (black circles) and real stiffness (black, dash-dotted line). Bottom - Power consumption  $P_{m,a}$  (grey, solid) and  $P_{m,s}$  (black, dash-dotted line).

due to operation above the collocation limit determined from (4.14). The middle plot gives the stiffness  $K_s$  set by the variable stiffness control strategy. With a value of  $124.84 \text{ Nm rad}^{-1}$ , it corresponds to the value calculated from (5.4). Additionally, it is observed that the desired value given by black circles is tracked accurately by the controller as shown by the dash-dotted line. The power consumption  $P_{m,a}$  of actuator 1 depicted as a grey solid line in the lower plot shows that very low power of less than 1 W would be required to move the pendulum under such ideal circumstances. In the beginning of the simulation, more power is required due to transient effects before the system reaches steady state motion. Power  $P_{m,s}$  required from actuator 2 is given by the black dash-dotted line and is zero, as stiffness is not changed throughout the simulation.

The right part of Figure 5.4 shows the results obtained for matching the second natural frequency to the trajectory. Link motion  $q_l$  corresponds to the desired task as for antiresonance tuning. Yet, actuator motion  $q_a$  shows the same phase delay but much higher values compared to the antiresonance case. This increased motion is in accordance with the results of Section 4.2.2, since low power consumption is achieved by low torques. The stiffness value of  $K_s = 74.10 \text{ Nm rad}^{-1}$  matches the one obtained from (5.5) and is tracked accurately by the controller. As for antiresonance tuning, power consumption  $P_{m,a}$  is distinctly below 1 W and transient effects are observed in the beginning. As stiffness is not changed due to the constant frequency of the trajectory, power  $P_{m,s}$  required from actuator 2 is zero.

The adaptation of the stiffness  $K_s$  during the chirp trajectories can be seen in Figure 5.5. The basic behavior of actuator motions  $q_a$  including their phase delays correspond to the ones observed previously. Low motion is performed when adjusting stiffness to the antiresonance using (5.4) and high motion amplitudes occur for matching the second natural frequency with (5.5). With increasing frequency of the link motion trajectory  $q_s$ , the selected stiffness  $K_s$  increases in both cases. As could be seen in Section 4.2.2, higher stiffness values  $K_s$  are required to match antiresonance. Regarding power consumptions of the drives, the power  $P_{m,a}$  of actuator 1 is very low but not as significant as for the sinusoidal trajectory in both tuning cases. Throughout the simulation, the requirements increase slightly due to the frequency [229] and the fact that stiffness is not ideally matched. Yet, power consumption stays below 10 W except in the last second. The increase in this part of the simulation is due to extrapolation of the stiffness trajectory and might thus be avoided by continuous trajectory generation from the desired stiffness values in practical implementation. Comparing the two adjustment laws, smaller power  $P_{m,a}$  is required when using antiresonance tuning. Beyond this, the consideration of the chirp trajectory allows for an examination of power consumption  $P_{m,s}$  required to adjust stiffness. Due to the friction loads, the peak values of the first oscillations

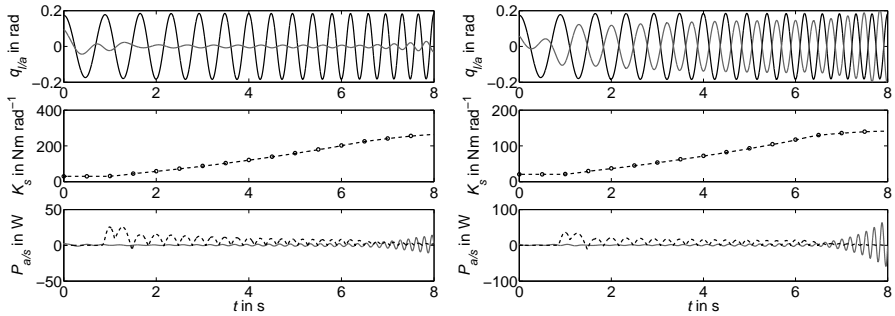


Figure 5.5: Chirp trajectory matched with antiresonance (left) or second natural frequency (right): Top - Position trajectories of actuator  $q_a$  (grey, solid) and link  $q_l$  (black, solid). Middle - Desired stiffness (black circles) and real stiffness (black, dash-dotted line). Bottom - Power consumption  $P_{m,a}$  (grey, solid) and  $P_{m,s}$  (black, dash-dotted line).

are about 26 W and 25 W for antiresonance adjustment compared to 22 W and 24 W for matching the second natural mode. In both, the power requirements decrease with increasing frequencies. Although those results are obtained specifically for the pendulum setup and friction effects are not considered the drive train actuating the link, it becomes obvious that stiffness variation can consume a significant share of power. The results show that setting constant stiffness over several cycles as it is proposed in [230] is appropriate. Further, it substantiates that power optimization should include requirements of both drive trains to find the most efficient solution.

In Figure 5.6 the spectrograms obtained by spectral analysis of the link trajectories  $q_l$  and the resulting stiffness trajectories are shown for the chirp trajectory. The left pair of plots gives the results adjusting stiffness to the antiresonance frequency based on an analysis of the link position trajectory  $q_l$ . In contrast to this, the right pair of plots gives analogue results based on the link torque trajectory  $\tau_e$  and thus allows for an assessment of the applicability to control methods that utilize force/torque trajectories. In the spectrogram plot of the left part of Figure 5.6 the increase of the motion frequency from  $f_0 = 1.0 \text{ Hz}$  to  $f_1 = 3.0 \text{ Hz}$  can be observed as a frequency shift of the power spectral density maximum over time. The corresponding stiffness trajectory  $K_s$  given by the black line is obtained by cubic interpolation of the nodes calculated from the spectrogram and indicated by black circles. The trajectory shows increasing stiffness  $K_s$  for increasing trajectory frequency and is according to the one in the left part of Figure 5.5. The spectrogram

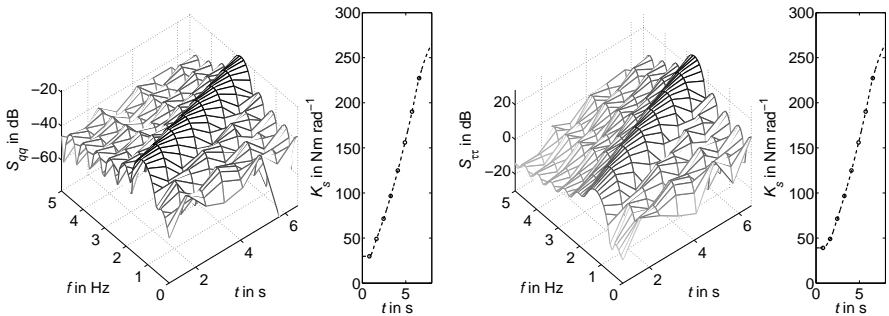


Figure 5.6: Spectrograms and stiffness trajectories  $K_s$  for chirp trajectory: Stiffness adjusted to antiresonance frequency based on link position trajectory  $q_l$  (left plots) and the link torque trajectory  $\tau_e$  (right plots). Black circles indicated stiffness trajectory nodes calculated from the spectrogram.

in the right pair of plots in Figure 5.6, shows that basic signal structure of the link torque trajectory  $\tau_e$  corresponds to the one of link motion  $q_l$ , although power spectral density  $S_{\tau\tau}$  is generally lower. The maximum of power spectral density is shifted with the increasing frequency as in the spectrogram of link motion. Hence, the stiffness trajectory is nearly identical. Only slight differences occur in the beginning of the simulation, as the maximum of power spectral density in the torque spectrogram is less distinct in this area. This exemplary result shows that the variable stiffness control method should be feasible for combination with control methods based on motion and force/torque trajectories.

Figure 5.7 presents the results from examining the dual-sine trajectory. For antiresonance tuning shown left, actuator motion  $q_a$  is distinctly lower than link motion  $q_l$  in compliance with the previous results. Anyhow, the difference is not as distinct as in the results obtained for the sinusoidal trajectory that are shown in Figure 5.4. For matching the second natural frequency, the upper right plot in Figure 5.7 shows that actuator motion  $q_a$  is of comparable size as link motion  $q_l$  for the dual-sine and thus in compliance with results from Section 4.2.2 and the simulations with the sinusoidal trajectory. In both, a phase delay of  $180^\circ$  between actuator motion  $q_a$  and the major frequency of link motion  $q_l$  is observed, since stiffness is tuned to the latter one. The accurately tracked stiffness values of  $K_s = 124.84 \text{ Nm rad}^{-1}$  and  $K_s = 74.10 \text{ Nm rad}^{-1}$  for matching the antiresonance and second natural frequency perfectly agree with the ones selected for the sinusoidal trajectory, as the major frequency of both trajectories is 2.0 Hz. Compared to the results of sinusoidal trajectory investigation, the power consumption  $P_{m,a}$  of actuator 1 is higher

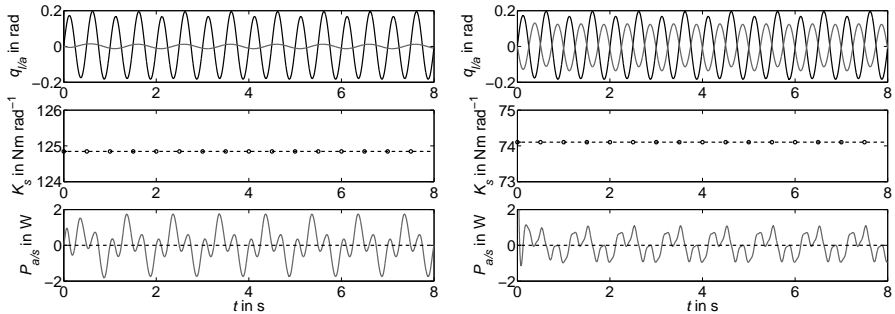


Figure 5.7: Dual-sine trajectory matched with antiresonance (left) or second natural frequency (right): Top - Position trajectories of actuator  $q_a$  (grey, solid) and link  $q_l$  (black, solid). Middle - Desired stiffness (black circles) and real stiffness (black, dash-dotted line). Bottom - Power consumption  $P_{m,a}$  (grey, solid) and  $P_{m,s}$  (black, dash-dotted line).

in both cases, which complies with the results from Section 4.2.2. This is due to the additional frequency component in the trajectory that does not match natural behavior. Due to the results from [230], the determination and setting of an average stiffness might thus additionally reduce required power. A comparison of the tuning methods shows that matching the second natural mode is advantageous for the dual-sine trajectory, since peak power during the task is about 1 W, while it is 2 W for matching the antiresonance. Irrespective of the stiffness adjustment law, power  $P_{m,s}$  required for stiffness variation is zero, since stiffness is constant.

The spectrograms and stiffness trajectories for the dual-sine trajectory are depicted in Figure 5.8. Results for adjusting stiffness to the second natural frequency considering the link position trajectory  $q_l$  are given in the left pair of plots, while the ones based on the link torque trajectory  $\tau_e$  are depicted in the right pair. The left pair of Figure 5.8 shows the two dominant frequencies of motion at 2.0 Hz and 1.0 Hz. In the analysis of the link torque trajectory that is shown by  $S_{\tau\tau}$  on the right, the lower frequency of the dual-sine has distinctly lower impact than in  $S_{qq}$ . Due to this, the major frequency can be detected more reliably. In both cases, stiffness is selected identically to be  $K_s = 124.84 \text{ Nm rad}^{-1}$  in compliance with the results shown in Figure 5.7. This substantiates the feasibility of the variable stiffness control strategy for combination with control methods based on motion as well as force/torque trajectories.

Figure 5.9 shows the system performing the same dual-sine trajectory. Yet, stiffness is manually modified to match the antiresonance frequency to either 1.98 Hz

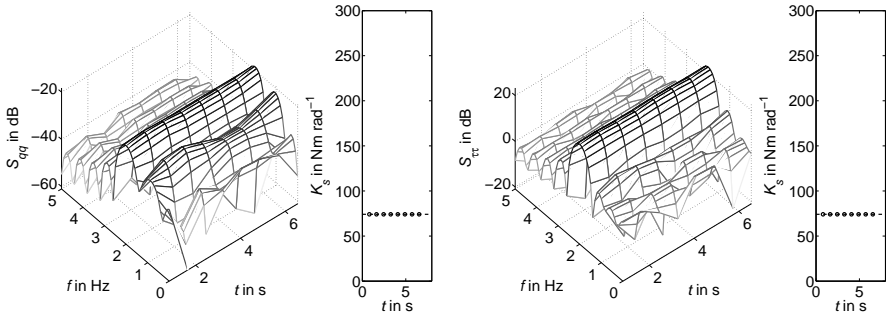


Figure 5.8: Spectrograms and stiffness trajectories  $K_s$  for dual-sine trajectory: Stiffness adjusted to the second natural frequency based on link position trajectory  $q_l$  (left plots) and the link torque trajectory  $\tau_e$  (right plots). Black circles indicated stiffness trajectory nodes calculated from the spectrogram.

(left) and 1.50 Hz (right) instead of 2 Hz. Those values are set between the two frequencies of the dual-sine to investigate if selecting an average stiffness as proposed in [230] leads to further reduction of power consumption for non-sinusoidal trajectories. When tuning stiffness to 1.98 Hz as colored left in Figure 5.9, a slightly decreased stiffness of  $K_s = 121.89 \text{ Nm rad}^{-1}$  is set. The resulting power consumption of actuator 1 is higher than the one observed in the left part of Figure 5.9.

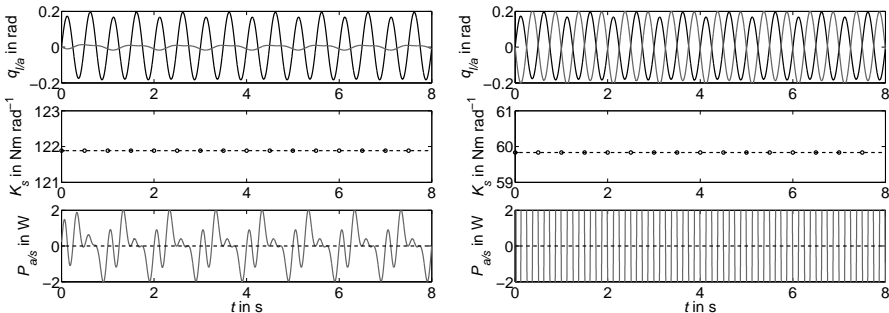


Figure 5.9: Dual-sine trajectory matching antiresonance to 1.98 Hz (left) and 1.50 Hz (right):  
Top - Position trajectories of actuator  $q_a$  (grey, solid) and link  $q_l$  (black, solid).  
Middle - Desired stiffness (black circles) and real stiffness (black, dash-dotted line).  
Bottom - Power consumption  $P_{m,a}$  (grey, solid) and  $P_{m,s}$  (black, dash-dotted line).

Choosing the real average of the two dual-sine frequencies of 1.5 Hz, stiffness is selected much lower with  $K_s = 59.83 \text{ Nm rad}^{-1}$ . Comparing this case to the results obtained for tuning to 2 Hz and 1.98 Hz, power consumption significantly increases to nearly 20 W. Hence, selecting stiffness based on the major frequency component is found to be the best of the investigated solutions, which deviates from the statements in [230].

### 5.2.2 Experimental evaluation

The experimental evaluation of the control strategy focuses on antiresonance as the impact of the second natural frequency is found to be less distinct in Section 4.1.5. Results obtained for a stiffness of  $75 \text{ Nm rad}^{-1}$  and dual-sine trajectories are depicted in Figure 5.10. In those, a frequency range of 1.7 – 2.0 Hz in steps of 0.1 Hz

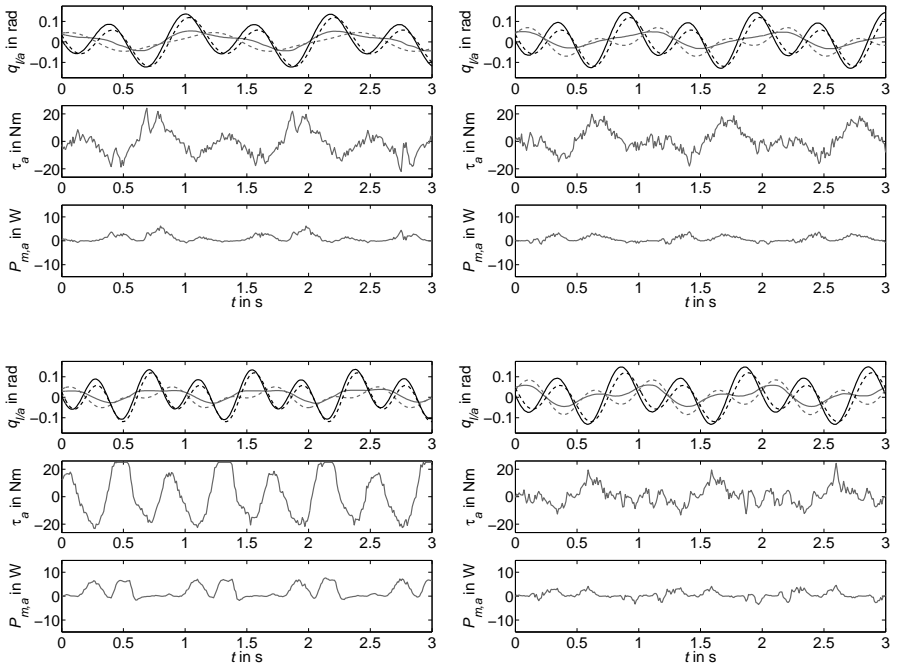


Figure 5.10: Dual-sine positions, torques and powers (link - black, actuator - grey, desired - dashed) at  $75 \text{ Nm rad}^{-1}$  and 1.7/1.35 – 2.0/1.0 Hz (upper left to lower right).

is considered for the major component (from upper left to lower right). Motion and torque data is shown besides power consumption. As in Section 4.2.3, black lines indicate link data, while actuator measurements are shown in grey and desired trajectories are depicted accordingly as dashed lines. Observing the development of power consumption over the frequencies shows that the lowest peak power values of less than 4.0 W are achieved at 1.9/0.95 Hz, which is close to the experimentally determined antiresonance frequency of 1.85 Hz. Accordingly, the transition from inphase to antiphase relative motion of actuator and link due to crossing the antiresonance frequency occurs in the observed frequency range. At 1.7/1.35 Hz peak powers are significantly higher than in antiresonance with more than 6 W, while peak power exceeds 4.5 W at 2.0/1.0 Hz. Since lowest power is observed when the major frequency component matches the antiresonance frequency, one can further see that assuming this in the stiffness control strategy is valid. According to inverse

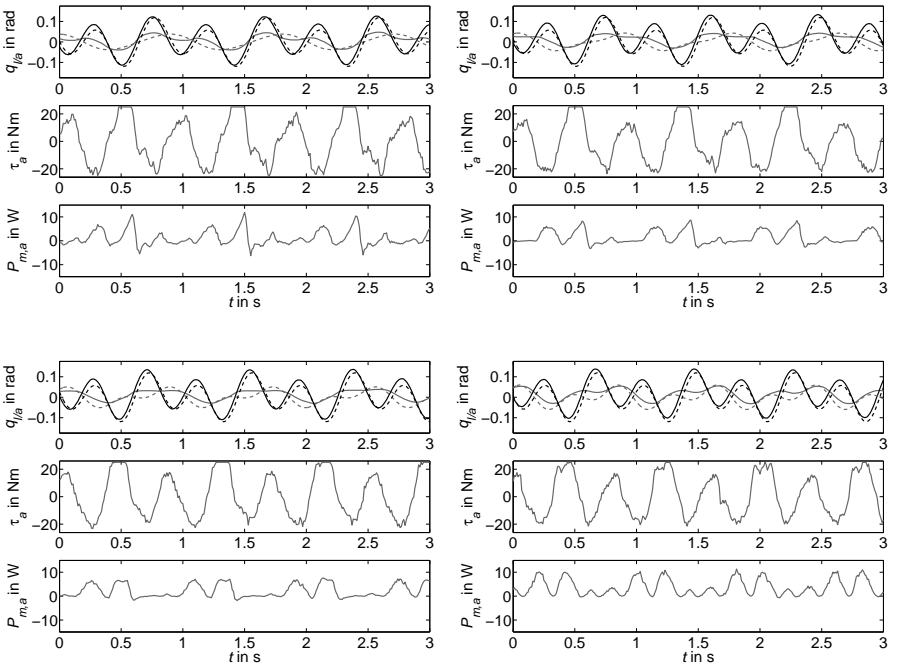


Figure 5.11: Dual-sine positions, torques and powers (link - black, actuator - grey, desired - dashed) at  $150 \text{ Nm rad}^{-1}$  and  $2.2/1.1 - 2.5/1.25 \text{ Hz}$  (upper left to lower right).

dynamics calculations, peak powers of 2.19 W, 3.24 W and 3.86 W would be required for direct actuation at 1.7/0.85 Hz, 1.9/0.95 Hz and 2.0/1.0 Hz. Comparing those to the ones obtained experimentally, confirms the low power requirements of the series elastic actuator in antiresonance operation.

For the experiments performed at a stiffness of 150 Nm rad<sup>-1</sup>, results for the frequency range 2.2/1.1 – 2.5/1.25 Hz are shown in Figure 5.11, since those cover the antiresonance frequency at 2.37 Hz. In compliance with the previously shown experiments, the lowest peak powers of about 7.5 W are found at 2.4/1.2 Hz due to the proximity of the major frequency component to the antiresonance at 2.37 Hz. It hence is comparable to the peak power of 7.06 W that would theoretically be required for direct actuation. Powers at lower and higher frequencies both exceed values of 10 W. Due to crossing the antiresonance frequency, the transition from inphase to antiphase motion is seen throughout the investigated frequency combinations. Considering the measured torques shows that the torque limitation is reached for frequencies of 2.2/1.1 – 2.4/1.2 Hz.

In the experiments with the automatic variation of stiffness mechanism, power consumption and control dynamics are investigated. Both aspects are observable in the left plots of Figure 5.12 that shows the results obtained for a sinusoidal trajectory with 1.6 Hz. In this, the position trajectories of  $q_l$  (black) and  $q_a$  (grey) are given in the upper plot, while  $q_s$  (black) is shown in the middle plot. The real positions are represented by solid lines and their desired values are given by dashed ones. The required mechanical powers  $P_{m,a}$  and  $P_{m,s}$  of the two actuators are given

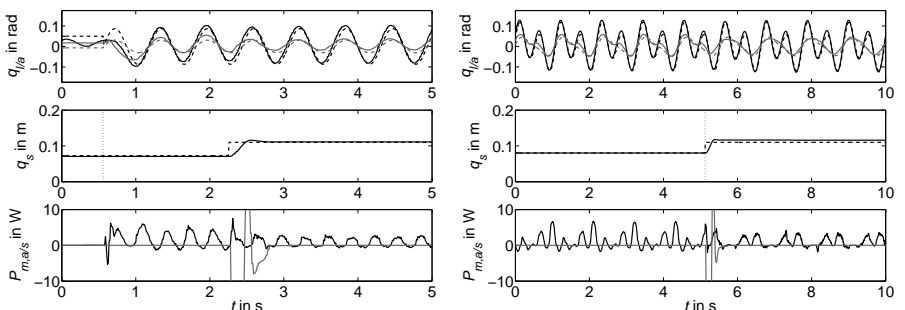


Figure 5.12: Variable stiffness control for sinusoidal (left) and dual-sine (right) trajectories: Positions of link / actuator (black / grey in upper plot) and counterbearing (black in middle plot) with desired values (dashed). Frequencies are 1.6 Hz for sinus and 1.8/0.9 Hz for dual sine.

in the lower plots by black and grey solid lines, respectively. In the beginning, both controllers are inactive and small residual pendulum motions  $q_l$  from a previous experiment can be seen. At 0.56 s, which is marked by the vertical dotted line in the middle plot, the controllers and the trajectory are started. While the top plot shows the sinusoidal motion of the pendulum  $q_l$ , the middle one presents the reaction of the adjustment mechanism. About 1.7 s after the trajectory is initiated, the stiffness control algorithm commands a change of the counter bearing position  $q_s$ . This is tracked by the PI-controller setting stiffness to 115.8 Nm rad<sup>-1</sup> in 0.5 s. Hence, the control algorithm is able to select and set stiffness appropriately considering the natural dynamics of the elastic drive train.

Although the model does not perfectly suit the prototype, this brings the antiresonance frequency close to the one of the trajectory, as actuator positions  $q_a$  decrease slightly. More importantly, the required power amplitudes reduce from above 5 W to less than 3 W. Since stiffness is only close to optimal and additional effort is required for friction compensation, this value is close to the requirement of 2.73 W direct actuation determined from inverse dynamics. Yet, the reduction of power is significant and further practically relevant, since required powers in direct actuation are expected to be distinctly higher if friction compensation is considered. The power consumed by the adjustment mechanism cannot be seen in Figure 5.12, since focus is set on power required for pendulum motion. Yet, the experimental results show that negative peak power is -64.71 W for accelerating, while it is 28.71 W for braking. As desired motion is commanded as a step, very high powers are required during acceleration. Those are limited by a motor torque saturation set to 0.11 Nm. In this drive train, recuperation is not possible since power is consumed for motions in both directions. Although power is required only shortly during adjustment, it has significant impact on global power consumption. This confirms that varying stiffness too frequently would be disadvantageous.

The results obtained for the dual-sine trajectory with 1.8/0.9 Hz that are shown right in Figure 5.12. In contrast to the previous experiment, the controls are active throughout the whole time range but the variable stiffness control is utilized beginning at 5.1 s (dotted vertical line, middle plot). The results confirm that power is reduced and most of the observed adjustment delay is due to spectral analysis. As the initial stiffness is not close to the optimal one, peak powers reduces from close to 7 W to slightly above 4 W, while stiffness is set in 0.4 s. As for the sinusoidal trajectory, this is slightly more than the theoretical value of 2.68 W for direct actuation, which anyhow would not be reached in practice. The peak power of the adjustment mechanism is -67.22 W for accelerating and 21.71 W for braking. Power required for acceleration is comparable to the one observed for the sinusoidal trajectory, as both include values exceeding the torque limitation.

The behavior of the variable stiffness control strategy for varying frequencies is shown by the results for chirp trajectories given in Figure 5.13. Frequency increases from 1.6 Hz to 2.2 Hz in 60 s. As for the sinusoidal one, all controllers are inactive before the trajectory starts. At that point, stiffness is initially adjusted three times using data from previous time steps that are partially zero. After that, desired stiffness is constant until a frequency of about 1.85 Hz is reached and before 2.1 hz are passed. This step-like adaptation of stiffness is due to the updating rate of spectral analysis. In the first of these intervals up to 1.85 Hz, real stiffness is slightly changing due to low control action of the PI-controller that reduces the steady-state control error based on the I-component. Considering actuator motions  $q_a$  in the top plot shows low amplitudes that decrease with increasing time. As additionally low powers are observed in the pendulum actuator power  $P_{m,a}$ , it becomes obvious that antiresonance tuning is performed successful. Yet, also power  $P_{m,a}$  shows decreasing amplitudes with increasing time after each adjustment. This is due to the deviation of the antiresonance frequency in the model and the prototype, where higher frequencies correspond to a specific stiffness. Hence, power reduces with increasing frequency, as the interrelation of stiffness and frequency approaches an optimal one. Theoretically, powers ranging from 1.74 W to 5.23 W would be required for direct actuation at frequencies from 1.6 Hz to 2.2 Hz. Hence, the final values of around 1.3 W, which are obtained shortly before stiffness is adjusted to a new and non-optimal value, show that antiresonance adjustment with an aligned model is suitable to significantly reduce power consumption. Beyond this, a better result might be achieved by improved spectral analysis to increase the required stiffness

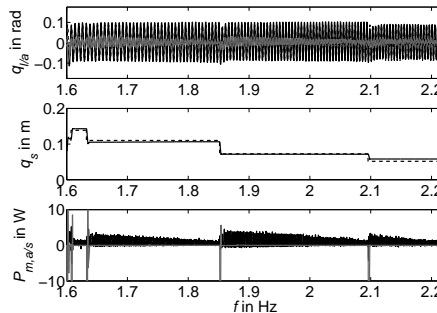


Figure 5.13: Variable stiffness control for a chirp trajectory: Positions of link / actuator (black / grey in upper plot) and counterbearing (black in middle plot) with desired values (dashed). Frequency increases from 1.6 Hz to 2.2 Hz in 60 s.

---

updating rate. In the chirp experiments, peak powers of  $-67.78\text{ W}$  for accelerating and  $25.45\text{ W}$  for braking are observed in the adjustment mechanism.

---

### 5.3 Conclusion

---

The investigated variable stiffness control strategy proposed by the author in [13] is based on spectral analysis and natural dynamics. Therefore, trajectories are analyzed regarding their power spectral density and the frequency component with the maximum signal power is selected using a bank of Goertzel filters. A power-optimal stiffness value is selected based on adjustment laws considering natural dynamics. With those, the drive train stiffness is tuned to match either the antiresonance or the second natural frequency.

For the examination and assessment of stiffness selection and tracking as well as power consumption of the link and stiffness adjustment actuators, forward dynamics simulation are performed. Such considering sinusoidal trajectories show very low power consumption required for moving the link if stiffness is adjusted to a power-optimal value with the proposed method. In case of constant frequency, no power is consumed by the stiffness adjustment actuator. The suitability of the strategy for automatic stiffness selection and tracking is investigated and confirmed by simulations with chirp signals as desired trajectories. Those further indicate that stiffness variation can account for a significant share of total power consumption of the system. As power consumption of the actuator driving the link is rather low for frequencies deviating slightly from the optimal ones, stiffness variation should thus not be performed too frequent. With this, adjustment power is kept low and the system can move in accordance with its natural behavior. This implies that stiffness should not be changed during a gait cycle but over several ones due to the high impact of adjustment power in prosthetic applications.

To assess the compatibility of the strategy with different control methods, the spectrograms of torque and position signals are analyzed. As those show that the major frequency can be detected from both, position and torque signals, the variable stiffness control strategy can be combined with a broad range of position and force/torque control methods including impedance control. Further, simulations with dual-sine trajectories confirm the beneficial effect of tuning to the antiresonance or second natural frequency as well as the feasibility of position and torque signals. Moreover, the dual-sine results prove that selecting stiffness based on the major frequency component is a valid assumption and thus a suitable approach, as minimum power consumption is achieved. Regarding all simulations, a delay between frequency changes in the trajectory and the adaptation of stiffness would occur in practical implementation due to spectral analysis. To improve the updat-

---

---

ing rate of spectral analysis for that purpose, two banks of Goertzel filters might be used in parallel and evaluated alternatingly. Alternatively, the detection of major frequency in prosthetic application might be performed by even simpler algorithms by means of counting the steps of the user based on ground contact measurements.

Experimental evaluations consider dual-sine trajectories as well. The corresponding results confirm that stiffness adjustment based on the frequency component with the major spectral power is an appropriate approach for selecting power-optimized stiffness values: Power consumption is observed to be minimal when the natural behavior of the system matches the frequency component of the trajectory with the maximum power share. As in Chapter 4, a distinct reduction of power consumption is seen in the case of antiresonance in contrast to insignificant ones for the first and second natural frequency. This can also be observed for sinusoidal, dual-sine and chirp trajectories if stiffness is adjusted automatically by the investigated algorithm. Although the adjustment mechanism reacts rather fast in the experiments, the updating rate should be increased by improved spectral analysis and power reduction would benefit from an aligned model. Yet, the results substantiate the suitability of the strategy. Further, they confirm that significant power is required to change stiffness and thus it should not be varied too frequent.



---

## 6 Exemplary design of a powered prosthetic knee

---

In the following, an exemplary design of a lower limb prosthetic system considering the human-machine-centered approach proposed in Chapter 3 is presented. Based on the results from Chapter 4 and Chapter 5, an actuation system using variable torsion stiffness is designed for implementation in a powered prosthetic knee as an application example. In this, the human-machine-centered approach presented in Chapter 3 is used to considering human factors as well as technical ones.

One major objective of this is to show the potential of the human-machine-centered approach and its impact on design decisions using the example. Based on a human-machine-centered list of requirements, simulations using human data and V model design, the concept for the powered prosthetic knee is elaborated. Within this, the possibility to geometrically integrate variable torsion stiffness within the envelope of the knee is assessed. As further functional integration is considered, the text is following the rough structure of the V model. Due to the high impact of stiffness on required power and energy, it is heuristically optimized with respect to those two criteria within design simulations according to [79]. Those simulations are using the advanced drive train model from Chapter 4. Finally, a first approach towards considering the interactions of the technical system and the human user in design simulations is outlined using the multi-body dynamics model from [248]. By considering the change of dynamics caused by the prosthesis, this simulation aims at understanding if design requirements are thus modified as well.

---

### 6.1 Methods

---

Various methods used in the exemplary design of the powered prosthetic knee are presented in Chapters 3 – 5. The design utilizes the design approach proposed in Chapter 3 and is thus based on a human-machine-centered requirements list. Inverse dynamics simulations are performed for system optimization considering the human gait models from [137, 248] and human gait data from [137] instead of the pendulum example given in Chapter 4. As a part of actuation design, geometric dimensioning of the elastic element as well as dimensioning and selection of the motor driving the joint, the corresponding transmission and an energy source are determined considering the results from simulation.

---

### 6.1.1 Human-machine-centered requirement analysis

---

The elaboration of the list of requirements is performed based on [63] taking into account the results from Chapter 3 in terms of a human-machine-centered prioritization and impacts of human factors on technical ones. As the exemplary design is limited to a selected number of essential aspects of a powered knee device, the list is simplified focusing on the main content instead of considering versioning, responsibility or other aspects of organization. In the list of requirements, components and system properties are listed and categorized according to the technical factor definitions presented in Section 3.2.1. They are further connected to a level in the V model based on the technical factor definitions and information on the most important impacts of human factors in (domain-)specific design are reported. To assess the single requirements, quality criteria or quantitative values to be achieved are collected as described in [63] based on the literature and human data from [137]. To investigate differences between purely technically motivated design and such with a human-machine-centered focus, the different development focuses determined in 3.2.1 and 3.2.3 are considered in terms of prioritization of the technical factors and corresponding requirements according to [63] and the influence of those rankings on design is discussed.

---

### 6.1.2 Concept of the actuation system

---

Using the list of requirements, a first selection of the actuator-transmission unit according to the required peak torques and angular velocities is performed based on human data for walking at  $1.6 \text{ m s}^{-1}$  and running at  $2.6 \text{ m s}^{-1}$  from [137]. Additionally, fundamental decisions on the overall system concept as well as its components like kinematics and energy source are made to prepare the basic concept to be investigated in the subsequent design simulations. Hence, this step corresponds to the one of system design in the V model. By utilizing the human-machine-centered design focus determined in Chapter 3, human and technical factors are considered in a balanced way.

---

### 6.1.3 Optimization with respect to human data

---

As the dimensioning of stiffness bandwidth and the resulting geometry of the elastic element is a very important issue for energy-efficient operation, it is determined based on optimizations of peak power or energy consumption during different types and velocities of gait according to [79]. Beyond this, the suitability of the actuator-transmission unit selected in the previous step is reconsidered. According to the

V model [231], these simulations are model-based methods applied for domain-specific design. In this, focus is set on the drive train and the energy source, since energy-efficient actuation is a major goal of this thesis. To consider and investigate the biomechanical loads on the knee joint during gait, human kinematic data acquired from participants without amputation in [137] is utilized. Those trajectories represent gait of an averaged unharmed person.

The resulting requirements regarding peak values of knee joint velocity  $\dot{q}_k$ , torque  $\hat{\tau}_k$  and mechanical power  $\hat{P}_{m,k}$  are taken from inverse dynamics simulation results of [137] and correspond to unharmed gait as well. Further, the impact of considering and neglecting the inertia  $I_a$  of the actuator-transmission unit is investigated by comparing the results obtained for those assumptions. The prosthetic knee to be designed is required to track the joint angle trajectories of the healthy subject by providing the corresponding torques, as inverse dynamics are calculated. Therefore, the measured joint trajectories  $q_k$ ,  $\dot{q}_k$  and  $\ddot{q}_k$  from [137] are substituted into (4.6) as link motions. The corresponding knee torques  $\tau_k$  taken from [137] are considered as loads replacing the pendulum load  $I_l \ddot{q}_l + G_l(q_l)$  yielding

$$K_s (q_k - q_a) = \tau_k \quad (6.1)$$

$$I_a \ddot{q}_a + K_s (q_a - q_k) = \tau_a . \quad (6.2)$$

In this,  $\tau_k$  contains the inertial and gravitational loads as well as others like ground contact during walking. To consider changed dynamics due to the prosthesis,  $\tau_k$  is alternatively calculated with the model from [248] adjusted to the specific case. Actuator motions  $q_a$  and its derivations are calculated using

$$q_a = q_l + K_s^{-1} \tau_k , \quad (6.3)$$

$$\dot{q}_a = \dot{q}_k + K_s^{-1} \dot{\tau}_k , \quad (6.4)$$

$$\ddot{q}_a = \ddot{q}_k + K_s^{-1} \ddot{\tau}_k . \quad (6.5)$$

Using the resulting velocities  $\dot{q}_a$  and  $\dot{q}_k$  and the corresponding torques  $\tau_a$  and  $\tau_k$ , powers  $P_{m,a}$  and  $\hat{P}_{m,a}$  are calculated using (4.20) and (4.21), respectively. As the derivations of the link torque  $\tau_k$  with respect to time are not contained in the data set from [137], both  $\dot{\tau}_k$  and  $\ddot{\tau}_k$  are calculated numerically from  $\tau_k$ . To avoid amplification of measurement noise by these numerical derivations, both signals are lowpass filtered using a zero-lag second order Butterworth filter with a cut-off frequency of 40 Hz according to ones used for filtering of kinematic data in [137]. Cut-off frequencies below this value cause distinct deviations in the trajectories of  $\dot{\tau}_l$  and  $\ddot{\tau}_l$  and should thus not be applied.

Aiming at an energy-efficient system, two kinds of optimizations are performed for design: On the one hand, peak power during the gait cycle is minimized to

decrease motor requirements and thus size and weight. On the other hand, efficiency is considered directly by optimizing the energy consumption required to perform one gait cycle. In both cases, the serial stiffness  $K_s$  is treated as the variable parameter to determine the required stiffness bandwidth and find optimal stiffness values for certain gait types and velocities. Both investigations consider walking at  $1.6 \text{ m s}^{-1}$  and running at  $2.6 \text{ m s}^{-1}$  using data available from [137]. Therefore, serial stiffness values in the range  $K_s = 100 - 1000 \text{ Nm rad}^{-1}$  are investigated in steps of  $1 \text{ Nm rad}^{-1}$ .

Among the design criteria, mechanical peak power is selected instead of average power to enable motor and transmission selection irrespective of the specific optimization objective. Beyond peak powers, the motor characteristics regarding possible combinations of the actuator torque  $\tau_a$  and the angular actuator velocity  $v_a = \dot{q}_a$  are considered. By comparing the absolute values of load curves to this characteristic line, suitability for four-quadrant operation and thus energy recuperation is examined. To investigate the impacts of considering and neglecting the inertia  $I_a$ , both ways to calculate the powers  $P_{m,a}$  and  $\bar{P}_{m,a}$  are compared. As an alternative to peak power, the optimization criterion energy consumption aims at increasing operating time. Therefore, mechanical energy consumptions corresponding to the powers  $P_{m,a}$  and  $\bar{P}_{m,a}$  are determined by integrating powers over the considered time frame as either

$$E_{m,a,a} = \int_{t_m} |P_{m,a}(t)| dt, \quad (6.6)$$

or

$$E_{m,a,r} = \begin{cases} \int_{t_m} \eta_a^{-1} P_{m,a}(t) dt, & P_{m,a}(t) \geq 0 \\ \int_{t_m} \eta_a P_{m,a}(t) dt, & P_{m,a}(t) < 0 \end{cases} \quad (6.7)$$

in analogy with (4.23) or (4.24). The presented torques, powers and energies are related to the average mass from [137] to investigate those values independently of subject mass. Energies are further related to stride length to consider a single gait cycle.

---

#### 6.1.4 Actuation integration and implementation

---

Evaluating the criteria and values resulting from the optimization step, an updated version of the human-machine-centered list of requirements is prepared. In this,

possible solutions are collected to finally support the design and specification of the powered knee device and its actuator-transmission unit. In compliance with the V model, this corresponds to assuring properties on component and system level by reconsidering and adjusting the requirements. In case of the actuator-transmission unit and the elastic element of the drive train, this is performed based on the velocities, torques and power obtained in the simulation. The elastic element is designed using (4.27) and the torsional moment of inertia corresponding to its shape as given in [84]. For a first specification of energy source capacity, mechanical energy consumptions determined in the design simulations are considered. The selection and configuration of appropriate storage components like batteries aims at delivering the required capacity and suiting the required motor voltage including a safety threshold. The required capacity  $C_{es}$  in mAh is determined by

$$C_{es} = 3.6 \frac{E_{min} d}{V_a l_{str}}, \quad (6.8)$$

where  $l_{str}$  is the actual stride length,  $d$  is the required walking distance,  $V_a$  is the motor voltage and  $E_{min}$  is the optimal mechanical energy consumption of one gait cycle determined from optimization. Hence, the required walking distance would not be possible if  $C_{es}$  is perfectly matched due to electrical losses. To ensure appropriate operating times, a safety margin is implemented by selecting a higher capacity. A main aspect of the step of system integration is the geometric and functional integration of the actuation system. The latter one is investigated considering damping through energy recuperation with the motor and realizing torque sensing in a model-based way, as both allow for improved or additional functionality without increased hardware complexity.

---

### 6.1.5 System integration issues

---

Two issues of system integration of the actuator concept are considered: On the one hand, the combination of the variable stiffness control strategy presented in Chapter 5 with the knee device is examined. On the other hand, a first investigation of the influence of considering the dynamic properties of the prosthesis in simulation is given. Both examinations rely on simulations with data from [137] and according models from [248]

For investigating the proposed variable stiffness control strategy, the shank angle trajectories of walking at  $1.6 \text{ m s}^{-1}$  and running at  $2.6 \text{ m s}^{-1}$  are analyzed regarding the frequency with the maximum signal power as in Chapter 5. For compatibility to the pendulum model, shank angle is considered with respect to the gravity vector as the difference  $q_h - q_k$  of hip and knee position (see 2.3). To focus on

dynamic motions, static components are not considered in spectral analysis and thus the signal mean values are removed prior to it. In spectral analysis, four subsequent gait cycles are evaluated with a bank of Goertzel filters covering a frequency range of  $0.0 - 15.0$  Hz and using a 256-point Kaiser window with a sidelobe attenuation of 0.5. The result of spectral analysis is compared with the mapping of power-minima to the natural behavior of the prosthesis using the contour plot for a sinusoidal trajectory as introduced in Section 4.1.4. In this, the amplitude of the trajectory is selected to be of comparable value as the amplitude of  $q_h - q_k$ . Due to using joint motion and torque data from [137], it is assumed that the dynamic properties of the link/prosthesis comply with those of the human leg, which are given in Table 6.1. Thus, the model is further compatible with the design simulations. From those, a first approximation of the link inertia through shank and foot with respect to the knee joint is given by

$$I_l = I_{sh} + m_{sh} p_{sh,a}^2 + I_{fo} + m_{fo} \left( (l_{sh} + p_{fo,a})^2 + p_{fo,g}^2 \right), \quad (6.9)$$

$$(6.10)$$

while the linearized torque caused by gravitation is

$$\gamma_l = m_{sh} g p_{sh,a} + m_{fo} g \sqrt{(l_{sh} + p_{fo,a})^2 + p_{fo,g}^2}. \quad (6.11)$$

$$(6.12)$$

In this, the foot is assumed not to move and  $I_{sh}$  and  $I_{fo}$  denote the inertias of shank and foot, respectively. The masses of shank and foot are given by  $m_{sh}$  and  $m_{fo}$ , while  $l_{sh}$  is the shank length. The positions of the centers of gravity of the limbs with respect to their axis of rotation are  $p_{sh,a}$  and  $p_{fo,a}$  for shank and foot corresponding to the leg axis while standing straight. The position of the center of gravity of the foot in the direction of gait is  $p_{fo,g}$ . Using this model, the natural dynamics for setting the stiffness values determined from optimization in Section 6.1.3 are determined and considered in comparison.

As a second issue of system integration, the potential of considering preliminary design results in human gait simulations to readjust system requirements is examined using the same data from [137] and modifying the model from [248]. For that

Table 6.1: Dynamics properties of the right leg in the human model from [248].

Parameter	$I_{sh}$	$I_{fo}$	$m_{sh}$	$m_{fo}$	$l_{sh}$	$p_{sh,a}$	$p_{fo,a}$	$p_{fo,g}$
Value	0.042	0.004	3.091	0.969	0.404	0.178	0.056	0.060
Unit	$\text{kg m}^2$	$\text{kg m}^2$	kg	kg	m	m	m	m

---

purpose, the simulation environment and models from [248] are utilized to compare the following cases:

- Mimicking of human biomechanics: The prosthesis has the same size, weight and inertial properties as the original limb of the subject. Hence, calculated required knee torques are identical with the ones for unharmed subjects.
- Consideration of real biomechanics: The real size, weight and inertial properties of the prosthesis are considered (iteratively) during the design process. Thus, calculated required torques approximate the real biomechanical load situation.

While the first case corresponds the assumptions of many previous studies like [98, 79] and the other simulations in this thesis, the second one is a step towards accommodating the changes in the dynamics of the overall human-mechatronic system. Although basically possible, this second approach is commonly not applied widely in prosthetic design as it is shown in Section 2.3.2. Investigating both cases is supported by [170], where it is stated that “discrepancy in knee torque and power between unimpaired subjects and below-knee amputees is very high“ and it is thus “difficult to deduct the requirements for a powered knee prosthesis from these data“. To implement the second case in the model from [248], the dynamic properties of the right leg of the human model are replaced by the ones of the prosthesis, which are determined from a CAD model of the system as well as datasheets of the components. As this model is a two-dimensional one with respect to sagittal plane that considers less effects than the one used in [137], the cases of mimicking human biomechanics and considering real biomechanics are simulated with it to allow for direct comparison of both cases.

---

## 6.2 Results

---

Subsequently, the results of the exemplary design of the powered prosthetic knee concept are given. A human-machine-centered list of requirements is determined based on the literature and human gait data. The results obtained from this list are compared to those determined with a purely technically motivated design focus. Further, the list is used to set up a fundamental concept of the device. Inverse dynamics simulations help to heuristically optimize system efficiency based on stiffness selection. With this information, the list of requirements is revised and updated. Based on this, a first proposal for the realization of the knee device is established. The dynamic properties of this design are considered in an additional simulation to investigate potential impacts of the changed dynamics in design.

---

### 6.2.1 Human-machine-centered requirement analysis

---

The first version of the list of requirements including the rankings of human-machine-centered design (HMCD) and purely technically motivated design (Tech.) is given in Table 6.2. In this, the technical factors are arranged according to their HMCD-rank and the corresponding level in the V model (V-level) is given as well as the impact of specific human factors according to the results from 3.2.3. As focus is set on energy efficiency and actuation hardware, aspects of *Gait planning / state recognition* (GPR) and *Controls* (CON) are only considered in terms of system integration in this example and based on the stiffness control strategy proposed in Chapter 5. Although the requirements regarding *Actuation / drive train* (ACT), *Functionality* (FUN), *Mechanics / kinematics* (MEC), *Operating time* (OPT), *Weight* (WEI), *Size/ volume* (SIZ) and *Sensors* (SEN) are not exclusively defined on one of the V-levels, the predominant one is given according to the categorization in Chapter 3. Hence, requirements regarding the *Actuation / drive train* are interpreted as component requirements (comp.) but are also relevant on system level (sys.).

The list of requirements shows the decrease of human factor impact on the technical factors with decreasing HMCD-rank. As the basic requirement for a knee prosthesis is to enable walking, the corresponding peak joint velocity, torque and power are taken from the human data from [137] regarding *Actuation / drive train*. Beyond this, the configuration and implementation of the elasticity in the drive train are to be considered. Issues regarding *Functionality*, are mainly motivated by the possible types and velocities of gait as well as the adaptation. Hence, the requirements for running are extracted from human data of [137] and collected including the stiffness bandwidth required for adjustment. *Mechanics / kinematics* comprise the implementation of the mechanic knee joint and its range of motion based on the maximum and minimum joint angles according to [137], while damping is only considered in terms of its implementation. The three subsequent technical factors *Operating time*, *Weight* and *Size/ volume* are representing system properties. A main issue of *Operating time* is the energy source, which is required to enable a locomotion distance of 10 km for all possible gait velocities (inspired by the value from [218]).

The requirements regarding *Weight* and *Size/ volume* are determined based on anthropometric data from [43] and [76], respectively. The results of various studies analyzed in [43], estimate the average mass of a human shank to be 3.3–4.8 kg. The requirement is set to the average of this range of about 4.0 kg for the whole shank including foot actuation components. This is assumed as motors driving the ankle are often attached to the shank to keep the foot lightweight (e.g., [18, 95, 6, 21]).

Table 6.2: First version of the (human-machine-centered) list of requirements considering actuation of a powered prosthetic knee.

	<b>TF</b>	<b>V-lev.</b>	<b>HF-imp.</b>	<b>HMCID</b>	<b>Tech.</b>	<b>Requirement</b>	<b>Value/Criteria</b>
<b>ACT</b>	BSI, SUP, MOB, OUT	2 2 2 2		7 7 7 7	Peak velocity (walk) Peak torque (walk) Peak power (walk) Elastic energy storage	7.18 rad s <sup>-1</sup> [137] 62.19 Nm [137] 121.26 W [137]	
					Config., implem.		
	SAT, SUP, MOB	3 3 3		2 2 2	Stiffness range (walk/run) Peak velocity (run) Peak torque (run) Peak power (run)	Up to 600 N m rad <sup>-1</sup> [170] 10.53 rad s <sup>-1</sup> [137] 178.21 Nm [137] 686.63 W [137]	
	Sys. Sys.						
<b>FUN</b>	FOS, SUP	4 4		7 7	Joint implementation Range of motion (walk) Range of motion (run)	none 1.95 – 3.07 rad [137] 1.55 – 2.97 rad [137]	
					Damping		Implementation
	MOB	5		9	Actuator/gear efficiency	high	
	Sys.				Energy source capacity	10 km [218]	
<b>OPT</b>	WEI	none		1	Weight	2.5 kg [43]	
	SIZ	Sys.		8	6	Size	0.086 · 0.379 m [76]
<b>SEN</b>	none	8		4	Position	Range of motion	
	SEN			4	Torque		Range of load torques

To ensure weight capacities for appropriate ankle actuation, knee weight is limited to 2.5 kg, as the foot designed in [21] contributes about 1.5 kg to shank mass and is considered exemplary for a complete transfemoral prosthesis in the remainder of the chapter. As the depth of the shank is in parallel with the direction of locomotion and thus not as crucial for *Size/ volume* as its width and length, the latter ones are focused. Yet, depth should have a comparable dimension as width according to the biological leg. The dimensions of the prosthetic knee are required to suit the knee width and shank length of an average young women with a body height of 1.68 m. This includes 95% of male subjects from [76] as well as the average assumed in [137]. User weight is not considered in this example specifically, as focus is set on energy efficiency and the functional design of the prosthetic drive train. Further, the stiffness adjustment mechanism is not dimensioned, as the load situation is rather complex due to being dominated by friction and should be assessed by experiments. Anyhow, the main components are to be approximated for a first estimation of system size and weight.

---

### 6.2.2 Concept of the actuation system

---

Considering the requirements collected in Table 6.2, a crucial step in powered prosthetic knee design is the selection of the actuator. As electromechanical actuation like DC or EC motors is mostly used in literature (e.g., [144, 218]) and received high ratings in the technical assessment given in [193], this type of actuators is focused. An additional advantage of those is that they enable four-quadrant operation and thus can increase energy efficiency and operating time by recuperating energy. For a first motor selection, it is assumed that only 60% of the maximum required power of 686.63 W is required, if a serial elasticity is introduced, as reduction to approximately 50% are observed for running in [79]. If this assumption is valid, a motor with a peak power of about 400 W should be sufficient to fully provide and resist joint power even during running. Yet, this might not even be necessary to support users if adding power they cannot create themselves is sufficient. As such lower requirements are reported in the literature [146, 144, 216, 218], an approach to consider this is presented as an aspect of subsequent system integration. To suit the requirements, a 3890048CR DC motor with a peak power of 406 W from Dr. Fritz Faulhaber GmbH & Co. KG, Schönaich, Germany is chosen exemplarily. It can be combined with transmissions like the 38A series from the same manufacturer. A first estimation of the required gear ratio is determined based on the required angular velocity of  $\nu_a = 10.53 \text{ rad s}^{-1}$  and the no-load motor velocity of  $575.96 \text{ rad s}^{-1}$  as well as the required torque of 178 Nm and the stall torque of the motor, which is 2.91 Nm. The quotients of those pairs of values are 54.70

---

and 61.17 for velocities and torques, respectively. As only a reduction ratio of 60 is provided by the manufacturer, this is chosen.

Due to the literature and previous findings of this thesis, series elastic actuator-elasticity configurations can increase energy efficiency, be adapted to very versatile tasks, improve human-machine interaction due to better predictability, and supports user safety. Hence, a serial elastic configuration is selected for actuator design. The investigated example further aims at assessing the potential for geometric integration of variable torsion stiffness, which is examined in Chapter 4 and Chapter 5. The feasibility is substantiated by first experiments with prototype hardware in Section 4.2.3, which can be understood as hardware-in-the-loop experiments in the process of the V model development. Due to [170], joint elasticities of up to  $600 \text{ N m rad}^{-1}$  occur in gait of unharmed humans. Using (4.27), the elastic element can be designed to suit this requirement. From a functional perspective, the variation of stiffness is demanded to enable adaptation to different users or certain kinds of gait mainly aiming at energy efficiency [96, 79, 242]. Variable torsion stiffness belongs to the group of structure-controlled variable stiffness approaches that received high rating in the assessment regarding lower limb prosthetics in [193]. Specifically, variable torsion stiffness provides a very simple design and thus might be suitable for geometric integration in the joint itself without needing complex and huge kinematics, as it is a rotational elasticity. Hence, a single joint design as discussed in [170] seems to be a simple design solution that can be combined with a series variable torsion elasticity as proposed in [238].

Considering such a single axis design, achieving the required range of motion is straightforward. Yet, a limitation by mechanical stops might be beneficial for the user, e. g., to  $0 - 120^\circ$  as in [146]. The inclusion of dissipative mechanical damping components is not considered, as a main design objective is energy efficiency. Yet, damping can be realized by functional integration through the electromechanic actuator and thereby power can be recuperated [224]. According to [224], “legged locomotion entails a number of functions that require net dissipation of mechanical power, especially at the knee“ but “unlike the human musculoskeletal system which requires net metabolic energy consumption during contraction (whether concentric, eccentric, isometric, or isotonic), an actively powered artificial limb has the potential to leverage energy storage mechanisms for improved overall energetic performance“. Further, this functional integration leads to a smaller number of components. Although a damping mechanism without an actuator might be sufficient for running and only a small motor should be required for walking due to [79], using a high power motor instead of a damper thus provides both functionalities, supplying full joint power and increasing operating times due to recuperation. As energy sources, lithium polymer batteries are widely used due to their high energy

---

density as shown in Section 2.3 and thus those are considered in this design example as well.

As the remaining design aspects achieved low rankings in human-machine-centered design, less effort should be invested in meeting the requirements concerning those. To comply with those of *Weight* and *Size / volume*, lightweight and small components are preferred in selection. Further, a combination of the investigated knee concept with the foot from [21] is considered in the requirements. The frontal dimensions of the prosthesis are demanded to stay within  $0.086 \text{ m} \cdot 0.379 \text{ m}$  for knee width times shank length. As shank depth in sagittal plane is less important and usually not evaluated in studies like [76], it is not specifically taken into account but inspired by the biological leg. Despite rank of a technical factor the corresponding requirements have to be acquired carefully since basic compliance with those might be important to assure quality of other ones, e. g., *Sensors for Gait planning / state recognition* and *Controls*. Since measurements of ground contacts are to be performed within the prosthetic foot, sensing the actual drive train state is assessed to be most important in prosthetic knee design. In the elastic drive train, it should be beneficial to measure the positions of both, link  $q_k$  and actuator  $q_a$  regarding objectives like control performance. This can be achieved by the integration of optical or magnetic encoders. Taking into account those used in the prototype, one can see that covering the full range of joint motion is simple, since those are not limited mechanically regarding rotation. Beyond positions, encoders further provide the link and actuator velocities of the knee joint drive train. Considering system integration, measuring both positions facilitates acquiring the joint torque  $\tau_k$  without a torque sensor, as this is intrinsically contained within the system: In the solution of [212], joint torque is calculated model-based using the encoder positions and current joint stiffness as  $K_s(q_a - q_k)$ .

---

### 6.2.3 Optimization with respect to human data

---

The optimization of power and energy requirements with respect to stiffness is a model-based approach to increase actuation efficiency and supports domain-specific design regarding the actuator-transmission unit and the required stiffness range. Figure 6.1 shows peak powers related to subject weight versus stiffness and powers required during a gait cycle for peak power optimization. The left plots show the optimization results for walking at  $1.6 \text{ m s}^{-1}$ , while the right ones depict those of running at  $2.6 \text{ m s}^{-1}$ . The upper left plot shows that peak power can be reduced by selecting an appropriate elasticity for walking. If actuator-transmission inertia  $I_a$  is not considered, the optimal value is found at the upper boundary of the investigated stiffness range. As peak power converges to the one of direct drive (black

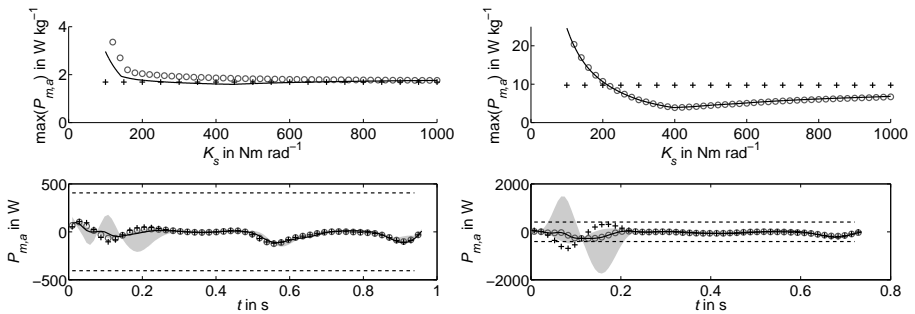


Figure 6.1: Peak powers related to subject weight versus stiffness and powers required during a gait cycle for peak power optimization (walking - left, running - right, no recuperation): Direct actuation (black plus signs) compared to SEA with neglecting  $I_a$  (grey circles) and considering  $I_a$  (solid black). Power over gait cycle is compared to motor peak power (dashed black) and envelope of powers along stiffness range (shaded grey area).

plus signs), the selection of a rigid connection and thus direct actuation would be recommended as in [79]. Yet, peak power shows a distinct minimum in the investigated stiffness range when considering  $I_a$ . With a value of  $1.59 \text{ W kg}^{-1}$  at a stiffness of  $446 \text{ Nm rad}^{-1}$ , it lies below the one of direct actuation at  $1.69 \text{ W kg}^{-1}$  and hence the optimization objective is met. From this, it becomes distinct that considering  $I_a$  is important for design, as a real optimum can be found for walking in contrast to the results from [79]. Considering power over the gait cycle confirms these results and further shows that the selected motor has distinct reserves regarding peak power in walking. The effect of optimizing stiffness can be observed by comparing power considering  $I_a$  (black line) with human joint power (black plus signs). To indicate the range of powers corresponding to the investigated stiffness range the envelope of this range is given by the shaded grey area. As can be seen in Figure 6.1, power is significantly reduced compared by selecting the optimal stiffness value but can be distinctly increased considering different ones.

The right plots in Figure 6.1 show the analogue results for running. In this case, an optimal stiffness of  $398 \text{ Nm rad}^{-1}$  and a significant peak power reduction from  $9.74 \text{ W kg}^{-1}$  to  $3.90 \text{ W kg}^{-1}$  is found irrespective of the consideration or neglection of  $I_a$ . This is in compliance with the results from [79] that also show a peak power minimum of comparable value and neglects  $I_a$ . Power requirements over the gait cycle show the significant reduction of peak power. Only through this

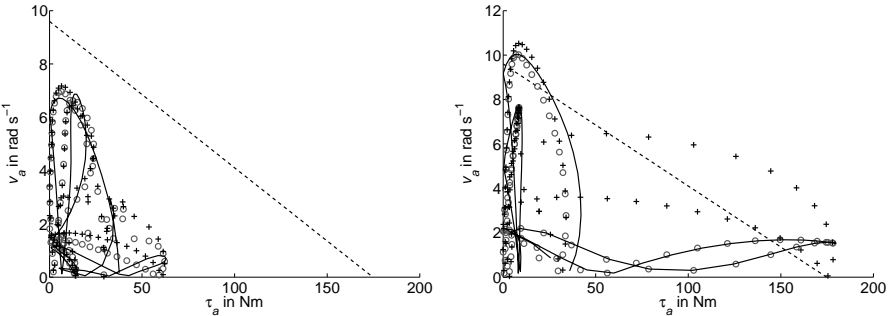


Figure 6.2: Angular velocity  $v_a$  versus torque  $\tau_a$  at the transmission output for peak power optimization in walking (left) and running (right): Direct actuation (black plus signs) compared to SEA with neglecting  $I_a$  (grey circles) and considering  $I_a$  (solid black) and motor characteristics (dashed black).

reduction, it is possible to handle full joint power with the proposed motor due to the high negative power peak during early stance phase.

To examine if the selected motor is appropriate for the required loads in combination with optimized serial stiffness, the absolute values of the velocity-torque trajectories at the transmission output are compared with the characteristic lines of the motor in Figure 6.2. The results for walking in the left plot show that the motor is suitable for driving the joint and regenerating energy in all three cases, as all trajectories including the one of direct actuation (black plus signs) are below the characteristic line of the motor (dashed black line). In running, torque as well as velocity exceed the characteristics of the motor in high and low load situations as can be seen right in Figure 6.2. Yet, the trajectory of direct actuation is exceeding the characteristic line across a wider part of the operating range. Hence, the combination of motor and optimized serial stiffness should allow for a wide range of possible gait velocities. Running at  $2.6 \text{ m s}^{-1}$  seems not to be possible if handling the full amount of positive and negative gait powers is required. Yet, this might not be necessary if users are satisfied with partial support.

Figure 6.3 shows the results obtained for optimizing serial stiffness aiming at minimum energy consumption. In walking, which is shown in the left plots, a significant reduction of energy consumption can be reached as it is found in [79]. Comparing the results regarding the consideration of actuator-transmission inertia  $I_a$  shows that optimal stiffness is shifted from  $409 \text{ Nm rad}^{-1}$  to  $375 \text{ Nm rad}^{-1}$  taking it into account. Meanwhile, consumed energy is increased to  $0.28 \text{ J m}^{-1} \text{ kg}^{-1}$  instead of  $0.27 \text{ J m}^{-1} \text{ kg}^{-1}$ . The lower left plot in Figure 6.3 presents corresponding

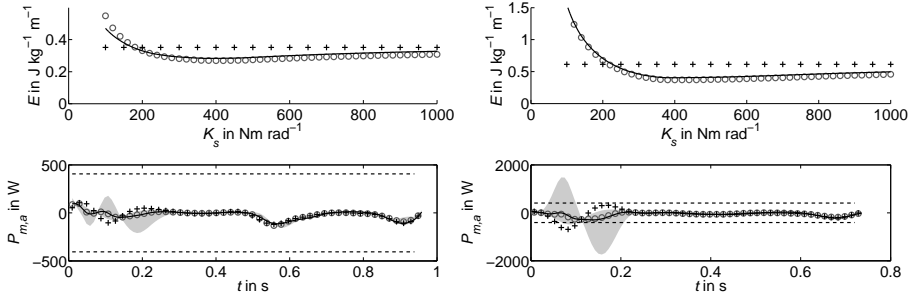


Figure 6.3: Optimized energy consumptions related to subject weight and stride length versus stiffness and powers required during a gait cycle (walking - left, running - right, no recuperation): Direct actuation (black plus signs) compared to SEA with neglecting  $I_a$  (grey circles) and considering  $I_a$  (solid black). Power over gait cycle is compared to motor peak power (dashed black) and envelope of powers along stiffness range (shaded grey area).

power requirements over the gait cycle. As for optimization of peak power, those keep within the motor limitations in all three cases. Results for running are given right in Figure 6.3. In the top plot, a distinct reduction of energy consumption to  $0.37 \text{ J m}^{-1} \text{ kg}^{-1}$  at  $417 \text{ Nm rad}^{-1}$  for neglecting  $I_a$  is observed in compliance with [79]. Further, a reduction to  $0.40 \text{ J m}^{-1} \text{ kg}^{-1}$  at  $379 \text{ Nm rad}^{-1}$  is found when considering  $I_a$ . As for peak power optimization, power over the gait cycle shows that the serial elastic drive train enables to reduce gait power. The velocity-torque trajectories given in Figure 6.4 show that as for peak power optimization, the selected motor has sufficient reserves for walking but not for running. Hence, gait power cannot be fully provided and might thus increase energy effort of the users.

An overview on the optimization results is given in Table 6.3. It becomes distinct that considering energy recuperation has no effect on power and stiffness in peak power optimization but on optimizing energy consumption. In this latter case, slightly modified but feasible stiffness values are found for running. For walking, a higher deviation of stiffness is found in combination with distinctly increased peak power if recuperation is considered. Globally, the stiffness values obtained for optimization of peak power and energy consumption show that adaptation of the drive train to specific locomotive tasks can be achieved by stiffness variation. Further, the resulting mechanical powers and energies required for gait are of comparable value for both kinds of optimization. Thus, the required energy source capacity approximated based on the mechanical energy consumption is comparable

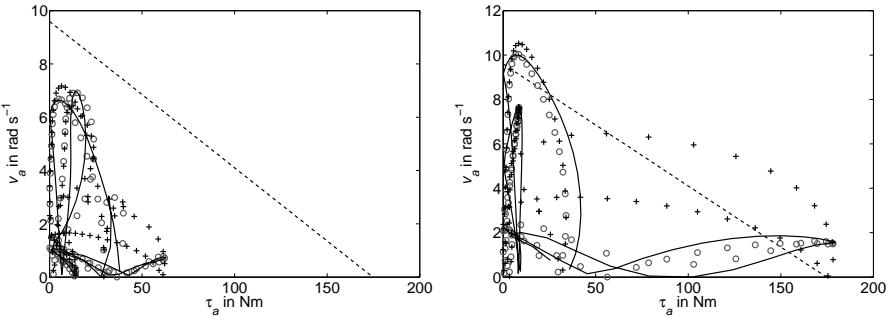


Figure 6.4: Angular velocity  $v_a$  versus torque  $\tau_a$  at the transmission output for energy consumption optimization in walking (left) and running (right): Direct actuation (black plus signs) compared to SEA with neglecting  $I_a$  (grey circles) and considering  $I_a$  (solid black) and motor characteristics (dashed black).

as well. Although being theoretical values and a battery should be necessary in real applications, the negative consumptions occurring with recuperation indicate the potential of power regain. Very low differences occur between the optimizations with respect to peak power and energy consumption. Hence, optimization to peak power is recommended, as it should result in more feasible solutions with reduced drive train size and weight. Comparing the results presented in Table 6.3

Table 6.3: Stiffness, peak power and related energy consumption values for optimization of peak power and energy consumption without (w/o) and with (w/) recuperation in walking and running with consideration of actuator-transmission inertia  $I_a$ . In the bottom line energy source capacity required for running is given.

		Peak power optimized		Energy con. optimized	
		w/o recup.	w/ recup.	w/o recup.	w/ recup.
Walking	Stiffness in $\text{Nm rad}^{-1}$	446	446	376	100
	Peak power in W	112.92	112.92	114.8	210.09
	Energy con. in $\text{J kg}^{-1} \text{m}^{-1}$	0.37	-0.36	0.28	-0.2
	Stiffness in $\text{Nm rad}^{-1}$	398	398	378	355
	Peak power in W	276.5	276.5	290.58	325.09
	Energy con. in $\text{J kg}^{-1} \text{m}^{-1}$	0.4	-0.27	0.4	-0.27
<b>Req. energy source cap. in mAh</b>		1657.16	-1121.44	1656.4	-1135.68

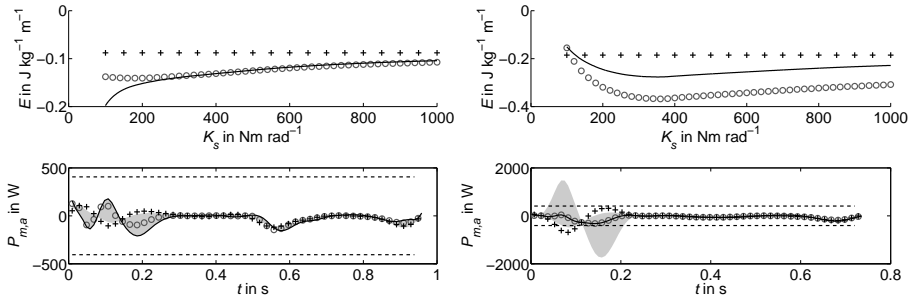


Figure 6.5: Optimized energy consumptions related to subject weight and stride length versus stiffness and powers required during a gait cycle (walking - left, running - right, with recuperation): Direct actuation (black plus signs) compared to SEA with neglecting  $I_a$  (grey circles) and considering  $I_a$  (solid black). Power over gait cycle is compared to motor peak power (dashed black) and envelope of powers along stiffness range (shaded grey area).

with those in [79] shows that stiffness values optimized for peak power reduction are higher than those optimized minimizing energy consumption. Considering the difference between walking and running, increased stiffness values are observed for running when optimizing energy consumption, while for peak power optimization higher values are found for walking. Although these basic characteristics are in compliance with those given in [79], an important difference is that an optimal stiffness for power optimization in walking is found if both inertias are considered only.

Despite the energy consumptions shown in Figure 6.3 are optimized based on (6.6) and thus do not consider recuperation, the power plots show the potential of using it. Energy recuperation can be investigated by using (6.7) and considering the high negative powers in the calculation of the required (req.) energy source capacity (cap.). Yet, the energy consumption criterion itself can be determined utilizing on (6.7) as well. The results of optimization with this criterion are given in Figure 6.5 corresponding with Table 6.3. In the case of walking, which is shown left, the consideration of recuperation in optimization leads to maximization of required motor powers according to the possibilities provided by the stiffness range. This is due to the fact that negative powers are major during walking and thus their amplification theoretically increases energy efficiency. Anyhow, this would lead to the selection of a motor with distinctly increased size and weight and should thus finally result in worse efficiency especially from a practi-

cal point of view and solutions that do not comply with user demands. In the results for running that are given in the right plots, minimum energy consumption is found at  $355 \text{ Nm rad}^{-1}$  with a value of  $-0.37 \text{ J m}^{-1} \text{ kg}^{-1}$  for neglecting  $I_a$  and at  $355 \text{ Nm rad}^{-1}$  with  $-0.28 \text{ J m}^{-1} \text{ kg}^{-1}$  including the influence of  $I_a$ . Further, it shows that using (6.7) as the criterion of optimization is possible for running and that energy-optimal stiffness is shifted by considering recuperation. Yet, this is not the case for walking, as the theoretical optimization result is not practically feasible. Hence, results of optimization with and without considering recuperation should be compared during design. When optimizing peak power requirements, neglection and consideration of energy recuperation does not impact the results as can be seen in Table 6.3.

---

#### 6.2.4 Actuation integration and implementation

---

Based on the results from simulations and optimization, an updated list of requirements including a possible solution for the design task is determined and presented in Table 6.4. Therefore, results from optimization of peak power without applying energy recuperation are utilized. According to those results, the requirements regarding peak velocities, torques and powers on the motor are adjusted. Beyond this, the energy source requirements are determined in detail considering that recuperation is not included in the concept. However, recuperation is intended to be used and due to the resulting safety margin, the fulfillment of function should be assured despite the theoretical estimation based on the mechanical energy consumption.

The stiffness range of the elastic element in the variable torsion stiffness drive train is adjusted to slightly lower values due to the results of the optimization. Yet, the elastic element is designed to the value from the first version to safely cover the requirements. To decrease complexity, the elastic element is designed as a polyamide rod with a square cross-section and implemented concentrically with the knee joint, which is represented by a single axis mechanism. Considering the available knee width of  $0.086 \text{ m}$ , the maximum active length of the elastic element should be less than  $q_{s,min} = 0.066 \text{ m}$  to provide sufficient space for bearings and gear components. The square profile provides a stiffness bandwidth of  $50 - 600 \text{ N m rad}^{-1}$  if edge length is set to  $0.0139 \text{ m}$  according to (4.27) and the torsional moment of inertia given in [84]. Regarding damping, the realization by energy recuperation through the DC motor decreases the number of hardware components by means of functional integration. With this, operating time should be increased significantly even in practical realization, although the negative energy balance observed in Table 6.3 is expected to diminish due to un-

Table 6.4: Updated (human-machine-centered) list of requirements considering actuation of a powered prosthetic knee.

TF	V-lev.	HF-imp.	HMCD	Tech.	Requirement	Value/Criteria	Solution
ACT	BSI, SUP, MOB, OUT	Comp., Sys.	2 2 2 2	7 7 7 7	Peak velocity (walk) Peak torque (walk) Peak power (walk) Elastic energy storage	6.21 rad s <sup>-1</sup> 63.01 N m 112.26 W Config., implem.	DC motor, peak power 406 W, Planetary gear box, 60 : 1
	SAT, SUP, MOB	Comp., Sys.	3 3 3	2 2 2	Stiffness range (walk/run) Peak velocity (run) Peak torque (run) Peak power (run)	Up to 500 N m rad <sup>-1</sup> 10.02 rad s <sup>-1</sup> 179.71 N m 276.50 W	600 N m rad <sup>-1</sup> maximum
	FUN	Comp., Sys.	3	2	Joint implementation Range of motion (walk) Range of motion (run)	none 1.95 – 3.07 rad [137] 1.55 – 2.97 rad [137]	single axis joint [170]
					Damping	Implementation	Recuperation (DC motor)
MEC	FOS, SUP	Comp., Sys.	4 4	7 7	Actuator/gear efficiency Energy source capacity	high over 1700 mAh	79.2% (DC motor and gears) Lithium Polymer batteries
	MOB	WEI	5	9			
SIZ	Sys.	none	7	1	Weight	2.5 kg [43]	-
SEN	Comp., Sys.	none	8	4	Size Position Torque	0.086 · 0.379 m [76] Range of motion Range of load torques	Encoders Model-based w/ encoders

---

modeled effects like friction. The global electromechanical efficiency of motor and transmission shows a maximum value of 79.2%.

Energy is planned to be supplied to the drive train by a package of five Lithium Polymer batteries in serial configuration. Providing an overall voltage of 55.5 V, batteries of the type ROXXY Evo 3–45030C from robbe Modellsport GmbH & Co. KG, Grebenhain, Germany are selected. This voltage corresponds to about 115% of the voltage required by the motor and should thus provide a sufficient safety margin for high load conditions. The package has a weight of 0.23 kg and a capacity of 2250 mAh that should cover the requirement of 10 km gait distance despite unconsidered electrical losses (compare Table 6.3). Due to the conceptual state of development no sensors are selected but it is assumed to use encoders for motion sensing and determine joint torque in a model-based fashion. After another design iteration including control algorithms, specific encoders with appropriate properties could be selected. In this subsequent iteration, a motor with higher power might be selected as well if the requirement of supporting full joint torques for running at  $2.6 \text{ m s}^{-1}$  or other gait types with high load is maintained. For slightly lower gait velocities, the current motor should be sufficient for providing power and recuperating energy.

Figure 6.6 shows several perspectives of the first implementation concept of the prosthetic knee in combination with the powered foot presented in [21]. Comparing the requirements given in Table 6.4 to the knee design shows the result of the human-machine-centered concept design: Among the two most important technical factors, requirements of *Actuation / drive train* are fulfilled completely, while such of *Functionality* might not be met in extreme situations. Anyhow, it would be a significant benefit for prosthetic users if running at velocities close to  $2.6 \text{ m s}^{-1}$  is enabled by the prosthetic knee. The determination of the threshold velocity would require more human data covering speeds between walking at  $1.6 \text{ m s}^{-1}$  and running at  $2.6 \text{ m s}^{-1}$ . Further, human-in-the-loop experiments might show, if support of the users is experienced to be sufficient even if less than the full joint power is provided. Issues of *Mechanics / kinematics* are met regarding joint kinematics as well as damping, which is realized integrated with the joint actuator. *Operating time* requirements are exceeded, as those benefit from variable stiffness optimization in terms of drive train efficiency and the energy source capacity is designed with an extensive safety margin due to the early state of the concept. Knee and shank *Weight* limitations of 2.5 kg and 4.0 kg are slightly exceeded by the concept, as those are predicted to be 2.67 kg and 4.13 kg including mechanical elements like bearings based on [238]. Due to the lower importance of *Weight* according to the human-machine-centered design focus, this fact is accepted in this first iteration. In contrast to this, the low rated issues of *Size / volume* and *Sensors* are both



Figure 6.6: CAD models of the proposed prosthetic knee in combination with the foot designed in [21]: Front view (left), rear view (middle) and detail rear view of conceptual knee mechanics and drive train (right).

met completely. Regarding *Sensors*, an aspect of system integration is included by calculating the elastic torque from position measurements based on a model of the elasticity. Knee width corresponds to the required value of 0.086 m, while knee length is even less than the requirement with 0.225 m and this provides sufficient space to integrate the knee with the foot from [21]. The resulting overall concept meets the size requirements of length, width, and depth. This and Figure 6.6 show that integration of a variable torsion stiffness drive train into a prosthetic knee is possible. The model suits the requirements defined in Table 6.4, although the foot design consumes a higher share of the shank length than assumed.

As the stiffness adjustment mechanism is not designed due to the unknown load situation, the estimation of system size and weight is based on a first concept of this second drive train. It assumes that stiffness is varied using a smaller, second motor that actuates the relocatable slider of the counter bearing. This second motor is the right one shown in the rear views in Figure 6.6. As in the prototype and indicated in the CAD models, rotatory motions of the motor are intended to be transformed to linear slider motions by a ball-screw. To determine a first approximation of the motor mass and inertia, a DC gear motor 1.61.046.311 from Bühler Motor GmbH, Nuremberg, Germany is included, as it has a mass of 0.15 kg, which is approximately one third of the mass of the motor driving the link. Since this selection is performed on the assumption of the mass properties only, the motor might not be able to suit the unknown power requirements in prosthetic application and is just used exemplary.

Comparing the human-machine-centered and the technically motivated ranking in Table 6.4, it becomes obvious that engineering based on the latter ones can lead to completely different solutions: Due to the fact that *Weight* receives the highest rating and *Actuator/ drive train* is rated to be of low importance in this case, a more light weight design with less support through actuators might seem appropriate to the engineers. Further, the realization of damping with the actuator might not be chosen in this case since it increases *Operating time* but also *Weight*. Thus, it could be assessed to be too heavy, while only leading to benefit regarding *Operating time*, which was rated to have the lowest importance.

Referring to the design requirements themselves, one can see that those increase with extended demand of biomechanical functionality (e.g., for including running) and recuperation. Both result in higher required motor peak power, as the current design is optimized to provide and regain full joint powers of unharmed gait. Yet, users might experience sufficient support even if only partial power is provided, and the requirements might further decrease in reality, as the prosthesis might be lighter than the real leg. To consider the latter case in design, the prosthesis should be integrated to the model used for inverse dynamics analysis of the human data from [137]. Such lower requirements can also be seen in experiments with prostheses as in [146, 144, 216, 218], where decreased joint powers are measured with the prosthetic prototypes. However, decreased requirements connected to lower demands of the users cannot be simulated up to now. To observe and consider such effects in early development, human-in-the-loop experiments with the Prostheses-User-in-the-Loop simulator might be feasible as proposed in Chapter 3.

---

### 6.2.5 System integration issues

---

Considering system integration of the exemplary knee design, the combination of the developed drive train with suitable algorithms for stiffness control is required. The characteristic frequencies of the natural dynamics observed in the prosthetic system considering the results from optimization of peak power and energy consumption are presented in Table 6.5. Therefore, the methods utilized in Chapter 4 and Chapter 5 are applied aiming at a clarification of the interrelation of natural dynamics and power consumption. The left plot in Figure 6.7 shows the results of spectral analysis of the shank trajectories with respect to the gravity vector for walking and running from [137]. It becomes distinct that one major frequency of about 1.0 Hz occurs in walking at  $1.6 \text{ m s}^{-1}$ , while two at 1.3 Hz and 2.6 Hz are observed in running with  $2.6 \text{ m s}^{-1}$ . In running, the higher power spectral density occurs in the component with lower frequency. This substantiates that the biolog-

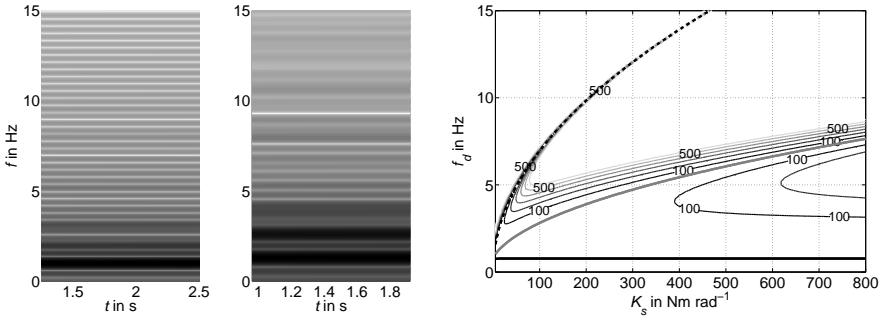


Figure 6.7: Spectrograms of mean-adjusted shank motion trajectories of walking (left) and running (middle) and comparison of natural limb dynamics with power consumption contour (right,  $\hat{q}_l = 20^\circ$ ).

ical motions are basically compatible with the synthetic sinusoidal, dual-sine, and chirp trajectories investigated in Chapter 4 and Chapter 5.

In all cases presented in Table 6.5, the values obtained for antiresonance and the second natural mode are outside the frequency range that occurs during gait. Yet, the plot comparing natural dynamics and power consumption that is given right in Figure 6.7, shows that the first natural frequency lies in the range of the major frequency components of the trajectory. It is found at about 0.775 Hz and

Table 6.5: Characteristic frequencies of natural dynamics in the prosthetic system calculated based on the stiffness values obtained from optimization of peak power and energy consumption.

	Stiffness in Nm rad <sup>-1</sup>	Peak power optimized		Energy con. optimized	
		w/o recip.	w/ recip.	w/o recip.	w/ recip.
Walking	Stiffness in Nm rad <sup>-1</sup>	446	446	376	100
	1 <sup>st</sup> nat. mode in Hz	0.775	0.775	0.775	0.774
	Antiresonance mode in Hz	5.73	5.73	5.27	2.81
	2 <sup>nd</sup> nat. mode in Hz	14.69	14.69	13.49	6.96
Running	Stiffness in Nm rad <sup>-1</sup>	398	398	378	355
	1 <sup>st</sup> nat. mode in Hz	0.775	0.775	0.775	0.775
	Antiresonance mode in Hz	5.42	5.42	5.29	5.13
	2 <sup>nd</sup> nat. mode in Hz	13.88	13.88	13.52	13.11

nearly insensitive against stiffness variation. Although the highly stiffness-sensitive second natural frequency and antiresonance might reach such low frequency values to match the gait trajectory spectrum, this would require values of  $50 \text{ Nm rad}^{-1}$  and below and should thus be infeasible for practical application.

Due to these results, there is an incomplete link between adapting natural dynamics via stiffness and power optimal operation that is observed in actuator design. Yet, the consideration of natural dynamics is essential since the optimal values are varied by the consideration and neglection of actuator inertia. Anyhow, it seems not to be possible to understand the connection of stiffness adaptation and reduced power consumption with linear models. The observations might be due to unmodeled effects that specifically occur at certain gait types or velocities. Such might be related to unconsidered nonlinear effects like variations of the natural frequencies due to high position amplitudes or the equilibrium position used for linearization. Further, the unconsidered foot motions could possible influence the result. Hence, the proposed stiffness control strategy is not directly applicable for the prosthetic knee example. Nevertheless, these results substantiate the necessity of considering actuator inertia in the design of powered prostheses with elastic actuation. Regarding V model development, this means that design of this software component that is not focused in this application example needs to be fed back to the concept level for adjustment to the new requirements. An updated version might assure required properties by exchanging the adjustment laws. Therefore, subsequent steps of development or future research needs to reveal the stiffness-specific effects causing optimality with respect to peak power or energy consumption.

To compare the cases of mimicking human biomechanics or considering the real biomechanics including the proposed prosthetic concept, the peak power optimization for walking is repeated. Figure 6.8 compares the results of both cases obtained using the data from [137] but calculating torques and thus powers with the model from [248]. The model parameters of a prosthesis including the knee concept and the powered foot from [21], which is not subject to this thesis, are given in Appendix A.2. In the simulation of the prosthesis, unrealistically high torque values occur in the first time step that seem to be caused by slight differences in the dimensions of the limbs. As all other values are meaningful, the first one is set to equal the second, while the rest is kept. Powers obtained considering the dynamic properties of the human leg depicted in the left part of Figure 6.8 are higher than those observed considering the prosthesis shown right: Peak power decreased to  $163.5 \text{ W}$  instead of  $180.6 \text{ W}$  and power-optimal stiffness is found at  $332 \text{ Nm rad}^{-1}$  instead of  $356 \text{ Nm rad}^{-1}$  due to the lower values of most inertial parameters. For running, similar results are found with peak power decreasing from  $1009.1 \text{ W}$  to  $689.3 \text{ W}$  and power-optimal stiffness being shifted from  $2728 \text{ Nm rad}^{-1}$  to  $726 \text{ Nm rad}^{-1}$ .

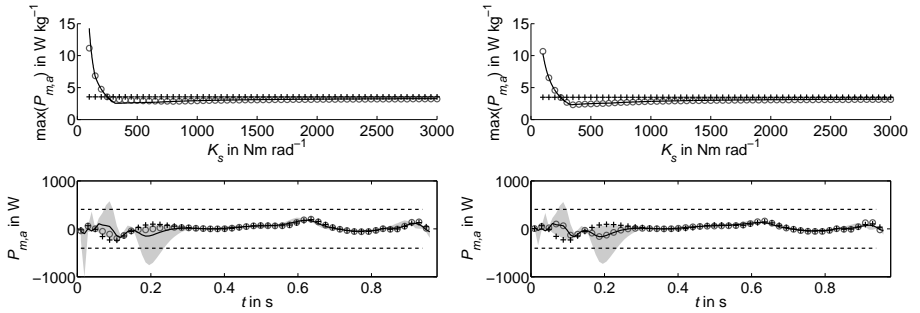


Figure 6.8: Inverse dynamics simulation of human gait using the model from [248]. Peak powers during walking related to subject weight versus stiffness and powers required during a gait cycle for peak power optimization (human biomechanics - left, prosthetic biomechanics - right, no recuperation): Direct actuation (black plus signs) compared to SEA with neglecting  $I_a$  (grey circles) and considering  $I_a$  (solid black). Power over gait cycle is compared to motor peak power (dashed black) and envelope of powers along stiffness range (shaded grey area).

Comparing those results to the ones from [137] reveals that the model from [248] generally estimates higher torques and powers, since the motion trajectories are identical. Beyond differing model parameters, this might be due to neglection of wobbling mass dynamics, model uncertainties and different other issues given in [137]. Hence, the results are only used to show the potential of the second case but are not used for design simulations. Yet, the approach to consider the dynamics of the prosthesis in a second step of design simulations and optimization is promising, as relevant changes can be seen in their comparison. The decrease of required actuator power by about 10% in walking shows that holistic modeling of the human-mechatronic system might leverage better designs through a more realistic prediction of the requirements.

### 6.3 Conclusion

As a major aspect, the potential of the proposed human-machine-centered design approach is considered. Following the design procedure proposed in the framework introduced in Chapter 3, a powered prosthetic knee is developed exemplarily. In a list of requirements, issues and values are summarized and ordered according to the human-machine-centered development focus. Technical design is performed complying with the V model methodology and its human-machine-centered exten-

sions proposed in Chapter 3. Although this includes issues of system design and integration, focus is set on knee actuation hardware, which is also considered as a component design example. As the human-machine-centered development focus shows distinct deviations compared to the purely technical one, engineering decisions might be made differently using those. While *Functionality* receives high importance in both rankings, *Weight* is considered to be more important than *Actuator / drive train*, *Mechanics / kinematics* and *Operating time* in the technical ranking compared to the human-machine-centered one. Hence, the proposed solution for a prosthetic knee might not be selected with a purely technical approach due to its increased weight. Yet, human-machine-centered rating indicates that users might accept this as a drawback, as it is accompanied by significantly improved *Support*, *Mobility* and *Functionality*. This might be in line with the statement from [44] that even very light prosthetic legs are perceived to be heavy (assumably passive ones). Finally, every prosthesis needs to be assessed by users and only beyond this step a definite comparison of the technical and the human-machine-centered design approaches is possible. Therefore, the extension by human-in-the-loop experiments could enable considering real user requirements, which might for instance show if partial support is sufficient, throughout the design process.

Optimization of peak power and energy consumption are helpful tools to increase the efficiency of powered prosthetics. Based on the method from [96, 79], stiffness values leading to minimum peak power or energy consumption are searched. Stiffness values optimizing the specific criterion are found in all cases and confirm those reported in [79] that consider the same type of prosthesis and uses identical biomechanical data as this thesis. Yet, a very interesting effect is found, when considering actuator inertia. Although its impact on the level of minimum peak power and energy consumption as well as the corresponding stiffness value is rather low, a minimum is found for walking in contrast to [79]. The conclusion of [79] that a rigid connection would be advantageous is confirmed in this thesis if actuator inertia is not considered. Taking into account the potential of energy recuperation shows that optimal stiffness values are shifted only slightly but dramatic influence on energy efficiency is observed, since a high share of power can be regained at the knee during locomotion. Drive trains incorporating stiffness values obtained from optimizations with respect to peak power and energy consumption show comparable power and energy requirements. Thus, the one resulting from peak power optimization should be selected, since it decreases motor size and weight, which might finally decrease user efforts and even the energy balance of the prosthesis due to the decreased inertial and gravitational loads in a leaner overall system.

A combination of the variable stiffness control strategy from Chapter 5 with the optimization results shows not to be straightforward. Peak power and energy

---

consumption minima do not vary with frequency due to natural dynamics. The major frequencies of locomotion are of lower value than the natural dynamics of the prosthesis with the stiffness values from optimization. Further, the adaptation of the drive train to these frequencies would require infeasible low stiffness values. Yet, natural dynamics are important from a design perspective, since it influences the level of the stiffness values found in optimization. As an issue of systems engineering, the reasons of variation among the optimization results of different gait types and velocities should be examined and considered in an updated version of variable stiffness control due to the V model procedure.

In the conceptual design of the powered knee device geometrical and functional integration of the variable torsion stiffness concept in a prosthetic component are examined. The optimization results are used as a basis for selecting an actuator driving the joint and enabling energy recuperation by considering four-quadrant operation. The proposed solution is based on a 400 W DC motor driving a single-axis joint via variable torsion stiffness with simplified elastic element geometry. So far, this design is assumed not to provide the full joint torques and velocities of the maximum required running velocity. Anyhow, it is designed to cover a wide range of walking and running velocities and thus might provide sufficient *Functionality* to the users. Although a main reason for the selection of the high-power actuator is energy recuperation in walking in running, it should be helpful in high-load situations like stair climbing (consider [176]). Using lithium polymer batteries, the whole device has a weight of approximately 2.67 kg, which slightly exceeds the requirement. Volume suits the desired values, as it fits the anthropometric envelope. *Operating time* should be higher than the required 10 km of fast walking or even running due to optimization, energy recuperation, and the safety margin applied in energy source dimensioning. Concerning functional integration of the proposed prosthesis according to V model development, damping properties of the knee are realized by energy recuperation through the joint actuator and torque can be determined from position sensing using the system model. Hence, both technical functionalities do not demand additional components and thus a lower share of system volume.

Considering the change of dynamics through the prosthesis in inverse dynamics, shows relevant reductions of power requirements and is thus promising for design. Yet, the simulation model from [248] is only suitable to identify such indications but should not be used in technical design due to an overestimation of torques and powers.



---

## 7 Overall discussion and conclusion

---

Subsequently, a global discussion of the findings and results of this thesis and an overall conclusion are given. In the discussion, the outcomes of the thesis are summarized and questioned critically. Finally, the main results and their overall impact are concluded referring to the open questions stated in Chapter 1 leading to an outlook on future works.

---

### 7.1 Overall discussion

---

The discussion is subdivided with respect to aspects of the human-machine-centered prosthetic design and variable stiffness actuation.

---

#### 7.1.1 Human-machine-centered design

---

The novel human-machine-centered approach to prosthetic design proposed in Chapter 3 aims at designing technical solutions that integrate with their users as synergetic human-mechatronic systems. To ensure an equal consideration of human and technical factors in technical design, a framework incorporating the analysis of those factors is proposed. By the analysis of human factors based on topic-specific questionnaires and interviews as well as expert studies, a human factor set modeling seven human factors is determined with respect to (powered) lower limb prosthetics. In human factor analysis, focus is set to technical development potentials that are due to user requirements and the impact of human factors on technical design is examined in contrast to purely psychological studies. The seven factors of the developed model are: *Satisfaction, Feeling of Security, Body Schema Integration, Support, Socket, Mobility, and Outer Appearance*. In an expert study, the model is basically confirmed and *Body Schema Integration, Socket* and *Outer Appearance* show to be most robust, while *Support* and *Mobility*, which appear to be highly relevant to powered prosthetics, are not separated clearly based on the current human survey data.

To assess the human-machine-centered design approach, the design of a powered prosthetic knee is considered. The corresponding technical factors are determined from the literature: *Mechanics / kinematics, Actuation / drive train, Sensors, Gait planning / state recognition, Controls, Weight, Size / volume, Operating time* and *Functionality*. Joining the aspects from both domains is a key issue of human-machine-centered design. This is solved by using quality function deployment

(QFD) to examine interrelations between human and technical factors and determine a design focus. This focus prioritizes technical factors according to their relevance for the users. Regarding the knee example, *Gait planning / state recognition*, *Actuation / drive train* and *Functionality* are assessed to be the most important technical factors in human-machine-centered prosthetic design. The results further substantiates the relevance of the human factors *Body schema integration*, *Support*, and *Mobility* in powered prosthetics, although the latter two ones are not confirmed statistically by the expert study. Another development focus, which is determined with respect to the technical factors only, shows distinct differences in technical factor importance: The ranking of *Weight* is increased distinctly, while *Actuation / drive train* receives significantly lower assessment for instance. From this, the potential of finding different solutions with the human-machine-centered approach becomes obvious.

Within the design framework, V model development methodology is suggested for systems engineering and extended to consider human factors based on human-machine-centered list of requirements and a corresponding design focus determined by QFD. The resulting combination of QFD and V model enables integration of the user perspective with issues of systems engineering. To foster this, V model design is suggested to be extended by human-in-the-loop experiments to integrate user throughout the design process. For that purpose, two experimental facilities are proposed: Prosthesis-user-in-the-loop for early user tests with simulations instead of prototype evaluations and the Int<sup>2</sup>Bot to examine specific aspects of *Body schema integration* and possibilities to manipulate it.

To assess the overall potential of the human-machine-centered design approach, a powered prosthetic knee is designed using it as an application example in Chapter 6. Based on the methodology and findings from Chapter 3, a human-machine-centered requirement analysis is performed and considered in V model development. Due to the distinct deviations between the human-machine-centered and the purely technical design focus, engineering decisions resulting from both are expected to differ. For instance, the technical solution proposed in Chapter 6 is determined by the human-machine-centered approach that focuses on *Actuator / drive train*, *Mechanics / kinematics* and *Operating time*. This solution might not be chosen in a purely technical development due to its relatively high weight, as this approach emphasizes the importance of *Weight*.

Critical consideration of the proposed human-machine-design approach and corresponding results indicates that particular human factors like *Support* and *Mobility* should be investigated in more detail, as they show to be important in powered prosthetics but are not separated clearly by experts.

An optimized version of the custom-built questionnaire developed in connection with this thesis is supposed to clarify such issues and validate the human factor set. Therefore, a factor analysis and the identification of structure equation models that are both not realizable with the current number of questionnaire participants should be conducted. With those, the interrelations of the human factors can be modeled and the missing relative importance weighting of human factors could further be added to the QFD-process. Given a sufficient response, the particular demands of specific user groups, which are not considered so far, can be examined by a cluster analysis and modeled with a Kano approach [63]. Beyond issues concerning the factors themselves, results obtained by using engineering design methods like QFD or pair-wise comparison might differ between the methods or even be influenced by their rating scales. To cope with this, such impacts should be investigated in comparative studies, and statistical validation of their results is required to confirm the prevalence of those. Ultimately, the feasibility of the proposed human-machine-centered design framework and possibly resulting benefits for the users can only be assessed in trials, where human subjects test prosthetics designed with this approach. As the results of this thesis indicate that engineering decisions might be done differently with the proposed approach, the basic concept is concluded to be promising. This further applies for human-in-the-loop experiments in systems engineering, as those allow for the early examination of user issues and can improve development by a steady integration of users. Although the proposed framework is intended for the use in lower limb prosthetics development, it can be applied to other human-mechatronic systems with distinct human-machine interaction due to the universality of the considered engineering design methods. Thus, other types of prostheses including upper limb ones can be covered as well as orthotics, exoskeletons and general wearable robotics by adjusting the human and technical factors to the particular design task. As those all show distinct human-machine interrelations due to the body-proximity of the technical system and its interaction with the user, the specific human factors should have comparable characteristics in contrast to those in classical ergonomics (e.g., [54]).

---

### 7.1.2 Variable stiffness actuation

---

Regarding prosthetic actuation, this thesis focuses on elastic actuation with variable stiffness, as such is expected to achieve the aim of energy efficiency by exploiting natural dynamics. Considering a leg-inspired pendulum, serial and parallel actuator-elasticity configurations are examined and compared with respect to their natural dynamics and corresponding power requirements in Chapter 4. The observation of two natural frequencies and an antiresonance mode shows that considering

actuator inertia by advanced modeling is crucial to exploit natural dynamics. It thus should be considered in actuator design in contrast to the approaches of various other works on powered prosthetics. In such, only antiresonance is found using basic models that neglect actuator inertia, as it depends on the link dynamics only. Antiresonance achieves further importance, as it marks the transition point from inphase to antiphase motion of the inertias and the collocation limit of control design. Unlike serial elastic actuation, only one natural frequency is found in its parallel counterpart, as both inertias are rigidly coupled irrespective of the utilized model.

Analyzing average power consumption of serial and parallel elastic actuation shows significantly decreased power consumption over a reasonable stiffness-frequency range in proximity to the natural frequencies, when compared to direct actuation of the joint. The consideration of efficiencies and energy recuperation does not change global characteristics of average power consumption but the latter one reduces the required energy significantly. Hence, both effects are not relevant for searching optimal stiffness values but should be considered in design.

In both configurations, the occurring power minima can be traced to the natural dynamics. For serial elastic actuation, minimal desired motion in antiresonance and minimal required torques in natural frequencies decrease the consumed power. Due to this connection of power consumption and natural dynamics, the capabilities for adjusting the latter ones by varying stiffness are superior in serial elastic actuation, as antiresonance and second natural frequency are sensitive to stiffness variation. Regarding serial elastic actuation, these insights are evaluated experimentally with a variable torsion stiffness prototype corresponding to the model used in the simulations. The results indicate a shift of the natural and antiresonance frequencies compared to model due to uncertainties, unmodeled effects, and unideal friction compensation. Yet, the feasibility of antiresonance for stiffness selection is confirmed, while the effects of the natural frequencies is not that distinct in the prototype.

A variable stiffness control strategy aiming at the exploitation of the observed natural dynamics is investigated in Chapter 5. In this, trajectories are analyzed regarding maximum power frequency component using Goertzel filters and power-optimal stiffness is selected to match antiresonance or second natural frequency to this major component. Forward dynamics simulations show that stiffness adjustment to varying as well as multiple frequencies is possible with the algorithm. The power consumed to do so can have a significant impact on power consumption of the system. Hence, it should not be performed too frequent. Simulations further indicate that selecting stiffness based on the major frequency component is a valid assumption. This is confirmed by experiments with the variable torsion stiffness

---

prototype. The experiments further show that model accuracy as well as the updating rate of spectral analysis need to be improved. The suitability of the method to minimize power consumption as well as the significant impact of adjustment power are confirmed in the experiments. Besides spectral analysis of the position trajectory, simulations prove that the major frequency component can alternatively be found by analyzing torque trajectories, which confirms the compatibility of the method to motion and force/torque control methods.

The insights on variable stiffness actuation are finally considered in the exemplary application of the design of a powered prosthetic knee in Chapter 6. Optimization of peak power and energy consumption based on basic and advanced modeling confirms validity of the results from [79]. Yet, one distinct deviation from those shows that an optimal stiffness exists for walking that is only found if the advanced model is used. Hence, the mechanical dynamics should be considered entirely in system design. Energy recuperation is found to distinctly decrease of energy requirements and is thus important for design. Yet, it has only low impact on the stiffness resulting from optimization. For practical application, an optimization of the design with respect to peak power is concluded beneficial, as it leads to a leaner technical system without affecting energy efficiency significantly. Yet, the connection of power optimization of the prosthesis to the variable stiffness control strategy from Chapter 5 requires additional research, since the points of optimal operation cannot be predicted by linear system dynamics.

Another issue tackled in Chapter 6 concerns the possibility of geometrical and functional integration of the variable torsion stiffness concept in a prosthetic component, which is confirmed by the proposed knee design. Developed based on the human-machine-centered approach from Chapter 3, the outlined system should enable nearly full locomotion support even during running and is energy-efficient through optimization of the series elastic drive train and energy recuperation. It is expected to allow for long operation of more than the required 10 km in fast walking and even running. Although few requirements are not ideally met by the concept, this might be interpreted as an acceptable drawback or even not experienced by users. Functional integration of mechanical damping is realized by regenerative braking with the actuator and torque sensing can be solved model-based using signals from position measurement.

Reviewing the results regarding variable stiffness actuation shows that the consideration of actuator dynamics in terms of actuator inertia shows to be essential in general and in prosthetics, as it unveils design and control aspects not seen in basic models. Yet, nonlinear effects on natural dynamics are not considered as the linearized transfer functions are analyzed. Power consumptions obtained with the nonlinear models show a good accordance with natural dynamics calculated from

---

linearized models in the pendulum. Yet, considering effects like nonlinearity or foot motion in natural dynamics determination might give insights with respect to the prosthetic example in a subsequent design iteration.

Beyond this, the models do not describe influences like damping and friction that might be crucial in practical application, e. g., operation with the second natural frequency is not power-optimal in the experiments. Besides warping natural dynamics, model uncertainties and unideal friction compensation impacts on stiffness selection and the accuracy of feedback linearization control in practice. Thus, the models used in control should be aligned with the dynamics of the real system. As only antiresonance is observed clearly in the experiments, it can be argued that advanced modeling might not be necessary. Yet, considering actuator inertia in prosthetic application shows significant impact on design, e. g., due to the optimal stiffness found for walking. Further, efficiencies are only considered in a best-case-scenario and should be modeled as functions of the load situation for practical design for better model accuracy. Yet, efficiencies do not show significant impact on the fundamental system characteristics and thus seem to be irrelevant in early steps like concept development and drive train optimization.

The designed knee concept is rather heavy and voluminous, as a very high power actuator is required to provide full joint power during driving and decelerating the link. This might not be necessary to suit user requirements and could be examined by human-in-the-loop experiments leading to a more human-machine-centered design. System integration of the overall prosthesis shows that the developed variable stiffness control strategy needs to be adjusted to the prosthetic application as the interrelation of power and energy minima with natural dynamics cannot be described with the utilized linear models. Promising aspects for future research are the variation of the natural frequencies due to high motion amplitudes and the equilibrium position. Further issues might be found in practical prosthetic application, as only antiresonance is observed clearly in the variable torsion stiffness prototype and delayed generation of the required stiffness trajectory due to spectral analysis that could increase power consumption. The first challenge might be solved by the examinations suggested above, while other methods for searching the major power frequency might be more feasible in prosthetic application, e. g., counting steps. Eventually, the findings on natural dynamics and power consumption in variable stiffness actuation as well as the specific ones on variable torsion stiffness might be used in general tasks that require efficient cyclic motion.

---

## 7.2 Overall conclusion

---

In this thesis, human-machine-centered design approach for lower limb prosthetic systems is given. Aiming at a synergetic integration of human and prosthesis acting jointly as a human-mechatronic system, psychological issues and human factors are considered as well as technical ones. Among technical ones, focus is set on variable stiffness actuation and control that represent enabling technologies.

Investigating the relevance of human factors in prosthetic design reveals seven factors that impact on prosthetic design. A comparison of assessing technical factors on themselves or with respect to the modeled human factors shows that the resulting design focus can deviate distinctly. In order to consider this in prosthetic design, a human-machine-centered design methodology incorporating technical and human factors analysis, a transfer step joining those and systems engineering enriched by human data and human-in-the-loop experiments is proposed. In this, modeling the determined human factors is of major importance and deducted based on human survey data. High ratings of *Body schema integration* in the exemplary application of the methodology to design a powered prosthetic knee indicate that this is a crucial aspect. Further, its strong relation to the top-rated technical factor *Gait planning / state recognition* is shown. *Actuation / drive train* receives high ratings as well and shows to be related to the *Support* of the users and to their *Mobility*. The most important system property is *Functionality*. The two presented human-in-the-loop experiments provide the possibility to investigate both: Actuation that suits *Support* and *Mobility* requirements of the users can be explored with the Prostheses-User-in-the-Loop simulator concept, while the Int<sup>2</sup>Bot helps to investigate *Body schema integration* and how to manipulate it technically.

Future works on the human-machine-centered prosthetic design approach should examine the interrelations of human and technical factors in more detail. Besides, a validation of the corresponding models and the design framework based on the assessment of the users is required. Essentially, the applied methods of engineering design should be investigated regarding their feasibility in comparative studies and fostered by the incorporation of statistical data from users and experts. Within this, the approach might be extended to other domains of engineering design, e. g., a human-machine centered version of *failure mode and effects analysis* (FMEA, see [63]) might increase the fault tolerance of the human-mechatronic system as a whole. As human survey data is of major importance for the complete approach, an optimized version of the custom-built questionnaire will be developed. Based on user response to this, the set of human factors could be validated and specific requirements of particular types of users might be considered. Another questionnaire might be designed to reveal detailed interrelations of enabling and predisposing fac-

---

tors, i. e., technologies and their perception. For a more detailed investigation of such issues, both proposed human-in-the-loop experiments should be implemented and investigated. The elaborated human-machine-centered design framework could further be applied to other lower limb prosthetic components or transferred to other types of prostheses, orthoses and wearable robots.

Regarding variable stiffness actuation, the relationship of natural dynamics and power-optimized operation is clarified for the leg-inspired pendulum example. In this as well as in the exemplary application in the design of a prosthetic knee, advanced modeling including actuator inertia shows to unveil effects that are not observed with common models. Remarkably, it shows that a power-optimal stiffness value can be found in the data from [137] for walking. Further, optimization with respect to peak power is concluded to be beneficial for practical realization. Using it leads to leaner prosthetic system and energy efficiency is decreased only slightly compared to the value for optimal energy consumption. Considering those findings in design leads to energy-efficient prostheses with a wide functional spectrum and long operating time, as it becomes obvious in the proposed knee concept. With this concept, the feasibility of applying variable torsions stiffness actuation in powered lower limb prosthetics is shown. In designing actuators for such systems, issues like functionality and operating time receive more importance and increase system requirements if human factors are considered. A first simulation considering the real biomechanics due to interactions of the human user and the technical system show promising results, as requirements might further be reduced by this.

Aiming at increased functionality and operating time, appropriate control techniques for stiffness variation are required to adapt to the current gait type or velocity. Therefore a variable stiffness control strategy using the advanced models and spectral trajectory analysis is discussed. By adapting stiffness to match the natural dynamics of the system to the trajectory frequency, energy efficiency and functional versatility can be improved. Yet, stiffness should not be adjusted too frequent due to the fact that it consumes a significant share of overall power consumption, i. e., rather during various gait cycles than during a single one. As the connection between power-optimal stiffness, natural dynamics and frequencies in the position signals of gait cannot be clarified with the applied linear models, the algorithm has to be revised for application in prosthetics based on more advanced modeling and the results from power optimization using gait data. Therefore, the investigation of nonlinear effects on the first natural frequency seems to be promising.

Hence, the investigation of unmodeled effects and search for the connection of natural dynamics and power minima in prostheses is a major aspect to future research. A nonlinear version of the presented variable stiffness control strategy

---

---

might support the adjustment to prosthetic application and improve suitability for other applications demanding energy-efficient performance of cyclic tasks. To cover a wider range of gait types and velocities more human data comprising those is required. A suitable inverse dynamics model of human gait might enable more optimized designs by considering the real biomechanical loads due to the prosthesis. Further, a prosthetic prototype actuated by variable torsion stiffness should be set up based on the proposed design concept. Beyond the examination of technical issues, this prototype would also contribute in the validation of the proposed human-machine-centered prosthetic design approach. Finally, only experimental trials with human subjects can show whether a prosthetic solution is accepted and perceived as a fully integrated replacement or not.



---

## A Appendix

---

### A.1 Human and technical factors

---

Subsequently, the items of the different versions of the custom-built questionnaire used in this thesis and initially designed in [57] are listed. The non-demographic and non-freetext items of the first version are presented in Table A.1.

Table A.1: German items of the custom-built questionnaire.

#	Item
1	Sind Sie mit Ihrer Prothese im Alltag zufrieden?
2	Wie zufrieden sind Sie mit der Passung Ihrer Prothese an Ihren Stumpf?
3	Wie zufrieden sind Sie mit dem Gewicht Ihrer Prothese?
4	Wie zufrieden sind Sie mit Ihrer Prothese beim Stehen?
5	Wie zufrieden sind Sie mit Ihrer Prothese beim Gehen/Laufen?
6	Wie zufrieden sind Sie mit Ihrer Prothese beim Sitzen?
7	Haben Sie Probleme mit dem Gleichgewicht beim Stehen?
8	Haben Sie Probleme mit dem Gleichgewicht beim Gehen?
9	Wie oft fühlen Sie sich physisch erschöpft, wenn Sie Ihre Prothese im täglichen Bedarf verwenden?
10	Haben Sie Probleme beim Anziehen der Prothese?
11	Schränkt Sie die Größe der Prothese in Ihrem Alltag ein?
12	Wie oft macht Ihre Prothese Geräusche (Quietschen, Klickgeräusche o.ä.)?
13	Fühlen Sie sich durch diese Geräusche unwohl?
14	Fühlen Sie sich gesellschaftlich eingeschränkt?
15	Sind Sie mit der Akkuleistung Ihrer Prothese zufrieden?
16	Wie oft haben Sie Druckstellen an Ihrem Stumpf, durch einen schlecht anliegenden Schaft?
17	Wie oft haben Sie Blasen an Ihrem Stumpf, durch einen schlecht anliegenden Schaft?
18	Wie oft haben Sie Schwellungen an Ihrem Stumpf, durch einen schlecht anliegenden Schaft?
19	Haben Sie nach längerer Tragezeit Probleme mit der Passung Ihrer Prothese?
20	Fühlen Sie sich durch eine nicht gut anliegende Prothese in Ihrem Alltag eingeschränkt?
21	Wird durch Schweißbildung die Passung von Ihrem Stumpf zur Prothese beeinträchtigt?

- 
- 22 Verwenden Sie eine technische Hilfe um die Passung zwischen Ihrem Stumpf und der Prothese zu verbessern?
- 23 Wie oft, an einem Tag, müssen Sie den Schaft an Ihren Stumpf anpassen?
- 24 Würden Sie eine technische Hilfe in Anspruch nehmen, die dem Verlust des Volumens im Stumpf entgegenwirkt?
- 25 Wie oft haben Sie Schwierigkeiten im Alltag aufgrund eines geschwollenen Stumpfes?
- 26 Verwenden Sie Textilien die das reduzierte Volumen Ihres Stumpfes ausgleichen?
- 27 Würden Sie einen Schaft bevorzugen, der sich selbstständig an die Form und das Volumen des Stumpfes anpasst?
- 28 Belasten Sie beide Beine beim Stehen gleichzeitig?
- 29 Benötigt das Gehen mit der Prothese mehr Muskelkraft als die Bewegungen des gesunden Beines?
- 30 Wäre es für Sie von Vorteil, wenn das Gehen mit der Prothese durch mechanische Unterstützung weniger Muskelkraft erfordern würde?
- 31 Haben Sie Schmerzen/schmerhaftes Ziehen an Ihrem Stumpf, verursacht durch den Schaft der Prothese?
- 32 Wären Sie bereit, um mit weniger Kraftanstrengung gehen zu können, eine osseointegrierte (Prothesenschaft ist mit dem Knochen im Stumpf verbunden) Prothese zu tragen?
- 33 Sind Sie mit der Stabilität während der Standphase Ihrer Prothese zufrieden?
- 34 Sind Sie mit der Stabilität während der Schwungphase Ihrer Prothese zufrieden?
- 35 Sind Sie mit Ihrem Erscheinungsbild in der Öffentlichkeit zufrieden?
- 36 Haben Sie das Gefühl, ein natürliches Gangbild zu haben?
- 37 Sind Sie mit der Schwungbewegung Ihrer Prothese zufrieden?
- 38 Sind Sie mit der Möglichkeit, Ihre Prothese Ausstrecken zu können, zufrieden?
- 39 Wünschen Sie sich mehr mechanische/elektronische Unterstützung beim Strecken ihrer Prothese?
- 40 Sind Sie mit der Möglichkeit, Ihre Prothese Beugen zu können, zufrieden?
- 41 Wünschen Sie sich mehr mechanische/elektronische Unterstützung beim Beugen Ihrer Prothese?
- 42 Ändern Sie häufig Ihre Ganggeschwindigkeit während des Laufens?
- 43 Fühlen Sie sich unwohl, wenn Sie Ihre Ganggeschwindigkeit nicht variieren können?
- 44 Haben Sie Probleme beim Wechseln der Ganggeschwindigkeit mit Ihrer momentanen Prothese?
- 45 Möchten Sie in der Lage sein, Ihre Ganggeschwindigkeit selbstständig zu ändern?
- 46 Sind Sie mit dem Wechsel vom Stand in die Gangphase zufrieden?
- 47 Ist Ihnen eine mechanische/elektronische Unterstützung beim Übergang von der Stand- in die Gangphase wichtig?
- 48 Ist das Treppensteigen für Sie schwierig?
- 49 Fühlen Sie sich unsicher mit Ihrer Prothese als mechanisches Hilfsmittel?

- 
- 50 Ist Ihre Prothese für das Treppensteigen ausgelegt?
- 51 Wie oft bleibt Ihr Fuß beim Treppensteigen an der Stufe hängen?
- 52 Können Sie so Treppensteigen, dass Sie abwechselnd beide Füße auf je eine Stufe aufsetzen?
- 53 Steigen Sie Treppen, indem Sie das gesunde Bein zuerst auf die Stufe stellen und dann die Prothese nachziehen?
- 54 Können Sie sich mit ihrer Prothese bücken?
- 55 Können Sie schwere Gegenstände, die tief stehen, hochheben?
- 56 Sind Sie mit den Bewegungen des Kniegelenks zufrieden?
- 57 Sind Sie mit dem Widerstand des Kniegelenks beim Abbremsen der zufrieden?
- 58 Fühlen Sie sich sicher und stabil, wenn Sie mit der Prothese einen Gleichgewichtsverlust ausgleichen müssen (z. B. bei einem Ausfallschritt um den Körper bei Ungleichgewicht zu stabilisieren)?
- 59 Sind Sie mit der Dämpfung beim Fersenkontakt zufrieden?
- 60 Sind Sie mit der Dämpfung der Prothese beim Strecken zufrieden?
- 61 Sind Sie mit den Dämpfungseigenschaften der Fußprothese zufrieden?
- 62 Haben Sie mit der Fußprothese Probleme bei unebenem Boden oder bei Steigungen?
- 63 Passt sich das Fußgelenk an den jeweiligen Untergrund an?
- 64 Wie oft bleiben Sie mit der Fußprothese an Unebenheiten am Boden hängen?
- 65 Heben Sie Ihren Fuß mit Hilfe der Hüfte an, damit das Bein genügend Abstand zum Boden hat?
- 66 Wenn Sie Gehen, unterstützen Sie diese Bewegung mit einem Anheben der gesunden Hüfte?
- 67 Stoßen Sie sich stärker mit Ihrem gesunden Bein ab, damit Sie einen größeren Abstand zum Boden erhalten?
- 68 Halten Sie eine mechanische/elektronische Unterstützung beim Abrollen des Fußes für notwendig?
- 69 Können Sie mit Ihrer Prothese Schuhe mit unterschiedlicher Absatzhöhe tragen?
- 70 Wäre eine Fußprothese, die sich an die Absatzhöhe ihrer Schuhe anpasst, wünschenswert?
- 71 Haben Sie Schmerzen in der Hüfte auf der Seite der Amputation?
- 72 Haben Sie Schmerzen in der Hüfte auf der gesunden Seite, die aufgrund der Prothese entstanden sind?
- 73 Haben Sie Schmerzen im Rücken, die aufgrund der Prothese entstanden sind?
- 74 Haben Sie Schmerzen im Bein der gesunden Seite?
-

The English versions of the non-demographic and non-freetext items of the questionnaire designed in [57] are presented in Table A.2.

Table A.2: English items of the custom-built questionnaire.

#	Item
1	Are you satisfied with your prosthesis in everyday life?
2	How satisfied are you with the fitting of your prosthesis to your stump?
3	How satisfied are you with the weight of your prosthesis?
4	How satisfied are you with your prosthesis during standing?
5	How satisfied are you with your prosthesis during walking/running?
6	How satisfied are you with your prosthesis during sitting?
7	Do you have balance problems while standing?
8	Do you have balance problems while walking?
9	If you use your prosthesis during daily tasks, how often do you feel mentally exhausted?
10	Do you have problems to apply your prosthesis?
11	Are you restricted in everyday life by the size of your prosthesis?
12	How often is your prosthesis making noises (squeaking, clicking,...)?
13	Do you feel uncomfortable by this noises?
14	Do you feel socially restricted?
15	Are you satisfied with the battery performance of your prosthesis?
16	How often do you have pressure marks on your stump, based on a badly fitting shaft?
17	How often do you have blisters on your stump, based on a badly fitting shaft?
18	How often do you have swellings on your stump, based on a badly fitting shaft?
19	After you have worn the prosthesis for a longer period (without interruption), do you have problems with the fitting?
20	Are you restricted in your everyday life by a badly fitting prosthesis?
21	Is the fitting of your prosthesis to your stump affected due to perspiration?
22	Do you use any kind of technical assistance to enhance the fitting between your stump and the prosthesis?
23	How often, at one day, do you have to adjust the shaft on your stump?
24	If it would reduce the loss of your stump volume, would you use a technical assistance?
25	How often in your everyday life do you have problems because of a swollen stump?
26	Do you use textiles to reduce the loss of your stumps volume?
27	Would you prefer a shaft which fits itself onto the stump automatically (form and volume)?
28	While standing, do you load both legs contemporary (balanced weight bearing)?
29	Does walking with the prosthesis use more muscle power than the movement of sound leg?

- 
- 
- 30 Would it be advantageous for you if walking with mechanical supported prosthesis would need less muscle power?
- 31 Do you have twinge pain at your stump because of the prosthesis shaft?
- 32 Would you be ready for an osseointegrated prosthesis (prosthesis shaft is connected with the bone of the stump) to walk with less physical effort?
- 33 Are you satisfied with the stability of your prosthesis during stance phase?
- 34 Are you satisfied with the stability of your prosthesis during swing phase?
- 35 Are you satisfied with your appearance in public?
- 36 Do you think you have a natural gait pattern?
- 37 Are you satisfied with the swing movement of your prosthesis?
- 38 Are you satisfied with the possibility of your prosthesis in extension?
- 39 Do you wish more mechanical/electronic assistance during the extension of your prosthesis?
- 40 Are you satisfied with the possibility of your prosthesis in flexion?
- 41 Do you wish more mechanical/electronic assistance during the flexion of your prosthesis?
- 42 Do you often change your gait speed during walking?
- 43 Do you feel comfortable when you cannot change gait speed?
- 44 Do you have problems with your prosthesis while changing gait speed?
- 45 Do you want to be able to change your gait speed yourself?
- 46 Are you satisfied with the transition from standing to walking?
- 47 Is a mechanical/electronic support for the transition from standing to walking important for you?
- 48 Is stair climbing difficult for you?
- 49 Do you feel uncertain with your prosthesis as a mechanical assistant?
- 50 Is your prosthesis designed for stair climbing?
- 51 How often you get caught on a step with the foot?
- 52 Are you able to climb stairs alternately with both feet?
- 53 Are you climbing stairs in the way that you use the sound leg for the first step and than afterwards drag behind the prosthesis?
- 54 Are you able to bend down with your prosthesis?
- 55 Are you able to lift low lying heavy things?
- 56 Are you satisfied with the movements of the knee joint?
- 57 Are you satisfied with the resistance of the knee joint during decelerating?
- 58 Do you feel certain and stable when you have to clear the loss of balance (e.g. to stabilize the body by unbalance during a lunge/sidestep)?
- 59 Are you satisfied with the damping/absorption by heel-contact?
- 60 Are you satisfied with the damping/absorption during the extension of your prosthesis?
- 61 Are you satisfied with the damping/absorption quality of your foot prosthesis?
- 62 Do you have any problems with your foot prosthesis on uneven ground or inclines?

- 
- 63 Does the ankle joint adjust to any particular ground?  
 64 How often you get caught with your foot prosthesis on uneven ground?  
 65 Do you lift your foot with the aid of your hips so that your leg has got enough distance to the ground?  
 66 If you are walking, do you support the movement with lifting of the sound hip?  
 67 Do you push off more intense your sound leg so that you have got ground clearance?  
 68 Do you think a mechanical/electronical support is necessary for roll your foot from heel to toe?  
 69 Are you able to wear shoes with different heel levels with your prosthesis?  
 70 Is a foot prosthesis which adjusts itself on different heel levels preferable?  
 71 Are you in pain at the hip on the side of the amputation?  
 72 Are you in pain at the hip of the sound side, because of the prosthesis?  
 73 Do you have back pain because of the prosthesis?  
 74 Are you in pain at the leg of the sound side?
- 

The German items regarding body schema integration are given in Table A.3.

Table A.3: German items on body schema integration.

#	Item
1	Erscheint Ihnen ihre Prothese beim Blick auf Ihre Beine im Alltag als wäre sie ein Teil ihres Körpers?
2	Hat sich Ihre Wahrnehmung der Prothese im alltäglichen Gebrauch an die des entsprechenden echten Körperteils angelehnt?
3	Haben Sie das Gefühl, dass die Prothese ein Teil von Ihnen ist?
4	Haben Sie das Gefühl, dass die Prothese Ihr neues echtes Bein ist?
5	Haben Sie das Gefühl, dass die Prothese ein Teil Ihres Körpers ist?
6	Nehmen Sie die Prothese an der Stelle wahr, an der sie das entsprechende Körperteil lokalisieren würden?
7	Befindet sich die Prothese an der Stelle, wo sich Ihre ehemalige echte Extremität befand?
8	Spüren Sie die Position Ihrer Prothese im Raum ohne diese anzuschauen?
9	Fühlen Sie die Beschaffenheit des Untergrundes durch Ihre Prothese?
10	Nehmen Sie Berührungen an der Prothese als Berührung des entsprechenden Körperteils wahr?
11	Erscheint es Ihnen so, als könnten Sie die Prothese zu jeder Zeit kontrollieren?
12	Haben Sie das Gefühl, die Bewegungen Ihrer Prothese kontrollieren zu können?
13	Können Sie ein Jucken am entsprechenden Körperteil durch Kratzen an der Prothese lindern?

---

The English items regarding body schema integration are given in Table A.4.

Table A.4: English items on body schema integration.

#	Item
1	Does your prosthesis seem to be a part of your body when you look at it in daily life?
2	Did your perception of the prosthesis approach the one of the according real part of the body?
3	Do you have the feeling that the prosthesis belongs to you?
4	Do you have the feeling that the prosthesis is your new real leg?
5	Do you have the feeling that the prosthesis is part of your body?
6	Do you perceive the prosthesis in the location where you would localize the corresponding part of the body?
7	Is the prosthesis in the location where your former real extremity was located?
8	Do you feel the spatial position of your prosthesis without looking at it?
9	Do you feel the structure of the ground surface through your prosthesis?
10	Do you perceive contacts with the prosthesis as contacts with the corresponding part of the body?
11	Does it seem to you like you can control the prosthesis at any time?
12	Do you have the feeling to be able to control the movements of your prosthesis?
13	Can you relieve itching at the corresponding part of the body by scratching the prosthesis?

Figure A.1 shows technical solutions, criteria and further information determined in technical factor analysis of powered prosthetic knees.

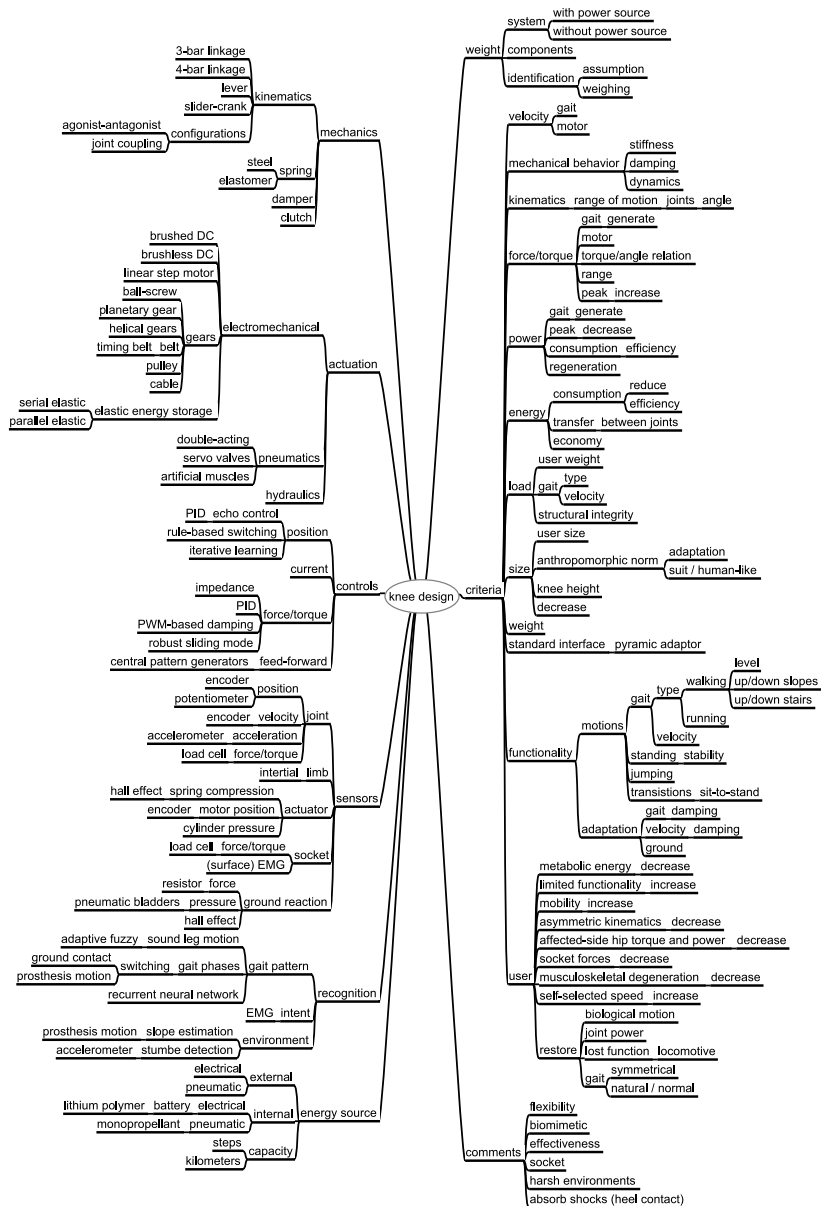


Figure A.1: Complete list of technical solutions, criteria and further information.

---

## A.2 Model parameters of the proposed prosthetic concept

---

Table A.5 gives the model parameters reflecting the dynamics properties of the proposed prosthetic concept with respect to the model from [248].

Table A.5: Dynamics properties of the proposed prosthetic concept with respect to the model from [248].

Parameter	$I_{sh}$	$I_{fo}$	$m_{sh}$	$m_{fo}$	$l_{sh}$	$p_{sh,a}$	$p_{fo,a}$	$p_{fo,g}$
Value	0.065	0.001	4.13	0.337	0.404	0.192	0.042	0.027
Unit	kg m <sup>2</sup>	kg m <sup>2</sup>	kg	kg	m	m	m	m

---

## A.3 Component list of the variable torsion stiffness prototype

---

Table A.6 lists the components of the variable torsion stiffness prototype.

Table A.6: Component list of variable torsion stiffness prototype.

Component	#	Manufacturer	Type
Motor	1	Bühler Motor GmbH, Nuremberg, GER	1.13.075.214
Planetary gears	1	Neugart GmbH, Kippenheim, GER	PLE 80-80
Bellows coupling	1	HAFNER Maschinenbau GmbH	MKJ-S 100 ST
Link drive		Kleinwallstadt, GER	
Roller bearings	4	Standard parts	61804/5/7/8 RS
Motor	1	Bühler Motor GmbH, Nuremberg, GER	1.13.075.214
Planetary gears	1	Neugart GmbH, Kippenheim, GER	PLE 40-4
Bellows coupling	1	HAFNER Maschinenbau GmbH, Kleinwallstadt, GER	MKJ 45
Ball-screw	1	Bosch-Rexroth AG, Lohr am Main, GER	20X10RX3
Fixed bearing	1	Bosch-Rexroth AG, Lohr am Main, GER	SEB-F-Z 12
Floating bearing	1	Bosch-Rexroth AG, Lohr am Main, GER	SEB-L-S 12
Stiffness adjustment			
Linear guiding rail	2	SKF GmbH, Schweinfurt, GER	TSX25-D
Linear carriage	2	SKF GmbH, Schweinfurt, GER	RWU25-D-FE-G2-V2
Sleeve bearing	2	igus GmbH, Cologne, GER	iglidur Z
Motor controller	2	Granite Devices Oy, Tampere, Finland	VSD-XE
Power supply	1	MEAN WELL Enterprises Co., Ltd., Taipei, Taiwan	HRP-600-48
Electronics			
Control platform	1	National Instruments Germany GmbH, Munich, GER	CompactRio 9082
Incremental Encoder	3	PWB encoders GmbH, Eisenach, GER	ME 22

---

## Acknowledgements

---

The author would like to thank Prof. Dr.-Ing. Stephan Rinderknecht for the supervision of this work and providing a great creative freedom as well as Prof. Dr. rer. nat. Oskar von Stryk for agreeing to act as the second examiner and his critical and constructive perspective on the content of this work.

Further gratitude is owed to Dr. Oliver Christ, Dr.-Ing. Torsten Felzer, Dr.-Ing. Daniel Labisch, Jochen Schuy, Tim Schürmann, Dr.-Ing. Bruno Strah, and Janis Wojtusch for supporting this work with intensive discussions and reviewing the manuscript. The early encouragement regarding the inclusion of psychological aspects and design methodology by Marita Unden and Moritz Keim is highly appreciated by the author. Another thanks goes to Prof. Dr. Jan Peters, Prof. Dr. André Seyfarth, and Prof. Dr. Joachim Vogt for the pleasant collaboration and discussions. Tribute is paid to Philipp Erler, Christian Framing, Florian Stuhlenmiller, Michael Windrich, and David Wartenberg for their eager support in the laboratory, to Walter Rausch and Uwe Rodenhäuser for manufacturing parts for the prototype as well as Dr. Susanne Lipfert for providing human gait data and Ines Passier for moderating the QFD-discussion. Regarding layout and administrative issues the author thanks Sabine Backhaus, Birgit Lampert, and Ursula Willner.

Beyond this, thanks go to the colleagues supporting this work at the *Institute for Mechatronic Systems in Mechanical Engineering* and those from *Intelligent Autonomous Systems Lab*, the *Locomotion Lab, Simulation, Systems Optimization and Robotics Group* as well as *Work and engineering psychology group*, who create a stimulating, interdisciplinary research environment at *Technische Universität Darmstadt*. The support from *Bundesinnungsverband für Orthopädie. Technik, Bundesverband für Menschen mit Arm- oder Beinamputation, Chas A Blatchford and Sons Ltd., Fraunhofer IPA Stuttgart, German Jordanian University, Heidelberg Motion Lab, medi GmbH & Co. KG, MediClin AG, Össur Europe BV, Otto Bock HealthCare GmbH, Sanitätshaus Klein Dieburg, Selbsthilfegruppe für Arm und Beinamputierte Bayern e.V Coburg, Universiteit Twente, University of Alabama, Vanderbilt University and Vrije Universiteit Brussel* is valued. Thanks for hardware donations go to *Bühler Motor GmbH, National Instruments Germany, HAFNER Maschinenbau GmbH, and Igus GmbH*.



---

## Bibliography

---

- [1] M. Ackermann. *Dynamics and Energetics of Walking with Prostheses*. PhD thesis, University of Stuttgart, 2007.
- [2] Y. Akao, editor. *Quality Function Deployment - Integrating Customer Requirements into Product Design*. Productivity Press, 1990.
- [3] A. Albu-Schäffer. *Regelung von Robotern mit elastischen Gelenken am Beispiel der DLR-Leichtbauarme*. Dissertation, Technische Universität München, 2002.
- [4] A. Albu-Schäffer, S. Wolf, O. Eiberger, S. Haddadin, F. Petit, and M. Chalon. Dynamic modelling and control of variable stiffness actuators. In *IEEE International Conference on Robotics and Automation*, 2010.
- [5] S. K. Au, P. Dilworth, and H. Herr. An ankle-foot emulation system for the study of human walking biomechanics. In *IEEE International Conference on Robotics and Automation*, 2006.
- [6] S. K. Au, J. Weber, and H. Herr. Powered ankle-foot prosthesis improves walking metabolic economy. *IEEE Transactions on Robotics*, 25 (1):51 – 66, 2009.
- [7] A. T. Bahill and W. L. Chapman. A tutorial on quality function deployment. *Engineering Management Journal*, 5 (3):24 – 35, 1993.
- [8] R. Baumgartner and P. Botta. *Amputation und Prothesenversorgung*. Thieme, 2008.
- [9] P. Beckerle, O. Christ, M. Windrich, S. Rinderknecht, J. Vogt, and J. Wojtusch. A methodological approach to integrate psychological factors to lower limb prosthetic functional design. In *International Society of Prosthetics and Orthotics World Congress*, 2013.
- [10] P. Beckerle, O. Christ, M. Windrich, G. Schütz, J. Vogt, and S. Rinderknecht. User-centered prosthetic design: A methodological approach to transfer psychological factors to technical development. In *European Conference Technically Assisted Rehabilitation*, 2013.
- [11] P. Beckerle, O. Christ, J. Wojtusch, J. Schuy, K. Wolff, S. Rinderknecht, J. Vogt, and O. von Stryk. Design and control of a robot for the assessment

- of psychological factors in prosthetic development. In *IEEE International Conference on Systems, Man and Cybernetics*, 2012.
- [12] P. Beckerle, L. Lahnstein, J. Wojtusch, S. Rinderknecht, and O. von Stryk. Conception and design of a hardware simulator for restoring lost biomechanical function. In *IEEE International Conference on Systems, Man and Cybernetics*, 2013.
  - [13] P. Beckerle and S. Rinderknecht. A variable stiffness control strategy using system dynamics and spectral trajectory analysis. In *International Workshop on Human-Machine Systems, Cyborgs and Enhancing Devices*, 2013.
  - [14] P. Beckerle, F. Schültje, J. Wojtusch, and O. Christ. Implementation, Control and User-Feedback of the Int<sup>2</sup>Bot for the Investigation of Lower Limb Body Schema Integration. In *IEEE International Symposium on Robot and Human Interactive Communication*, 2014.
  - [15] P. Beckerle, J. Wojtusch, S. Rinderknecht, and O. v. Stryk. Mechanical influences on the design of actuators with variable stiffness. In *International Symposium on Adaptive Motion of Animals and Machines*, 2013.
  - [16] P. Beckerle, J. Wojtusch, S. Rinderknecht, and O. von Stryk. Analysis of system dynamic influences in robotic actuators with variable stiffness. *Smart Structures and Systems*, 13 (4):711 – 730, 2014.
  - [17] P. Beckerle, J. Wojtusch, J. Schuy, B. Strah, S. Rinderknecht, and O. v. Stryk. Power-optimized stiffness and nonlinear position control of an actuator with variable torsion stiffness. In *IEEE/ASME International Conference on Advanced Intelligent Mechatronics*, 2013.
  - [18] R. D. Bellman, M. A. Holgate, and T. G. Sugar. Sparky 3: Design of an active robotic ankle prosthesis with two actuated degrees of freedom using regenerative kinetics. In *IEEE International Conference on Biomedical Robotics and Biomechatronics*, 2008.
  - [19] D. Berry. Microprocessor prosthetic knees. *Physical Medicine and*, 17:91 – 113, 2006.
  - [20] S. Blumentritt, M. Bellmann, E. Ludwigs, and T. Schmalz. Zur biomechanik des mikroprozessorgesteuerten prothesenkniegelenks genium. *Orthopädie Technik*, 1:24 – 35, 2012.

- 
- [21] S. Böker, P. Beckerle, J. Wojtusch, and S. Rinderknecht. A novel design approach and operational strategy for an active ankle-foot prosthesis. In *International Symposium on Adaptive Motion of Animals and Machines*, 2013.
- [22] R. Borjian, J. Lim, M. B. Khamesee, and W. Melek. The design of an intelligent mechanical active prosthetic knee. In *Annual Conference of IEEE Industrial Electronics*, 2008.
- [23] J. Bortz. *Statistik für Human- und Sozialwissenschaftler*. Springer, 2005.
- [24] M. Botvinick and J. Cohen. Rubber hands 'feel' touch that eyes see. *Nature*, 391:756, 1998.
- [25] V. Bouchereau and H. Rowlands. Quality function deployment: the unused tool. *Engineering Management Journal*, Feb:45 – 52, 2000.
- [26] D. J. Braun, F. Petit, F. Huber, S. Haddadin, P. van der Smagt, A. Albu-Schäffer, and S. Vijayakumar. Optimal torque and stiffness control in compliantly actuated robots. In *IEEE/RSJ International Conference on Intelligent Robots and Systems*, 2012.
- [27] D. J. Braun, F. Petit, F. Huber, S. Haddadin, P. van der Smagt, A. Albu-Schäffer, and S. Vijayakumar. Robots driven by compliant actuators: Optimal control under actuation constraints. *IEEE Transactions on Robotics*, 29 (5):1085 – 1101, 2013.
- [28] J. W. Breakey. Body image: The lower-limb amputee. *Journal of Prosthetics and Orthotics*, 9 (2):58 – 66, 1997.
- [29] B. Brogliato, R. Ortega, and R. Lozano. Global tracking controllers for flexible-joint manipulators: a comparative study. *Automatica*, 31:941 – 956, 1995.
- [30] R. Carloni and L. Marconi. Limit cycles and stiffness control with variable stiffness actuators. In *IEEE/RSJ International Conference on Intelligent Robots and Systems*, 2012.
- [31] M. Catalano, G. Grioli, F. Bonomo, R. Schiavi, and A. Bicchi. Vsa-hd: From the enumeration analysis to the prototypical implementation. In *IEEE/RSJ International Conference on Intelligent Robots and Systems*, 2011.
- [32] L.-K. Chan and M.-L. Wu. Quality function deployment: A literature review. *European Journal of Operational Research*, 143:463 – 497, 2002.

- 
- [33] P. Cherelle, V. Grosu, A. Matthyss, B. Vanderborght, and D. Lefeber. Design and validation of the ankle mimicking prosthetic (amp-) foot 2.0. *IEEE Transactions on Neural Systems and Rehabilitation Engineering*, 22 (1):138 – 148, 2014.
- [34] J. Choi, S. Hong, W. Lee, S. Kang, and M. Kim. A robot joint with variable stiffness using leaf springs. *IEEE Transactions on Robotics*, 27:229 – 238, 2011.
- [35] O. Christ, P. Beckerle, J. Preller, M. Jokisch, S. Rinderknecht, J. Wojtusch, O. von Stryk, and J. Vogt. The rubber hand illusion: Maintaining factors and a new perspective in rehabilitation and biomedical engineering? *Biomedical Engineering*, 57(S1):1098 – 1101, 2012.
- [36] O. Christ, P. Beckerle, S. Rinderknecht, and J. Vogt. Usability, satisfaction and appearance while using lower limb prostheses: Implications for the future. *Neuroscience Letters*, 500 (S1):e50, 2011.
- [37] O. Christ, A. Elger, K. Schneider, P. Beckerle, J. Vogt, and S. Rinderknecht. Identification of haptic paths with different resolution and their effect on body scheme illusion in lower limbs. *Technically Assisted Rehabilitation*, 2013.
- [38] O. Christ, M. Jokisch, J. Preller, P. Beckerle, S. Rinderknecht, J. Wojtusch, O. von Stryk, and J. Vogt. User-centered prosthetic development: Comprehension of amputees' needs. *Biomedical Engineering*, 57(S1):1098 – 1101, 2012.
- [39] O. Christ and M. Reiner. Perspectives and possible applications of the rubber hand and virtual hand illusion in non-invasive rehabilitation: Technological improvements and their consequences. *Neuroscience and Biobehavioral Reviews*, 2014.
- [40] O. Christ, J. Wojtusch, and P. Beckerle. Robotic mirroring of movements in the lower limbs: signal delay of a consumer device sensor. *SAN2014 Meeting, Book of Abstracts*, 2014.
- [41] O. Christ, J. Wojtusch, P. Beckerle, K. Wolff, J. Vogt, O. von Stryk, and S. Rinderknecht. Prosthesis-User-in-the-Loop: User-Centered Design Parameters and Visual Simulation. In *Annual International Conference of the IEEE EMBS*, 2012.
- [42] J. Churcher. Implications and applications of piaget's sensorimotor concepts. *Adaptive Control of Ill-Defined Systems*, 16:289 – 304, 1984.

- 
- 
- [43] E. Churchill, L. L. Laubach, J. T. McConville, and I. Tebbetts. Anthropometric source book. Volume I: anthropometry for designers. NASA, 1978.
  - [44] J. Cole. *Psychoprosthetics*, chapter Virtual and Augmented Reality, Phantom Experience, and Prosthetics, pages 119 – 129. Springer, 2008.
  - [45] S. H. Collins and A. D. Kuo. Recycling energy to restore impaired ankle function during human walking. *PLoS ONE*, 5 (2):e9307, 2010.
  - [46] R. R. Craig and A. J. Kurdila. *Fundamentals Of Structural Dynamics*. John Wiley & Sons, 2011.
  - [47] A. De Luca. Feedforward/Feedback Laws for the Control of Flexible Robots. In *IEEE International Conference on Robotics and Automation*, 2000.
  - [48] A. De Luca, R. Farina, and P. Lucibello. On the control of robots with visco-elastic joints. In *IEEE International Conference on Robotics and Automation*, 2005.
  - [49] A. De Luca, F. Flacco, A. Bicchi, and R. Schiavi. Nonlinear decoupled motion-stiffness control and collision detection/reaction for the vsa-ii variable stiffness device. In *IEEE/RSJ International Conference on Intelligent Robots and Systems*, 2009.
  - [50] A. De Luca and L. Lanari. Robots with elastic joints are linearizable via dynamic feedback. In *IEEE Conference on Decision and Control*, 1995.
  - [51] A. De Luca, S. Panzieri, and G. Ulivi. Stable inversion control of flexible link manipulators. In *IEEE International Conference on Robotics and Automation*, 1998.
  - [52] R. Dedic and H. Dindo. Smartleg: An intelligent active robotic prosthesis for lower-limb amputees. In *International Symposium on Information, Communication and Automation Technologies*, 2011.
  - [53] S. Delp, F. C. Anderson, A. S. Arnold, P. Loan, A. Habib, C. T. John, E. Guendelman, and T. D. G. Opensim: Open-source software to create and analyze dynamic simulations of movement. *IEEE Transactions on Biomedical Engineering*, 54 (11):1940 – 1950, 2007.
  - [54] DIN Deutsches Institut für Normung e.V. EN ISO 9241-9:2000, Ergonomische Anforderungen für Bürotätigkeiten mit Bildschirmgeräten, 2000.

- 
- [55] H. Dresig and F. Holzweißig. *Maschinendynamik*. Springer, 2012.
- [56] O. Eiberger, S. Haddadin, M. Weis, A. Albu-Schäffer, and G. Hirzinger. On joint design with intrinsic variable compliance: derivation of the DLR QA-Joint. In *IEEE International Conference on Robotics and Automation*, 2010.
- [57] M. Engel. Entwurf eines Fragebogens zur Erhebung des Verbesserungspotentials bei Beinprothesen. Studienarbeit, Institute for Mechatronic Systems in Mechanical Engineering, Technische Universität Darmstadt, 2010.
- [58] P. Erler. Regelung eines Prüfstandes zur Untersuchung eines Antriebsstranges mit variabler Torsionssteifigkeit. Master's thesis, Institute for Mechatronic Systems in Mechanical Engineering, Technische Universität Darmstadt, 2013.
- [59] P. Erler, P. Beckerle, B. Strah, and S. Rinderknecht. Experimental comparison of nonlinear motion control methods for a variable stiffness actuator. In *IEEE International Conference on Biomedical Robotics and Biomechatronics*, 2014.
- [60] M. Eslamy, M. Grimmer, S. Rinderknecht, and A. Seyfarth. Does it pay to have a damper in a powered ankle prosthesis? A Power-Energy Perspective. In *IEEE International Conference on Rehabilitation Robotics*, 2013.
- [61] M. Eslamy, M. Grimmer, and A. Seyfarth. Effects of unidirectional parallel springs on required peak power and energy in powered prosthetic ankles: Comparison between different active actuation concepts. In *IEEE International Conference on Robotics and Biomimetics*, 2012.
- [62] C. Everarts, B. Dehez, and R. Ronsse. Variable stiffness actuator applied to an active ankle prosthesis: Principle, energy-efficiency, and control. In *IEEE/RSJ International Conference on Intelligent Robots and Systems*, 2012.
- [63] J. Feldhusen and K.-H. Grote, editors. *Pahl/Beitz Konstruktionslehre*. Springer Vieweg, 2013.
- [64] K. Fite, J. Mitchell, F. Sup, and M. Goldfarb. Design and control of an electrically powered knee prosthesis. In *IEEE International Conference on Rehabilitation Robotics*, 2007.
- [65] W. Friedl, H. Höppner, F. Petit, and G. Hirzinger. Wrist and Forearm Rotation of the DLR Hand Arm System: Mechanical Design, Shape Analysis

and Experimental Validation. In *IEEE/RSJ International Conference on Intelligent Robots and Systems*, 2011.

- [66] R. S. Gailey, K. E. Roach, E. B. Applegate, B. Cho, B. Cunniffe, S. Licht, M. Maguire, and M. S. Nash. The amputee mobility predictor: An instrument to assess determinants of the lower-limb amputee's ability to ambulate. *Archives of Physical Medicine and Rehabilitation*, 83:613 – 627, 2002.
- [67] P. Gallagher and M. MacLachlan. Development and psychometric evaluation of the trinity amputation and prosthesis experience scales (tapes). *Rehabilitation Psychology*, 45 (2):130 – 154, 2000.
- [68] S. Gallagher and J. Cole. Body Schema and Body Image in a Deafferented Subject. *Journal of Mind and Behavior*, 16:369 – 390, 1995.
- [69] M. Garabini, A. Passaglia, F. Belo, P. Salaris, and A. Bicchi. Optimality principles in variable stiffness control: The vsa hammer. In *IEEE/RSJ International Conference on Intelligent Robots and Systems*, 2011.
- [70] C. Gauthier-Gagnon, M. C. Grisé, and P. D. Enabling factors related to prosthetic use by people with transtibial and transfemoral amputation. *Archives of Physical Medicine and Rehabilitation*, 80 (6):706 – 713, 1999.
- [71] J. Geeroms, L. Flynn, R. Jimenez-Fabian, B. Vanderborght, and D. Lefeber. Ankle-Knee Prosthesis with Powered Ankle and Energy Transfer for CYBERLEGs  $\alpha$ -Prototype. In *IEEE International Conference on Rehabilitation Robotics*, 2013.
- [72] Y. Geng, X. Xu, L. Chen, and P. Yang. Design and analysis of active transfemoral prosthesis. In *36th Annual Conference on IEEE Industrial Electronics Society*, 2010.
- [73] Y. Geng, P. Yang, X. Xu, and L. Chen. Design and simulation of active transfemoral prosthesis. In *Chinese Control and Decision Conference*, 2012.
- [74] H. Geyer and H. Herr. A muscle-reflex model that encodes principles of legged mechanics produces human walking dynamics and muscle activities. *IEEE Transactions on Neural Systems and Rehabilitation Engineering*, 18 (3):263 – 273, 2010.
- [75] M. J. Giumenti, S. J. Gibson, N. Georgiou-Karistianisa, and J. L. Bradshaw. Mechanisms underlying embodiment, disembodiment and loss of embodiment. *Neuroscience and Biobehavioral Reviews*, 32:143 – 160, 2008.

- 
- [76] H. Greil. Körpermaße 2000: Aktuelle Perzentilwerte der deutschen Bevölkerung im jungen Erwachsenenalter. *Brandenburgische Umwelt Berichte*, 2001.
- [77] B. Greitemann, H. Bork, and L. Brückner. *Rehabilitation Amputierter*. Göttinger Verlag, 2002.
- [78] M. Grimmer, M. Eslamy, S. Gliech, and A. Seyfarth. A comparison of parallel- and series elastic elements in an actuator for mimicking human ankle joint in walking and running. In *IEEE International Conference on Robotics and Automation*, 2012.
- [79] M. Grimmer and A. Seyfarth. Stiffness adjustment of a series elastic actuator in a knee prosthesis for walking and running: The trade-off between energy and peak power optimization. In *IEEE/RSJ International Conference on Intelligent Robots and Systems*, 2011.
- [80] M. Grimmer and A. Seyfarth. Stiffness adjustment of a series elastic actuator in an ankle-foot prosthesis for walking and running: The trade-off between energy and peak power optimization. In *IEEE International Conference on Robotics and Automation*, 2011.
- [81] S. S. Groothuis, G. Rusticelli, A. Zucchelli, S. Stramigioli, and R. Carloni. The vsaUT-II: A novel rotational variable stiffness actuator. In *IEEE International Conference on Robotics and Automation*, 2012.
- [82] D. Gross, W. Hauger, J. Schröder, and W. A. Wall. *Technische Mechanik 3: Kinetik*. Springer, 2010.
- [83] D. Gross, W. Hauger, J. Schröder, and W. A. Wall. *Technische Mechanik 2: Elastostatik*. Springer, 2012.
- [84] K.-H. Grote and J. Feldhusen, editors. *Dubbel - Taschenbuch für den Maschinenbau*. Springer, 2005.
- [85] K. L. Gwet. *Handbook of Inter-Rater Reliability*. Advanced Analytics, LLC, 2012.
- [86] S. Haddadin, A. Albu-Schaeffer, A. De Luca, and Hirz. Collision detection and reaction: A contribution to safe physical human-robot interaction. In *IEEE International Conference on Robotics and Automation*, 2008.

- 
- [87] S. Haddadin, F. Huber, and A. Albu-Schäffer. Optimal control for exploiting the natural dynamics of variable stiffness robots. In *IEEE International Conference on Robotics and Automation*, 2012.
  - [88] S. Haddadin, M. C. Özparpucu, and A. Albu-Schäffer. Optimal control for maximizing potential energy in a variable stiffness joint. In *IEEE Conference on Decision and Control*, 2012.
  - [89] B. J. Hafner and D. G. Smith. Differences in function and safety between medicare functional classification level-2 and -3 transfemoral amputees and influence of prosthetic knee joint control. *Journal of Rehabilitation Research & Development*, 46 (3):417 – 434, 2009.
  - [90] B. J. Hafner, L. L. Willingham, N. C. Buell, K. J. Allyn, and D. G. Smith. Evaluation of function, performance, and preference as transfemoral amputees transition from mechanical to microprocessor control of the prosthetic knee. *Archives of Physical Medicine and Rehabilitation*, 88(2):207 – 217, 2007.
  - [91] S. I. Hailmann. Interviewstudie zur Körperintegritätswahrnehmung von Beinprothesenträgern. Studienarbeit, Work and engineering psychology research group & Institute for Mechatronic Systems in Mechanical Engineering, Technische Universität Darmstadt, 2011.
  - [92] G. Heller, Günster, and E. Swart. Über die Häufigkeit von Amputationen unterer Extremitäten in Deutschland. *Deutsche Medizinische Wochenschrift*, 130 (28/29):1689 – 1690, 2005.
  - [93] M. J. Highsmith, J. T. Kahle, D. R. Bongiorni, B. S. Sutton, S. Groer, and K. R. Kaufman. Safety, energy efficiency, and cost efficacy of the c-leg for transfemoral amputees: A review of the literature. *Prosthetics and Orthotics International*, 34 (4):362 – 377, 2010.
  - [94] J.-M. Hoc. *The Oxford Handbook of Cognitive Engineering*, chapter Human-Machine Cooperation, pages 395 – 403. Oxford University Press, 2013.
  - [95] M. A. Holgate, J. K. Hitt, R. D. Bellman, T. G. Sugar, and K. W. Hollander. Sparky (spring ankle with regenerative kinetics) project: Choosing a dc motor based actuation method. In *IEEE International Conference on Biomedical Robotics and Biomechatronics*, 2008.
  - [96] K. W. Hollander, R. Ilg, and T. G. Sugar. Design of the robotic tendon. In *Design of Medical Devices Conference*, 2005.

- 
- [97] K. W. Hollander, R. Ilg, T. G. Sugar, and D. Herring. An efficient robotic tendon for gait assistance. *Journal of Biomechanical Engineering*, 128:788 – 791, 2006.
- [98] K. W. Hollander, T. G. Sugar, and D. Herring. Adjustable robotic tendon using a ‘jack spring’<sup>TM</sup>. *IEEE International Conference on Rehabilitation Robotics*, pages 113 – 118, 2005.
- [99] C. D. Hoover, G. D. Fulk, and K. B. Fite. The design and initial experimental validation of an active myoelectric transfemoral prosthesis. *Journal of Medical Devices*, 6 (1):011005, 2012.
- [100] M. Howard, D. J. Braun, and S. Vijayakumar. Constraint-based equilibrium and stiffness control of variable stiffness actuators. *IEEE International Conference on Robotics & Automation*, 2011.
- [101] T.-H. Huang, J.-Y. Kuan, and H.-P. Huang. Design of a new variable stiffness actuator and application for assistive exercise control. In *IEEE/RSJ International Conference on Intelligent Robots and Systems*, 2011.
- [102] A. M. Huff, B. E. Lawson, and M. Goldfarb. A running controller for a powered transfemoral prosthesis. In *Annual International Conference of the IEEE EMBS*, 2012.
- [103] S. Huh, G. Tonietti, and A. Bicchi. Neural network based robust adaptive control for a variable stiffness actuator. In *Mediterranean Conference on Control and Automation*, 2008.
- [104] S.-H. Huh and Z. Bien. Robust sliding mode control of a robot manipulator based on variable structure-model reference adaptive control approach. *IET Control Theory & Applications*, 1 (5):1355 – 1363, 2007.
- [105] J. W. Hurst, J. E. Chestnutt, and A. A. Rizzi. An actuator with physically variable stiffness for highly dynamic legged locomotion. In *IEEE International Conference on Robotics and Automation*, 2004.
- [106] IEA. Iea triennial report, 2000 - 2003. Technical report, IEA Press, 2003.
- [107] R. Isermann. *Mechatronische Systeme - Grundlagen*. Springer, 1999.
- [108] R. Isermann and M. Münchhof. *Identification of Dynamic Systems - An Introduction with Applications*. Springer, 2011.

- 
- 
- [109] G. E. Jacques, S. Ryan, S. Naumann, M. Milner, and W. L. Cleghorn. Application of quality function deployment in rehabilitation engineering. *IEEE Transactions on Rehabilitation Engineering*, 2 (3):158 – 164, 1994.
  - [110] A. Jafari, N. G. Tsagarakis, and D. G. Caldwell. AwAS-II: a new actuator with adjustable stiffness based on the novel principle of adaptable pivot point and variable lever ratio. In *IEEE International Conference on Robotics and Automation*, 2011.
  - [111] A. Jafari, N. G. Tsagarakis, B. Vanderborght, and D. G. Caldwell. A novel actuator with adjustable stiffness (AwAS). In *IEEE/RSJ International Conference on Intelligent Robots and Systems*, 2010.
  - [112] M. Jokisch, J. Preller, A. Schropp, O. Christ, P. Beckerle, and J. Vogt. The rubber hand illusion paradigm transferred to the lower limb: A physiological, behavioral and psychometric approach. *International Journal of Psychophysiology*, 85 (3):421 – 422, 2012.
  - [113] A. Kannenberg, B. Zacharias, and M. Bellmann. Difficulty and safety of performing activities of daily living with two different microprocessor controlled prosthetic knee joints. In *American Academy of Orthotists & Prosthetists: 38th Academy Annual Meeting and Scientific Symposium*, 2012.
  - [114] A. O. Kapti and M. S. Yucenur. Design and control of an active artificial knee joint. *Mechanism and Machine Theory*, 41 (12):1477 – 1485, 2006.
  - [115] K. R. Kaufman, J. A. Levine, R. H. Brey, S. K. McCrady, D. J. Padgett, and M. Joyner. Energy expenditure and activity of transfemoral amputees using mechanical and microprocessor-controlled prosthetic knees. *Archives of Physical Medicine and Rehabilitation*, 89 (7):1380 – 1385, 2008.
  - [116] R. Kelly, V. Santibáñez Davila, and J. A. Loría Perez. *Control of Robot Manipulators in Joint Space*. Springer, 2005.
  - [117] J. G. Ketelaar, L. C. Visser, S. Stramigioli, and R. Carloni. Controller design for a bipedal walking robot using variable stiffness actuators. In *IEEE International Conference on Robotics and Automation*, 2013.
  - [118] B.-S. Kim and J.-B. Song. Hybrid dual actuator unit: A design of a variable stiffness actuator based on an adjustable moment arm mechanism. In *IEEE International Conference on Robotics and Automation*, 2010.

- 
- 
- [119] B.-S. Kim and J.-B. Song. Design and control of a variable stiffness actuator based on adjustable moment arm. *IEEE Transactions on Robotics*, 28 (5):1145 – 1151, 2012.
  - [120] K. Koganezawa, Y. Shimizu, H. Inomata, and T. Nakazawa. Actuator with non linear elastic system (ANLES) for controlling joint stiffness on antiaonistic driving. In *IEEE International Conference on Robotics and Biomimetics*, 2004.
  - [121] R. Kramme. *Technische Medizin*. Springer, 2004.
  - [122] M. Laffranchi, T. N. G, and D. G. Caldwell. Variable physical damping actuators (vpdas): Facilitating the control and improving the performance of compliant actuation systems. In *IEEE International Workshop on Advanced Motion Control*, 2012.
  - [123] M. Laffranchi, T. N. G, and D. G. Caldwell. Analysis and development of a semiactive damper for compliant actuation systems. *IEEE/ASME Transactions on Mechatronics*, 18 (2):744 – 753, 2013.
  - [124] M. Laffranchi, N. Tsagarakis, , and D. G. Caldwell. A compact compliant actuator (compact) with variable physical damping. In *IEEE International Conference on Robotics and Automation*, 2011.
  - [125] D. Lakatos, G. Garofalo, F. Petit, C. Ott, and A. Albu-Schäffer. Modal limit cycle control for variable stiffness actuated robots. In *IEEE International Conference on Robotics and Automation*, 2013.
  - [126] J. R. Landis and G. G. Koch. The measurement of observer agreement for categorical data. *Biometrics*, 33 (1):159 – 174, 1977.
  - [127] B. E. Lawson, A. H. Shultz, and M. Goldfarb. Evaluation of a coordinated control system for a pair of powered transfemoral prostheses. In *IEEE International Conference on Robotics and Automation*, 2013.
  - [128] B. E. Lawson, H. A. Varol, and M. Goldfarb. Standing stability enhancement with an intelligent powered transfemoral prosthesis. *IEEE Transactions on Biomedical Engineering*, 58 (9):2617 – 2624, 2011.
  - [129] B. E. Lawson, H. A. Varol, A. Huff, E. Erdemir, and M. Goldfarb. Control of stair ascent and descent with a powered transfemoral prosthesis. *IEEE Transactions on Neural Systems and Rehabilitation Engineering*, 21 (3):466 – 473, 2013.

- 
- 
- [130] B. E. Lawson, H. A. Varol, F. Sup, and M. Goldfarb. Stumble detection and classification for an intelligent transfemoral prosthesis. In *Annual International Conference of the IEEE EMBS*, 2010.
  - [131] S.-H. Lee and J.-B. Song. Acceleration estimator for low-velocity and low-acceleration regions based on encoder position data. *IEEE/ASME Transactions on Mechatronics*, 6 (1):58 – 64, 2001.
  - [132] M. W. Legro, G. Reiber, M. del Aguila, M. J. Ajax, D. A. Boone, J. A. Larsen, D. G. Smith, and B. Sangeorzan. Issues of importance reported by persons with lower limb amputations and prostheses. *Journal of Rehabilitation Research & Development*, 36:155 – 163, 1999.
  - [133] M. W. Legro, G. D. Reiber, D. G. Smith, M. del Aguila, J. Larsen, and D. Boone. Prosthesis evaluation questionnaire for persons with lower limb amputations: assessing prosthesis-related quality of life. *Archives of Physical Medicine and Rehabilitation*, 79:931 – 938, 1998.
  - [134] J. Lenarčič, T. Bajd, and M. M. Stanišić. *Robot Mechanisms*. Springer, 2013.
  - [135] T. Lens and O. von Stryk. Investigation of safety in human-robot-interaction for a series elastic, tendon-driven robot driven robot arm. In *IEEE/RSJ International Conference on Intelligent Robots and Systems*, 2012.
  - [136] E. Lewis and D. M. Lloyd. Embodied experience: A first-person investigation of the rubber hand illusion. *Phenomenology and the Cognitive Sciences*, 9:317 – 339, 2010.
  - [137] S. W. Lipfert. *Kinematic and dynamic similarities between walking and running*. PhD thesis, Friedrich-Schiller Universität, 2010.
  - [138] G. D. Logan and D. F. Radcliffe. Potential for use of a house of quality matrix technique in rehabilitation engineering. *IEEE Transactions on Rehabilitation Engineering*, 5 (1):106 – 115, 1997.
  - [139] M. R. Longo and P. Haggard. Sense of agency primes manual motor responses. *Perception*, 38:69 – 78, 2009.
  - [140] M. R. Longo, F. Schüür, M. P. M. Kammers, T. M, and P. Haggard. What is embodiment? A psychometric approach. *Cognition 107*, 107:978 – 998, 2008.
  - [141] J. Lunze. *Regelungstechnik 1*. Springer, 2013.

- 
- [142] A. F. T. Mak, M. Zhang, and D. A. Boone. State-of-the-art research in lower-limb prosthetic biomechanics-socket interface: A review. *Journal of Rehabilitation Research & Development*, 38 (2):161 – 174, 2001.
- [143] R. Marino and M. W. Spong. Nonlinear control techniques for flexible joint manipulators: A single link case study. In *IEEE International Conference on Robotics and Automation*, 1986.
- [144] E. C. Martinez-Villalpando and H. Herr. Agonist-antagonist active knee prosthesis: a preliminary study in level-ground walking. *Journal of Rehabilitation Research & Development*, 46 (3):361 – 373, 2009.
- [145] E. C. Martinez-Villalpando, J. Weber, G. Elliott, and H. Herr. Biomimetic prosthetic knee using antagonistic muscle-like activation. In *ASME International Mechanical Engineering Congress and Exposition*, 2008.
- [146] E. C. Martinez-Villalpando, J. Weber, G. Elliott, and H. Herr. Design of an agonist-antagonist active knee prosthesis. In *IEEE International Conference on Biomedical Robotics and Biomechatronics*, 2008.
- [147] A. Mayer, K. Kudar, K. Bretz, and J. Tihanyi. Body schema and body awareness of amputees. *Prosthetics and Orthotics International*, 32 (3):363 – 382, 2008.
- [148] D. Meschede. *Gerthsen Physik*. Springer, 2002.
- [149] U. Mettin, P. X. La Hera, L. B. Freidovich, , and A. S. Shiriaev. Parallel elastic actuators as a control tool for preplanned trajectories of underactuated mechanical systems. *International Journal of Robotics Research*, 29(9):1186 – 1198, 2009.
- [150] S. A. Migliore, E. A. Brown, and S. P. DeWeerth. Biologically inspired joint stiffness control. In *IEEE International Conference on Robotics and Automation*, 2005.
- [151] W. C. Miller, M. Speechley, and A. B. Deathe. Balance confidence among people with lower-limb amputations. *Physical Therapy*, 82 (9):856 – 865, 2002.
- [152] D. Mitrovic, S. Klanke, M. Howard, and S. Vijayakumar. Exploiting sensorimotor stochasticity for learning control of variable impedance actuators. In *IEEE International Conference on Humanoid Robots*, 2010.

- 
- 
- [153] T. Morita and S. Sugano. Design and development of a new robot joint using a mechanical impedance adjuster. In *IEEE International Conference on Robotics and Automation*, 1995.
  - [154] T. Morita and S. Sugano. Development and evaluation of seven-d.o.f. mia arm. In *IEEE International Conference on Robotics and Automation*, 1997.
  - [155] C. D. Murray. An interpretative phenomenological analysis of the embodiment of artificial limbs. *Disability and Rehabilitation*, 26 (16):963 – 973, 2004.
  - [156] C. D. Murray. *Psychoprosthetics*, chapter Embodiment and Prosthetics, pages 119 –130. Springer, 2008.
  - [157] C. D. Murray and J. Fox. Body image and prosthesis satisfaction in the lower limb amputee. *Disability and rehabilitation*, 24 (17):925 – 931, 2002.
  - [158] R. Nordmann. *Mechatronische Systeme Teil I*. Shaker Verlag, 2005.
  - [159] R. Nordmann and H. Birkhofer. *Maschinenelemente und Mechatronik I*. Shaker Verlag, 2003.
  - [160] A. V. Oppenheim, R. W. Schafer, and J. R. Buck. *Discrete-Time Signal Processing*. Prentice Hall, 1998.
  - [161] C. Ott. *Cartesian impedance control of redundant and flexible-joint robots*. Springer, Berlin, 2008.
  - [162] S. Ozgoli and H. D. Taghirad. A survey on the control of flexible joint robots. *Asian Journal of Control*, 8 (4)(4):332 – 344, 2006.
  - [163] G. Pahl, W. Beitz, J. Feldhusen, and K.-H. Grot. *Engineering Design - A Systematic Approach*. Springer, 2007.
  - [164] G. Palli and C. Melchiorri. Robust control of robots with variable joint stiffness. In *International Conference on Advanced Robotics*, 2009.
  - [165] G. Palli and C. Melchiorri. On the control of redundant robots with variable stiffness actuation. In *IEEE/RSJ International Conference on Intelligent Robots and Systems*, 2012.
  - [166] J.-J. Park, Y.-L. Lee, J.-B. Song, and B.-S. Kim. Safe joint mechanism based on nonlinear stiffness for safe human-robot collision. In *IEEE International Conference on Robotics and Automation*, 2008.

- 
- [167] J. Perry, J. M. Burnfield, C. J. Newsam, and C. P. Energy expenditure and gait characteristics of a bilateral amputee walking with c-leg prostheses compared with stubby and conventional articulating prostheses. *Archives of Physical Medicine and Rehabilitation*, 85:1711 – 1717, 2004.
- [168] F. Petit and A. Albu-Schäffer. Cartesian impedance control for a variable stiffness robot arm. In *IEEE/RSJ International Conference on Intelligent Robots and Systems*, 2011.
- [169] F. Petit and A. Albu-Schäffer. State feedback damping control for a multi dof variable stiffness robot arm. In *2008 IEEE International Conference on Robotics and Automation*, 2011.
- [170] S. Pfeifer, R. Riener, and H. Vallery. An actuated transfemoral prosthesis with optimized polycentric knee joint. In *IEEE International Conference on Biomedical Robotics and Biomechatronics*, 2012.
- [171] M. R. Pitkin. *Biomechanics of Lower Limb Prosthetics*. Springer, 2010.
- [172] G. A. Pratt and M. M. Williamson. Series elastic actuators. In *IEEE/RSJ International Conference on Intelligent Robots and Systems*, 1995.
- [173] H. V. Quy, L. Aryananda, F. I. Sheikh, F. Casanova, and R. Pfeifer. A novel mechanism for varying stiffness via changing transmission angle. In *IEEE International Conference on Robotics and Automation*, 2011.
- [174] S. G. Rabinovich. *Evaluating Measurement Accuracy - A Practical Approach*. Springer, 2013.
- [175] S. Rao, R. Carloni, and S. Stramigioli. A novel energy-efficient rotational variable stiffness actuator. In *Annual International Conference of the IEEE EMBS*, 2011.
- [176] R. Riener, M. Rabuffetti, and C. Frigo. Joint powers in stair climbing at different slopes. In *Annual International Conference of the IEEE EMBS*, 1999.
- [177] G. M. Rommers, L. D. W. Vos, J. W. Groothoff, and W. H. Eisma. Mobility of people with lower limb amputations: scales and questionnaires: a review. *Clinical Rehabilitation*, 15:92 – 102, 2001.

- 
- 
- [178] B. Rosen, H. H. Ehrsson, C. Antfolk, C. Cipriani, F. Sebelius, and G. Lundborg. Referral of sensation to an advanced humanoid robotic hand prosthesis. *Scandinavian Journal of Plastic and Reconstructive Surgery and Hand Surgery*, 43:260 – 266, 2009.
  - [179] E. J. Rouse, L. M. Mooney, E. C. Martinez-Villalpando, and H. M. Herr. Clutchable series-elastic actuator: Design of a robotic knee prosthesis for minimum energy consumption. In *IEEE International Conference on Rehabilitation Robotics*, 2013.
  - [180] G. Salvendy. *Handbook of Human Factors and Ergonomics*. John Wiley & Sons, Inc., 2006.
  - [181] I. Sardellitti, G. Medrano-Cerda, N. G. Tsagarakis, A. Jafari, and D. G. Caldwell. A position and stiffness control strategy for variable stiffness actuators. In *IEEE International Conference on Robotics and Automation*, 2012.
  - [182] I. Sardellitti, G. A. Medrano-Cerda, T. N., A. Jafari, and D. G. Caldwell. Gain scheduling control for a class of variable stiffness actuators based on lever mechanisms. *IEEE Transactions on Robotics*, 29 (3):791 – 798, 2013.
  - [183] E. M. Schaffalitzky. *Optimising the prescription and use of lower limb prosthetic technology: A mixed methods approach*. PhD thesis, Dublin City University, 2010.
  - [184] E. M. Schaffalitzky, P. Gallagher, M. MacLachlan, and N. Ryall. Understanding the benefits of prosthetic prescription: exploring the experiences of practitioners and lower limb prosthetic users. *Disability & Rehabilitation*, 33 (15-16):1314 – 1323, 2011.
  - [185] E. M. Schaffalitzky, P. Gallagher, M. MacLachlan, and S. T. Wegener. Developing consensus on important factors associated with lower limb prosthetic prescription and use. *Disability & Rehabilitation*, 34 (24):2085 – 2094, 2012.
  - [186] E. M. Schaffalitzky, S. N. Mhurchadha, P. Gallagher, S. Hofkamp, M. MacLachlan, and S. T. Wegener. Identifying the values and preferences of prosthetic users: A case study series using the repertory grid technique. *Prosthetics and Orthotics International*, 33 (2):157 – 166, 2009.
  - [187] R. Schiavi, G. Grioli, S. Sen, and A. Bicchi. VSA-II: a novel prototype of variable stiffness actuator for safe and performing robots interacting with humans. In *IEEE International Conference on Robotics and Automation*, 2008.

- 
- [188] T. L. Schmitz and K. S. Smith. *Mechanical Vibrations - Modeling and Measurement*. Springer, 2012.
- [189] M. A. Schubert. Quality function deployment - a comprehensive tool for planning and development. In *IEEE 1989 National Aerospace and Electronics Conference*, 1989.
- [190] F. Schültje, P. Beckerle, M. Grimmer, J. Wojtusch, and S. Rinderknecht. Comparison of Trajectory Generation Methods for a Human-Robot Interface based on Motion Tracking in the Int<sup>2</sup>Bot. In *IEEE International Symposium on Robot and Human Interactive Communication*, 2014.
- [191] T. Schürmann. Psychological acceptance and engineering decisions: Evaluation of expert opinions in prosthesis development. Master's thesis, Work and engineering psychology research group, Technische Universität Darmstadt, 2013.
- [192] T. Schürmann, P. Beckerle, J. Vogt, and O. Christ. Sind Urteile von Experten unterschiedlicher Berufsbiografien einstimmig? Eine Studie zur professionellen Beurteilung von Beinprothesen. *Orthopädie Technik*, 2:30 – 35, 2014.
- [193] J. Schuy. Entwicklung von beinprothesenkonzepten zur aktiven unterstützung des nutzers. Diplomarbeit, Institute for Mechatronic Systems in Mechanical Engineering, Technische Universität Darmstadt, 2011.
- [194] J. Schuy, P. Beckerle, J. Faber, J. Wojtusch, S. Rinderknecht, and O. von Stryk. Dimensioning and evaluation of the elastic element in a variable torsion stiffness actuator. In *IEEE/ASME International Conference on Advanced Intelligent Mechatronics*, 2013.
- [195] J. Schuy, P. Beckerle, J. Wojtusch, S. Rinderknecht, and O. von Stryk. Conception and Evaluation of a Novel Variable Torsion Stiffness for Biomechanical Applications. In *IEEE International Conference on Biomedical Robotics and Biomechatronics*, 2012.
- [196] M. Seidel. *Methodische Produktplanung - Grundlagen, Systematik und Anwendung im Produktentstehungsprozess*. PhD thesis, Universität Karlsruhe, 2005.
- [197] H. Senra, R. Aragao Oliveira, I. Leal, and C. Vieira. Beyond the body image: a qualitative study on how adults experience lower limb amputation. *Clinical Rehabilitation*, 26:180 – 191, 2011.

- 
- [198] W. H. J. Shaw. Design feature dominance in quality function deployment. In *Innovation in Technology Management - The Key to Global Leadership. PICMET '97: Portland International Conference on Management and Technology*, 1997.
- [199] X. Shen and Gol. Independent stiffness and force control of pneumatic actuators for contact stability during robot manipulation. In *IEEE International Conference on Robotics and Automation*, 2005.
- [200] P. V. Shendge and P. V. Suryawanshi. Sliding mode control for flexible joint using uncertainty and disturbance estimation. In *World Congress on Engineering and Computer Science*, 2011.
- [201] B. Siciliano, L. Sciavicco, L. Villani, and G. Oriolo. *Robotics: Modelling, Planning and Control*. Springer, 2009.
- [202] J. J. E. Slotine and W. Li. *Applied Nonlinear Control*. Prentice Hall, 1991.
- [203] J. Song and B. Kim. Three types of dual actuator units for variable impedance actuation. In *IEEE International Conference on Robotics and Automation*, 2010.
- [204] L. Song, X. Wang, S. Gong, Z. Shi, and L. Chen. Design of active artifical knee joint. In *Asian-Pacific Conference on Medical and Biological Engineering*, 2008.
- [205] A. W. Spong. Modeling and control of elastic joint robots. *Journal of Dynamic Systems, Measurement, and Control*, 109:310 – 318, 1987.
- [206] M. W. Spong. Adaptive control of flexible joint manipulators. *System & Control Letters*, 13:15 – 21, 1989.
- [207] M. W. Spong. On the force control problem for flexible joint manipulators. *IEEE Transactions on Automatic Control*, 34 (1):107 – 111, 1989.
- [208] M. W. Spong, J. Y. Hung, S. A. Bortoff, and F. Ghorbel. A comparison of feedback linearization and singular perturbation techniques for the control of flexible joint robots. In *American Control Conference*, 1989.
- [209] M. W. Spong, K. Khorasani, and P. V. Kokotovic. A slow manifold approach to feedback control of nonlinear flexible systems. In *American Control Conference*, 1985.

- 
- [210] M. W. Spong, J. S. Thorp, and J. M. Kleinwaks. The control of robot manipulators with bounded input: Part II: robustness and disturbance rejection. In *IEEE Conference on Decision and Control*, 1984.
- [211] M. W. Spong and M. Vidyasagar. Robust linear compensator design for non-linear robotic control. *IEEE Journal of Robotics and Automation*, 3 (4):345 – 351, 1987.
- [212] A. H. Stienen, E. E. Hekman, H. ter Braak, A. M. Aalsma, F. C. van der Helm, and H. van der Kooij. Design of a rotational hydro-elastic actuator for an active upper-extremity rehabilitation exoskeleton. In *IEEE International Conference on Biomedical Robotics and Biomechatronics*, 2008.
- [213] S. Stramigioli, G. van Oort, and E. Dertien. A concept for a new energy efficient actuator. In *IEEE/ASME International Conference on Advanced Intelligent Mechatronics*, 2008.
- [214] J. S. Sulzer, M. A. Peshkin, and J. L. Patton. MARIONET: An exotendon-driven rotary series elastic actuator for exerting joint torque. In *IEEE International Conference on Rehabilitation Robotics*, 2005.
- [215] F. Sup, A. Bohara, and M. Goldfarb. Design and control of a powered knee and ankle prosthesis. In *IEEE International Conference on Robotics and Automation*, 2007.
- [216] F. Sup, A. Bohara, and M. Goldfarb. Design and control of a powered trans-femoral prosthesis. *International Journal of Robotics Research*, 27 (2):263 – 273, 2008.
- [217] F. Sup, H. A. Varol, J. Mitchell, T. Withrow, and M. Goldfarb. Design and control of an active electrical knee and ankle prosthesis. In *IEEE International Conference on Biomedical Robotics and Biomechatronics*, 2008.
- [218] F. Sup, H. A. Varol, J. Mitchell, T. J. Withrow, and M. Goldfarb. Self-contained powered knee and ankle prosthesis: Initial evaluation on a trans-femoral amputee. In *IEEE International Conference on Rehabilitation Robots*, 2009.
- [219] K. G. Taylor. How to make a success of quality function deployment. In *IEE Colloquium on Customer Driven Quality in Product Design*, 1994.

- 
- 
- [220] P. J. Theeven, B. Hemmen, R. Geers, R. Smeets, P. Brink, and H. Seeleen. Influence of advanced prosthetic knee joints on perceived performance and everyday life activity level of low-functional persons with a transfemoral amputation or knee disarticulation. *Journal of Rehabilitation Medicine*, 44 (5):454 – 461, 2012.
  - [221] I. Thorson, M. Svimin, S. Hosoe, F. Asano, and K. Taji. Design considerations for a variable stiffness actuator in a robot that walks and runs 2007. In *JSME Conference Robotics and Mechatronics*, 2007.
  - [222] G. Tonietti, R. Schiavi, and A. Bicchi. Design and control of a variable stiffness actuator for safe and fast physical Human/Robot interaction. In *IEEE International Conference on Robotics and Automation*, 2005.
  - [223] N. G. Tsagarakis, M. Laffranchi, B. Vanderborght, and D. G. Caldwell. A compact soft actuator unit for small scale human friendly robots. In *IEEE International Conference on Robotics and Automation*, 2009.
  - [224] M. R. Tucker and K. B. Fite. Mechanical damping with electrical regeneration for a powered transfemoral prosthesis. In *IEEE/ASME International Conference on Advanced Intelligent Mechatronics*, 2010.
  - [225] T. Umedachi and A. Ishiguro. A development of a fully self-contained real-time tunable spring. In *IEEE/RSJ International Conference on Intelligent Robots and Systems*, 2006.
  - [226] R. Ünal. *WalkMECH - Design and Control of an Energy Recycling Transfemoral Prosthesis*. PhD thesis, University of Twente, 2014.
  - [227] R. Van Ham, T. G. Sugar, B. Vanderborght, K. W. Hollander, and D. Lefeber. Compliant Actuator Designs Review of Actuators with Passive Adjustable Compliance/Controllable Stiffness for Robotic Applications. *IEEE Robotics & Automation Magazine*, 16:81 – 94, 2009.
  - [228] B. Vanderborght, A. Albu-Schaeffer, A. Bicchi, E. Burdet, D. G. Caldwell, R. Carloni, M. Catalano, O. Eiberger, W. Friedl, G. Ganesh, M. Garabini, M. Grebenstein, G. Grioli, S. Haddadin, H. Hoppner, A. Jafari, M. Laffranchi, D. Lefeber, F. Petit, S. Stramigioli, N. Tsagarakis, M. Van Damme, R. Van Ham, L. C. Visser, and S. Wolf. Variable impedance actuators: A review. *Robotics and Autonomous Systems*, 61 (12):1601 – 1614, 2013.

- 
- [229] B. Vanderborght, R. Van Ham, D. Lefeber, T. G. Sugar, and K. W. Hollander. Comparison of Mechanical Design and Energy Consumption of Adaptable, Passive-compliant Actuators. *International Journal of Robotics Research*, 28:90 – 103, 2009.
- [230] B. Vanderborght, B. Verrelst, R. Van Ham, M. Van Damme, P. Beyl, and D. Lefeber. Development of a compliance controller to reduce energy consumption for bipedal robots. *Autonomous Robots*, 24 (4):419 – 434, 2008.
- [231] Verein Deutscher Ingenieure. VDI 2206, Design methodology for mechatronic systems, 2004.
- [232] B. Verrelst, F. Daerden, D. Lefeber, R. van Ham, and T. Fabri. Introducing pleated pneumatic artificial muscles for the actuation of legged robots: a one-dimensional set-up. In *Climbing and Walking Robots*, 2000.
- [233] R. Versluys, A. Desomer, G. Lenaerts, P. Beyl, M. Van Damme, B. Vanderborght, I. Vanderniepen, G. Van der Perre, and D. Lefeber. From Conventional Prosthetic Feet to Bionic Feet: A Review Study. In *IEEE International Conference on Biomedical Robotics and Biomechatronics*, 2008.
- [234] R. Versluys, A. Desomer, G. Lenaerts, M. Van Damme, P. Beyl, G. Van der Perre, L. Peertaer, and D. Lefeber. A pneumatically powered below-knee prosthesis: Design specifications and first experiments with an amputee. In *IEEE International Conference on Biomedical Robotics and Biomechatronics*, 2008.
- [235] D. R. Vickers, C. Palk, A. S. McIntosh, and K. T. Beatty. Elderly unilateral transtibial amputee gait on an inclined walkway: A biomechanical analysis. *Gait and Posture*, 27:518 – 529, 2008.
- [236] O. von Stryk, P. Beckerle, O. Christ, S. Rinderknecht, and J. Vogt. Verfahren und Testeinrichtung zur Durchführung von Tests mit einer Prothese, 2012.
- [237] O. von Stryk, P. Beckerle, O. Christ, S. Rinderknecht, and J. Vogt. Verfahren und Vorrichtung zum Durchführen von Tests mit einer Testprothese, 2012.
- [238] D. Wartenberg. Auslegung, Konstruktion und Prototypenaufbau eines aktiven Prothesenkniegelenks mit variabler Steifigkeit. Bachelor Thesis, Institute for Mechatronic Systems in Mechanical Engineering, Technische Universität Darmstadt, 2012.

- 
- [239] R. L. Waters, J. Perry, D. Antonelli, and H. Hislop. Energy cost of walking of amputees. *Bone and Joint Surgery*, 58 (1):42 – 46, 1976.
- [240] G. Waycaster, S.-K. Wu, and X. Shen. Design and control of a pneumatic artificial muscle actuated above-knee prosthesis. *Journal of Medical Devices*, 5 (3):031003, 2011.
- [241] R. Weiber and D. Mühlhaus. *Strukturgleichungsmodellierung*. Springer Gabler, 2014.
- [242] E. C. Wentink, H. F. J. M. Koopman, S. Stramigioli, J. S. Rietman, and P. H. Veltink. Variable stiffness actuated prosthetic knee to restore knee buckling during stance: A modeling study. *Medical Engineering & Physics*, 35:838 – 845, 2013.
- [243] H. H. Wetz. Einfluss des C-Leg-Kniegelenk-Passteiles der Fa. Otto Bock auf die Versorgungsqualität Oberschenkelamputierter. *Der Orthopäde*, 4:298 – 319, 2005.
- [244] M. W. Whittle. *Gait analysis: An introduction*. Elsevier, 2007.
- [245] T. Wimbock, C. Ott, A. Albu-Schäffer, A. Kugi, and G. Hirzinger. Impedance control for variable stiffness mechanisms with nonlinear joint coupling. In *IEEE/RSJ International Conference on Intelligent Robots and Systems*, 2008.
- [246] M. Windrich. Integration psychologischer Faktoren in die technische Entwicklung von aktiven Beinprothesen. Bachelor Thesis, Institute for Mechatronic Systems in Mechanical Engineering, Technische Universität Darmstadt, 2012.
- [247] M. Windrich. Überblick zu aktiven beinprothesenkomponenten. Research seminar, Institute for Mechatronic Systems in Mechanical Engineering, Technische Universität Darmstadt, 2014.
- [248] J. Wojtusch, P. Beckerle, O. Christ, K. Wolff, O. von Stryk, S. Rinderknecht, and J. Vogt. Prosthesis-user-in-the-loop: A user-specific biomechanical modeling and simulation environment. In *Annual International Conference of the IEEE EMBS*, 2012.
- [249] S. Wolf, O. Eiberger, and G. Hirzinger. The DLR FSJ: Energy based design of a variable stiffness joint. In *IEEE International Conference on Robotics and Automation*, 2011.

- 
- 
- [250] S. Wolf and G. Hirzinger. A new variable stiffness design: Matching requirements of the next robot generation. In *IEEE International Conference on Robotics and Automation*, 2008.
  - [251] M. Yalcin, B. Uzunoglu, E. Altintepe, and Patoglu. VNs<sub>a</sub>: Variable negative stiffness actuation based on nonlinear deflection characteristics of buckling beams. In *IEEE/RSJ International Conference on Intelligent Robots and Systems*, 2013.
  - [252] S. Zahedi. *ATLAS OF Prosthetics*, chapter Lower Limb Prosthetic Research In The 21st Century. Endolite Institute, 2001.
  - [253] K. Ziegler-Graham, E. MacKenzie, P. Ephraim, T. TG, and B. R. Estimating the Prevalence of Limb Loss in the United States: 2005 to 2050. *Archives of Physical Medicine and Rehabilitation*, 89:422 – 429, 2008.

---

---

---

## Wissenschaftlicher Werdegang<sup>1</sup>

---

- 06/2002                    Allgemeine Hochschulreife
- 10/2003 — 05/2009      Studium Maschinenbau (Mechatronik)  
an der Technischen Universität Darmstadt
- 05/2009                    Diplom Maschinenbau (Mechatronik)
- 05/2009 — 07/2014       Wissenschaftlicher Mitarbeiter  
Institut für Mechatronische Systeme im Maschinenbau,  
Fachbereich Maschinenbau, TU Darmstadt
- seit 08/2014               Oberingenieur  
Institut für Mechatronische Systeme im Maschinenbau,  
Fachbereich Maschinenbau, TU Darmstadt

---

<sup>1</sup> gemäß § 20 Abs. 3 der Promotionsordnung der TU Darmstadt